

A thermogravimetric study of oxygen diffusion in $\text{YBa}_2\text{Cu}_3\text{O}_{7-\delta}$

María Dolores Vázquez-Navarro



A dissertation submitted to the University of Cambridge for the
Degree of Doctor of Philosophy

Corpus Christi College
Cambridge

August 1998

To my parents

Recte vives Licini, neque altum
semper urgendo neque, dum procellas
cactus horrescis, nimium pretendo
litus iniquum

Auream quisquis mediocritatem
diligit tunc caret obsoleti
sordibus tecti, caret invidenda
sobrius aula

Saepe ventis agitur ingens
pinus et celsae graviore casu
decidunt turres feriuntque summos
fulgura montes

Sperta infestis, metuit secundis
alterum sortem bene preparatum pectus,
informes hieles reducit Iupiter,
idem summovet.

Non si male nunc, et olim sic erit:
quondam cithara tacentem suscitavit
Musam neque semper arcum
tendit Apollo

Rebus angusti animosus atque fortis
appare; sapienter idem
contrahes vento nimium secundo
turgida vela.

Horace

Vivirás mejor, Licinio, no instando siempre
a la alta mar ni, por evitar prudente
las tormentas, acercándote demasiado a la
peligrosa orilla.

Quien ama la dorada medianía
carece seguro de la miseria de un
techo impropio; carece de un sobrio
palacio envidiable.

Con más frecuencia es zarandeado por los vientos el
pino ingente, las elevadas torres se precipitan
con más dura caída y los rayos hieren
los montes más altos.

Espera en la dificultad, y teme en la
prosperidad la suerte contraria con el pecho
bien dispuesto. Júpiter trae los espantosos inviernos;
también los remueve.

No porque ahora vaya mal será así siempre:
a veces la cítara motiva a la callada musa,
y no siempre Apolo
tiende su arco.

En la circunstancia adversa muéstrate animoso
y fuerte: de igual modo sabiamente
reducirás las hinchadas velas a
un viento favorable.

You will take a better course, Licinius,
if you do not always thrust over the deep sea,
or hug the dangerous coast too close,
shivering at the prospect of squalls.

Whoever loves the Golden Mean
is safe (no squalor for him in a filthy garret),
and temperate (for him no mansion
that men will envy).

The hughe pine is more cruelly tossed
by the winds, the loftiest towers
have the heaviest fall and lightning strikes
the tops of mountains.

The heart well prepared hopes in adversity
for a change in fortune, and fears in prosperity.
Jupiter brings back ugly winters
and Jupiter

removes them. If all goes badly now, some day
it will not be so. Sometimes Apollo rouses
the silent Muse with his lyre. He does not always
stretch his bow.

In difficult straits show spirit
and courage, and when the wind
is strong at your back, be wise
and shorten the bulging sail.

SUMMARY

$\text{YBa}_2\text{Cu}_3\text{O}_{7-\delta}$ (YBCO) was one of the first high temperature superconductors discovered, and its superconducting properties are strongly dependent on oxygen stoichiometry. A large amount of work has been done on the variation of stoichiometry and its effect on the superconducting properties of the material. However, in spite of all the work done, the results published in the literature are very scattered.

This thesis presents a thermogravimetric study of oxygen diffusion in YBCO under isothermal and non-isothermal conditions and tries to reconcile the data available based on the results obtained and taking into account the factors that may have affected the data presented by other groups, such as the effects of the microstructure and the different diffusion coefficients measured with the techniques used. An Arrhenius expression for the chemical diffusion of oxygen has been calculated from the analysis of isothermal oxygenation data, and it has been corroborated by a study of the non-isothermal experiments carried out. This work includes the development of a macroscopic model for oxygen diffusion in YBCO based on the diffusion coefficient calculated from experimental data. The model is used to simulate for the first time oxygenations under both isothermal and non-isothermal conditions.

The study of non-isothermal oxygenations has led directly to the design of novel cooling procedures that can be introduced at the end of the processing stage of YBCO samples, producing highly oxygenated specimens in shorter times than for conventional isothermal and ramped oxygenation procedures.

The final section of this dissertation presents a study of the Direct Current Zoning effect. The generation of a mobile hot zone in a polycrystalline YBCO bar when passing a current across it is directly linked to the diffusion of oxygen ions in the material. A mechanism for the motion of the zone along the sample has been suggested. A computer model has been developed to reproduce this process taking into account the motion of ions due to chemical diffusion and the potential difference established. The results from this model have corroborated the mechanism suggested and give for the first time the opportunity to study this phenomenon in more detail.

PREFACE

This thesis describes the work carried out in the Department of Materials Science and Metallurgy of the University of Cambridge between October 1994 and July 1998 under the supervision of Prof. J.E. Evetts.

The work described is original except where reference is made to the work of others. No part of this work has been submitted for any other degree at this or another university. The work described has not been done in collaboration with others and it does not exceed 60,000 words in length.

I would like to thank the Engineering and Physical Sciences Research Council, E.A. Technology, the Interdisciplinary Research Centre (IRC) in Superconductivity, and Corpus Christi College, Cambridge, for financial support during this research. I am also grateful to Prof. C.J. Humphreys, Prof. A.H. Windle and Prof. Y. Liang for the provision of laboratory facilities in the Department of Materials Science and Metallurgy and at the IRC in Superconductivity.

Some of the work described in this dissertation has been published as follows:

“Microwave assisted oxygenation of melt-processed bulk $\text{YBa}_2\text{Cu}_3\text{O}_{7-\delta}$ ceramics”. A.T. Rowley, R. Wroe, D. Vázquez-Navarro, Wai Lo and D.A. Cardwell, *J. Mat. Sci.*, Vol. **32** (1997) pp. 4541-4547.

“Analysis and Modelling of Oxygen Diffusion in $\text{YBa}_2\text{Cu}_3\text{O}_{7-\delta}$ under Non-isothermal Conditions”. M.D. Vázquez-Navarro, A. Kuršumović, C.Chen and J.E. Evetts, *Inst. Phys. Conf. Ser.* No. **158** (paper presented at the *European Conference on Applied Superconductivity*, The Netherlands, 30 June-3 July, 1997) pp. 1037-1040.

M^a Dolores Vázquez-Navarro

August 1998

ACKNOWLEDGEMENTS

I am very grateful to all that have helped me during my career as a research student. I would like to thank my supervisor, Dr. (now Prof.) Jan Evetts for his support, encouragement and patience during these years. I am extremely grateful to Dr. Lindsay Greer, for allowing me to use his Thermal Analysis System, and to Dr. Ilan Blech and Dr. José Ruiz for their help with the development of the theoretical models to the DCZ effect and macroscopic oxygen diffusion (respectively). I would also like to thank Dr. Chen for kindly supplying the single crystals used. I am very grateful to Dr. Ahmed Kuršumovic for arriving just at the right time to give me the breath of encouragement and positiveness towards my work I needed at the time. No matter what happens, it is always good to have a smile ready for everyone!. Thanks a lot too to Andrew Moss, Dave Nicol , and Bryan Barber and Carol Best for their help when I had to use the X-rays, SEM and needed to print just that little bit of the photograph (but twenty of them, please!).

I once was told that we spend most of our lives working (not counting the time we are asleep, of course); in the case of a PhD student this working life seems to be much longer than anybody else's. I would therefore like to thank everyone in the lab for making it a nicer place where to spend all those hours: Gavin (incredibly patient with my computer-related questions), Wilfred (thanks for all the support and for your help in making the 'box'... I am sure it will be useful to coming generations!), Richard (being positive and enthusiastic all the time), Bee-San (ah, those long talks during the long weekends!), Peter (you will always get the highest score!), Kim (go slowly, go slowly!), Andrés (thanks for answering all my physics questions and for the morning chats about almost everything! - and apologies to the rest of the office for the loud Spanish natter). To you all and the rest of the lab (Mark, Zoe, Bartek... the ones that are still here and those that have already left), "heaps of thanks" for having had the patience to share all this time with a (very often) stressed Dolores who used to go to Coffee and never went to Tea.

Thanks to Margaret for always being there and for giving me a room in 25 Cranmer Rd., as I had the chance of sharing the house with Jon (best 'uncle' ever!), Alison :-), Meera (thanks for all the de-stress lunches and so much more!) and Emma. There

won't be a place like no. 25. And to everyone in Leckhampton, especially the 'Venezuelan contingent': Juan Carlos, Deisy, Steve, Alena, Ernesto, Nadia and Thomas for introducing me to Latin American music, going to all those dance-till-you-drop parties and memorable punting trips to Grantchester (plus other random celebrations).

I am most grateful to my London connection: Pablo, Javier (Molero), Javier (Madurga), Dalia, Tatiana, Pete & Co. for being such good listeners and preserving my sanity by giving me the chance of running away from Cambridge to good ol' London every now and then.

A very special 'thanks' to Miguel, for his support and advice during these years, always being at the other end of the phone/E-mail line to listen to whatever I had to say. I wouldn't have been able to get this far on my own. (Apologies for the long coach journeys to and fro!).

And finally, I would like to thank my parents and sister for all they have done for me all these years, and without whose love, encouragement and understanding I would not be writing these lines. You are next, Marga!.

Chapter 1

Introduction to $YBa_2Cu_3O_{7-\delta}$

1.1 Introduction

This chapter presents a brief introduction to the subject of superconductivity: its discovery and the search for a room temperature superconducting material. The phenomenon of superconductivity is briefly outlined and the chapter ends with a description of the dependence of the $YBa_2Cu_3O_{7-\delta}$ chemical structure on its oxygen stoichiometry.

1.2 Discovery

In the early decades of this century, after having successfully liquefied helium in 1909, the Dutch physicist Kamerlingh Onnes conducted a study of the electrical properties of metals at low temperatures. He observed that when mercury was cooled to temperatures in the range of the boiling point of liquid helium, its resistivity suddenly decreased to such a small value that he was unable to measure it.

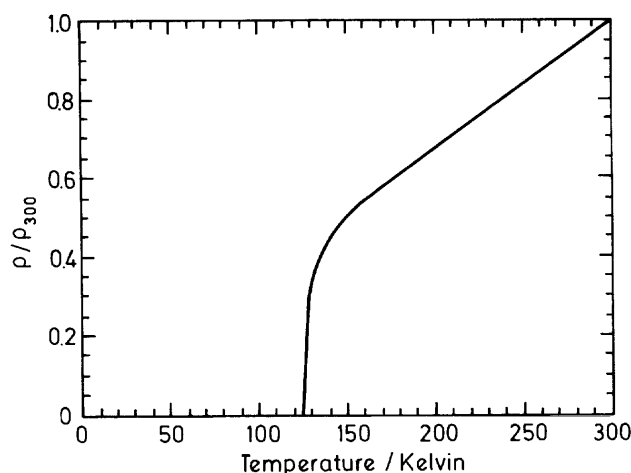


Fig. 1.1 Relative variation in resistance ρ/ρ_{RT} vs. temperature (K) similar to that observed by K. Onnes in Hg. This plot corresponds to the change in resistance with temperature of $Tl_2Ba_2Ca_2Cu_3O_{10}$ (from Cyrot and Pavuna (1992))

Onnes observed that below 4 K, mercury passed into a new state with electrical properties unlike those previously known. This new state was called the “superconducting state”. Superconducting materials offer no resistance to the flow of electrical currents through them as long as their temperature is below a certain value known as critical temperature: T_c . The discovery of superconductivity in mercury was the starting point of the quest for a room temperature superconductor. This material would allow the transport of energy without any losses, increasing the efficiency of this process to 100 %.

During the following years it was found that more than 20 metallic elements exhibited superconductivity at low temperatures. In 1913 Pb was found to be superconducting at 7.2 K and in 1930 Nb was discovered to have a critical temperature of 9.2 K, the highest of all pure metals.

The study to find new materials with higher T_c 's continued with alloys and compounds, which have higher critical temperatures than elemental metals. Nb compounds have become very important, as they can be used in a large number of small and large scale applications (e.g. magnetic field sensors and superconducting magnets respectively). Nb_3Ge exhibits the highest critical temperature of the group, with $T_c = 23.3$ K. Further work on this field led to the discovery of superconductivity in the Chevrel phases. The highest critical temperature in the series was 15 K, measured in $PbMo_6S_8$. Organic superconducting materials were also discovered in the early 1980's. However, their critical temperatures are much lower than those of any of the inorganic compounds mentioned so far, the highest being 10 K.

From 1973 to 1986 the 23 K figure of Nb_3Ge remained at the top of the list of critical temperatures. Oxide ceramics, such as the perovskites $SrTiO_3$ and $BaBiO_3$ could be made to superconduct at low temperatures by reduction or by doping, but their T_c was lower than that of Nb_3Ge . In 1986, however, Bednorz and Müller (1986) synthesised $La_{2-x}Ba_xCuO_4$ (LBCO). The crystal structure of this compound is based on that of the first superconducting oxide, the perovskite $SrTiO_3$. This compound was the first of what are known today as high temperature superconductors, with a $T_c = 35$ K. After this encouraging discovery an increasing amount of work was dedicated to studying and developing new perovskite-like structures and in 1987, Wu and co-workers (Wu

et al. (1987)) and Zhao *et al.* (1987) found that substituting the La with Y resulted in a compound, $\text{YBa}_2\text{Cu}_3\text{O}_{7-\delta}$ (YBCO), with a T_c of 93 K, almost 40 degrees higher than LSCO. This was a revolutionary discovery because finally, the material discovered had a T_c above the boiling point of liquid nitrogen (77 K). This meant that the applications for this superconducting compound would not require such a complex cooling system as with the other materials that needed liquid He for their operation. In the same year another superconducting compound, Bi-Sr-Ca-Cu-O (BSCCO) was discovered. Of the two superconducting phases of this compound, $\text{Bi}_2\text{Sr}_2\text{Ca}_2\text{Cu}_3\text{O}_{10+\delta}$, (2223) has the highest critical temperature: 110 K. Shortly after another compound with the same crystal structure, $\text{Tl}_2\text{Ba}_2\text{Ca}_2\text{Cu}_3\text{O}_{10}$, was found to superconduct at 125K. In 1993 a mercury compound with a similar structure was discovered, $\text{HgBa}_2\text{Ca}_2\text{Cu}_3\text{O}_{8-x}$, and its critical temperature is the highest observed up to date: 133 K. If the material is subjected to high pressure the T_c can be increased to 164 K. The discovery of high temperature superconductors seems to have reached a temporary standstill due to the increased complexity of the crystal structures of the compounds discovered. This structure also limits the extent of their industrial applications, as these materials are brittle and difficult to form and process for most large scale applications.

1.3 Structure and stoichiometry of $\text{YBa}_2\text{Cu}_3\text{O}_{7-\delta}$

Most high T_c superconducting oxides are cuprate compounds with a characteristic layered structure. The unit cell of superconducting cuprates of the $\text{RBa}_2\text{Cu}_3\text{O}_{7-\delta}$ type (R = rare earth) is developed from that of a tetragonal perovskite repeated along the c axis, and it consists of a sequence of copper-oxygen layers. This section presents a review of the structure of $\text{YBa}_2\text{Cu}_3\text{O}_{7-\delta}$ as an introduction to the work presented in this thesis.

The perovskite structure has the general formula ABO_3 . It was first found from the mineral perovskite CaTiO_3 and it consists of Ti^{4+} ions contained in octahedral cages of O^{2-} ions leaving a large cuboctahedral hole where the larger Ca^{2+} ion sits (see Fig. 1.2). Changes in temperature alter the coordination of the Ti ions with its

neighbouring oxygen ions, and this modifies the crystal structure of the material: from tetragonal at low temperatures to orthorhombic and orthogonal at high temperatures.

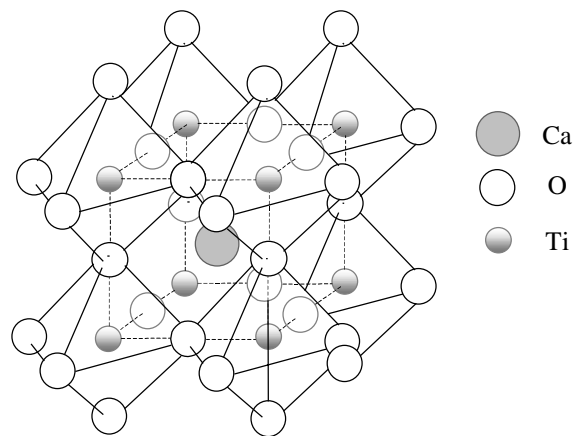


Fig. 1.2 The perovskite structure

The crystal structure of YBCO consists of three perovskite-like unit cells stacked one above the other. The central cell has an Y atom sandwiched between two corrugated CuO_2 planes. Above and below these CuO_2 planes there is a BaO_2 layer on top of which lies a Cu-O basal plane with a variable oxygen content. The whole structure is symmetrical with respect to the Y ion that can be substituted by a number of rare earths (except Pr and Yb) without losing its superconducting properties.

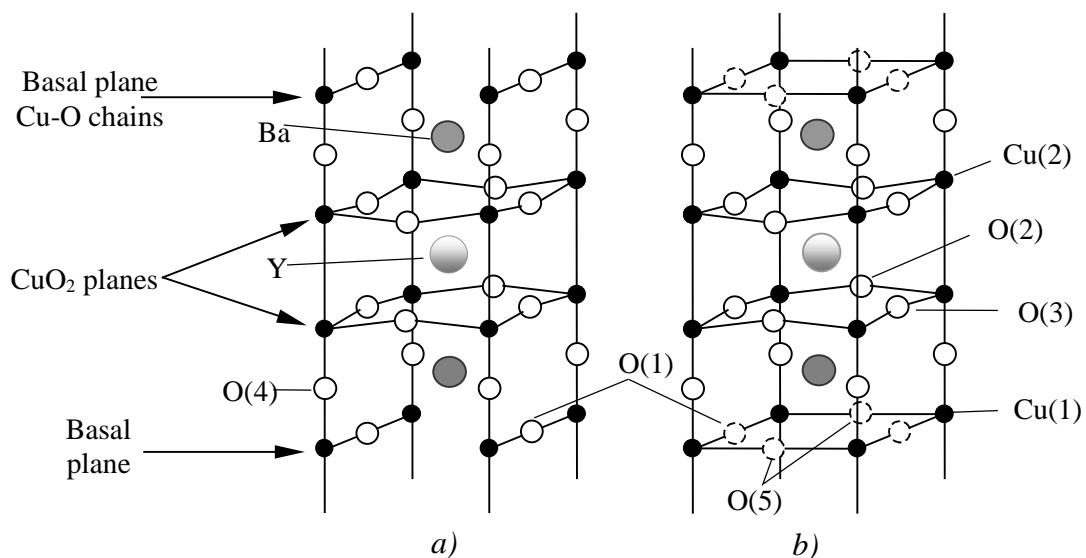


Fig. 1.3 a) Structure and model unit of layered $YBa_2Cu_3O_7$, and, b) $YBa_2Cu_3O_{7-\delta}$. When the oxygen content is < 7 , O(1) and O(5) sites are partially filled

The stoichiometry of $\text{YBa}_2\text{Cu}_3\text{O}_{7-\delta}$ varies with temperature and partial oxygen pressure, the value of δ ranging from 0 to 0.85 (see Fig. 1.5). As oxygen is added to or removed from the structure the oxygen ions rearrange themselves in the Cu-O basal plane with a predominant tendency to form Cu-O chains (Poulsen *et al.* (1991) and Jorgensen *et al.* (1990)). This change in oxygen content modifies the crystal structure of YBCO and its superconducting properties. The decrease in oxygen has a marked effect on the critical temperature, T_c (Fig. 1.4). Table 1.1 shows that there is some disagreement in the published values linking the critical temperature of YBCO to its characteristic oxygen content. Some authors observe a peak in the critical temperature for oxygen contents of 6.97, while others have measured a constant value of T_c in this region. It appears that the measurement of properties related to the oxygen stoichiometry in YBCO is always associated to a certain amount of uncertainty in the values calculated. This is probably due to the errors associated to the measurement of the oxygen content of the material.

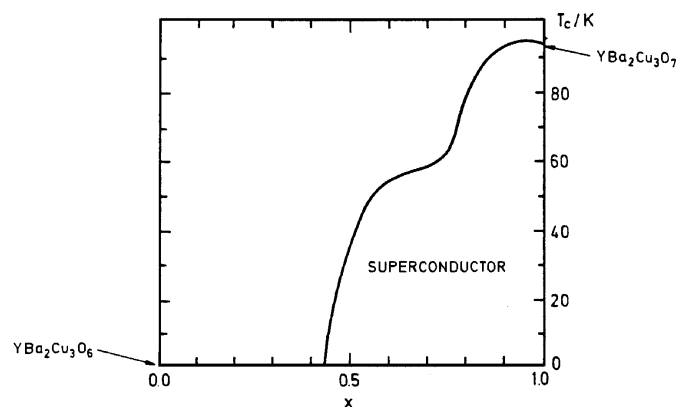


Fig. 1.4 Schematic variation of critical temperature with oxygen content (from Cyrot and Pavuna (1992))

Oxygen content	T_c (K) (1)	T_c (K) (2)	T_c (K) (3)
6.99	94	93	94
6.98	93	94	93
6.97	92	93	92
6.96	90	93	90
6.91	84.3	91	90
6.87	63	86.5	89
6.7	60	66.5	82.9
6.62	57.1	61	68.6
6.54	50	58	60
6.45	47.1	54.2	57.6
6.4	31	47.9	57.5

Table 1.1 Variation of critical temperature with oxygen content from different authors: (1) Jacobson *et al.* (1987), (2) Poulsen *et al.* (1989), (3) Cava *et al.* (1987)

1.3.1 Orthorhombic to Tetragonal Transition

The stoichiometry of YBCO is the most important factor to consider in order to optimise its superconducting properties, and a great deal of work has been dedicated to the study of the variation in oxygen content of this material. It has been found that the equilibrium stoichiometry depends both on temperature and partial oxygen pressure (Gallagher (1987), Kishio *et al.* (1987), etc.). Fig. 1.5 shows data by Gallagher that represents the variation in oxygen content in YBCO with respect to temperature as well as partial oxygen pressure.

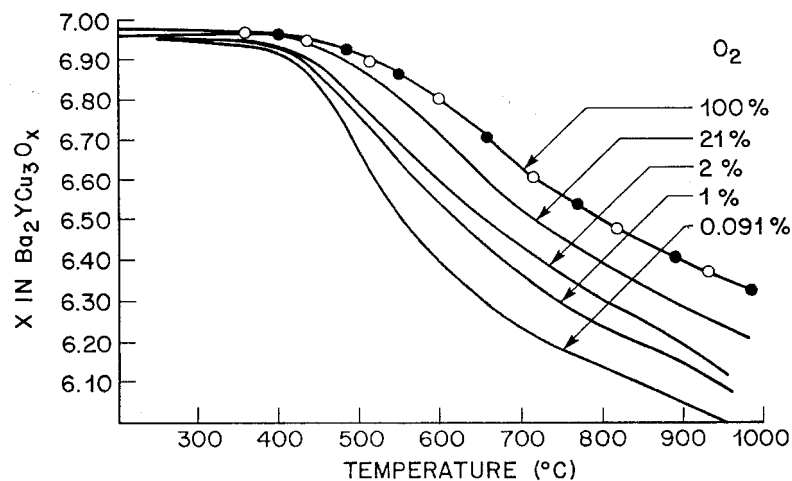


Fig. 1.5 Variation in oxygen content with temperature and oxygen pressure (from Gallagher (1987))

If we take a sample of YBCO at equilibrium ($\delta = 0$), the oxygen ions in the Cu-O basal plane are ordered on the O(1) sites only (the O(5) sites remain empty), forming one-dimensional linear Cu-O chains along the b axis. The crystal structure has orthorhombic ($Pmmm$) symmetry ($a \neq b$). If the temperature of the sample is increased, oxygen is lost from the structure (see Fig. 1.5). This decrease in oxygen content results in a disorder of the ordered orthorhombic structure; oxygen ions move into the adjacent and vacant O(5) sites until the loss of oxygen is so great that the oxygen-oxygen interactions are not strong enough to maintain the orthorhombic structure and the material undergoes a structural transformation to a tetragonal symmetry ($P4/mmm$) (see Fig. 1.6).

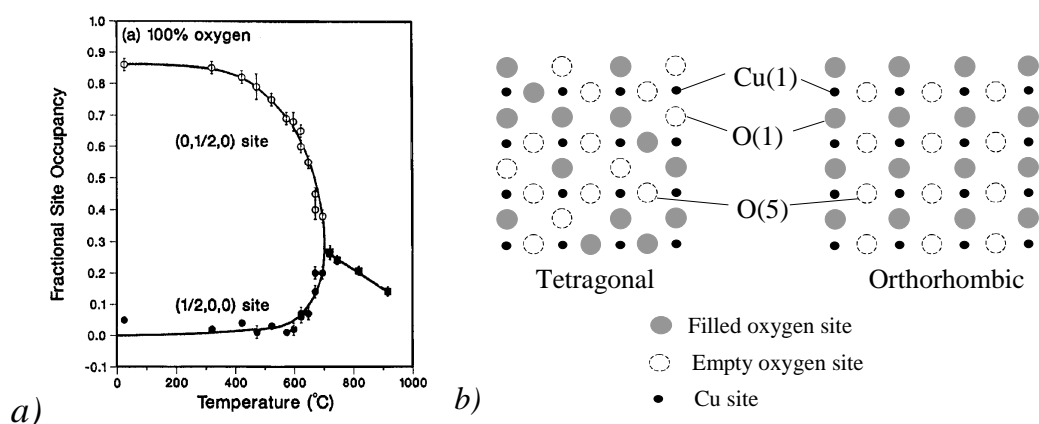


Fig. 1.6 a) Occupancy of oxygen ions in lattice sites (from Jorgensen *et al.* (1987-a)), and b) orthorhombic and tetragonal basal planes

Neutron diffraction studies carried out by Jorgensen *et al.* (1987-a) show the change in the occupancy of the O(1) ($1/2, 0, 0$) and O(5) ($0, 1/2, 0$) sites in the crystal structure as it loses or gains oxygen (see Fig. 1.6 a)). Strauven *et al.* (1988) measured changes in oxygen occupancy from 0.85 to 0.25 for ($1/2, 0, 0$) and from 0 to 0.25 for ($0, 1/2, 0$) as fully oxygenated samples were heated in air from room temperature to 720 °C, agreeing with the results presented by Jorgensen and co-workers. The difference in oxygen content, 0.35, evolves from the material into the surrounding atmosphere. This transition from orthorhombic to tetragonal crystal structure has been found to be a second order order-disorder transformation (Freitas and Plaskett (1987)) and it depends on partial oxygen pressure as well as on the kinetics of oxygen diffusion in the material (Shi (1989)).

The results of data published by the different authors on this subject are fairly consistent. The transition has been found to occur at temperatures ranging from 676 to 700 °C in pure oxygen (Specht *et al.* (1988), Jorgensen *et al.* (1987-b)) to approximately ≤ 520 °C at 0.09 atm O_2 (O'Bryan and Gallagher (1987)).

The value of the oxygen content at which the orthorhombic to tetragonal transition occurs has not been observed to depend on partial oxygen pressure, and the values reported for the oxygen content at the transition vary from 6.5 (Freitas and Plaskett (1987)) to 6.68 (Kishio *et al.* (1988)) (see Fig. 1.7 b)). The scatter in the data is very likely to be the result of differences in sample preparation or poorly controlled experimental conditions. This transition is a direct consequence of the oxygen content and its ordering in the crystal structure.

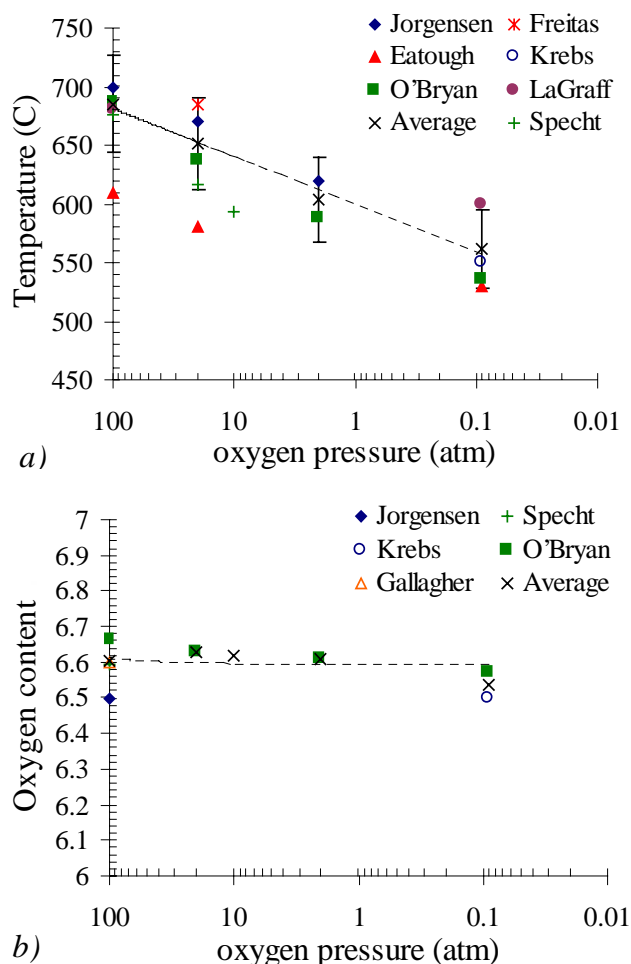


Fig. 1.7 a) O-T transition temperature values, and b) O-T oxygen contents at different oxygen pressures collected from literature

The O-T transition has been found to be irreversible in inert atmospheres, this is a direct consequence of its relation to oxygen content. On heating, the orthorhombic material loses oxygen to the surrounding atmosphere. If this atmosphere is an inert gas, such as N_2 or He, oxygen cannot be absorbed back from it when the temperature decreases, so the sample remains tetragonal and no O-T transformation is observed.

The authors mentioned so far have also measured the variation in the values of the lattice parameters with oxygen content and partial oxygen pressure. a and b have been observed to become shorter with decreasing oxygen content until they become equivalent (tetragonal crystal structure); c , on the other hand, is observed to increase slowly with decreasing oxygen content (Jorgensen *et al.* (1987-b), Schuller *et al.* (1987), LaGraff *et al.* (1990)).

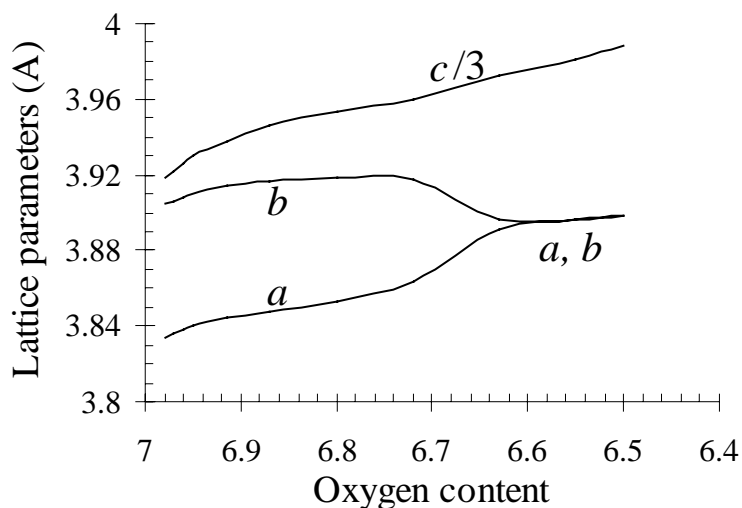


Fig 1.8 Change in lattice parameters of YBCO with oxygen content (average of data collected from literature)

For an oxygen content of 6.91, the crystal lattice of YBCO is orthorhombic with lattice parameters: $a = 0.382$ nm, $b = 0.388$ nm and $c = 1.168$ nm, and the values for the tetragonal structure (for an oxygen content equal to 6.62) are: $a = b = 0.387$ nm and $c = 1.172$ nm (Datta (1992)).

1.3.2 Ortho I and Ortho II phases

It has been mentioned in section 1.2.1 that the critical superconducting temperature, T_c , varies with oxygen content. The generally accepted view is that superconductivity

is intimately related to the CuO_2 planes, and the variation of T_c is the result of a charge redistribution in the structure that increases the hole content in these planes. This is directly related to the oxygen content of the material.

Cava *et al.* (1990) observed a non-linear decrease in the electronic charge with decreasing oxygen content in the copper of the CuO_2 plane; this corresponds exactly to the variation of T_c with oxygen content. LaGraff *et al.* (1990) observed in their resistance measurements of YBCO that as the oxygen content decreased so did the carrier concentration (electron holes). This agrees with theoretical work by Zaanen *et al.* (1988). However, Veal *et al.* (1990) observed that after annealing an orthorhombic sample at low temperature (≈ 150 °C) the T_c increased; they point out that this is due to a rearrangement of the oxygen ions in the basal plane. Veal and co-workers suggest that when the Cu-O chains are ordered, there is an increase in the in-plane carrier concentration that alters the T_c . The preference of the oxygen ions to align themselves into chains maximises the number of 2-coordinated monovalent coppers. Each Cu acquires an electron from the CuO_2 planes, maximising the hole concentration and increasing the critical transition temperature. In this process oxygen ions that are in normally vacant chain sites (O(5)) move to normally chain occupied sites (O(1)). High resolution electron microscopy and electron diffraction studies (Beyers *et al.* (1989)) support the observations made by Veal and co-workers; these show the tendency for oxygen to order in 2-dimensional chain structures with all the O(1) sites in a chain along the b axis being either full or empty and with no oxygens on the O(5) sites on the a axis.

The variation of the critical temperature due to a rearrangement of the oxygen ions in the structure but not as a consequence of a change in stoichiometry stresses the importance of the study of the different crystallographic structures present in YBCO. X-ray diffraction, neutron diffraction, high resolution electron microscopy and theoretical studies have been carried out for this purpose. The most important orthorhombic structures in YBCO are known as Ortho I and Ortho II (OI and OII), and they have been found to correspond to the two plateaux present in the variation of T_c with composition at 93 K and 58 K (see Fig. 1.9 a).

The OI (93 K) phase is characteristic of a fully oxygenated material and it consists of a sequence of full Cu-O chains (parallel to the b axis). As the oxygen in the structure decreases many kinds of short range ordered full-empty chain arrays are observed until at the 58 K plateau, the OII phase dominates. This structure has alternating full and empty Cu-O chains (see Fig. 1.9 b)). Poulsen *et al.* (1991) suggests that the 58 K plateau is a consequence of the dynamic coexistence of domains (or clusters) of the OI and OII phases.

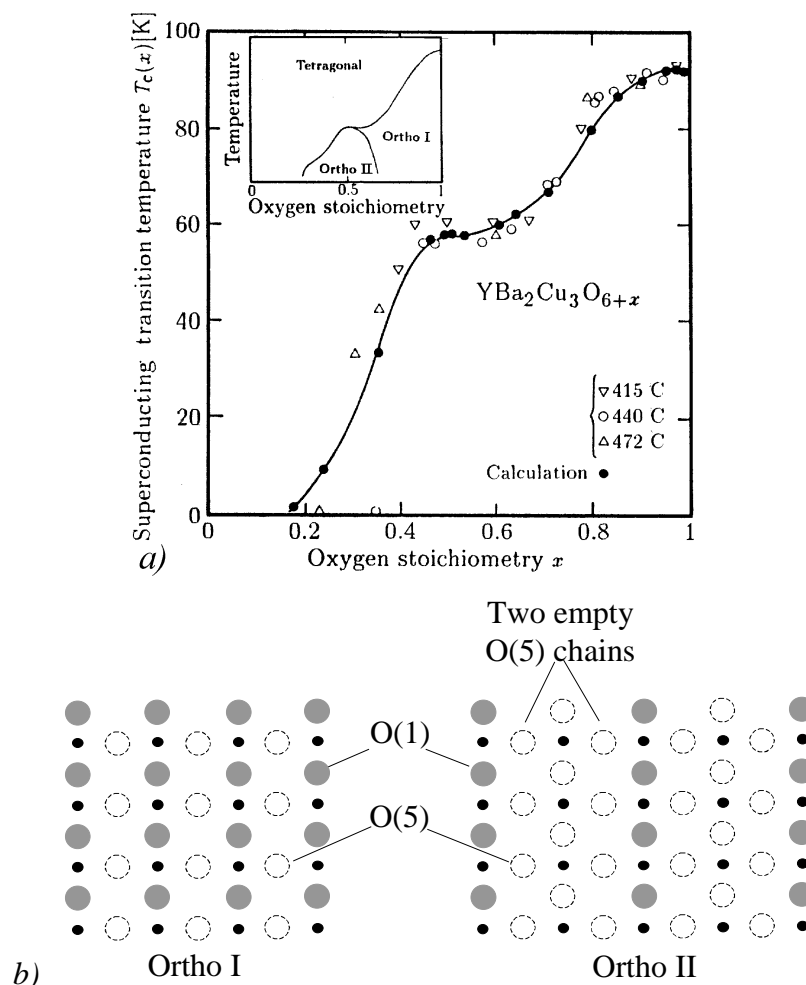


Fig 1.9 a) Variation of T_c with oxygen content (Poulsen *et al.* (1991)), and b) Ortho I and Ortho II structures

The formation of the orthorhombic structure due to the incorporation of oxygen to the tetragonal lattice results in an increase in the length of the b lattice parameter; this gives rise to a crystal lattice distortion generating stresses in the crystal structure (see Figs. 1.10 a) and b)) that are relieved by the formation of twins along the 110 planes. In the ideal compound $YBa_2Cu_3O_6$, the basal plane is free from oxygen ions and the

structure is tetragonal, with a lattice parameter equal to 3.82 \AA ($a = b$). However, as oxygen is incorporated to the lattice, it occupies either the O(1) or O(5) sites (see chapters 1 and 3), increasing the length of the a and b parameters to 3.88 \AA . This difference in length is accommodated by the material with the formation of twins, as shown in Fig. 1.10.

Twins can be observed by simple optical microscopy (see Fig. 1.11). This optical examination was used by Beyers *et al.* (1989) to follow the O-T transition in YBCO. They found that at oxygen contents as low as 6.28 it was possible to see the formation of microdomains with a tweed microstructure, and that macroscopic twins were clearly present for oxygen contents between 6.5 and 6.65. The presence of these twins makes of optical examination a quick way of checking whether the material has been oxygenated.

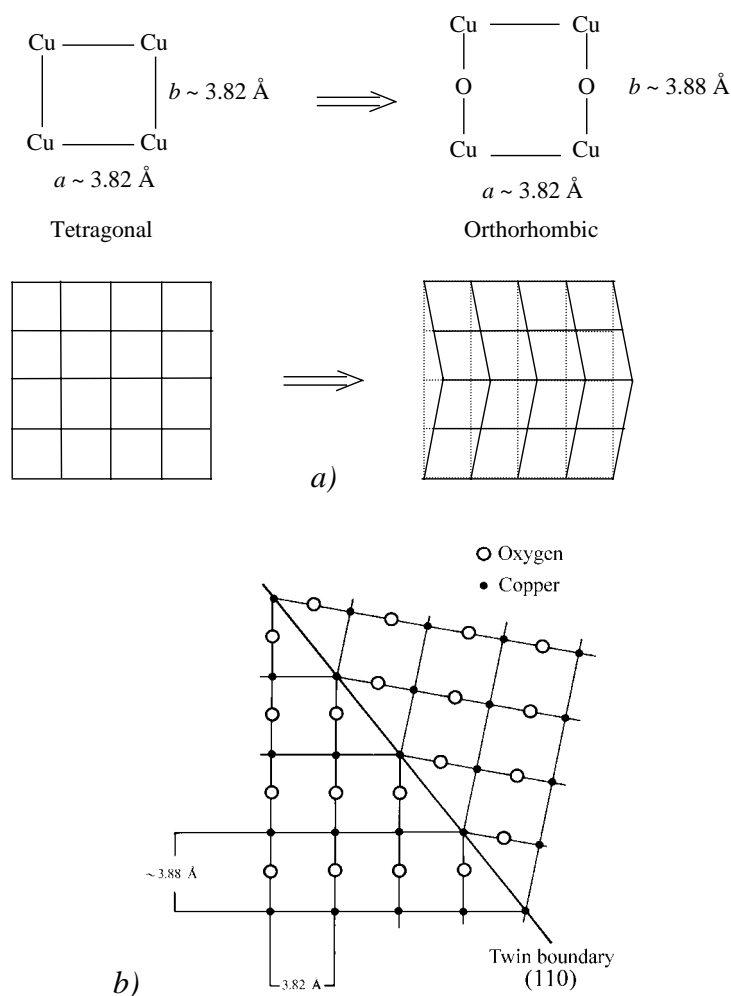


Fig. 1.10 a) Lattice parameters of deoxygenated and oxygenated basal plane showing schematic of lattice deformation, and b) diagram showing how the lattice parameter difference is accommodated in a twin boundary in $YBa_2Cu_3O_7$

Fig. 1.11 Twinned orthorhombic grains 0.15 mm

This section has reviewed the changes in the crystal structure of YBCO that result from the variation of its oxygen stoichiometry. This compound has been observed to undergo a second order order-disorder transition from an orthorhombic structure (high oxygen content) to a tetragonal structure (low oxygen content) at an oxygen content of approximately 6.5. The transition temperature is observed to depend on partial oxygen pressure. Within the range of oxygen contents at which YBCO is superconducting, a number of orthorhombic structures have been identified (OI and OII among others – see chapter 3) either by experimental methods or theoretical calculations. The results present in the literature related to this orthorhombic to tetragonal transition and the arrangement of oxygen ions in the crystal structure are fairly consistent.

1.4 Superconductivity

Soon after the discovery of superconductivity in mercury it was found that temperature was not the only limiting factor for the transition from normal to superconducting state. Onnes discovered that electrical currents could flow through the superconductor without resistance as long as the current per unit cross-sectional area did not exceed a certain value known as critical current, I_c . He also observed that if the superconductor was placed in a magnetic field, the magnitude of this field had a critical value, B_c , above which the superconductor would also revert to its normal state.

1.4.1 Meissner effect

Meissner and Ochsenfeld (1933) observed that when a metal becomes a superconductor when it is cooled in the presence of a magnetic field, it expels the magnetic flux from its interior. This phenomenon is known as the Meissner effect. It occurs because when the material is in its superconducting state, the presence of a magnetic field sets up screening electrical currents on the surface of the superconductor producing a magnetic field equal in strength but opposite in direction to the externally applied one. These screening currents make the magnetic field inside the sample exactly zero. The expulsion of the magnetic field occurs independently of the sequence used in cooling or applying the magnetic field, which means that the superconducting state is a true thermodynamic state.

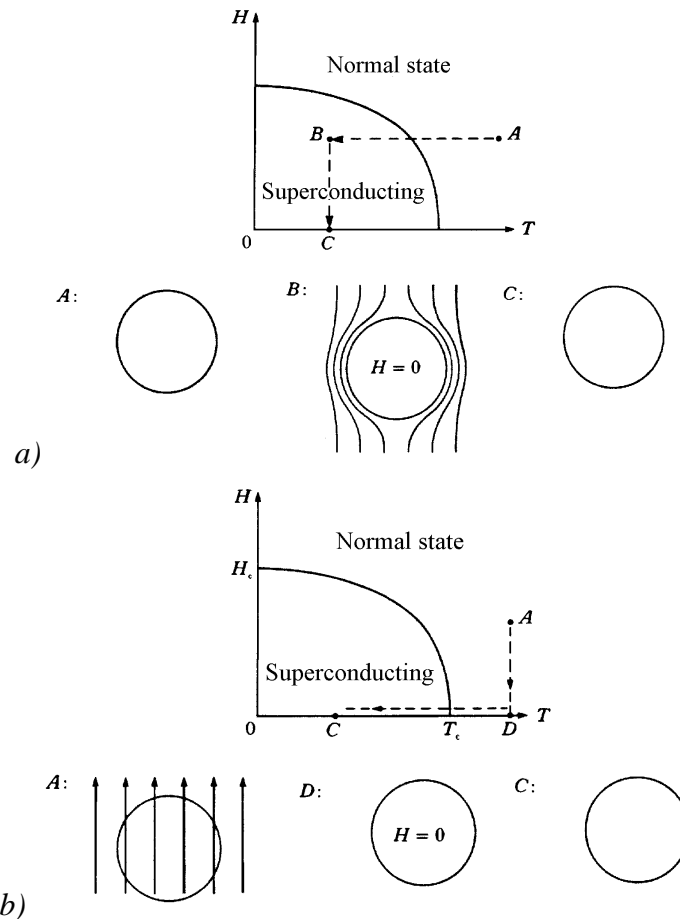


Fig. 1.12 Schematic of Meissner effect showing that the magnetic field inside the superconductor will be equal to 0 independently of the path followed to reach the superconducting state (from: Rose-Innes (1988))

1.4.2 Penetration depth

From the discovery of the Meissner effect, F. and H. London (1950) studied the relationship between the magnetic field and electrical currents in superconductors, and predicted that the applied magnetic field did penetrate in a small region near the surface in spite of the opposing screening currents. They suggested that the applied field would penetrate in the superconductor over a characteristic length (λ). This length is known as the penetration depth; the magnetic field decreases as $\exp(-x/\lambda)$ where x is the distance from the sample surface.

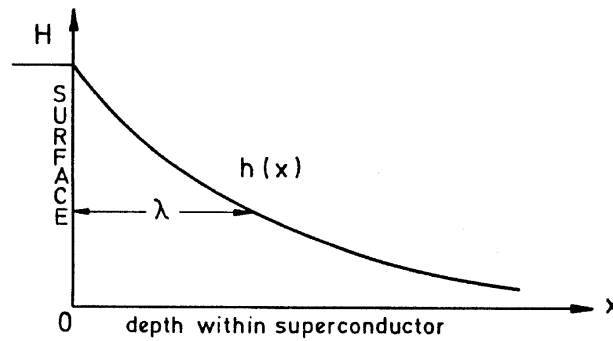


Fig. 1.13 Schematic decay of the magnetic field in a superconductor (from: Cyrot and Pavuna (1992))

1.4.3 Type I and Type II superconductors

The type of superconductor described in the previous sections is known as Type I; when the magnetic field exceeds a critical value, B_c , it penetrates inside the sample eliminating its superconducting properties. The ability of these materials to exclude magnetic fields makes them the perfect materials to use in ultrasensitive magnetic instruments. However, the current densities carried by these materials are very low, which makes them useless for many large scale applications (e.g. wires for electromagnets). Most metallic elements are Type I superconductors.

In 1957 Abrikosov showed that certain superconductors exhibited a different behaviour in the presence of a magnetic field. These materials allow the magnetic field to penetrate in groups of quantised magnetic flux lines called vortices, each vortex containing a single quantum of magnetic flux $\Phi_0 = h/2e = 2 \times 10^{-15}$ Wb. The vortices arrange themselves into a regular lattice (the lowest possible energy state) and the material is said to be in the mixed state. These are called Type II superconductors

and they enter the normal state when the magnetic field applied is so large that no more vortices can be packed into the sample. Transition elements like Nb and V are Type II superconductors, as well as alloys and copper oxides.

Type II superconductors can carry much larger currents than Type I, which increases enormously their field of application (e.g. large permanent magnets, wires and tapes).

1.5 Conclusions

This chapter has reviewed the history of superconducting materials and it has given an insight into the complex structure of $YBa_2Cu_3O_{7-\delta}$, one of the first high temperature superconductors discovered. The change in the stoichiometry of YBCO modifies its crystal structure and its electrical properties, as the material changes from being a semiconductor at low oxygen contents to becoming a superconductor at high oxygen contents.

The superconducting properties of YBCO are beyond the scope of this work and therefore have been reviewed briefly. The following chapters are going to deal in more detail with the study of diffusion and the optimisation of the oxygen stoichiometry in this superconducting material.

Chapter 2

Theory of diffusion

2.1 Introduction

There are a large number of processes that involve the transport of a physical quantity via a generalised flux from one part of the system to another under the action of a force which often takes the form of a gradient of another physical quantity. These are known as transport phenomena.

The following table summarises a number of these phenfomena:

<i>Phenomenon</i>	<i>Gradient</i>	<i>Flux</i>	<i>Law</i>
Heat transfer κ = thermal conductivity	Temperature, T	Energy, $(1/2)mv^2$	Fourier, $j_z = -\kappa (\partial T/\partial z)$
Chemical diffusion D = diffusion coefficient	Concentration, C	Mass, m	Fick, $j_z = -D (\partial C/\partial z)$
Viscosity η = viscosity coefficient	Velocity, v	Momentum, mv	Newton, $j_z = -\eta (\partial v/\partial z)$
Electrical current σ = electrical conductivity	Potential difference, V	Current, I	Ohm, $j_z = -\sigma (\partial V/\partial z)$

Table 2.1 Transport phenomena

Of all these processes, this study is going to concentrate on diffusion. This phenomenon is very important because it is fundamental to many physical processes, such as phase transformations, solid state reactions, sintering, etc.. Diffusion controls for instance the achievement of a uniform concentration within a single phase where there is an initial concentration gradient¹ or a chemical potential gradient (see

¹ There are exceptions to this situation. In the case of diffusion of interstitial C in Fe, for example, diffusion occurs in the direction of increasing C concentration (spinodal decomposition). This is known as "up-hill" diffusion and it increases the concentration gradient.

equations (2.17)-(2.20)). This results in a reduction of the total free energy of the system.

The diffusion process can be analysed by looking at the atomic mechanism through which it takes place or by considering a macroscopic diffusion coefficient that makes no reference to the atomic nature of matter and therefore does not specify the atomic processes taking place. The following sections are going to consider these two aspects, starting with the overall study of diffusion and following with the atomic mechanisms. The various diffusion coefficients that can be measured and the relationship between them will also be discussed. The chapter will finish with the derivation of a number of solutions to the diffusion equation that will be used in the study of the oxygen diffusion process in YBCO (chapter 5).

2.2 Definitions and fundamental relationships

The starting point for the study of the diffusion process is its definition by means of a flux equation. Let us consider a volume of unit cross sectional area; the rate of transfer of a diffusing substance through this section of unit area is proportional to the concentration gradient measured normal to the section, i.e.

$$j = -D \left(\frac{\partial C}{\partial x} \right), \quad (2.1)$$

where j is the rate of mass transfer per cross-sectional area, C the concentration of diffusing species, x the distance travelled by the species in the direction perpendicular to the cross-sectional area considered and D is the diffusion coefficient. This equation is known as *Fick's first law*. The negative sign indicates that diffusion occurs in the direction opposite to that of increasing concentration. This equation describes the effect of a concentration or chemical potential gradient of one type of particle present in the absence of an electric field and it is only valid for an isotropic system with a

In the case of fast ionic conductors, diffusion can also occur in the absence of a concentration gradient. There is a direct link between the chemical diffusion and the ionic conductivity of the diffusing substance (Nernst-Einstein equation), and it is going to be seen in chapter 6 how the presence of an electric field can modify the concentration profile within a sample of a fast ionic conducting material such as $\text{YBa}_2\text{Cu}_3\text{O}_{7.8}$.

concentration gradient in the x direction. If the flux equation described the flow in all three crystallographic directions, it would be expressed:

$$j = -\left(D_x \frac{\partial C}{\partial x} + D_y \frac{\partial C}{\partial y} + D_z \frac{\partial C}{\partial z}\right). \quad (2.2)$$

However, to simplify the study and analysis of the diffusion process, from now on the system in which diffusion occurs is going to be considered isotropic ($D_x = D_y = D_z$) unless stated otherwise. In the case of diffusion in the YBCO system considered in this thesis, tracer diffusion measurements (Rothman *et al.* (1991)) have shown that diffusion in the ab plane is approximately 10^6 times faster than along the c direction. This large difference in the diffusion values justifies the assumption that oxygen diffusion in YBCO occurs in a two-dimensional system (see chapters 3 and 5). For this introductory analysis of the diffusion process, diffusion is going to be considered to occur only along the x axis.

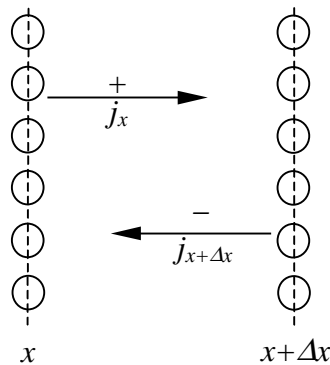


Fig. 2.1 Schematic of diffusion process in one dimension (along the x -axis)

Fick's first law can be derived as follows: let us take two adjacent planes where diffusion is occurring by nearest neighbour jumps of one type of atoms between those planes (Fig. 2.1). In this case the diffusion coefficient is taken to be independent of concentration. The number of atoms per unit area of the plane at x is N_x and that of the plane at $x + \Delta x$ is $N_{x+\Delta x}$.

We must introduce a new quantity: the mean jump frequency of the diffusing atoms, Γ ; this is the average number of times an atom changes lattice sites per second.

The flux of atoms moving from x to $x + \Delta x$ and from $x + \Delta x$ to x is:

$$j_x = \frac{1}{2}\Gamma N_x, \text{ and } j_{x+\Delta x} = \frac{1}{2}\Gamma N_{x+\Delta x}, \text{ respectively.} \quad (2.3)$$

The net flux between both planes is therefore given by:

$$j = j_{x+\Delta x} - j_x = \frac{1}{2}\Gamma(N_{x+\Delta x} - N_x). \quad (2.4)$$

This can also be expressed in terms of number of atoms per unit volume:

$$j = \frac{1}{2}\Gamma(\Delta x) \frac{(N_{x+\Delta x} - N_x)}{\Delta x}. \quad (2.5)$$

Since $N_x/(\Delta x)$ is equal to C , the concentration, substituting and taking limits we have:

$$j = -\frac{1}{2}\Gamma(\Delta x)^2 \frac{\partial C}{\partial x}, \text{ or } j = -D \frac{\partial C}{\partial x}. \quad (2.6)$$

Δx is equal to the lattice spacing, d , (the distance of separation between nearest neighbours). It can be seen that in this case describing linear diffusion the value of the diffusion coefficient can be expressed by: $D = 1/2\Gamma(\Delta x)^2$. In cubic lattices diffusion is isotropic and therefore equally likely to occur in any of the orthogonal directions, so the above expression would change to:

$$j = -\frac{1}{6}\left(\Gamma_x d^2 \frac{\partial C}{\partial x}\right), \quad (2.7)$$

which is equivalent to:

$$j = -D \frac{\partial C}{\partial x}, \quad \text{with } D = \frac{1}{6}\Gamma_x d^2. \quad (2.8)$$

For f.c.c. systems, $D = \frac{1}{12}\Gamma d^2$ and for b.c.c. systems: $D = \frac{1}{24}\Gamma d^2$.

The dimensions of the terms of equations (2.1) to (2.7) are the following:

$$\begin{aligned} x &= [\text{L}], & D &= [\text{L}^2\text{T}^{-1}], \\ d &= [\text{L}], & \Gamma &= [\text{T}^{-1}]. \end{aligned}$$

The concentration can be expressed in several ways, since the units of the flux must be consistent, they depend on those given to the concentration. For example, if the concentration is given in g/cm^3 ($[\text{ML}^{-3}]$), the flux will be given in: $\text{g/cm}^2\text{s}$ ($[\text{ML}^{-2}\text{T}^{-1}]$).

However, if the concentration is given in moles/cm³, the units of the flux will be moles/cm²s, this is: $C = [L^{-3}]$ and $j = [L^{-2}T^{-1}]$. D is usually expressed in cm²/s.

Fick's first law only applies if the system considered is in *steady state*, this is, the concentration at every point is invariant: $\frac{\partial C}{\partial t} = 0$.

To deal with *non-steady state* flow in which C changes with time, let us consider an element of volume of unit cross sectional area with a thickness equal to Δx . If this distance is very small, the flux at x can be expressed as:

$$j = j_{x+\Delta x} - \Delta x \frac{\partial j}{\partial x}. \quad (2.9)$$

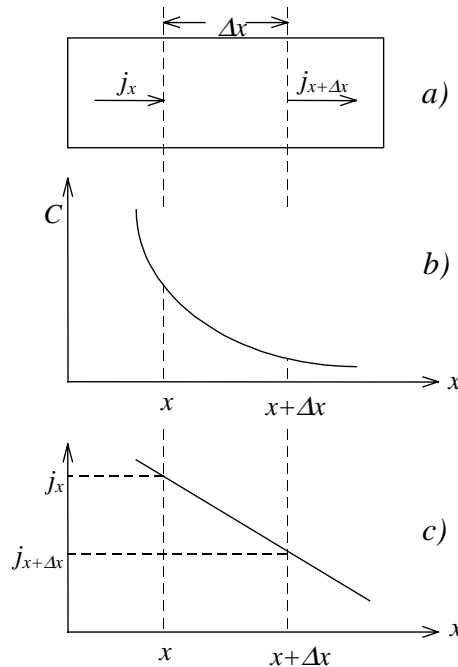


Fig. 2.2 a) Element of volume, b) assumed concentration profile $C(x)$, and c) flux of material, $j(x)$ in this element of volume

The amount of material that enters the element per unit time, j_x , is different from that which leaves it, $j_{x+\Delta x}$, therefore the concentration in the element changes so that the net increase in matter in the element can be expressed by:

$$j_x - j_{x+\Delta x} = -\Delta x \frac{\partial j}{\partial x} = \Delta x \frac{\partial C}{\partial t}. \quad (2.10)$$

Fick's first law is valid at any point in time, so Eq. (2.1) can be substituted into (2.10) giving:

$$\frac{\partial C}{\partial t} = \frac{\partial}{\partial x} \left(D \frac{\partial C}{\partial x} \right) = \frac{\partial^2 j}{\partial x^2}. \quad (2.11)$$

This is known as *Fick's second law* of diffusion. In three directions it becomes:

$$\frac{\partial C}{\partial t} = \frac{\partial}{\partial x} \left(D_x \frac{\partial C}{\partial x} \right) + \frac{\partial}{\partial y} \left(D_y \frac{\partial C}{\partial y} \right) + \frac{\partial}{\partial z} \left(D_z \frac{\partial C}{\partial z} \right) = \nabla j. \quad (2.12)$$

2.3 Mechanisms of diffusion

The diffusion process must also be examined in the context of the mechanism by which it takes place. This mechanism can involve interstitial atoms, vacancies or a complex combination of these. The mobility of these particles can also be affected by the imperfections of the lattice such as dislocations, grain boundaries, point defects, etc.

The atoms that form the lattice oscillate around their equilibrium positions and sometimes this oscillation is so big that they change sites contributing to the diffusion process. This can occur in several ways that are going to be reviewed in the following sections:

2.3.1 Interstitial mechanism

This is one of the simplest mechanisms (see Fig. 2.3 a)). Atoms that have dissolved in a host lattice into interstitial positions move through the interstices of the lattice without displacing permanently any of the matrix atoms.

This type of diffusion is controlled by the energy needed to distort the host lattice enough so that the change from one site to another is possible. This mechanism is common in alloys where the solute normally dissolves interstitially, such as C in α - or γ -iron, or in matrices damaged with radiation, where atoms that are normally in the lattice have shifted to interstitial positions.

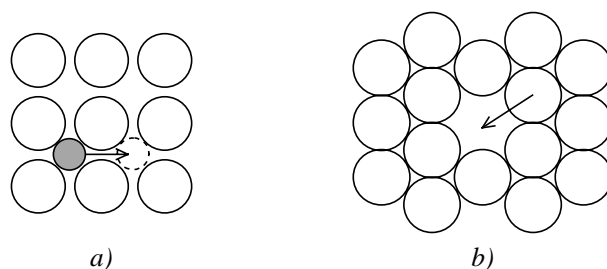


Fig. 2.3 Schematic diagrams of: a) interstitial diffusion, and b) vacancy diffusion

2.3.2 Vacancy mechanism

This is the most general and important of all mechanisms (see Fig. 2.3 b)). Diffusion occurs via an exchange of position of one atom with an adjacent vacancy. Therefore, a flux of diffusing atoms in any direction requires a vacancy flux of equal magnitude in the opposite direction. This type of diffusion is controlled by the energy needed to form a vacancy plus the energy required to move it within the lattice. This mechanism predominates in close packed metals and substitutional solutes in alloys. It is also found in ionic compounds and oxides.

This mechanism was confirmed by the experiments carried out by Kirkendall. The setup used for these experiments consisted of an α -brass/copper couple with the interface between both alloys marked by Mo wires (Fig. 2.4).

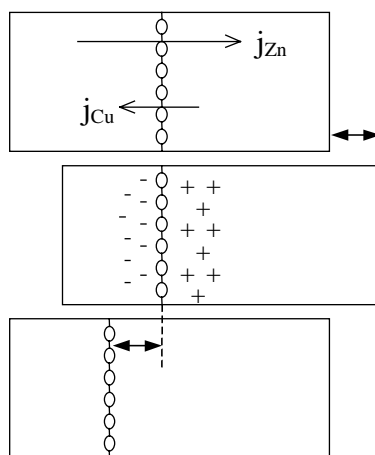


Fig. 2.4 Kirkendall effect

It was observed that after annealing the sample the markers had shifted to the side closer to the α -brass end showing that the zinc atoms diffuse out of the alloy faster

than the copper atoms diffuse in. This can be explained in terms of vacancies: they seem to exchange places more readily with the zinc atoms and as a result of the loss of Zn pores are created in the brass side while on the Cu side of the couple the material increases volume due to the diffusion of Zn into the structure.

2.3.3 Interstitialcy and Crowdion mechanisms

These mechanisms occur in situations where the interstitial atom is so large that if interstitial diffusion were to occur it would produce a very large distortion of the lattice. The activation energy required for interstitial diffusion to occur in this case would be too big, so either of these two mechanisms become active. The interstitialcy mechanism (Fig. 2.5 a)) is a combination of an interstitial and a substitutional process. An interstitial atom moves onto a regular lattice site by pushing the atoms on that site into an interstitial position and therefore interstitialcy diffusion occurs instead.

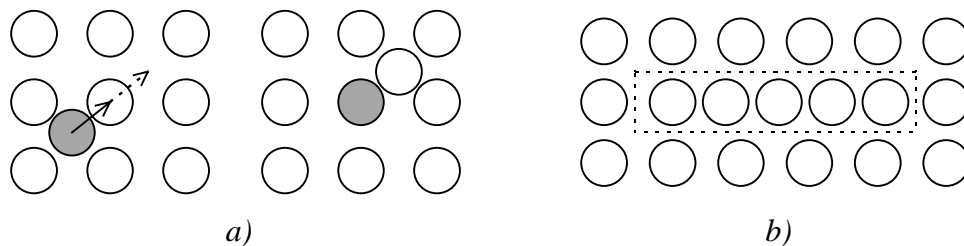


Fig. 2.5 Schematic illustration of: a) interstitialcy mechanism and b) Crowdion mechanism

Atoms may adopt a Crowdion configuration to accommodate for the extra atom introduced in the lattice (usually as the result of radiation damage). In this case $n+1$ atoms occupy n lattice sites. This configuration looks like an edge dislocation because the distortion is spread out along a line (Fig. 2.5 b)). The energy to move this array of atoms is also smaller than if an interstitial mechanism took place.

2.4 Types of diffusion coefficient

Diffusion processes can be studied with various techniques and some of these measure different types of diffusion coefficients. This section reviews the different coefficients and the relation between them.

2.4.1 Self diffusion

The self diffusion coefficient, D_{si} , of the species i in a material is the diffusivity due to thermal excitation in a homogeneous solid in the absence of a chemical potential gradient. The motion of the ions can be modelled by a random walk analysis (Le Claire *et al.* (1975)) to give (in an isotropic cubic lattice – see section 2.2):

$$D_{si} = \frac{1}{6} \Gamma_i r_i^2 \quad (2.13)$$

where r_i is the jump distance and Γ_i is the mean jump frequency of each particle. Γ_i depends on the fraction of ions that have sufficient thermal energy to overcome the activation barrier for hopping and the number of vacant sites available for atoms to hop into.

This coefficient can be estimated using a technique known as *internal friction*. It involves applying stress to a sample that will induce a rearrangement of the mobile atoms or ions to accommodate the stress. The stress is then released and the solid returns to its original atomic configuration. In both cases the diffusion of atoms is thermally activated. The value of the diffusion coefficient of the mobile species can be calculated measuring the relaxation time necessary for the diffusing species to return to the equilibrium configuration.

2.4.2 Tracer diffusion

This occurs when a radioactive tracer diffuses in a chemically homogeneous solid. In a completely homogeneous material the mean square displacement of the tracer atoms is experimentally determined from the spatial distribution of the tracer particles (tracer concentration profile). This can be carried out by taking sections of the material perpendicularly to the principal diffusion axis and measuring the radioactivity of each section.

There are cases in which radioactive isotopes are not available, such as when oxygen diffusion is being studied. A stable isotope of the diffusing species is then chosen as a tracer. The penetration of this tracer as a function of distance is observed after the diffusion experiment using Secondary Ion Mass Spectrometry (SIMS). This technique

is very powerful because it can analyse very small samples and it can be used to determine the possible anisotropy of the tracer diffusion coefficient, D^* , as a function of crystallographic direction.

It should be noted that when the radioactive tracer chosen is of the same element as the matrix material (e.g. ^{57}Fe in Fe or ^{22}Na in Na), the process is also known as *self diffusion*, although it is not the same as the one discussed in the previous section, as it is discussed below:

2.4.3 Correlation factors

The self diffusion coefficient, D_s , is a measure of the mobility of diffusing particles in a matrix. But this diffusion of particles can occur via different mechanisms that may not be equivalent.

If the jumps of i in the lattice are random, the path followed by all i particles can be described as a “random walk”. According to the random walk theory, the diffusion coefficient in an isotropic material is proportional to the mean square displacement of the diffusing particles in time t (see section 2.2):

$$D_s \propto \frac{\langle x^2 \rangle}{6} \quad (2.14)$$

where $\langle x \rangle$ is the mean distance between jumps. This is known as the Einstein diffusion equation.

Let us compare two cases: self diffusion of A in A (as described in section 2.4.1) and the diffusion of a radioactive tracer, A^* in A. The diffusion mechanism is via vacancies in both cases.

If we consider the first situation, A particles will diffuse in the matrix of A with all the diffusing jumps being equivalent to each other and the random walk approach can be applied. This does not occur in the second case, where once particle A^* has taken the place of the next nearest vacancy the probability of the particle exchanging sites with the same vacancy and cancelling the diffusional step is greater than the probability that A^* will move in any other direction with the help of another vacancy coming along. This means that diffusion of A^* in the A lattice is not a random walk. However,

diffusion of vacancies in the A lattice is a random walk, so A* will keep on jumping back and forth, exchanging positions with the original vacancy until another vacancy becomes its next nearest neighbour.

In this case the jumps of the tracer atoms are said to be correlated and the comparison between self diffusion and tracer diffusion is expressed by:

$$D_s = fD^* \quad (2.15)$$

where D^* denotes the tracer diffusion coefficient. The correlation factor, f , accounts for the non-random motion of tracers and it is a measure of the efficiency of atomic jumping for long distance migration.

The value of the correlation factor is always going to be less than 1 because the diffusion process is always less efficient than in a perfectly random situation. f is a function of the displacement between jumps and the angle between them. Therefore, its value changes depending on the type of crystal structure and on the diffusion mechanism. Table 2.2 summarises the value of the correlation factor for vacancy diffusion for different lattice structures.

<i>Crystal structure</i>	<i>f</i>
<u>Two dimensional diffusion:</u>	
– Honeycomb	0.5
– Square	0.46694
– Hexagonal	0.56006
<u>Three dimensional diffusion:</u>	
– Diamond	0.5
– Simple cubic	0.65311
– BCC	0.72722
– FCC	0.78146
– HCP	0.78121 (⊥ to c)
	0.78146 (// to c)

Table 2.2 Values of the correlation factor for vacancy diffusion in various lattices (after J.R. Manning, (1968))

The correlation factor is also present when comparing different diffusion mechanisms, e.g., when diffusion occurs via interstitials or vacancies. Solvent particles B diffusing through interstitials in A will move with a random walk because the particle always

finds itself in the same geometrical situation as in the previous step. However, when diffusion occurs via vacancies the possibility that the interaction between the solvent particle, B, and the vacancy be different from that between the vacancies and the atoms of the host lattice makes the jumps of B non-random and therefore a correlation factor, f , must be included when comparing diffusion occurring by both mechanisms.

2.4.4 Chemical diffusion

When a concentration gradient is imposed on a non-stoichiometric compound, re-equilibration of the diffusing substance may occur by a diffusional process involving the propagation of a concentration gradient throughout the specimen to minimise the concentration differences in the sample. There are some special cases, such as that of spinodal decomposition, where the concentration differences are not minimised by the diffusion process, but increased.

The rate constant that describes the chemical diffusion process is known as chemical diffusion coefficient, \tilde{D} , and it is the constant of proportionality in Fick's second law of diffusion. In a one-dimensional case this law can be expressed as:

$$\frac{\partial C}{\partial t} = \frac{\partial}{\partial x} \left(\tilde{D} \frac{\partial C}{\partial x} \right), \quad (2.16)$$

where C is the concentration of the mobile species, t is the time and x is the diffusion distance.

The chemical diffusion coefficient, \tilde{D} , and the self diffusion coefficient, D_s are related by a thermodynamic enhancement factor that can be derived as follows:

In order to achieve equilibrium in a system the value of chemical potentials of the different mobile particles of the system must be constant. Let us consider a system where particles, i , and vacancies, v , are the only mobile species. Gradients in their chemical potential, μ , will generate a flux expressed by:

$$j_i = -L_{ii} \frac{\partial \mu_i}{\partial x} - L_{iv} \frac{\partial \mu_v}{\partial x}, \text{ and}$$

$$j_v = -L_{vi} \frac{\partial \mu_i}{\partial x} - L_{vv} \frac{\partial \mu_v}{\partial x}, \quad (2.17)$$

where the L terms are the transport coefficients of i and v , and μ_x is the chemical potential of particles ($x = i$) and vacancies ($x = v$) in the system.

For the above expressions to be correct the sum of the fluxes present in the system must be zero, i.e. $j_i + j_v = 0$. Taking the off-diagonal terms to be so small that they can be neglected and considering that all the vacancies are at equilibrium in the system (the vacancies that flow through the material are created at one end ($x = 0$) and annihilated at the other) leaves $\mu_v = 0$ and $(\partial\mu_i/\partial x = 0)$. We have that the flux equals:

$$j_i = -L_{ii} \frac{\partial\mu_i}{\partial x} = -D_{si} \frac{\partial C_i}{\partial x}. \quad (2.18)$$

If we compare Fick's first law with this equation we have that the value of L_{ii} is:

$$L_{ii} = -D_{si} \frac{\partial C_i}{\partial \mu_i} \quad (2.19)$$

The chemical potential can be expressed by: $\mu_i = \mu_i^o + kT \ln a_i$, where μ_i^o is the chemical potential of i at $T = 0$ K and a_i is its activity. The self diffusion coefficient can be considered a measure of the rate at which atoms diffuse in an ideal solution, therefore the activity of the diffusing particle can be expressed as its mole fraction in the system, $a_i = n_i$, and the chemical potential becomes: $\mu_i = \mu_i^o + kT \ln n_i$

Substituting in the flux equation for both cases we have:

$$\text{Chemical diffusion: } j_i = -\tilde{D}_i \frac{\partial C_i}{\partial x} - L_{ii} \frac{\partial \mu_i}{\partial x} = -L_{ii} kT \frac{\partial \ln a_i}{\partial x}, \text{ and}$$

$$\text{Self diffusion: } j_i = -D_{si} \frac{\partial C_i}{\partial x} - L_{ii} \frac{\partial \mu_i}{\partial x} = -L_{ii} kT \frac{\partial \ln n_i}{\partial x}. \quad (2.20)$$

Assuming that the transport coefficients are the same in both cases and defining the activity coefficient as $\gamma_i = a_i/n_i$, we obtain:

$$\tilde{D}_i = -D_{si} \frac{\partial \ln a_i}{\partial \ln n_i} = -D_{si} \left(1 + \frac{\partial \ln \gamma_i}{\partial \ln n_i} \right). \quad (2.21)$$

Where $\left(1 + \frac{\partial \ln \gamma_i}{\partial \ln n_i} \right)$ is the *thermodynamic enhancement factor*. This factor takes into account that chemical diffusion occurs in the presence of a concentration gradient whereas this gradient is absent in the self diffusion process.

Very few studies have been made of the value of this thermodynamic factor for oxygen diffusion in YBCO. Faupel and Hehenkamp (1993) propose a relationship between the thermodynamic factor, Φ , and oxygen content as shown in Fig. 2.6. Chapter 3 will analyse these data in the context of the diffusion results present in the literature.

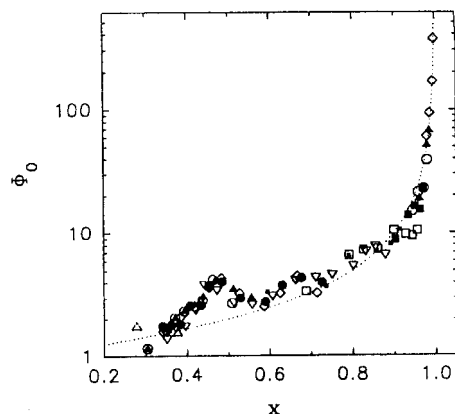


Fig. 2.6 Variation of thermodynamic factor with oxygen content for $YBa_2Cu_3O_{6+x}$ (from Faupel and Hehenkamp (1993))

The thermodynamic factor links the individual chemical diffusion coefficient with the self diffusion coefficient by a concentration dependent activity coefficient, γ . This γ describes the interaction of the diffusing substances with respect to the lattice. The value of γ is constant at small concentrations of the diffusing substance (Henry's law) and equals one as the mole fraction, n_i , tends to one (Raoult's law). In these cases the chemical diffusion coefficient is approximately equal to the self diffusion coefficient.

When the mixing process decreases the net enthalpy of the system, there is an increased tendency towards interdiffusion and in this case the thermodynamic factor is greater than one. This results in a chemical diffusion coefficient faster than the self diffusion coefficient. When mixing increases the net enthalpy the thermodynamic factor is less than unity, and the rate at which mixing occurs is reduced. In this case chemical diffusion occurs more slowly than self diffusion.

2.4.5 Factors affecting diffusion

The diffusion coefficient can be affected by a large number of factors, the most important ones being composition, temperature and structure.

- Composition

There are cases in which the diffusion coefficient changes with composition. This makes the analysis of the diffusion process more complicated since there is one extra variable to be taken into account. The Kirkendall effect mentioned in section 2.2.1 is a good example of a concentration dependent diffusion system. Boltzmann–Matano analysis can be used to calculate the diffusion coefficient for each concentration. There is a good review of the study of concentration dependent diffusion in Crank (1975). The diffusion coefficient depends on concentration because the value of the binding energies of the vacancy to the diffusing ion may vary with the amount of diffusing ions present in the material. The value of the diffusion coefficient may decrease when the number of vacant sites is reduced. The change in D may be greater than an order of magnitude over a very small concentration range (10^{-4} atomic percent). An example of this concentration dependent diffusion is that of Fe ions diffusing in Fe_{1-x}O . It can be seen in Fig. 2.7 how at 802 °C the value of D decreases with increasing Fe content.

The diffusion coefficient considered in this thesis is assumed to be independent on concentration, so the possible solutions to the diffusion equation and the analysis of the process presented will only refer to concentration-independent diffusion. The range of activation enthalpies for diffusion processes observed experimentally is considerable. Values can vary from approximately 0.1 eV allowing interstitial motion at low temperatures to 1-2 eV, characteristic of vacancy motion in oxides at higher temperatures (hundreds of degrees).

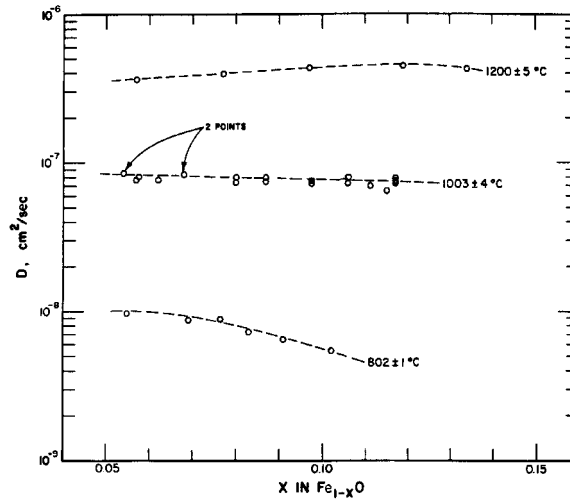


Fig. 2.7 Log D as a function of deviation from stoichiometry for cation self-diffusion: ^{59}Fe in Fe_{1-x}O , at different temperatures (from N.L. Peterson (1973))

- Temperature

From diffusion experiments the dependence of the diffusion coefficient on temperature can be expressed by an Arrhenius type relationship:

$$D = D_o \exp(-A_e/kT) \quad (2.22)$$

where D_o and A_e are independent of temperature. The activation energy of the diffusion process, A_e , is associated to the energy required for the formation of defects, and that necessary for their motion. D_o , the pre-exponential term, is proportional to the entropy of formation and motion of these particles as well as to the bond strength and the jump frequency of the diffusing particles:

$$D_o = \frac{1}{6} r^2 f \Gamma \exp((S_f + S_m)/k), \quad (2.23)$$

$$(2.24)$$

Where r is the jump distance and Γ is the jump frequency of the diffusing particles; f is the correlation factor already mentioned in section 2.4.3. If self diffusion occurs via vacancies the activation energy is equal to the enthalpy of formation and motion of these vacancies (bond strength), while in interstitial diffusion it is not necessary to form a defect for diffusion to occur and the activation energy would be the value of the enthalpy of motion of the diffusing particle through interstitials in the lattice. Diffusion of weakly bonded ions (metals) will have lower activation energies than those that are strongly bonded to the lattice (ionic solids).

In the case of oxygen diffusion in YBCO, the activation energy is equal to the binding energy of the oxygen ions to the lattice. The creation of vacancies in the ab plane would not alter significantly the final value, since even in the case of a lattice that is almost fully oxygenated there are always O(5) sites available for the motion of oxygen ions. Even though this thesis concentrates on the macroscopic aspects of diffusion, chapter 3 reviews some of the theoretical work carried out to study the ionic motion in the YBCO lattice during the diffusion process. It has already been mentioned at the beginning of section 2.2 that diffusion in YBCO can be considered a two-dimensional process, as the motion of oxygen ions and vacancies in the ab plane occurs around 10^6 times faster than in the c direction (see also chapter 3).

- Structure

D increases with lattice irregularity. Due to a reduction in packing density in dislocations and grain boundaries, atoms can diffuse along these paths more easily. Analysis of grain boundary diffusion will be dealt with in more detail in the following section. Since the grain boundary area to volume ratio of a polycrystalline solid is small, grain boundary diffusion only becomes important in certain phenomena, like sintering or oxidation. It seems that grain boundary diffusion has a more pronounced effect on D at lower temperatures because its lower activation energy makes it less sensitive to temperature changes in this range. As the temperature decreases the value for the diffusion rate along grain boundaries decreases more slowly than that of diffusion through the bulk.

2.5 Application to real geometries. Solutions of the diffusion equation

The diffusion process is a very important phenomenon, but it can be very complicated in the general case of an anisotropic, inhomogeneous, multicomponent system subject to various driving forces. General solutions of the diffusion equation can be obtained for a number of initial and boundary conditions provided the diffusion coefficient is constant.

2.5.1 Thin film solution

Let us first consider a *non-steady state* situation where two solute-free infinite rods are joined by the ends with a thin film of solute concentration C_0 between them (see Fig. 2.8). The equation that describes this situation is Fick's second law of diffusion:

$$\frac{\partial C}{\partial t} = \frac{\partial}{\partial x} \left(-\tilde{D} \frac{\partial C}{\partial x} \right); \quad (2.16)$$

by differentiation we can see that:

$$C = \frac{A}{\sqrt{t}} \exp\left(-x^2/4\tilde{D}t\right) \quad (2.25)$$

is a solution of the above equation. The total amount of solute per unit cross section, M , is equal to: $M = \int_{-\infty}^{\infty} C dx$; substituting and integrating we can calculate the value of

A : $A = \frac{M}{2\sqrt{\pi\tilde{D}}}$. so the variation in concentration along the rods can be expressed by:

$$C = \frac{M}{2\sqrt{\pi\tilde{D}}} \exp\left(-x^2/4\tilde{D}t\right). \quad (2.26)$$

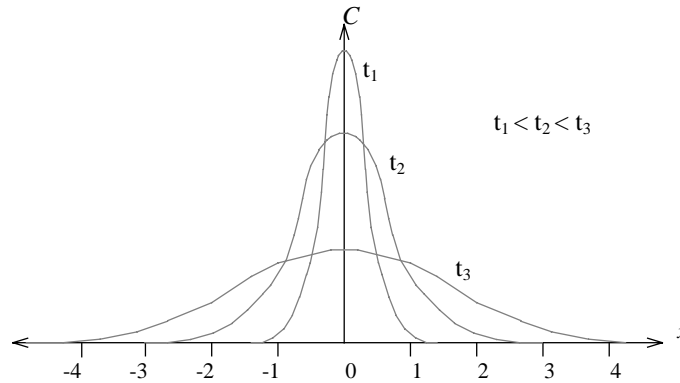


Fig. 2.8 Time sequence of diffusion profiles displaying thin film diffusion into an infinite rod

2.5.2 Semi-infinite sources

There are cases in which the initial distribution is not just confined to a plane but it occupies a finite region, as it happens in the case where a *semi-infinite* rod with a constant solute concentration is attached to a solute-free rod, i.e.:

$$C = C_o \text{ for } x < 0, t = 0$$

$$C = 0 \text{ for } x > 0, t = 0$$

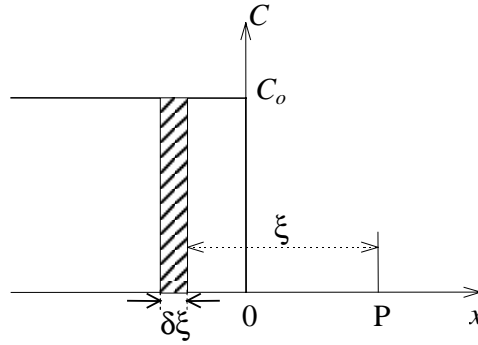


Fig. 2.9 Definition of the symbols used in this section. Case of diffusion from a semi-infinite source

Taking a small element of volume of thickness $\delta\xi$ and unit area, the concentration at P at any point in time is:

$$C = \frac{C_o \delta\xi}{2\sqrt{\pi\tilde{D}t}} \exp\left(-\xi^2/4\tilde{D}t\right). \quad (2.27)$$

Doing a summation of all the $\delta\xi$ elements:

$$C = \frac{C_o \delta\xi}{2\sqrt{\pi\tilde{D}t}} \int_{-\infty}^{\infty} \exp\left(-\xi^2/4\tilde{D}t\right) d\xi = \frac{C_o}{\sqrt{\pi}} \int_{x/2\sqrt{\tilde{D}t}}^{\infty} \exp(-\eta^2) d\eta, \quad (2.28)$$

where $\eta = \xi/2\sqrt{\tilde{D}t}$, putting $\text{erf}(x) = \frac{2}{\sqrt{\pi}} \int_0^x \exp(-\eta^2) d\eta$, with $\text{erf}(-x) = -\text{erf}(x)$, and $\text{erf}(\infty) = 1$. Values of the error function can be found in many tabulations (Carslaw and Jaeger (1959)). The concentration profile varies according to:

$$C = \frac{C_o}{2} \left[1 - \text{erf}\left(\frac{x}{2\sqrt{Dt}}\right) \right]. \quad (2.29)$$

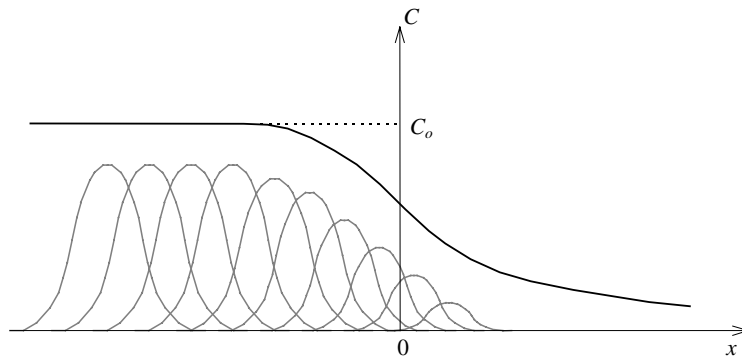


Fig. 2.10 Diffusion profile from a semi-infinite source at time $t > 0$. Black solid line represents the final solute distribution. Grey lines below the curve show the different error functions that describe the process and add up according to equation (2.29) to give the solute distribution shown.

2.5.3 Finite systems. Complete homogenisation

Let us consider the case of a plane of finite thickness with a solute concentration C_0 diffusing into two semi-infinite planes at each side. The boundary conditions are:

$$\begin{aligned} C &= C_0 \text{ for } 0 < x < l \text{ at } t = 0, \\ C &= 0 \text{ for } x = 0, \text{ and } C = 0 \text{ for } x = l \text{ for } t > 0 \end{aligned}$$

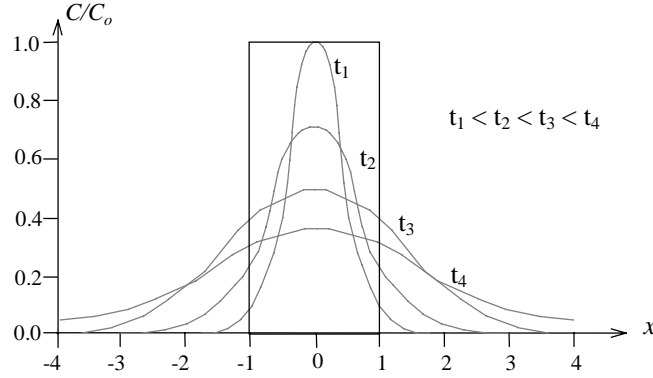


Fig. 2.11 Concentration-distance curves for diffusion from a finite source at $C = 0$ for different times

The final expression for the variation in concentration is:

$$C = \frac{4C_0}{\pi} \sum_{n=0}^{\infty} \frac{1}{(2n+1)} \exp\left(-\tilde{D} \frac{(2n+1)^2 \pi^2 t}{l^2}\right) \sin\left(\frac{(2n+1)\pi x}{l}\right). \quad (2.30)$$

2.5.4 Diffusion in a slab

In the case of the diffusion considered in this work, the situation can be approximated to that of diffusion in or out of a plane sheet. The diffusing species is assumed to enter through the x axis only, the initial concentration is uniform and the concentration at the surfaces is constant.

If the region $-1 < x < 1$ is initially at a uniform concentration C_0 , and the surfaces are kept at t constant concentration C_∞ , the solution of the diffusion equation becomes:

$$\frac{(C - C_0)}{(C_\infty - C_0)} = 1 - \frac{4}{\pi} \sum_{n=1}^{\infty} \frac{(-1)^n}{(2n+1)} \exp\left(-\tilde{D} \frac{(2n+1)^2 \pi^2 t}{4l^2}\right) \cos\left(\frac{(2n+1)\pi x}{2l}\right). \quad (2.31)$$

This solution gives the variation of the concentration profile with time t and distance x . If M_t is the total amount of diffusing substance that has entered the sheet at time t

and M_∞ is the corresponding quantity after infinite time, then the previous equation can be simplified to:

$$\frac{M_t}{M_\infty} = 1 - \sum_{n=1}^{\infty} \frac{8}{(2n+1)^2 \pi^2} \exp\left(-\tilde{D} \frac{(2n+1)^2 \pi^2 t}{4l^2}\right), \quad (2.32)$$

which gives the weight change with time in the diffusion process.

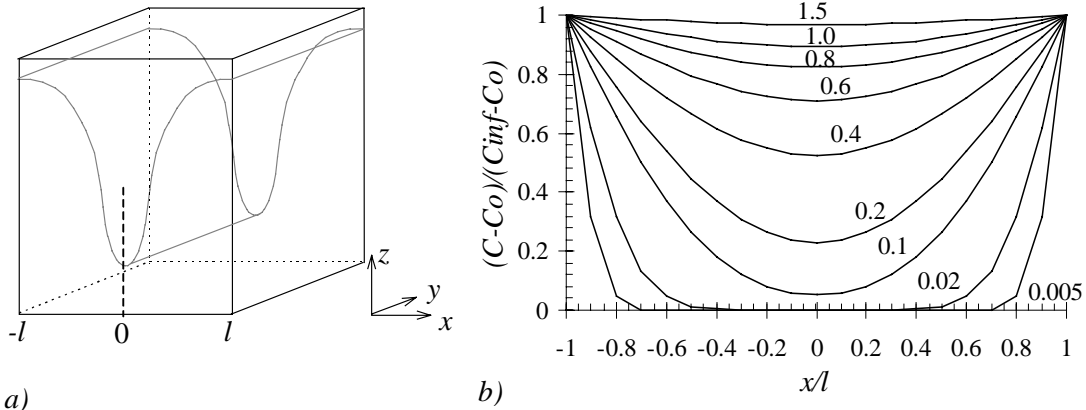


Fig. 2.12 a) Schematic of diffusion in a slab with concentration profile overlaid, and b) concentration distributions for the same diffusion situation at different times (equation (2.31)). Numbers next to the curves are the values of Dt/l^2

2.5.5 Grain boundary diffusion

All the solutions given above describe volume diffusion in perfect solids. Real solids, however, may have defects, dislocations or boundaries that affect the diffusion process, as mentioned in 2.3.5. This section is going to cover the mathematical solution to only one of these fast diffusion pathways: grain boundary diffusion. This type of diffusion is present in polycrystalline materials and its effect is more important at low temperatures. This phenomenon was first studied by Fisher (1951) and it has been followed by a number of authors that have proposed solutions to more complex situations (e.g.: Whipple, (1954), Suzuoka, (1964) and Kwok *et al.* (1984-a), (1984-b)).

Let us consider a grain boundary of thickness l perpendicular to a constant solute source of concentration C_0 . The rate of change in concentration for an element of grain boundary is given by:

$$\frac{\partial C}{\partial t} = \frac{1}{dyl} \left[l \left(j_y - j_y - \frac{\partial j_y}{\partial y} dy \right) - 2dyj_x \right] = -\frac{\partial j_y}{\partial y} - \frac{2}{l} j_x \quad (2.33)$$

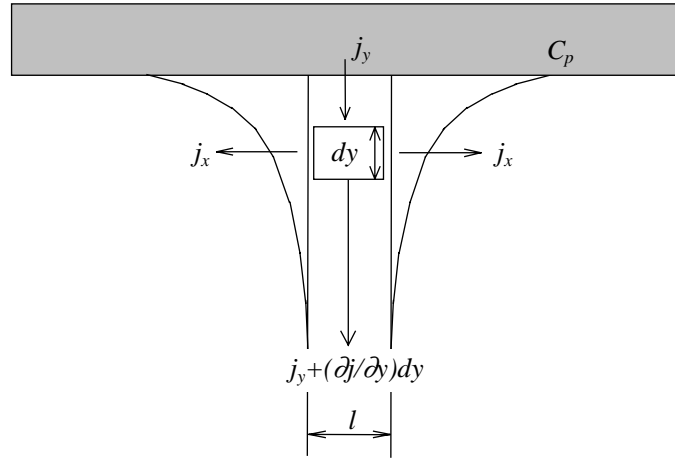


Fig. 2.13 Schematic of the concentration profile along a grain boundary and into the lattice in the case of grain boundary diffusion

Let D_{GB} be the diffusion coefficient at the grain boundary and that in the bulk be D_L . As long as $D_{GB} > D_L$ and the flux along the x direction is perpendicular to the boundary, the above equation can be solved taking the solution to the thin film case (Eq. (2.26)) and calculating an initially unknown factor that takes into account the effect of the fast diffusion on the boundary acting as a second source of solute that diffuses into the bulk:

$$C = C_o \exp \left(\frac{-y}{(\pi D_L t)^{1/4} \sqrt{l D_{GB} / 2 D_L}} \right) \left(1 - \operatorname{erf} \left(\frac{x}{2 \sqrt{D_L t}} \right) \right). \quad (2.34)$$

2.6 Methods of measurement

There are many approaches to measure the magnitude of a diffusion coefficient; these depend on the system studied and the characteristics of the diffusion process. Therefore, there are steady-state and transient methods, methods based on the analysis of concentration-distance curves or observation the overall rate or uptake or loss of diffusion substance by a specimen of known size and shape. The latter is going to be considered here. These methods are going to be applied to the analysis of oxygen diffusion data collected with thermogravimetry presented in chapter 5.

2.6.1 Sorption method. Constant \tilde{D}

This experiment has been used to determine the diffusion coefficient of dyes in cellulose sheet and of oxygen in muscle (Crank (1975)). The diffusion coefficient is assumed constant and the sheet does not change volume during the diffusion process. The experimental procedure used is thermogravimetry, where the weight change of the sheet is monitored as it is held at a certain temperature and the gas is diffusing in. The solution of the diffusion equation is equation (2.32):

$$\frac{M_t}{M_\infty} = 1 - \sum_{n=1}^{\infty} \frac{8}{(2n+1)^2 \pi^2} \exp\left(-\tilde{D} \frac{(2n+1)^2 \pi^2 t}{4l^2}\right). \quad (2.32)$$

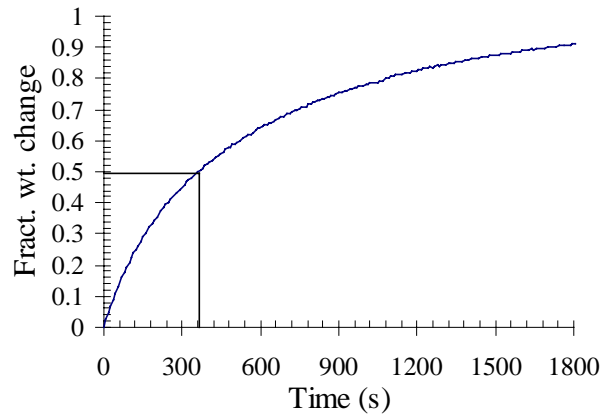


Fig. 2.14 Fractional weight change vs. t plot from experimental data of an oxygenation of $YBa_2Cu_3O_{7.8}$ powder at 400 °C. See chapter 5 for detailed analysis of experimental results

From this equation there are two ways of calculating the diffusion coefficient in the sheet. The first one considers the value of t/l^2 for which $M_t/M_\infty = 1/2$, $(t/l^2)_{1/2}$. This is well approximated by:

$$\left(t/l^2\right)_{1/2} = \frac{1}{\pi^2 D} \ln\left(\frac{\pi^2}{16} - \frac{1}{9}\left(\frac{\pi^2}{16}\right)^9\right), \quad (2.35)$$

the error being $\approx 0.001\%$. We then have:

$$\tilde{D} = \frac{0.0049}{\left(t/l^2\right)_{1/2}}. \quad (2.36)$$

Therefore, if the half-time of a sorption process is observed experimentally for a system with a constant diffusion coefficient the value of \tilde{D} can be determined from (2.36).

2.6.2 Initial rates of sorption and desorption

It is also possible to calculate an average diffusion coefficient from the initial gradient of the sorption curve when the fractional weight change is plotted against the square root of time. In the early stages of diffusion, for \tilde{D} constant and a sheet of thickness l , we have:

$$\frac{M_t}{M_\infty} = \frac{4}{\pi^2} \left(\frac{\tilde{D}t}{l^2} \right)^{1/2}. \quad (2.37)$$

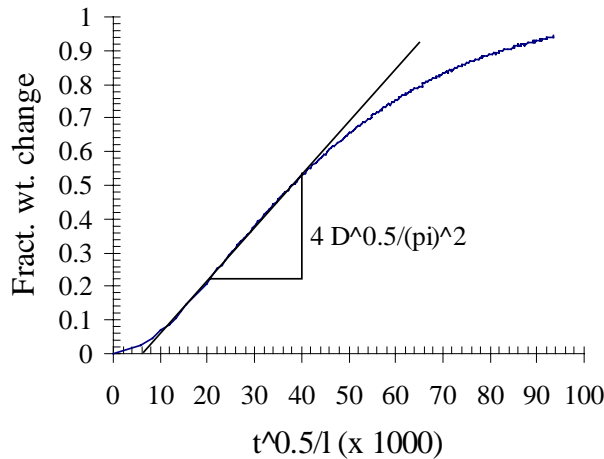


Fig. 2.15 Fractional weight change vs. $t^{1/2}/l$ plot from the initial data of an oxygenation of $\text{YBa}_2\text{Cu}_3\text{O}_{7.8}$ powder at 400 °C (particle diameter: 5.2 μm). See chapter 5 for detailed analysis of experimental data

2.6.3 Final rates of sorption and desorption

When the previous type of study is not possible there is a chance to calculate the value of the diffusion coefficient taking the later stages of the diffusion process. In this case only the first term of equation (2.32) needs to be considered and therefore, for diffusion in and out of a sheet of thickness l :

$$\frac{d(\ln(M_\infty - M_t))}{dt} = -\tilde{D} \frac{\pi^2}{l^2}. \quad (2.38)$$

The variation of the value of $\ln(M_\infty - M_t)$ with time gives a straight line from whose slope the value for \tilde{D} can be calculated.

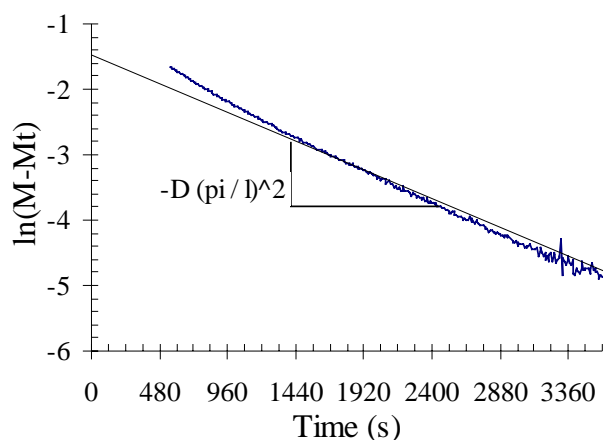


Fig. 2.16 Fractional weight change vs. t curve for experimental data of an oxygenation at 400 °C of $YBa_2Cu_3O_{7-\delta}$ powder (particle diameter: 5.2 μm). See chapter 5 for detailed analysis of experimental data

2.7 Conclusions

The diffusion process can be studied from two different points of view. The first one (microscopic) is concerned with the study of the movement of the ions within the crystal lattice. The second approach studies the diffusion process measuring the effect it has on the physical properties of the sample (change in resistivity, weight changes, etc.), without looking in detail at the movement of ions in the crystal structure. This is the macroscopic point of view, and it is going to be the one used in this thesis.

This chapter has reviewed the study of the diffusion process starting with the formulation of Fick's laws of diffusion. This has been followed by a presentation of the different mechanisms for diffusion (vacancy, interstitial, etc.) and the types of diffusion coefficients that can be measured depending on the technique used. The relationships between these coefficients have been discussed.

The chapter finishes with the application of Fick's laws to analyse and study diffusion data obtained from real experiments, taking into account the geometry of the sample, setting the appropriate boundary conditions for each case and giving the mathematical expressions of a number of diffusion situations. The solution to Fick's second law for

diffusion in a slab discussed here is going to be used in the analysis of the experimental results presented in chapter 5.

Chapter 3

Literature review

3.1 Introduction

Chapter 1 has introduced the subject of oxygen non-stoichiometry of YBCO, one of the parameters that determine its normal state and superconducting properties. Knowledge of the oxygen content of the samples as well as that of the rate at which it diffuses in and out of them has become a key issue in order to be able to optimise its properties.

The manufacture of YBCO samples involves (see chapter 4) heating the precursor powders so that they react and produce the required copper oxide with the right stoichiometric ratio between the Y, Ba and Cu ions. Once YBCO is obtained, polycrystalline samples are produced by sintering or melt-processing; single crystals are grown using a variety of methods, most of them involving heating to high temperatures. The oxygen content at these high temperatures is very low and in order to obtain YBCO with good superconducting properties an oxygenation step has to be included in the manufacturing process. This step involves heating the sample to temperatures below 500 °C to increase the oxygen content of YBCO and restore its superconducting properties. The annealing time during this step is determined not only by the diffusion coefficient, but also by the microstructural features that affect the diffusion process, such as porosity (interconnecting voids), grain size, twin density, grain orientation, sample surface area, impurity content and initial oxygen distribution.

In order to study the kinetics of oxygen diffusion a number of techniques have been used, but the results obtained differ considerably. One of the reasons is that sometimes the diffusion coefficient measured depends on the technique used, and the necessary correlation factors are not applied before comparisons are made. There has been a large amount of data published in this subject, but as it is going to be seen in the

following sections the variables affecting the diffusion process (especially in polycrystalline samples) are numerous and, in many cases, difficult to assess or control, giving rise to the wide range of values for oxygen diffusion shown.

3.2 Thermogravimetry (TG)

Thermogravimetric measurements can be used to study the chemical diffusion of a species in a material (see chapter 4 for a more detailed description of the technique). These measurements consist on placing a sample of the material in a balance in an enclosed atmosphere; the conditions of temperature and/or partial gas pressure – oxygen in this case – are changed so that a concentration gradient is established between the sample and the atmosphere and the diffusing species is either absorbed or desorbed from the sample, changing its weight. This change in weight is recorded with respect to time and temperature and is a direct measurement of the chemical diffusion process that is taking place.

Thermogravimetric analysis has been applied to the study of oxygen diffusion in YBCO powder and polycrystalline samples of varying density. The use of single crystals with this method has not been reported, perhaps due to the difficulty in producing the large amount of crystals needed so that the data from the weight measurements is outside the experimental error region inherent to the system used.

The scatter in the published data is quite large, as it is going to be seen in the following paragraphs. A summary of the results published using this technique is presented in Table 3.1. The difference between these results is thought to be due mainly to the high sensitivity of this technique; the variation in the microstructural features of the samples affects considerably the measurements taken (see chapter 5, section 5.2.3). But it could also have other reasons that are discussed in the following analysis:

The first pieces of work published with results from thermogravimetry concentrate on the measurement of the equilibrium oxygen content of YBCO with temperature and pressure. Gallagher (1987), Strobel *et al.* (1987) and Kishio *et al.* (1987) present data characterising the non-stoichiometry of YBCO at different partial oxygen pressures.

From their experiments, Gallagher and Strobel *et al.* (1987) have calculated the value for the activation energy of the diffusion process taking place. Gallagher (1987) obtained an activation energy equal to 1.03 - 1.15 eV while Strobel and co-workers calculated a higher value: 1.5 - 1.65 eV. The range in partial pressures used by both authors is the same, and so is the temperature range; since the activation energy characteristic of a vacancy diffusion process (see section 3.7 in this chapter and chapter 2) is approximately equal to 1 eV, the value of Strobel *et al.* (1987) is too high. Errors in the measurement or contamination of the sample could be two of the reasons for such a high activation energy.

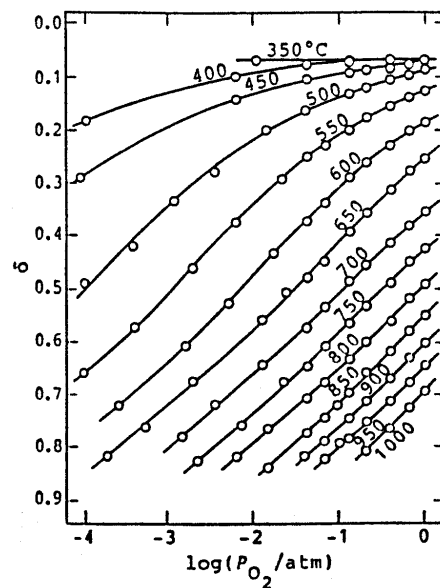


Fig 3.1 Oxygen stoichiometry vs. partial oxygen pressure diagram (Kishio *et al.* (1989-b))

In the two following papers published, Kishio *et al.* (1989-a), (1989-b) present a more complete version of their initial work (Kishio *et al.* (1987)). Comparing their concentration vs. partial oxygen pressure results with those from Strobel *et al.* (1987), it can be seen there is a difference of 0.05 in the oxygen content measured, which can be attributed to experimental error. Kishio and co-workers study in more depth the diffusion process, concluding that the diffusion coefficient is dependent on the oxygen content of the specimen, contradicting their initial assumption of a concentration-independent diffusion coefficient. They calculated an activation energy that changed with concentration between 1.38 eV (for $\delta = 1$) to 1.81 eV (for $\delta = 0$). The value of the pre-exponential coefficient changed in one order of magnitude with oxygen content. They find that their data, once converted to self-diffusion data with the

thermodynamic factor, agrees quite well with those from Ikuma and Akiyoshi (1988). Kishio *et al.* (1989-b) pointed out that more work should be done to investigate the effect of grain boundary diffusion in the final results obtained. The values of the diffusion coefficient calculated by this group have a very high activation energy and pre-exponential coefficient, which suggests that they could have used the dimensions of the polycrystalline pellets as their diffusion distance, instead of the grain size. Taking a longer distance increases the value of the diffusion coefficient, as it will be seen in chapter 5 (Table 5.1). In terms of the mechanism for diffusion, Strobel *et al.* (1987) only mention that it involves motion of oxygen ions from $(1/2, 0, 0)$ and $(0, 1/2, 0)$ sites in the ab plane. This mechanism is discarded by Kishio and co-workers (Kishio *et al.* (1989-b)) on the grounds that the chemical diffusion coefficient is said to be dependent on oxygen content, which is more typical of an interstitial mechanism. However, the proposed motion of oxygen along interstitials is due just to a change of reference point where the O(5) sites are not considered part of the crystal structure of YBCO, becoming interstitial sites.

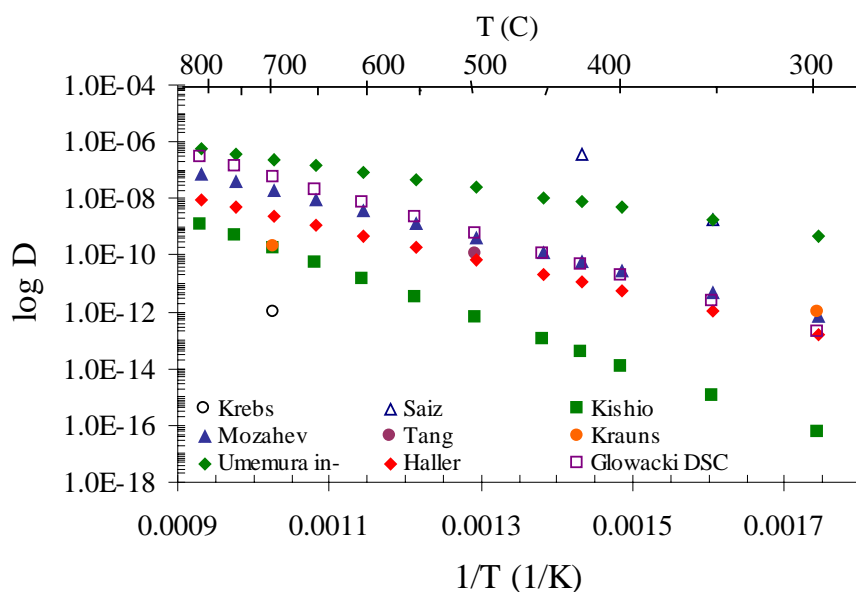


Fig. 3.2 Collected chemical diffusion data

Another study of oxygen diffusion that is going to be included in this section even though it was carried out using a different thermal analysis technique is that of Głowacki *et al.* (1988). They used differential scanning calorimetry to study the absorption and desorption of oxygen in YBCO. The experiments were carried out under non-isothermal conditions, unlike most of the thermogravimetry work presented

here, and they measured the heat released during the absorption of oxygen while the sample was heated at a certain rate in a pure oxygen atmosphere. These non-isothermal measurements present the advantage of giving information about the oxygenation process from very low temperatures (below 300 °C), which is not possible to do with other techniques. The activation energy of the absorption process was calculated to range between 1.5 and 1.6 eV, agreeing with that calculated by Tu and co-workers (1988), (1989) for out-diffusion of oxygen in their analysis of oxygen diffusion with resistance measurements (see section 3.4). These values are slightly higher than the rest of the activation energies found in the literature. This is justified by the authors proposing that the process is limited by the formation of a highly oxygenated layer that moves towards the centre of the sample (agreeing with Furukawa *et al.* (1992)), and suggesting that out-diffusion is surface reaction limited (see Tu *et al.* (1989) and LaGraff *et al.* (1991) in section 3.4).

It has been suggested by a number of authors that the value of the diffusion coefficient depends on the oxygen content of the sample. However, the bulk of the results presented in the literature describes the process with an Arrhenius equation. This means that a plot of $\ln D$ vs. $1/T$ is a straight line. Any concentration dependence of the diffusion coefficient would be reflected in this graph as a deviation from this straight line; as the dependence observed is an increase in the value of the activation energy with oxygen content, the $\ln D$ vs. $1/T$ plot would curve downwards to slower values of D (an increase in the slope of the line) as temperature decreased (see Fig. 3.3 a)). The arguments behind the increase in activation energy are that the relaxation curves of the property measured (weight change, resistivity, etc.) show a fast variation at the beginning of the measurement, when the oxygen content is low (Fig. 3.3 b)); this is followed by an apparent slowing down in the change of this property at longer times, when a large amount of oxygen has diffused in the sample. The diffusion study presented in this work (see chapter 5) shows that this behaviour is characteristic of a single diffusion process, independently of the amount of oxygen absorbed by the specimen, ruling out the proposed concentration dependence.

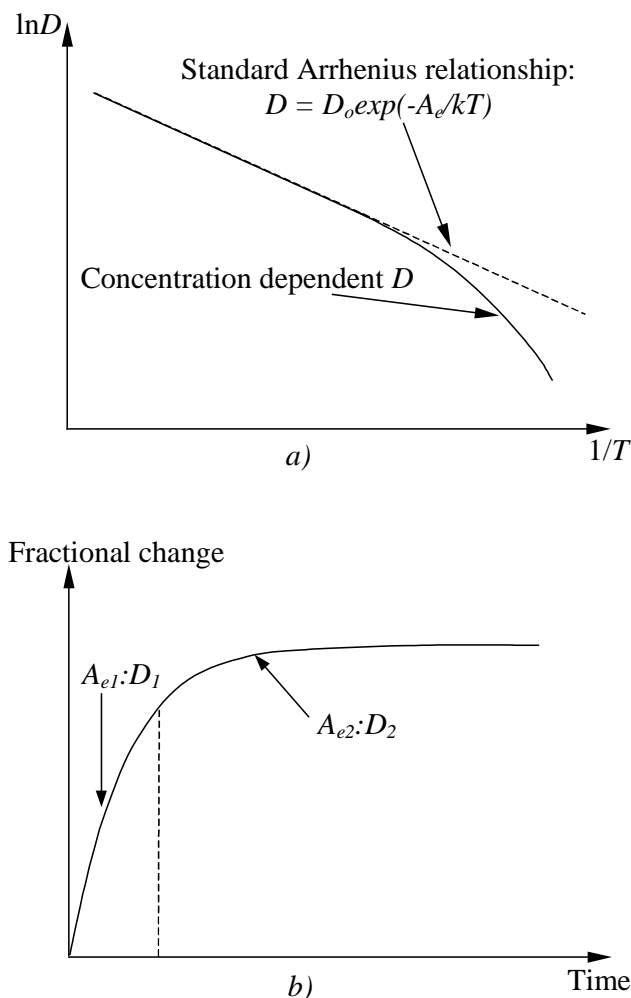


Fig. 3.3 a) Schematic of concentration-dependent and concentration-independent diffusion behaviour, and b) schematic of relaxation measurement with two apparent activation energy regions

Going back to the rest of the diffusion work, Saiz and Moya (1988) studied the influence of the microstructure on the diffusion coefficient and observed that the absorption of oxygen was up to 50 times faster in tetragonal samples than in orthorhombic samples. They also observed that for the polycrystalline samples used (grains 35 μm long, different densities), grain boundary diffusion was not the rate limiting factor for the diffusion process. The activation energies calculated for both processes (from a standard isothermal weight gain trace) were: 0.12 eV for tetragonal samples (the initial part of the curve) and 0.29 eV for orthorhombic samples (from the final part of the curve). These activation energy values are extremely low and have not been corroborated by any other work in the literature. It is difficult to explain the reason for these low values; perhaps the choice of the diffusion distance was not correct, or the samples were contaminated during the preparation process.

Haller *et al.* (1988) studied diffusion in a very porous polycrystalline sample and, assuming that the diffusion coefficient was independent of the oxygen content of the sample, they calculated an activation energy for the process equal to 1.15 eV and a pre-exponential term of $2.2 \times 10^{-3} \text{ cm}^2/\text{s}$. Using the calculated value of the diffusion coefficient, they also calculated the jump frequency of the oxygen ions in the lattice and they found it to be quite similar to that characteristic of a vacancy diffusion mechanism: 10^{-13} s^{-1} . They observed a slight variation in the values of the activation energy with oxygen content, but it was considered to be within the experimental error of the measurements taken.

From their oxygenation-deoxygenation cycles, Umemura *et al.* (1989) calculated two expressions for in- and out-diffusion. The activation energies of each are rather low: 0.7 and 0.5 eV respectively. An important aspect to consider again is the choice of the diffusion distance. Umemura and co-workers do not mention the grain size of their polycrystalline samples (diffusion distance), necessary to calculate the value of the diffusion coefficient. This leads to think that they have used the full dimensions of the sample as their diffusion distance; this could explain the fast values obtained for the pre-exponential factor and the activation energy. A peculiar behaviour in the weight relaxation times for in-diffusion suggests possible contamination of the samples or perhaps the onset of grain boundary diffusion.

The work presented by Lau *et al.* (1991) is contradicting, suggesting diffusion coefficients two orders of magnitude different for the same temperature. They have observed a non-Arrhenius dependence of the diffusion coefficient, also observed by Krauns and Krebs (1993), contradicting most of the results published. Krauns and Krebs (1993) carried out oxygenation studies in polycrystalline YBCO with a grain size of 1 to 5 μm and an average density of about 75%. The values they calculated for the activation energy from their experimental measurements change from 1.3 eV at 400 °C to 0.3 eV at 700 °C. They explain this change suggesting that the decrease in oxygen content at high temperatures enhances the diffusion process due to the increase in oxygen vacancies.

Even though the work carried out by Tang and Lo (1991) observed a concentration dependence of the diffusion coefficient, they show in a $\ln D$ vs. $1/T$ plot that their

diffusion values fall in a straight line, following an Arrhenius equation. This contradicts the previous statement of a concentration dependent diffusion coefficient. It has already been discussed (see Fig. 3.3 a)) that a concentration dependent diffusion coefficient deviates from the straight-line Arrhenius behaviour depending on the dependence on the oxygen content (upwards if the activation energy decreases and downwards if it increases with the amount of oxygen present in the sample). Tang and Lo (1991) worked with powder samples at temperatures around 500 °C and calculated an activation energy of 1.3 eV for the oxygenation process. The calculations were carried out based on a solution of the diffusion equation with the appropriate boundary conditions and at 500 °C the diffusion coefficient was found to be of the order of 10^{-10} cm²/s. They suggest that the source of disagreement between their calculations and other data published in literature is the presence of porosity in polycrystalline samples and the effect of large angle grain boundaries in the diffusion process.

On the same lines as Saiz and Moya (1988), Mozahev and co-workers (Mozahev *et al.*, (1992), Mozahev and Chernyaev, (1994)) studied the effect of sample porosity on the diffusion of oxygen in polycrystalline samples, obtaining a reasonable value of the activation energy equal to 1.2 eV. They observed that for sintered materials of densities lower \approx 80-85 % of the theoretical density, the oxygenation process could be described quite accurately with a model of a diffusion in a sphere. This means that both porous polycrystals and powders would have the same oxygenating behaviour. This could be due to the presence of a large number of open pores that facilitate the supply or removal of oxygen to and from inner parts of the polycrystal. If this were true, then the only factor to take into account in order to calculate the diffusion coefficient would be the diffusing distance, this is, the size of the grains in polycrystalline specimens and the powder particle diameter in powder samples. The temperatures at which their studies were carried out cover a very wide range (100–750°C), and the effect of grain boundaries does not appear to modify the diffusion results in the lower temperature region.

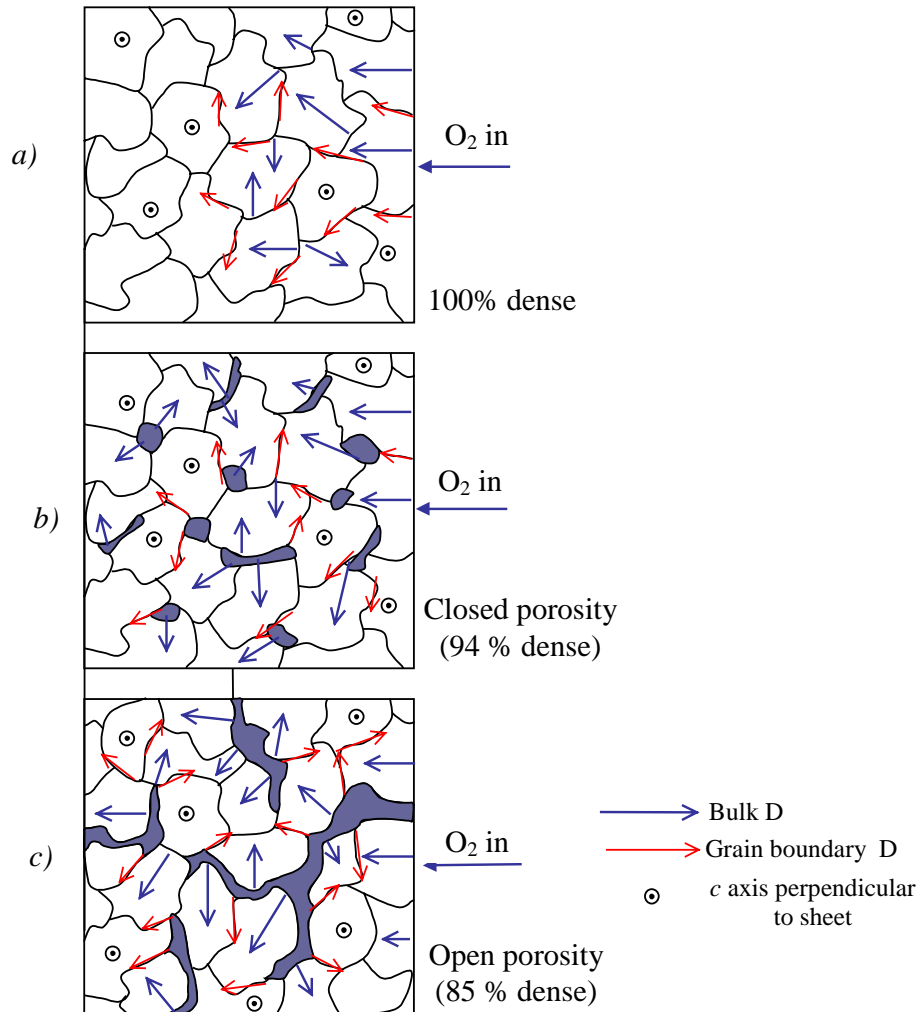


Fig. 3.4 Schematic of diffusion process in polycrystalline samples with different degrees of porosity

With respect to the effect of porosity on diffusion, three cases should be taken into account, depending on the degree of porosity present in the sample studied. It can be seen in Fig. 3.4 a) that if the sample is fully dense, the oxygen source is the atmosphere surrounding the sample and the only way this oxygen diffuses to the centre is via grain boundary diffusion and bulk diffusion. In this case the diffusion distance considered should be the dimensions of the sample (if the temperature at which this occurs is such that grain boundary diffusion effects can be ignored). The opposite situation would be that of a specimen with open porosity, where the oxygen diffuses in the sample not only from the surrounding atmosphere but also from the interconnected pores. These are a continuous oxygen source, as they are connected to the atmosphere outside the sample. In this case the diffusion process occurs more readily because oxygen can reach inner regions of the specimen through the pores, and

the diffusion distance considered should be that between interconnected pores (see Fig. 3.4 c)).

In the case of samples with closed porosity, (see Fig. 3.4 b)) some oxygenation would occur from the oxygen trapped in the closed pores into the material, but the amount would be so small that it would not have any major effect on the overall diffusion behaviour.

Furukawa *et al.* (1992) studied the oxygenation of YBCO powder at very low temperatures and at two different oxygen contents (fully deoxygenated and with an oxygen content equal to 6.44). They observed a slower oxygen uptake in the YBCO samples with a higher oxygen content (6.44), which suggests that the diffusion process is controlled by the speed at which the interface between the tetragonal and orthorhombic phases moves towards the centre of the sample. They have modelled this process using an “unreacted core model”, where the grains are spherical and, as soon as oxygenation starts, an orthorhombic skin forms and grows towards the centre of the particle. It seems that in this model the skin is fully orthorhombic at the highest oxygen content possible for that temperature and all the way across, which is difficult to believe since abrupt changes in concentration are not common in non-stoichiometric materials. The variation in concentration occurs gradually: there would be a decreasing concentration gradient towards the centre of the sample, where the outer surface is oxygenated to the highest possible oxygen content at the temperature the experiment is carried out and the oxygen content decreases gradually as the distance to the centre decreases. The slow oxygen uptake of the oxygenated sample could be due to surface contamination of the powder.

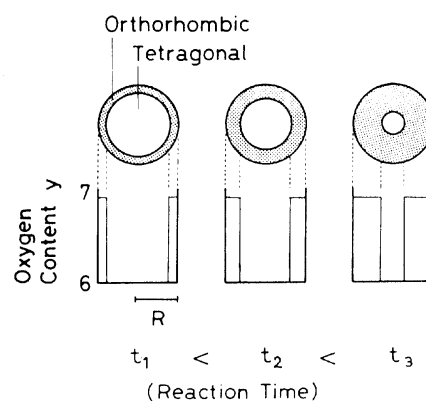


Fig. 3.5 Schematic of unreacted core model (after Furukawa *et al.* (1992))

3.2.1 Summary

Most of the thermogravimetric analysis of oxygen diffusion has been carried out in polycrystalline samples of varying density, although work on powdered YBCO has also been reported.

The values obtained with thermogravimetric analysis present a wide range of diffusion coefficients and activation energies. TGA gives a value for the chemical diffusion coefficient, i.e., diffusion in the presence of a concentration gradient, so the initial oxygen distribution in the sample as well as the microstructure can have a very important effect in the final result obtained. All the experiments have been carried out using polycrystalline samples of varying density and grain size, in most cases these variables have either been ignored or not mentioned in their publications, which makes it difficult to assess whether the result obtained is characteristic of that particular sample and agrees with a general value for D or the analysis of the collected data has been done incorrectly.

The use of polycrystalline samples for diffusion studies with thermogravimetry introduces a large source of uncertainties in the measurements. These specimens should be considered complex systems where a large number of factors can influence the diffusion process. The degree of densification (open or closed porosity), the size of the grains and the presence of grain boundaries should be taken into account before comparing the results obtained to those from powder specimens or to polycrystalline samples with different microstructural features.

3.3 Tracer diffusion experiments

Tracer diffusion studies to monitor oxygen diffusion in YBCO are carried out using ^{18}O as the tracer since there is no radioactive isotope of oxygen. Diffusion experiments are performed equilibrating the samples in ^{16}O , annealing them in ^{18}O , measuring the ^{18}O depth profile by SIMS and determining the value of D^* from a fit of the depth profile to the solution of the diffusion equation.

These studies can be carried out using single crystal or polycrystalline samples. The results obtained from tracer diffusion experiments are affected less by the different microstructural features of the samples (e.g. in polycrystalline materials), as SIMS depth profiles average the results over the different grain orientations of the specimen. The use of single crystals is very useful to obtain data from the behaviour in different orientations, although diffusion in the ab plane is limited by the small thickness of the crystals. Table 3.2 presents a summary of the results discussed below:

Rothman *et al.* (1989), (1991) and Routbort *et al.* (1990) have carried out a complete study of the phenomenon of oxygen tracer diffusion in YBCO. They have measured ^{18}O diffusion in polycrystalline and single crystal samples, calculating an expression for diffusion in polycrystals that is corroborated by most of the other works published (Turrillas *et al.* (1989), Sabras *et al.* (1990)). They did not observe a dependence of the tracer diffusion coefficient on partial oxygen pressure or oxygen content.

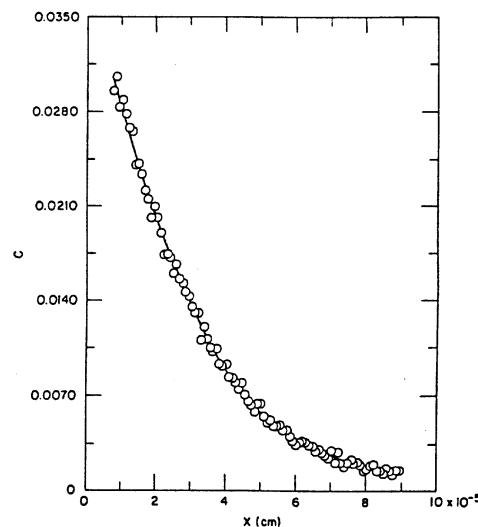


Fig 3.6 Penetration plot for YBCO polycrystal annealed for 1/2 h at 300 °C (after Rothman *et al.* (1991))

Their studies of diffusion on single crystals have been set as a reference point by all the diffusion work carried out later on as they were the first to measure the anisotropy in the diffusion process in the ab plane and along the c axis. The difference was calculated to be of the order of $10^4 - 10^6 \text{ cm}^2/\text{s}$. This has also been observed by other authors that conducted the same type of study on single crystals: both Bredikhin *et al.* (1991) and Tsukui *et al.* (1991-a), (1991-b) measured the difference between D_{ab}^* and D_c^* in a single crystal and found it to be of approximately five orders of magnitude.

Comparing the single crystal data with that from the polycrystalline samples, they observed that the diffusion coefficient of the latter was approximately the same as that measured in single crystal samples in the ab direction. This corroborates the initial assumption that tracer diffusion measurements are not affected by the microstructure of the specimen, giving an average value of the process in the sample. Since diffusion along the c axis occurs so slowly it is reasonable that the result from a polycrystalline sample is similar to that of diffusion along ab in a single crystal, the fastest of the two diffusion processes.

To complement the diffusion study, Rothman and co-workers (Rothman *et al.* (1991) and Routbort and Rothman (1994)) calculated the value of the tracer diffusion coefficient along the a and b directions in single crystal samples, finding a difference between them of one to two orders of magnitude. This is the only work that has measured such difference; the rest of the studies just consider diffusion in the ab plane and along the c axis. They propose a mechanism of diffusion based on organised diffusion along O(5) sites. This is similar to the diffusion mechanisms suggested by Ronay and Nordlander (1988).

There is a third piece of work (Tsukui *et al.* (1991-a), (1991-b)) that measured the value of D^* in single crystals with a stair-like shape; this configuration allowed them to carry out measurements along the ab and c directions in the same crystal, which they suggest gives more reliable results than if the studies had been carried out on different samples for each direction. However, they calculated a difference between the ab and c diffusion almost two orders of magnitude higher than that presented by Rothman *et al.* (1990). This could be due to the presence of impurities or flux on the surface of the crystal, as they report having observed the presence of flux in other crystals used, which altered the diffusion results obtained.

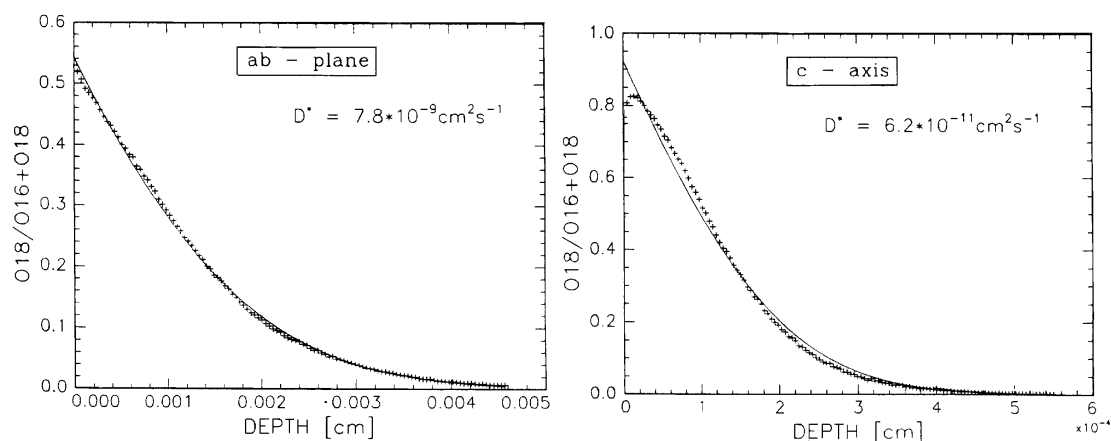


Fig 3.7 Isotopic penetration profiles along the *ab* and *c* directions for in-diffusion of ^{18}O at 800 °C in an YBCO single crystal (after Bredikhin *et al.* (1991))

Another study of D^* in single crystals is presented by Bredikhin *et al.* (1991). They carry out a systematic study at two different temperatures of the diffusion coefficient along the *ab* and the *c* directions, and although the results for D^* in the *ab* plane agree with those of Rothman and co-workers and the rest of the groups, the activation energy calculated for D^*_c is rather high (2.3 eV); this is understandable given the difficulty for the oxygen ions to move through the crystal structure in the *c* direction. The difference between the measured activation energies along the *ab* plane and the *c* axis seems to show that at one point at very high temperatures both values will coincide. However, this would occur beyond the melting point of YBCO. The activation energy calculated for D^*_{ab} is also slightly higher than that reported by Rothman and co-workers, although it is within the range energies that are expected for this type of process: around 1 eV.

It can be seen in Fig. 3.8 (and from the diffusion data collected with different measurements – see Tables 3.1 and 3.2) that the slopes of the tracer diffusion data are similar to those obtained for other chemical diffusion studies (Figs 3.2 and 3.11). This seems to indicate that the effect of the thermodynamic factor, Φ , mentioned in chapter 2 (Fig. 2.6) is not as large as expected from the data published by Faupel and Hehenkamp (1993). Their results show a considerable increase in the value of the thermodynamic factor with increasing oxygen content. This would mean that the difference between chemical and tracer diffusion data would be bigger at low temperatures, as in this region the equilibrium oxygen content of YBCO is higher. It

can be seen, however, that this is not the case, as most of the activation energies obtained for chemical and tracer diffusion processes are in the range of 0.9 – 1.2 eV. This could be an indication of the presence of a second effect that compensated the radical increase in Φ in this low temperature region. Salomons and de Fontaine (1990) have carried out MonteCarlo calculations to study theoretically the oxygen diffusion process and they have also presented the change in the thermodynamic factor with oxygen content in the sample. Their calculations present some variations with respect to the results of Faupel and Hehenkamp (1993), but the magnitude of the thermodynamic factor is also high for high oxygen contents of YBCO. They also observed a sharp increase in Φ around 6.5.

It has been suggested that the effects of a concentration dependence of the diffusion coefficient could counteract those of the thermodynamic factor, but the variation in the activation energy due to the change in oxygen content would have to be so large that it would have not passed unnoticed by the groups studying chemical diffusion. The dependence of the diffusion coefficient on concentration and how this can be observed using different measurement techniques should be the subject of a more detailed study so that these points can be clarified.

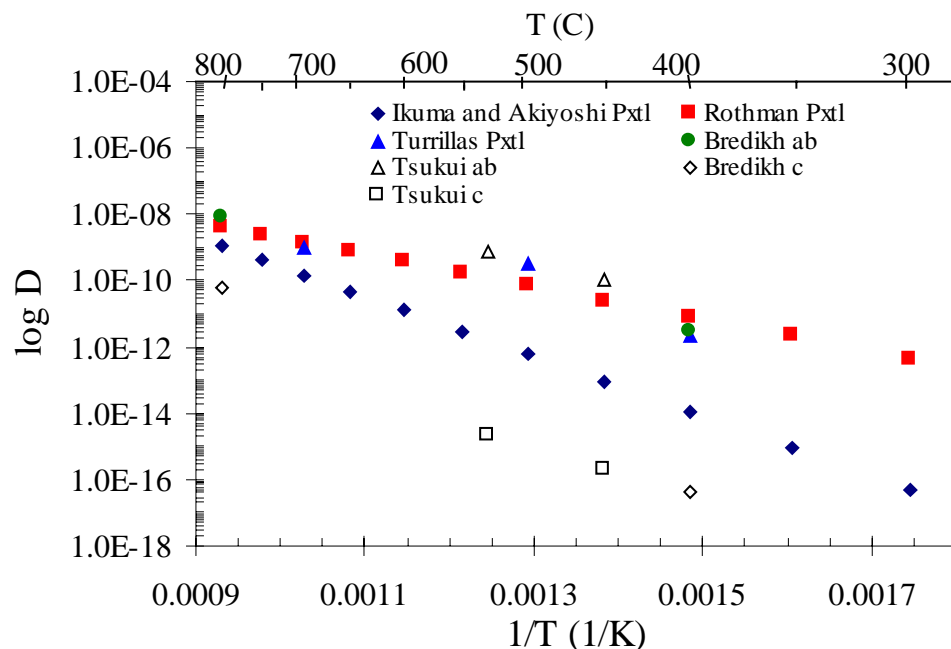


Fig. 3.8 Collected tracer diffusion data

There is another group of papers that studies the diffusion of ^{18}O in YBCO but do not use SIMS to evaluate the tracer diffusion coefficient. These groups use thermogravimetric analysis to calculate the speed at which oxygen is absorbed in the ^{16}O saturated sample. This work has been included in the tracer diffusion section although it does not fit in the standard tracer diffusion measurement group.

The first work published of this kind is that by Ikuma and Akiyoshi (1988), who studied oxygen isotope substitution in polycrystalline YBCO. They calculated an expression for this phenomenon with a very high activation energy (1.76 eV). This results in a lower value of the tracer diffusion coefficient. Rothman *et al.* (1989) suggest that the phenomenon measured by Ikuma and Akiyoshi may not represent diffusion. Their different result could be due to the presence of impurities in the polycrystal, as thermogravimetry is quite sensitive to microstructural changes. The decrease in D with increasing oxygen deficiency observed by these authors disagrees with the Arrhenius expression for the diffusion coefficient presented. According to this expression, D^* increases with increasing temperature and this is associated to a loss in oxygen, since the equilibrium oxygen content of YBCO decreases with increasing temperature (see Fig. 1.5). It is therefore not possible to observe a decrease in D^* with increasing oxygen deficiency as temperature increases, which indicates that there must be a flaw in their measurements.

The second work has been published by Conder and co-workers (Conder *et al.* (1993), Krüger *et al.* (1993)). They studied ^{18}O substitution in the YBCO lattice using thermogravimetry. They calculated the activation energies characteristic of the different types of ion exchange in the crystal structure. These range between 0.71 eV for substitution of ^{18}O in chains to 1.88 eV for the substitution of ^{18}O in planes, apex positions and chains. In a later paper, where they relate their study of the oxygen diffusion to the superconducting properties, Conder *et al.* (1994) give a slightly higher value for the activation energy of the isotope exchange in the chains: 1.23 eV. This agrees better with the rest of the data presented by other authors. They confirm the temperature (and not pressure or concentration) dependence of the oxygen diffusion coefficient in YBCO.

All their analysis has been carried out using a highly empirical method that consists on finding the best fit to the experimental data from a set of curves that are characteristic of a number of mechanisms (fifteen different types). The curve that seems to fit their results best is characteristic of diffusion controlled by the formation of an oxygen saturated outer region and the speed at which the ions diffuse through this layer, which agrees with the reaction core oxygenation process suggested by Furukawa *et al.* (1992), but disagree with the results obtained in this work. These results (see chapter 5) do not support the formation of a highly oxygenated outer layer that hinders the diffusion process.

3.3.1 Summary

Diffusion results from tracer diffusion measurements are in very good agreement with the exception of the work presented by Ikuma and Akiyoshi (1988). This technique presents the advantage of being independent of the microstructure of the sample used, as the results shown in Fig. 3.8 have been obtained from polycrystalline and single crystal specimens. A second advantage is the possibility of measuring the value of oxygen diffusion along the c axis, although it is necessary to have thick single crystals, which are not always easy to obtain.

However, its correlation with chemical diffusion through the thermodynamic factor, Φ , is not very clear, as this factor has been calculated to increase to very high values at high oxygen contents. This change in Φ with concentration would result in a non-Arrhenius dependence of D^* with temperature, disagreeing with all the experimental results published in the literature. More work should be carried out in this field to clarify the relationship between the tracer and chemical diffusion coefficients.

3.4 Resistance measurements

Resistance methods are based on the change in resistivity of YBCO with oxygen content. The resistivity of a material is determined by the product of the carrier concentration times their electronic mobility. It is known that holes in YBCO can be charge carriers and the concentration of these holes varies with oxygen doping.

Therefore, changes in resistivity can be related to oxygen stoichiometry and to the rate of change of this stoichiometry with time and temperature. Chapter 6 deals in more detail with the variation in the resistivity of YBCO with oxygen content in the high temperature range ($>300\text{ }^{\circ}\text{C}$).

The groups that have used resistance methods to measure the diffusion coefficient of oxygen in YBCO have studied this process in single crystals and polycrystalline specimens. As it has been seen in the previous sections, sometimes the work published does not give enough information about the microstructural features of the samples to be able to compare the data in the literature. The results of these measurements have been summarised in Table 3.3.

Tu *et al.* (1988-a), (1988-b) and (1989) studied the change in resistance during oxygenation and deoxygenation of polycrystalline samples. They carried out both isothermal and non-isothermal experiments.

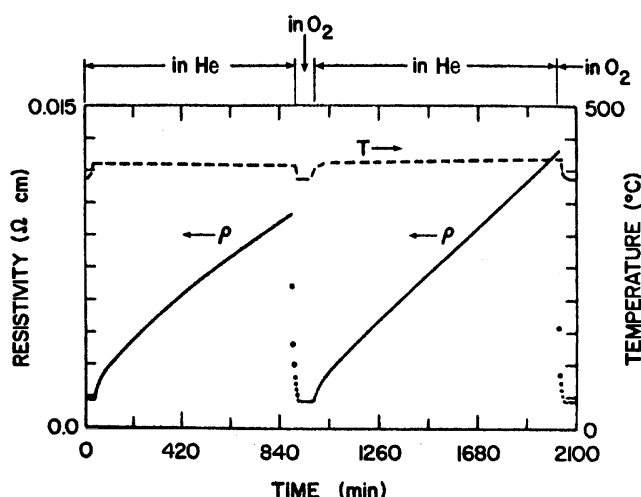


Fig 3.9 Isothermal resistivity measurements (after Tu *et al.* (1989))

The isothermal experiments showed an initial sharp decrease in the resistivity with a gradually decrease in slope with time which they attribute to a concentration dependent in-diffusion, as the process seems to occur much faster at the beginning of the measurement than at the end. From the slopes of the initial and final sections of the resistivity vs. time curve, they obtained two activation energies: 0.45 eV for $\delta = 0.38$ and 1.1 eV at saturation ($\delta = 0$). Tu *et al.* (1988-a) suggest that the difference in activation energies is due to the mechanism of oxygen diffusion. In the case of the lower activation energy, the oxide has a high concentration of oxygen empty sites in

the CuO planes and the energy required is that of oxygen motion down the plane. However, as the sample saturates with oxygen the diffusion process seems to slow down due to the reduction in the number of excess vacancies in the lattice, which means that for diffusion to occur these empty sites need to be created before oxygen can move within the material. This explains the higher value of the activation energy (A_e) at the end of the isothermal experiment; the value of A_e contains the energy for oxygen motion (0.48 eV) plus the energy for the formation of a defect (0.6 eV), giving the final calculated value of 1.1 eV. This apparent slowing down of the change of resistivity with time has been suggested by other authors to be characteristic of a concentration dependent diffusion coefficient (LaGraff *et al.* (1991), LaGraff and Payne (1993-a)).

However, chapter 5 will show that the shape of these measurements is characteristic of an Arrhenius behaviour controlled by a single diffusion coefficient. Although the speed at which oxygen diffuses in the material appears to slow down at longer times, what happens is that the sample is being saturated with the characteristic oxygen content for that temperature (see Fig. 1.5 for characteristic oxygen contents vs. temperature and Fig. 3.3 for variation from Arrhenius behaviour) and the amount of oxygen diffusing in the sample is less. The reduction in the variation of the oxygen stoichiometry results in a reduction of the change in resistivity, as it depends on the amount of oxygen present in the sample.

In the same work, Tu *et al.* (1988-a) observed that out-diffusion did not show the same concentration dependence reported for in-diffusion and calculated the activation energy of this process to be 1.76 eV. This high value is suggested to be the energy required to overcome the surface barrier to oxygen diffusion during deoxygenation. It should be taken into account that a small increase in the oxygen content will create high conductivity paths for the flow of current, causing the resistivity value to drop dramatically. The sudden decrease in resistivity observed by Tu *et al.* (1989) is therefore not an indication of a faster in-diffusion or of a surface controlled out-diffusion as it is suggested in their paper. This linear increase in resistivity with decreasing oxygen content observed has not been reported by other authors, which suggests that this effect might be a consequence of the behaviour of their

polycrystalline samples due to microstructural features or to the experimental method used. The value of the activation energy for out-diffusion compares only to that obtained by Kishio *et al.* (1989-b) and Ikuma and Akiyoshi (1988) by thermogravimetric analysis. There are other groups that agree with a surface-reaction limited out-diffusion, such as LaGraff *et al.* (1991); they suggest that oxygen evolution from the sample is controlled by the recombination and desorption process of oxygen ions. However, the activation energy calculated by LaGraff *et al.* (1991) for out-diffusion is much lower than that calculated by Tu and co-workers: 1.2 eV.

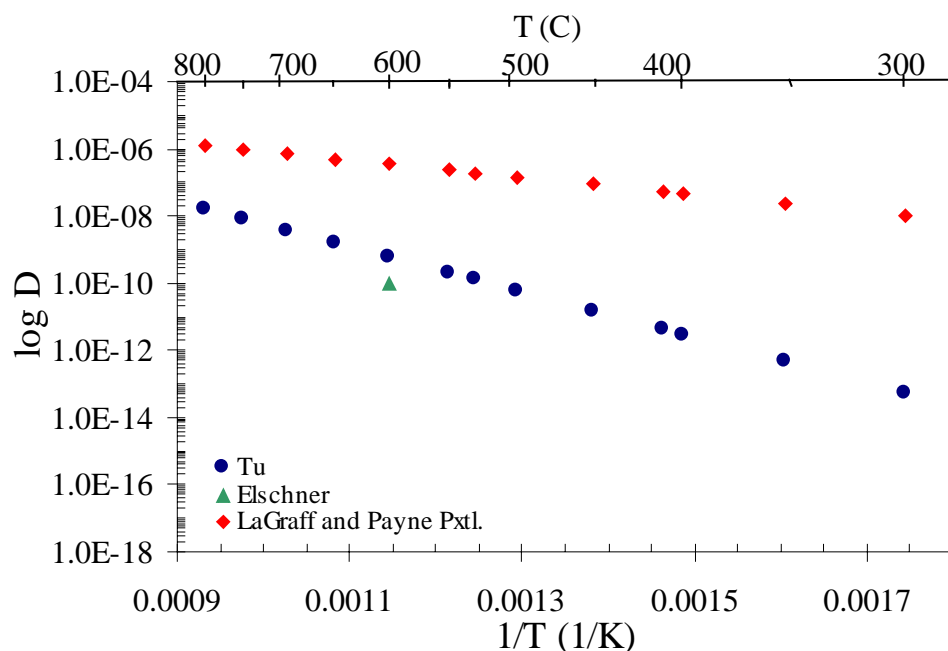


Fig. 3.10 Collected resistance data

From the non-isothermal studies of oxygen absorption, Tu *et al.* (1988-b), (1989) used Ozawa's thermal analysis (Ozawa (1970)) and calculated a value for the activation energy equal to 1.35 ± 0.1 eV (and a value of $D_o = 0.035$ cm²/s for $\delta = 0$). This activation energy is higher than that calculated from the data from the isothermal in-diffusion experiments and is thought to be a consequence of the formation of a highly oxygenated layer at the surface of the sample that hinders the in-diffusion process. These non-isothermal oxygenation curves have a very characteristic shape (see Fig. 3.11): when heating in pure oxygen a deoxygenated sample, the resistivity increases until around 300 °C, where a maximum is observed. This maximum is believed to mark the onset of diffusion into the sample. If the temperature is increased further, the

resistivity decreases as the oxygen content of the sample increases, but at temperatures around 500 °C the resistivity reaches a minimum value, thought to correspond with the point at which the sample has saturated with oxygen. From that point onwards the resistivity increases linearly again. Similar experiments have been carried out in this work using thermogravimetry giving the same characteristic curve, as it will be shown and discussed in more detail in chapter 5.

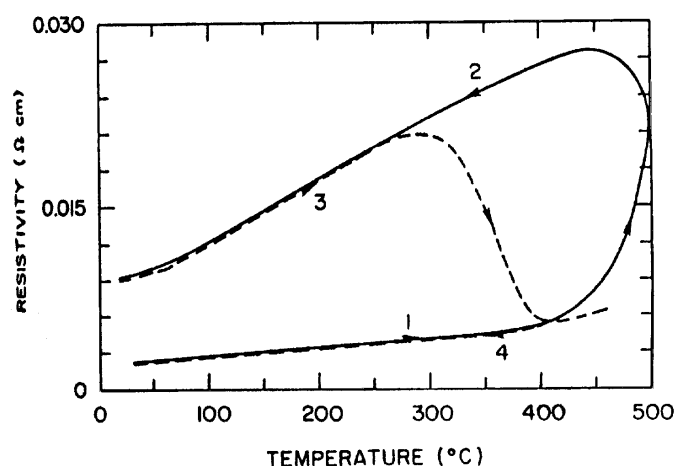


Fig 3.11 Non-isothermal resistivity measurements (after Tu *et al.* (1989)). 1 and 2 correspond to the variation in resistivity on heating and cooling at 3 °C/min in He, and 3 and 4 to the changes in resistivity when heating (3) and cooling (4) at 1 °C/min in O₂

Ottaviani *et al.* (1989), in their isothermal oxygenation experiments carried out with polycrystalline samples, have also calculated two different activation energies from the initial and final stages of the variation of resistivity with time, obtaining values equal to 0.4 eV for the beginning of the process (agreeing with Tu *et al.* (1988-b)) and 0.9 eV for the final part of the isothermal curve. Thermogravimetric measurements carried out simultaneously did not register any weight change in the last stages of the oxygenation. They suggest that the annealing at low temperatures in the presence of oxygen promoted the rearrangement of oxygen atoms from the (½, 0, 0) site where oxygen gives no additional carrier, to the (0, ½, 0) position where oxygen adds mobile charge carriers to the system. This process is activated by the rearrangement of a small number of oxygen atoms, and they only have to move to adjacent positions, which explains why the oxygen content does not change appreciably. The small change in position explains the low value of the activation energy calculated for this process.

Work done by Veal *et al.* (1990-a) (1990-b) supports this proposed rearrangement of oxygen within the sample without changing the oxygen content. They report an increase in the T_c of samples quenched from 520 °C after leaving the samples at room temperature for several days. This is attributed to an increase in the order of the vacancies in the sample, i.e. to an increase in the orthorhombicity of the sample that is not associated to any oxygen absorption (the temperatures used are too low for any significant diffusion to take place during the timescale of the experiments). The results presented by Ottaviani *et al.* (1989) should have been complemented with T_c measurements to corroborate their suggested rearrangement of oxygen ions into orthorhombic domains. This is a very interesting behaviour that should be studied in more detail, as it offers the possibility of improving the superconducting properties of a material with a given oxygen content by annealing at low temperatures (< 300 °C). There is also the possibility that their thermogravimetric system was not sensitive enough to record the small weight changes taking place during the last part of the diffusion process.

Elschner *et al.* (1992) studied the dependence of the microstructure on the different mechanisms of oxygen transport, working with polycrystals with different density and grain size. The samples used had densities equal to 85% and 100% of the theoretical density. Of the latter type, two samples were made by conventional sintering but in one of them some melting occurred, so the microstructure of the samples was different (40 μ m grains in the first one and presence of wide cracks 30 μ m apart in the second). They did not observe any difference between the in- and out-diffusion processes (see Fig. 3.12), disagreeing with Tu *et al.* (1988-a) and LaGraff *et al.* (1991). The activation energy they calculated for the diffusion process was the same for all the samples used, irrespective of their density and grain size. The value of obtained for the activation energy was equal to 0.5 eV. The pre-exponential coefficients were different for each of them, which marks the difference in diffusion coefficients between the three samples.

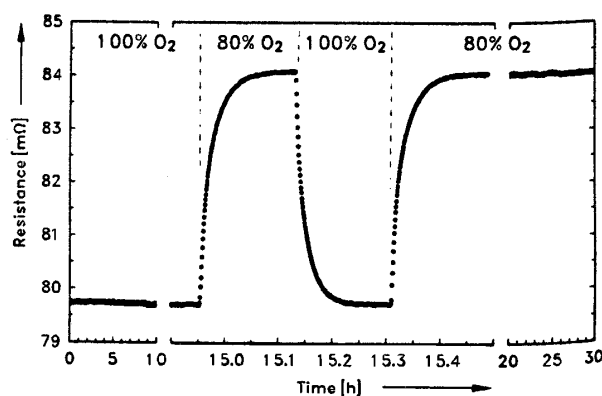


Fig 3.12 Time dependence of electric resistance with changing oxygen partial pressure at $T = 750\text{ }^{\circ}\text{C}$ (after Elschner *et al.* (1992))

It was observed that the diffusion of the 100 % dense sample sintered without melting remained constant at temperatures below $450\text{ }^{\circ}\text{C}$. Elschner *et al.* (1992) suggest that above this temperature the diffusion process measured is that occurring in the bulk of the samples, whereas below $450\text{ }^{\circ}\text{C}$ grain boundary diffusion takes over and controls the process. The activation energy observed for this grain boundary diffusion is equal to 0 eV. If this type of diffusion had such a low activation energy it would also be expected to be present in the other two samples, but this is not observed. This irregularity in the diffusion measurements is perhaps due to the presence of secondary phases or impurities in the specimen. The rate limiting factors suggested for each sample are bulk diffusion in the case of the 85% dense specimen and grain boundary diffusion (diffusion down cracks) for the highly dense specimens.

LaGraff and Payne (1993-a), (1993-b) and (1993-c) carried out experiments with single crystals at high temperatures and polycrystals with different grain sizes and porosity in a wider temperature range (see Fig. 3.13 a)). As it has been mentioned before, they found in-diffusion to be much faster than out-diffusion and the activation energy for the in-diffusion process in single crystals was calculated to be equal to 1.1 eV, whereas that for a 95% dense polycrystal was 0.4 eV. This value agrees with those presented by Ottaviani *et al.* (1989) and Tu *et al.* (1988-a). The lower activation energy was thought to be characteristic of grain boundary diffusion, while the higher one (1.1 eV) was suggested to be that of bulk diffusion. However, it has been mentioned above that the shape of the variation in resistivity with time during an isothermal experiment can be characteristic of a diffusional process with a single value for the diffusion coefficient, rather than of a combination of a fast and a slow

diffusion mechanism. They suggest the possibility of an important contribution of grain boundary diffusion in polycrystalline samples for temperatures above 350 °C, as it is the point above which they observe a non-linear variation of the resistivity increase in non-isothermal experiments (c.f. Tu *et al.* (1989)). Since this onset of non-linear resistivity occurs at 500 °C for single crystals, it has been suggested that 350 to 500 °C is the range within which grain boundary diffusion is faster than bulk diffusion and above 500 °C diffusion occurs mainly inside the grains.

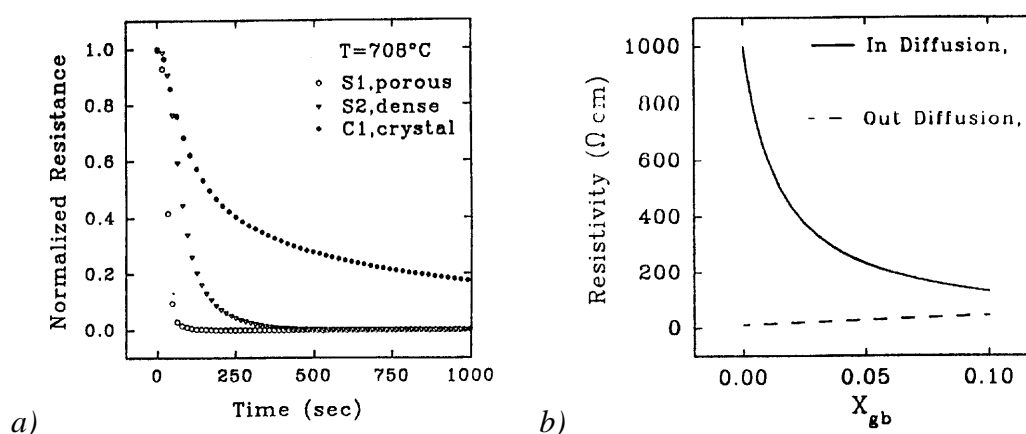


Fig 3.13 a) Resistance variation for oxygen in-diffusion at 708 °C in polycrystalline and single crystal YBCO (after LaGraff *et al.* (1993-b)), and b) change in resistivity during in- and out-diffusion measurements when a highly oxygenated layer and a highly deoxygenated layer are formed (respectively) in the samples.

Erb *et al.* (1996) carried out resistivity studies on single crystals and did not find any difference between in- and out-diffusion processes, agreeing with Elschner *et al.* (1992). Neither did they observe any dependence on the oxygen concentration. The activation energy calculated seemed slightly low (0.8 eV), which could be due to impurity effects. They point out that the method used to measure the changes in resistivity with time and temperature in the sample could affect the final results obtained, as some techniques are affected by grain boundary and surface effects whereas others only measure changes in the bulk of the sample.

3.4.1 Summary

The use of resistance methods to measure the oxygen diffusion coefficient presents a number of problems: one of them is that a small change in the oxygen content of the material can have a drastic effect on the value of the resistivity. LaGraff and Payne

(1993-a) calculated the effects the formation of a highly oxygenated shell and a deoxygenated shell would have on in- and out-diffusion respectively, and they found that a deoxygenated region formed during out diffusion would have a lesser effect on the change in resistivity than an equally thick oxygenated shell during in-diffusion (Fig. 3.13 b)). This oxygenated layer would form around the perimeter of the grains and in the necks formed between the grains during the sintering process. It would act as a short-circuiting pathway yielding resistivities not representative of the bulk material. The low activation energies calculated by Tu *et al.* (1988-a), (1988-b), (1989), LaGraff and co-workers (1991), (1992), (1993-a,b,c) and Elschner *et al.* (1992) could be due to the presence of this highly oxygenated region at the surface of the samples.

With respect to the evaluation of the diffusion coefficient from the change in resistivity of the specimen it should be noted that it is necessary to know the value of the effective diffusion length. When using resistance methods the external dimensions of the sample (in the case of single crystals) may not necessarily be the diffusion distances, so any diffusion coefficient given should be taken as an estimate of the upper limit of the value of this coefficient. Polycrystals with open porosity (density lower than 94 % of the theoretical value) present more internal surface area for oxygen exchange to occur. This means that the diffusion length will be shorter if the shell forms. Therefore the results are not representative of bulk behaviour.

It seems there is not an agreement on whether in-diffusion is faster or slower than out-diffusion. Some authors argue that out-diffusion is surface reaction limited and this is why it is slower than in-diffusion (Tu and co-workers), while this same argument is presented by other authors to justify their findings of slower in-diffusion than out-diffusion (LaGraff and Payne (1992)). The formation of a highly oxygenated layer is also another argument presented when trying to explain a slower in-diffusion process. At the same time, there are groups who have observed that both processes occur at the same rate (Elschner *et al.* (1992)). It seems that since diffusion occurs due to the presence of a chemical gradient, the oxygenation of the surface should not hinder but form part of the diffusion process. The argument against surface reaction limited out-diffusion has already been covered at the beginning of this section.

3.5 Internal friction methods

A number of authors have measured internal friction of oxygen ions in YBCO and related it to the diffusion of oxygen in this material (see Table 3.4). This technique measures the stress relaxation of individual atoms as they diffuse in a random walk through the structure. The activation energy of this process is the potential energy barrier that the oxygen atoms must overcome in the diffusion process. The measurements are not affected by the microstructure of the sample (e.g. presence of grain boundaries), as the distance considered (jump distance of an oxygen ion) is only a few Å, much smaller than the size of the microstructural features. This technique gives good results at low temperatures, where normal methods of studying diffusion are inoperative because of the very slow diffusion rates.

Internal friction measurements give a peak that in this case appears at 210 °C at 1.18 Hz and shifts to 800 °C for a vibration frequency of 40 Hz. This peak is attributed to be characteristic of hopping of oxygen ions between the O(1) and O(5) sites as the result of the applied stress. Most of the results obtained using this technique agree in that the activation energy for oxygen hopping is approximately equal to 1 eV, which is the characteristic value for the migration of point defects (e.g. vacancies).

Two groups (Tallon and Staines (1990) and Xie *et al.* (1989)) observe a change in the value of the activation energy with increasing temperature, but the final value of the diffusion coefficient is observed by Tallon and Staines (1990) to increase with temperature, while Xie *et al.* (1989) observed that D decreased as the temperature increased. The change in activation energy was attributed to a change in the potential energy of the O(1) and O(5) sites as the structure becomes tetragonal and the sites become equivalent, but this does not explain why the deviations from linearity go in opposite directions for each group.

Xie *et al.* (1989) suggest an explanation for the different in- and out-diffusion processes: The diffusion current is proportional to the density of oxygen-defective supercells and in the case of in-diffusion, oxygen atoms find that there are a large number of these in the structure, whereas in the case of out-diffusion the material is saturated with oxygen, which makes the process very slow since it restricts the

diffusion process to the outer deoxygenated layer of the sample. This argument is valid only for fully deoxygenated or fully oxygenated specimens. In the case of a partially oxygenated sample there should be enough defective supercells for both processes to occur at equivalent rates.

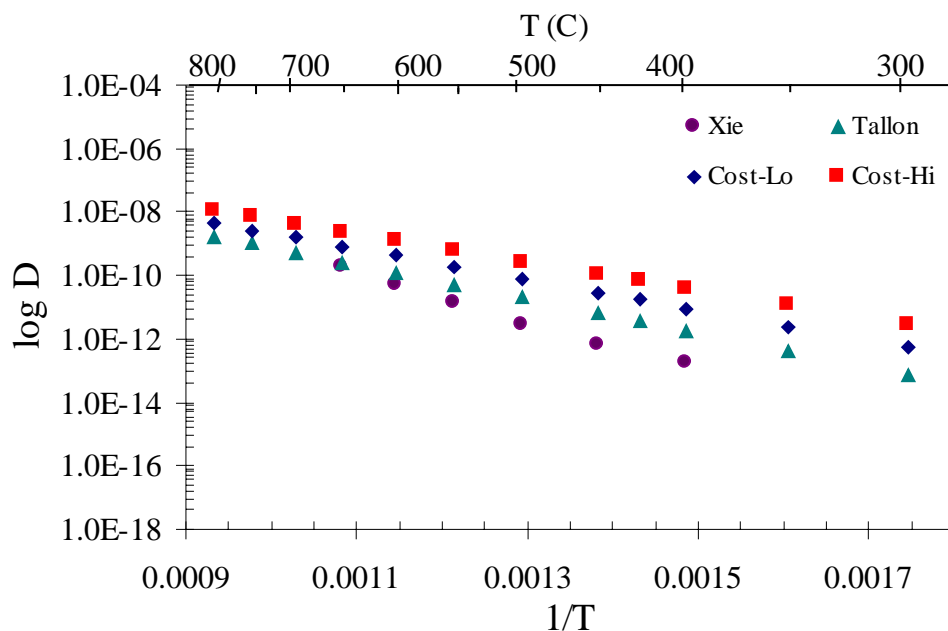


Fig. 3.14 Collected internal friction data

In two consecutive papers, Zhang and co-workers (Zhang *et al.* (1990-a), (1990-b)) present the results of very low frequency studies of oxygen relaxation deconvoluting a series of peaks from the initial ones obtained. Two of these deconvoluted peaks are associated to the motion of oxygen in the structure. This group is the only one that considers oxygen motion not only along the Cu-O chains, but in the CuO₂ planes and along the *c* axis. They give activation energies for these two types of displacement, for the in-plane approximately equal to 1 eV and for motion perpendicular to the CuO₂ planes and Cu-O chains equal to 1.35 - 1.5 eV. Further studies should be carried out to calculate the value of the pre-exponential coefficient to be able to compare these results with those obtained with other techniques.

Cost and Stanley (1991) have carried out an internal friction study over a wide range of frequencies which allowed them to calculate the activation energy for the relaxation of the motion of oxygen ions in the structure. The value of the activation energy was found to vary between 0.97-1.4 eV and the pre-exponential factor was equal to

$1.4 \times 10^{-4} \text{ cm}^2/\text{s}$ to $6.3 \times 10^{-4} \text{ cm}^2/\text{s}$; these values agree with those presented by Xie *et al.* (1989).

The relationship between oxygen diffusion and internal friction, however, is not completely certain. On one hand the activation energies agree fairly well, especially considering the range of energies obtained with other methods. But on the other hand the curved Arrhenius plots in different directions and the fact that the motion of oxygen ions occurs in the absence of a concentration gradient indicate that more work should be carried out to find the correlation between the internal friction results and chemical diffusion data.

3.6 Electrochemical methods

Using solid-state electrochemical cells it is possible to obtain information about diffusion and ion conduction processes. In the case of YBCO, oxygen ions can be driven in or out of the sample either by establishing a partial pressure gradient across the cell or applying a potential difference across it.

A typical galvanic cell may be represented as follows:



where: electrode = YBCO, electrolyte = fast ionic conductor, e.g. YSZ

The potential, E , of this oxygen concentration cell can be related to the difference in partial pressures on either side of the electrolyte by the Nernst equation:

$$E = -\frac{RT}{zF} \ln(P'_{\text{O}_2}/P''_{\text{O}_2}) \quad (3.1)$$

where (P'_{O_2}) and (P''_{O_2}) , are the oxygen pressures, R is the gas constant, F the Faraday constant and z is the number of units of charge carried.

A number of studies have carried out electrochemical measurements to calculate the oxygen diffusion coefficient of YBCO and their results are quite scattered. This method is dependent on the microstructure of the sample and on the type of interaction at the surface of the electrolyte, as reported by MacManus *et al.* (1992). The

dependence on the microstructural features of the sample may be the reason for the scatter in the results published:

O'Sullivan and Chang (1988) studied diffusion in a polycrystalline sample at 550 °C obtaining a value of 5×10^{-8} cm²/s for in- and out-diffusion, while this same value for the diffusion coefficient was obtained by Belzner *et al.* (1990) for a temperature of 800 °C. In a preliminary paper, MacManus *et al.* (1989) studied the introduction of oxygen in YBCO using an electrochemical cell. From decay curves of the current passing across the cell for set potentials applied, they calculated a value of the intrinsic (bulk) diffusion coefficient equal to 9×10^{-8} cm²/s for 600 °C, which can be compared with that reported by O'Sullivan and Chang (1988). Further experiments using resistance measurements are reported in this paper, giving values for the diffusion coefficient equal to 8×10^{-7} cm²/s for 600 °C and 1×10^{-4} cm²/s for 800 °C. The activation energy obtained from these two values is equal to 1.9 eV. These values are so high because the diffusion distance taken for the calculations was half the pellet thickness rather than half the average grain size.

In a following paper, MacManus *et al.* (1990) developed a computational model to reproduce the variation in oxygen content as the electrochemical conditions varied, and in an AC impedance analysis of various polycrystalline samples, the same group (MacManus *et al.* (1992)) calculated values for the activation energy of the in- and out-diffusion processes that agreed with Tu *et al.* (1989) (0.4 and 1.76 eV respectively).

AC impedance studies consist on applying a small alternating voltage across a galvanic cell and measuring the current response. Depending on the frequency of the alternating voltage it is possible to observe the different processes of ion transport in the cell, as each of them has a characteristic time constant. This type of measurements can differentiate between bulk diffusion, diffusion along grain boundaries and across the electrode. MacManus and co-workers found that the interface between the electrode and the electrolytes could modify the final result of the measurement. The values cited above were characteristic of an electrochemical cell with YBCO paste electrodes; however, if these electrodes were made of a polished polycrystalline sample the activation energy was found to be 1.5 eV. This activation energy is lower

than that calculated from the data in their earlier paper (MacManus *et al.* (1989)). However, as it was mentioned when analysing resistance methods all these activation energy values are too high compared with the typical values for a vacancy diffusion process and with the values calculated in this work (see chapter 5).

The diffusion coefficient calculated by Scolnik *et al.* (1991), 10^{-11} - 10^{-12} cm²/s, is four to five orders of magnitude faster than other values reported for oxygen diffusion at room temperature (e.g. Mogilevsky *et al.* (1994): 10^{-18} - 10^{-19} cm²/s). The reason why all the diffusion coefficients obtained by O'Sullivan and Chang (1988), MacManus *et al.* (1989) and the latter one by Scolnik *et al.* (1991) are so high compared to the rest is unknown. The need to use polycrystalline samples in this technique and the possible effects of grain boundary diffusion and the effect of the contact between electrodes and electrolytes could be the reason for these fast diffusion coefficients.

Patrakeev *et al.* (1993) point out that obtaining activation energies from an Arrhenius plot is not very accurate since the material is never at its equilibrium oxygen content. They carried out oxygen permeation measurements of YBCO polycrystalline samples and obtained a concentration dependent diffusion coefficient with activation energies ranging from 2.0 to 2.4 eV for concentrations varying between 6.35 and 6.6, which are amongst the highest values for activation energy reported.

These results are summarised in Table 3.5. The influence of sample microstructure on the results obtained using this technique and the effects of the contact between the electrode and electrolyte shows that great care must be taken when carrying out electrochemical measurements.

3.7 Theory

The study of oxygen diffusion from a theoretical point of view is important since it contributes to the understanding of the superconducting properties of YBCO and their dependence on oxygen ordering in the structure, as well as helping to clarify the diffusion process.

Alario-Franco and Chailout (1989) suggested a simple tunnelling mechanism by which oxygen atoms move in the *b* direction along the O(5) sites. This agrees with the

work presented by Ronay and Nordlander (1988), who, by using effective medium theory found that there is no potential energy barrier for oxygen motion in the $[1/2, b, 0]$ tunnel, whereas oxygen motion in the a and c directions requires overcoming barriers of 1.7 and 1.6 eV.

Bakker *et al.* (1988), (1989) presented a thermodynamic model to describe the oxygen content and ordering in YBCO, and a solution of the Ising model yielded a slight dependence of the diffusion coefficient on partial pressure of oxygen as well as a break at the orthorhombic-tetragonal transformation.

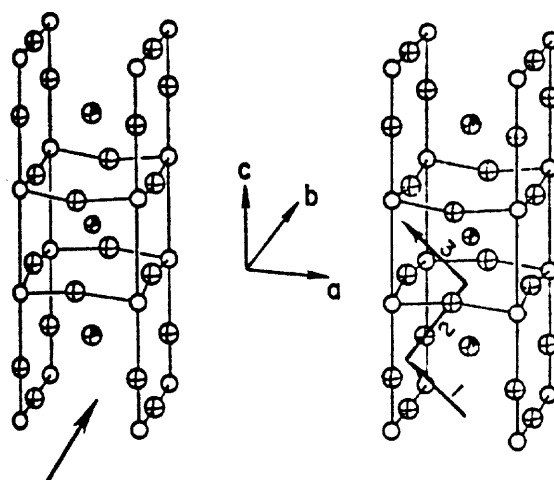


Fig 3.15 Possible routes for oxygen to move in the a and c directions (Ronay and Nordlander (1988))

Most of the studies agree in the tendency of oxygen atoms to align in chains, forming ordered regions within the material. De Fontaine and co-workers (de Fontaine *et al.* (1989), (1990-a), and (1990-b), Ceder *et al.* (1990), Asta *et al.* (1991) and Salomons and de Fontaine (1990)) used a Monte Carlo simulation of the antisymmetric next-nearest-neighbour Ising (ASYNNNI) model and a cluster variation method (CVM) to study oxygen diffusion in YBCO and related the different arrangement of the oxygen atoms in the α (along the a direction) and β (along the b direction) sublattices to the oxygen content and the critical temperature, T_c , characteristic for each oxygen concentration in YBCO and calculated a phase diagram relating the different orthorhombic ordered structures to the 60 and 90 K plateaux observed in T_c . This phase diagram is developed in more detail by Semenovskaya and Khatchaturyan (1992), who were able to distinguish not only the OI and OII phases, but also $\overline{\text{OI}}$, OIII and OIV. There is no calculation of the diffusion coefficient in the work by the group

of de Fontaine and co-workers although they predict a diffusion coefficient that depends strongly on concentration, noting the anisotropy between the diffusion along the a or b axis in the structure.

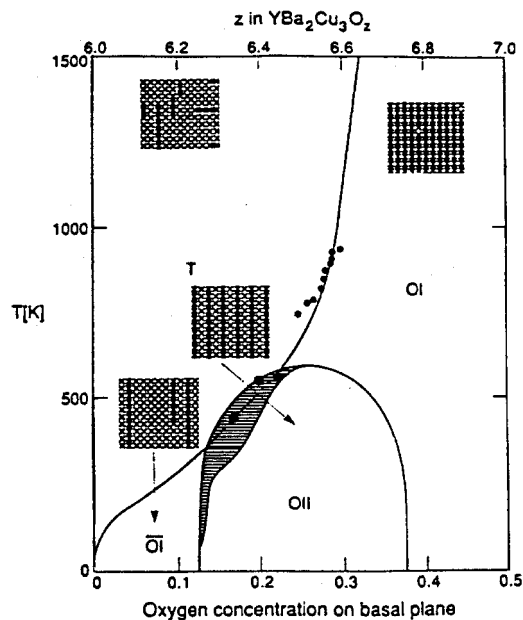


Fig. 3.16 Oxygen ordering phase diagram of YBCO (de Fontaine *et al.* (1990))

Ausloos and Pękalski (1995) also used the Ising model and they observed an irregularity in the value of the diffusion coefficient at an oxygen content of 6.5, which has already been mentioned by Bakker *et al.* (1988), (1989), as well as being noted by Salomons and de Fontaine (1990). Ausloos and Pękalski (1995) suggest that the diffusion process occurs along the Cu-O chains when the oxygen content is high (O(1)-O(1) or O(5)-O(5) jumps) and it is only at low concentrations of oxygen that O(1)-O(5) jumps occur.

Rothman and co-workers (Rothman *et al.* (1991)) propose an oxygen diffusion mechanism in which oxygen can only be removed from or be added to ends of ordered chains and move down tunnels within the crystal structure. They also suggest that the same type of jump is responsible for diffusion in the orthorhombic and tetragonal phases.

The study of the path that follows an oxygen atom in its diffusion through YBCO has been modelled by Islam (1990). The calculations yielded a series of diffusional jumps along the O(1)-O(4)-O(1) sites, which means that diffusion in the c direction would be more favourable than that in the ab plane, contradicting all the work presented so far.

A number of authors have calculated the rate of formation of oxygen vacancies at different positions in the lattice (Jorgensen *et al.* (1987-a), Capponi *et al.* (1987)), and the occupancy of the O(4), O(2) and O(3) sites is always much lower than that of the O(1) and O(5) sites, which makes diffusion along the *c* direction or in the CuO₂ planes a very restricted event.

With respect to the activation energies calculated with these theoretical methods, the scatter is not bigger than that present in other methods, varying from 0.8 eV for tetragonal YBCO (Choi *et al.* (1990)) to 1.2 eV (Salomons and de Fontaine (1990)).

It can be seen from the work reviewed in this section that no universally accepted theory of diffusion in YBCO is yet available.

3.8 Conclusions

The study of oxygen diffusion in YBCO has been carried out using a number of methods, and in spite of the large amount of work done in this field, this review chapter shows that the results presented vary considerably, in some cases up to five to six orders of magnitude.

The presence of microstructural features in the samples, such as porosity, grain size and orientation, twin density and presence of microcracks among others affect the final results of the diffusion process obtained when using certain experimental techniques (TGA, electrochemical methods, resistivity measurements). These effects are more noticeable when using polycrystalline samples, but using this type of samples is in some cases difficult to avoid, because the small size of single crystals limits the techniques that can be used.

Other techniques that are less affected by these microstructural features such as tracer diffusion and internal friction methods, however, measure a different type of diffusion coefficient: a process occurring in the absence of a concentration gradient. In order to be able to correlate these results to chemical diffusion processes it is necessary to know the value of the factors that link both types of diffusion (e.g. the thermodynamic factor – see chapter 2). The value of these factors is also subject of study but has not

been clarified completely, which makes the equivalence between diffusion in the absence and in the presence of a concentration gradient rather difficult.

A large number of studies are incomplete, only giving values of the activation energy of the diffusion process. This is an indication of how difficult it is for the oxygen ions to move in the lattice, it gives the slope of the line obtained when plotting the value of D vs. $1/T$, but it does not locate the diffusion values. It is necessary to know the pre-exponential coefficient (the intercept at $1/T = 0$ of the D vs. $1/T$ line) in order to be able to compare diffusion coefficients with each other. There are cases when the analysis of the data collected using the different techniques does not allow to calculate the pre-exponential coefficient; this limits the diffusion studies to a comparison of the activation energy values. This does not give enough to be able to use it for practical purposes of designing oxygenation stages during processing or calculating oxygenation times for different samples.

The ideal situation would be a study of the diffusion process in large single crystals; however, this is not very practical because of the extremely long times required to oxygenate them fully at low temperatures, when the equilibrium oxygen content is high and the superconducting properties can be optimised.

It has been shown that diffusion studies are very complex due to the large number of factors affecting the techniques used and because of the modifications to the diffusion behaviour introduced by the microstructural features of the samples studied. The following chapters show how a careful design of the experimental procedure can lead to a fairly complete study of the diffusion process and how these results can then be used to model the outcome of a theoretical heat treatment in terms of final oxygen concentration of the sample and distribution of oxygen within it, which can be applied to the optimisation of the oxygen content in different types of samples.

Chapter 4

Diffusion model and experimental procedure

4.1 Introduction

This chapter is divided in two sections: the first one contains a description of the diffusion model developed to reproduce the oxygenation process in YBCO. This model was written to complement the analysis of the oxygen diffusion data obtained experimentally, providing a means to follow the evolution of the distribution of oxygen within the sample as well as giving the chance to predict the outcome of hypothetical experiments and optimise the oxygenation during the cooling stage in the processing of YBCO samples (see chapter 5).

This is followed by a second section, where a brief account of the thermal analysis techniques available is given. This review concentrates on thermogravimetry, the technique chosen to study the oxygen diffusion process in YBCO. An overview of the preparation of the samples used in this work is presented, and the experimental procedure followed to carry out the diffusion study is summarised at the end of the chapter.

4.2 Modelling of oxygen diffusion in $\text{YBa}_2\text{Cu}_3\text{O}_{7-\delta}$

The aim of the present study of oxygen diffusion is to reconcile the widely scattered data present in the literature on this topic (see chapter 3). The computer programme written was developed to model the diffusion process theoretically. The diffusion study has been complemented with theoretical predictions of the outcome of oxygenating and deoxygenating experiments calculated with the model developed.

These oxygenations would have taken otherwise an unreasonable length of time to complete if they had been carried out experimentally (oxygenation of large single crystals). The use of this theoretical diffusion model is not limited to the prediction of final oxygen contents during isothermal experiments; it can also be applied to the study of the evolution of the oxygen content in multi-stage heat treatments and in non-isothermal oxygenations, where the temperature is continuously changing with time (see chapter 5).

4.2.1 Development of the model

It has been shown at the beginning of chapter 2 that heat conduction and diffusion are analogous transport phenomena. This model has been developed based on a finite element programme developed to study the heat transfer in steel specimens under the effects of a concentrated heat source (Ruiz *et al.* (1989), Rodríguez-Donoso *et al.* (1995)).

The model was initially designed for powder particles. These were assumed to be spheres of radius r . It has been mentioned in chapter 3 that diffusion in YBCO occurs more readily in the ab plane than along the c direction (Rothman *et al.* (1989)), so the sphere is divided in parallel sections a distance dh apart perpendicular to the c axis. This means that the circular faces of the flat cylinders are parallel to the ab plane (see Figs. 4.1 a) and b)). Each one of these cylinders is then divided into concentric rings separated by a distance dr .

The model calculates the rate of transfer of oxygen through each one of the rings in the discs with respect to the volume of each ring and integrates this value over the volume of the sphere.

When the distance dr is small compared to the radius of the sphere, it is possible to calculate the rate of transfer of material through a chosen element of the sample taking Fick's first law of diffusion

$$j = -D \left(\frac{\partial C}{\partial x} \right), \quad (4.1)/(2.1)$$

and applying it as follows:

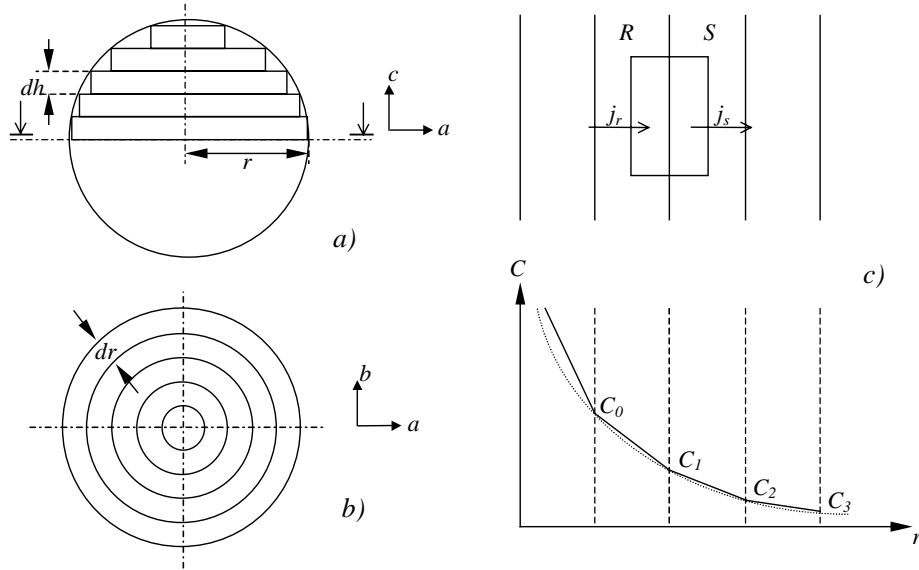


Fig. 4.1 Schematic of: a) side view, and b) top view of the divisions of the spherical particle for the model developed, and c) Fick's first law of diffusion

In a short time step, dt , the net amount of oxygen accumulated in the element shown in Fig. 4.1 c) is equal to the amount that flows in through R minus the amount that flows out of the element through S, this is:

$$j_{net} = j_r - j_s = -\frac{Ddt}{dr}(2\pi r_r dh)(2C_1 - C_0 - C_2) \quad (4.2)$$

where $2\pi r_r dh$ equals the cross sectional area of each ring of radius r , and dr and dh are the width and height of each ring, as shown in Figs. 4.1 a) and b). The variation in accumulation or loss of oxygen in the theoretical powder particle with diffusion time can be calculated integrating the above expression over the whole volume of the spherical particle.

It is assumed that the variation in concentration between the boundaries of two adjacent elements is linear and that the outer ring in each of the cylindrical slices is always at the equilibrium oxygen content for each temperature. Diffusion occurs due to the concentration gradient established within the sample and the change in the value of the diffusion coefficient with temperature. The process is not considered to be surface diffusion controlled and the effects of grain boundary diffusion or diffusion between the powder particles in agglomerates are ignored.

4.2.2 Optimisation of time increments and stability of solution

The stability of the calculation depends on the relationship between the size of the time steps, dt , and of the width of the rings, dr , in each cylindrical section.

It is necessary to find a compromise between the length of the time increments and the stability of the calculations. Computing time is reduced when the size of the time increments increases, but this decreases the accuracy of the calculations and the stability of the model.

To guarantee the stability of the model, the size of the time increment is chosen according to the dimensions of the distance elements; in this case the elements are concentric rings. Going back to Fick's first law of diffusion:

$$j = -D \left(\frac{\partial C}{\partial x} \right), \quad (4.1)/(2.1)$$

let Q be the number of oxygen atoms that pass through a plane of area A perpendicular to the oxygen concentration gradient in time dt . Substituting in the equation above:

$$Q = -AD \frac{dC}{dr} dt = -AD \frac{(C_{i+1} - C_i)}{dr} dt. \quad (4.3)$$

If N_i and N_{i+1} are the number of oxygen atoms in adjacent elements i and $i+1$, and since $C = N/V$, where V is the volume of the element considered, the above expression can be rewritten as:

$$Q = -D \frac{dt}{dr^2} (N_{i+1} - N_i) = K (N_{i+1} - N_i), \quad (4.4)$$

$$\text{this is: } K = D \frac{dt}{dr^2}. \quad (4.5)$$

The value of K needs to be chosen with care. If K is very large for a given value of dr , it would be possible to reverse the oxygen concentration gradient locally. If this happens the solution becomes unstable in the following time step.

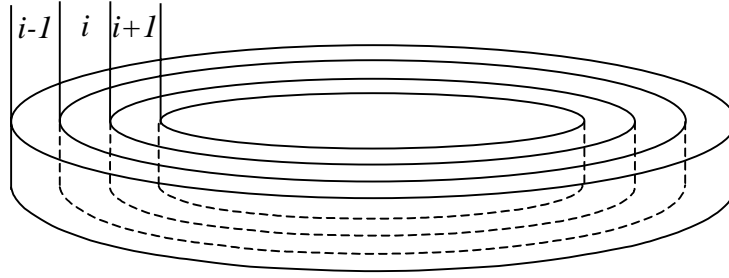


Fig. 4.2 Schematic of cylindrical elements in disk

The instability is limited to a region consisting of two adjacent elements plus first order neighbours within this time increment. In this model each element is surrounded by 2 elements. The concentration of the given finite element after a test time increment is given by $2KC_o$, where C_o is the total amount of material transferred per unit time through each step. The concentration of the first order neighbouring finite element is given by $(1-2K)C_o$; therefore, the critical value of K such that the gradient does not reverse is given by:

$$1-2K = 2K, \quad (4.6)$$

which implies that:

$$K_c = 1/2 \quad (4.7)$$

The simulation is stable provided K_c is not exceeded. For a given diffusion coefficient, the value of K is inversely proportional to the square of the distance step, dr (Eq. (4.5)). This distance is determined by the number of concentric rings into which each cylinder is divided, ka , and this number is chosen so that the inherent error introduced in the integration of the weight gain over the whole area is small. The value of kr chosen for powder particles has been 20 (so that $dr = r/20$), and that for single crystals has been 30 (with $dr = r/30$). The time interval between iterations, dt , is then chosen (see Eq. (4.5)) so that the value of K is set equal to or just below 0.5 (as shown above). Separate checks have shown no reduction in the accuracy of the fractional weight change results when the value of K was altered ($K < K_c$). Decreasing the value of K had the only effect of increasing computing time.

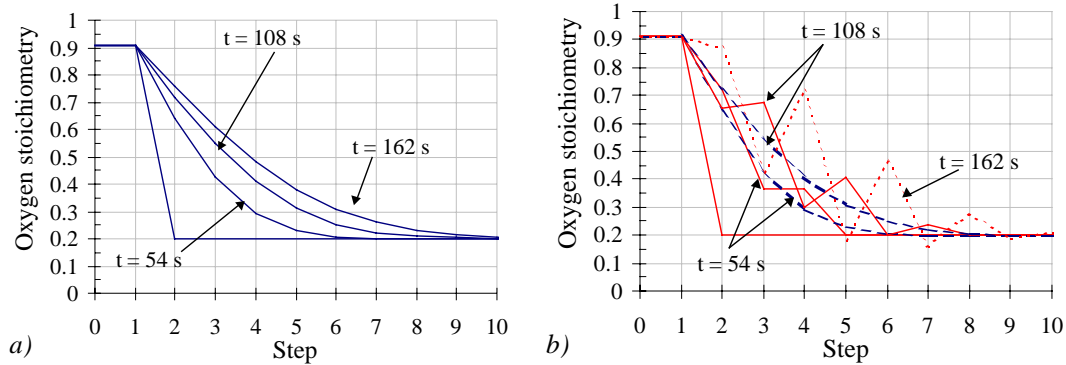


Fig. 4.3 a) Initial concentration traces for diffusion at 500 °C in a 2.1 μm radius particle when $K = 0.2$
 b) Red lines: Initial concentration traces for diffusion at 500 °C in a 2.1 μm radius particle when $K = 0.6$. Blue lines: Comparison with concentration traces shown in a)

4.2.3 Error due to the finite element method

Finite element error originates from the assumptions of the method (see 4.2.1). The first assumption made was that the concentration profile between two elements is linear, but in practice this profile is slightly curved. The second error is introduced because the centre of the oxygen distribution in an element does not quite coincide with its geometrical centre. The effect of diffusion between the agglomerated powder particles was not taken into account, as the agreement between the model for diffusion in a single particle and the experimental results is very good.

These errors are proportional to the finite element density. An increase in the number of elements in the calculation reduces the error introduced by the calculation in each step. The size of the finite elements was chosen as a compromise between the computation time and the required accuracy of the calculation.

4.2.4 Flowchart of the computer algorithm for the diffusion model

The computer algorithm was written in QBASIC. The diffusion and geometrical data necessary to do the calculations are stored as constants in the programme. These are: the pre-exponential factor of the diffusion coefficient, D_0 , the value of the activation energy, q , and the radius of the particle, r . The particle is divided into kr cylindrical sections and each cylinder into ka rings, which allows to calculate the height of the

cylindrical sections, dh , and the distance between the rings, dr . This first step also includes setting the appropriate time interval, dt , in order to avoid instability in the program at high temperatures according to what has been discussed in the previous section. A second group of geometrical factors is calculated for each cylindrical section: the external radius, volume and external surface area.

The user then inputs the initial oxygen concentration of the sample, the number of steps of the heat treatment, the initial and final temperature of each step and the time spent either changing the temperature between steps or keeping constant the temperature set at the beginning of the step.

Once the initial concentration of the particle is known, this value is set as the starting point for every ring and cylindrical slice, $C(kr,ka)$. This calculation is repeated as many times as cylinders there are (kr).

Time starts counting at this point; after each time increment the new temperature and value of the diffusion coefficient, $D(T)$, are calculated. From the variation in the equilibrium concentration profile with temperature, the program can calculate the new oxygen concentration for each ring $C(kr,ka)$ (Eq. (4.1)). This is followed by a series of iterations to calculate the change in concentration for all the rings with time and temperature. Once the concentration profile within the disc is calculated, the computer integrates the area below the curve obtained to calculate the relative weight change for that time step. This series of calculations is repeated until the whole heat treatment has been completed and the process starts again for the next disc in the sphere. Concentration profiles, times, temperatures and weight changes are exported to a file that can be read in spreadsheet form allowing the comparison between theoretical values and experimental data.

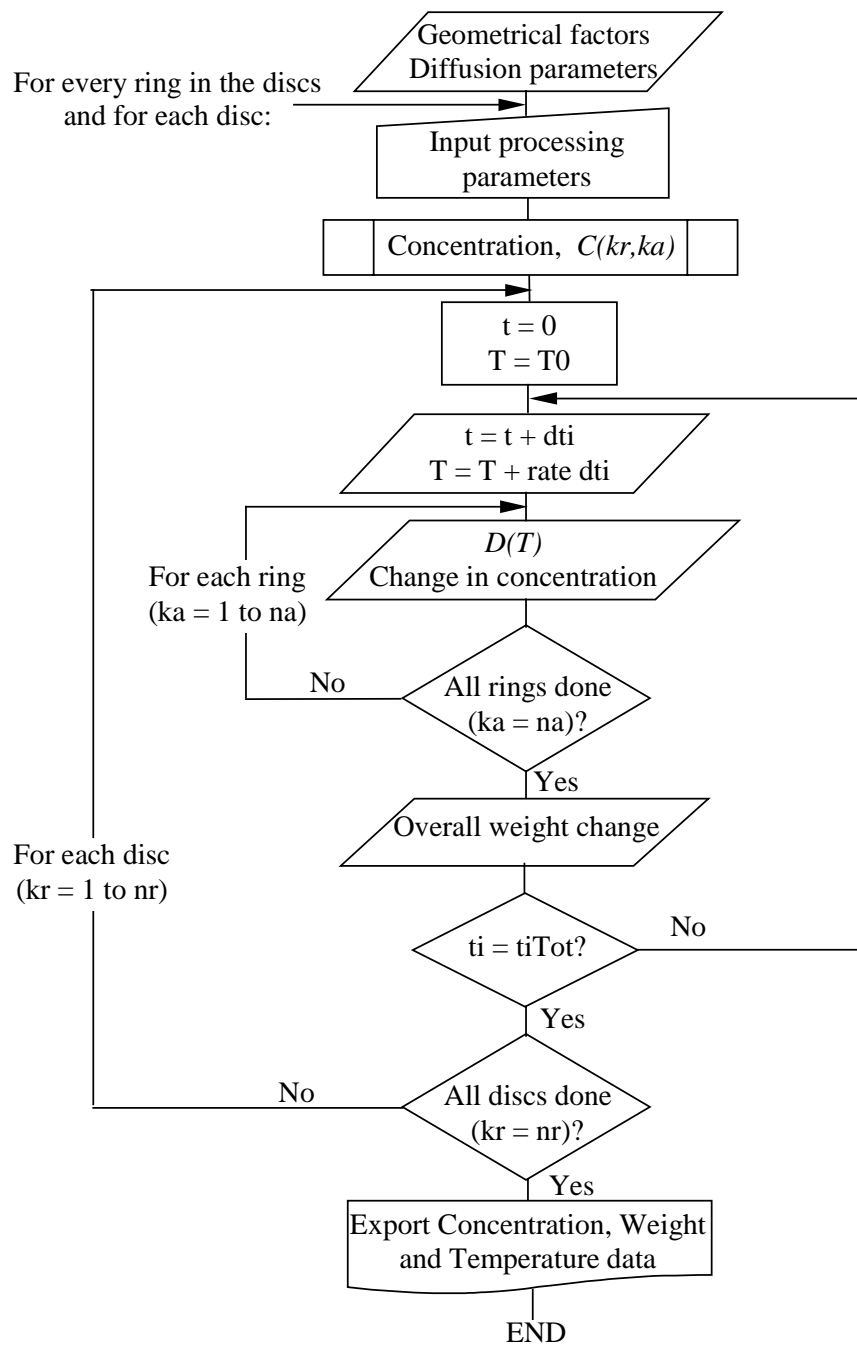


Fig. 4.4 Flowchart of the diffusion algorithm developed

4.3 Experimental techniques

The work presented in this thesis has been carried out using thermogravimetry. This section reviews this technique applied to the study the oxygen diffusion process in YBCO.

4.3.1 Thermogravimetry (TG)

Thermogravimetry (TG) a thermal analysis technique (see Table 4.1) that consists in the study of weight changes of a specimen as a function of temperature, time and/or surrounding atmosphere. This technique is used to quantify changes in weight resulting from chemical reactions, decompositions, Curie point transitions, transformations due to the interaction of a sample with the surrounding atmosphere (e.g. oxidation) and absorption or release of gases from a sample. The last application makes this technique particularly suitable for the study of the oxygen diffusion process in YBCO.

<i>Property</i>	<i>Technique</i>	<i>Abbreviation</i>
Mass	Thermogravimetry*	TG
	Derivative thermogravimetry	DTG
Temperature	Differential thermal analysis	DTA
Enthalpy	Differential scanning calorimetry	DSC
Dimensions	Thermodilatometry	
Mechanical properties	Thermomechanical analysis	TMA
	Dynamic mechanical analysis	DMA

*The term thermogravimetric analysis and its abbreviation TGA have not been accepted by the ICTA Nomenclature Committee.

Table 4.1 Thermal analysis techniques

4.3.1.1 TG design

The thermogravimetric analyser used in these experiments is a Perkin-Elmer TGA 7. This system operates between room temperature and 1000 °C. The sample size can have a maximum diameter of approximately 4 mm (bulk samples) and a volume of $\approx 12 \text{ mm}^3$ (powder specimens). The usual sample weights are 25-30 mg and according

to the manufacturer, the sensitivity of the balance is of $1\mu\text{g}$. The errors associated to the temperature and weight deviations in the system are discussed in more detail in chapter 5.

The standard thermogravimetric analyser consists of five elements: balance, temperature controller, furnace, atmosphere controller and a recording system. As it can be seen in Fig. 4.5, a sample pan (often made of Pt, Au or porcelain) is suspended from a high precision balance. In order to perform the experiments the sample pan has to be introduced in a furnace. A thermocouple is placed in the furnace very close to the pan but not touching it not to interfere with the weight measurements. The balance chamber and the furnace are placed in a hermetically sealed enclosure where the atmosphere can be controlled. Two flowmeters were connected to the gas intake for the system so that the atmosphere could be a single gas (e.g. O_2 , N_2 , Ar) or a controlled mixture of gases.

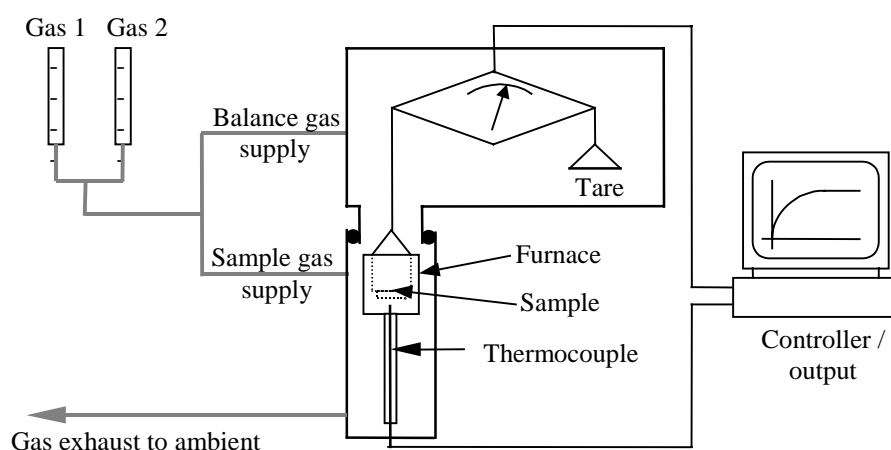


Fig. 4.5 Schematic of TGA

4.3.1.2 General operation and calibration

Thermogravimetry is a very sensitive technique and there are a number of variables that may alter the final result of the measurement and should therefore be taken into account. Experimental conditions must be carefully controlled and accurate calibration of the system is necessary.

- Control of the experimental conditions

One of the main problems in thermogravimetry is the effect buoyancy and convection currents of hot gas within the furnace enclosure may have on the final weight measurement. These effects are reduced by either altering the design of the furnace to minimise the convection currents or by keeping a certain flow rate that is, according to the manufacturer of the system, the optimum to minimise these effects. The gas flow rates recommended by Perkin-Elmer for this system are: 20 to 35 cm³/min for the sample gas supply and 40 to 60 cm³/min for the balance gas supply

It should also be taken into account that it is not possible to know the exact temperature of the sample without interfering in the weight measurement, so a general assumption must be made that the specimen is at the same temperature as the thermocouple, which, as it has been mentioned in the previous section, is located as close to the sample pan as possible.

With respect to the samples used, it is advised that the sample size is maintained approximately constant in all experiments. It is necessary to know the properties of the sample in advance and whether the reaction rate is going to be affected by the state of aggregation (powder, polycrystalline) of the specimen. Such is the case of diffusion experiments, where the use of polycrystalline samples modifies the results; this will be covered in more detail in the following chapter.

- Calibration

Thermogravimetric analysers are calibrated for weight and temperature. There is no accepted standard for weight and temperature calibration, and it is usual that the manufacturer supplies weight and temperature standards to calibrate the instrument.

Ferromagnetic samples with different Curie points are used for the temperature calibration of the TGA. These samples are placed in the balance and the total weight of the sample is altered by placing a magnet outside the furnace. When the temperature increases above the characteristic Curie point of the specimens, they lose their ferromagnetic properties and are no longer attracted by the magnet. This results in a sudden change in weight in the measurement recorded. The use of several

ferromagnetic materials is advised in order to extend the calibration over as wide a temperature range as determined by the experiments to be carried out.

With respect to the variation of temperature with time, it is very important to note that the heating rate modifies the lag of the sample temperature behind the programmed temperature. It is therefore necessary to quantify the magnitude of this temperature difference as a function of heating rate. Curie point measurements can also be used for this purpose. The difference between the thermocouple reading and the real Curie temperature of the sample at different heating and cooling rates gives the value of the temperature lag for each ramp rate. Results obtained on heating at several rates are shown in Fig. 4.6. The lag observed for the Fe sample, with a Curie temperature of 780 °C is much higher than that for Ni or Perkalloy, with lower Curie points. The temperatures at which the experiments are carried out in this work are in a lower temperature range: 300 to 550 °C. Therefore, the lag in the temperature measurements carried out in this work will never be higher than 20 °C.

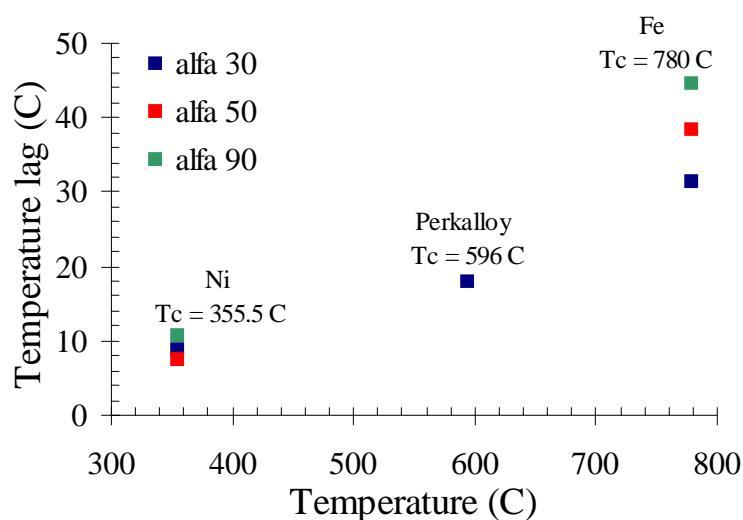


Fig. 4.6 Increase in thermal lag with heating rate for samples with different Curie temperatures.

4.3.1.3 TG data analysis

There are a number of ways of analysing the data collected in TGA measurements. One of the methods involves comparing the curves obtained to a set of already defined curves that have been formulated to describe the behaviours of transformations controlled by different mechanisms, such as boundary controlled growth or first or

second order reactions. However, this method is not appropriate for the series of experiments carried out in this dissertation since it is not known what mechanism controls the diffusion of oxygen in and out of $\text{YBa}_2\text{Cu}_3\text{O}_{7-\delta}$. The microstructure of the sample used can modify the value of the oxygen diffusion. It has been seen from the scatter in the data shown in chapter 3 that diffusion is a complex process regulated by different factors that vary with temperature: in bulk polycrystalline samples, for example, it is controlled by grain boundary diffusion at low temperatures, with the contribution from bulk diffusion becoming more important as the temperature increases. The point at which these two mechanisms overlap is not known, and assuming that only one of the two controls diffusion would be incorrect. Chapter 5 is going to present the possible ways of carrying out diffusion studies that are not affected by the microstructure of the samples.

The second method of analysis that can be used involves comparing the experimental data to the profile and weight gain obtained using the solution to Fick's second law that is formulated according to the conditions present in the experiments (see chapter 2 for the different boundary conditions and solutions to the diffusion equation). The study of initial rates of sorption and desorption also gives an approximation of the diffusion coefficient. This is the analysis used in this thesis and its results are described in more detail in the following chapter.

4.4 Materials and processing

The material used for these experiments was $\text{YBa}_2\text{Cu}_3\text{O}_{7-\delta}$ in powder, polycrystalline and single crystal form.

4.4.1 Powder

The powder used in the experiments was supplied by Seattle Speciality Ceramics, Inc. (SSC). The manufacturer states in the specifications that the stoichiometry of the material is $\text{YBa}_2\text{Cu}_3\text{O}_7$, which has been confirmed with X-ray diffraction analysis.

The particle size of the powder was measured using a Malvern Instruments Particle analyser SB.0C and it has been found that the average particle diameter is 5.2 μm , and the range of particle sizes present in more that 50 % in weight oscillated between 3 and 9 μm in diameter (see Fig. 4.7).

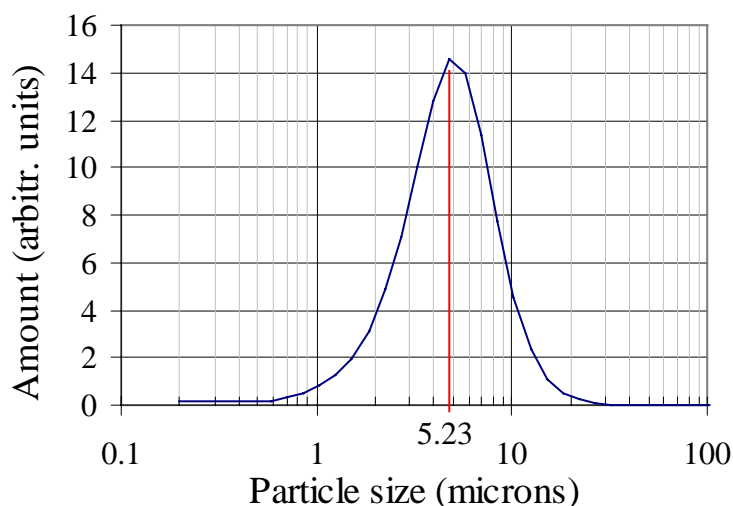


Fig. 4.7 Particle size distribution in SSC powder

Fabrication processes normally start with a homogeneous powder of a suitable particle size. Powder is frequently made using a solid state reaction method that involves calcining oxide and carbonate precursors (Y_2O_3 , BaCO_3 , CuO) mixed in the right proportions. After the precursor powder is calcined at temperatures near 900 $^\circ\text{C}$ in O_2 , the resulting material may contain secondary phases and unreacted components. The grinding and calcining steps are repeated a number of times in order to completely react the components into a phase pure powder. The YBCO powder used in this experiments (see Fig. 4.7) was made following a slightly different technique, in order to eliminate the effect of repeated grinding and calcining on the quality of the sample. This technique combines solution, spray drying and combustion synthesis to produce a homogeneous precursor powder consisting of an intimate mixture of Y_2O_3 , BaCO_3 and CuO (see Fig. 4.8). These powder particles were subsequently calcined and converted to phase pure $\text{YBa}_2\text{Cu}_3\text{O}_7$.

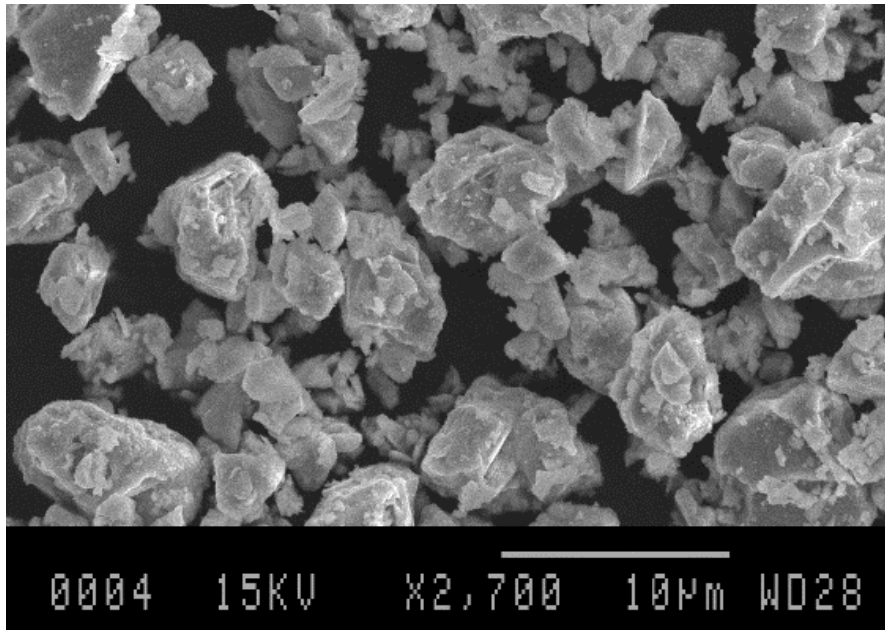


Fig 4.7 SEM micrograph of the $\text{YBa}_2\text{Cu}_3\text{O}_{7.8}$ powder used in this thesis. Average poarticle size: $5.23\mu\text{m}$

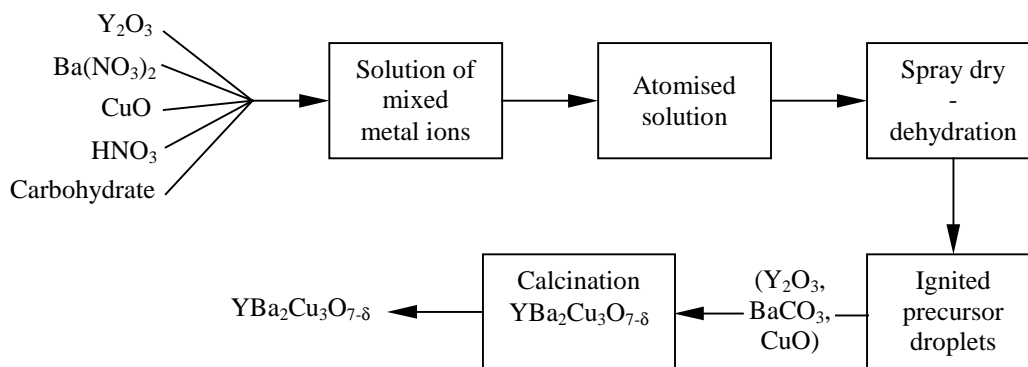


Fig 4.8 Powder processing

Other alternative techniques to produce YBCO powder have been reviewed extensively in Bourdillon and Bourdillon (1994) and Shi (1995).

4.4.2 Polycrystalline samples

The SSC powder was pressed at 50-76 MPa for two to five minutes to make pellets and slabs that were sintered in oxygen in a tube furnace to produce polycrystalline samples of different final densities. Before sintering the pellets were 1 cm in diameter and had a thickness of around 4 to 5 millimetres. The rectangular slabs were 5 cm long and 3 cm wide. The thickness was usually around 5-6 mm. Densification takes place during sintering and the final volume decreases 15-25 %.

Sintering depends strongly on temperature, and the choice of sintering temperature is determined by the phase equilibrium diagram of the Y-Ba-Cu-O system. It is important to have in mind that YBCO melts incongruently (decomposes peritectically into solid Y_2BaCuO_5 and an Y-poor liquid phase) at around 1000 °C (see Fig. 4.9 b)). Lindemer *et al.* (1991) review work done studying the decomposition of YBCO and on the dependence of phase stability on the partial oxygen pressure of oxygen, and they present a phase stability region depending on partial oxygen pressure and temperature shown in Fig. 4.9 a).

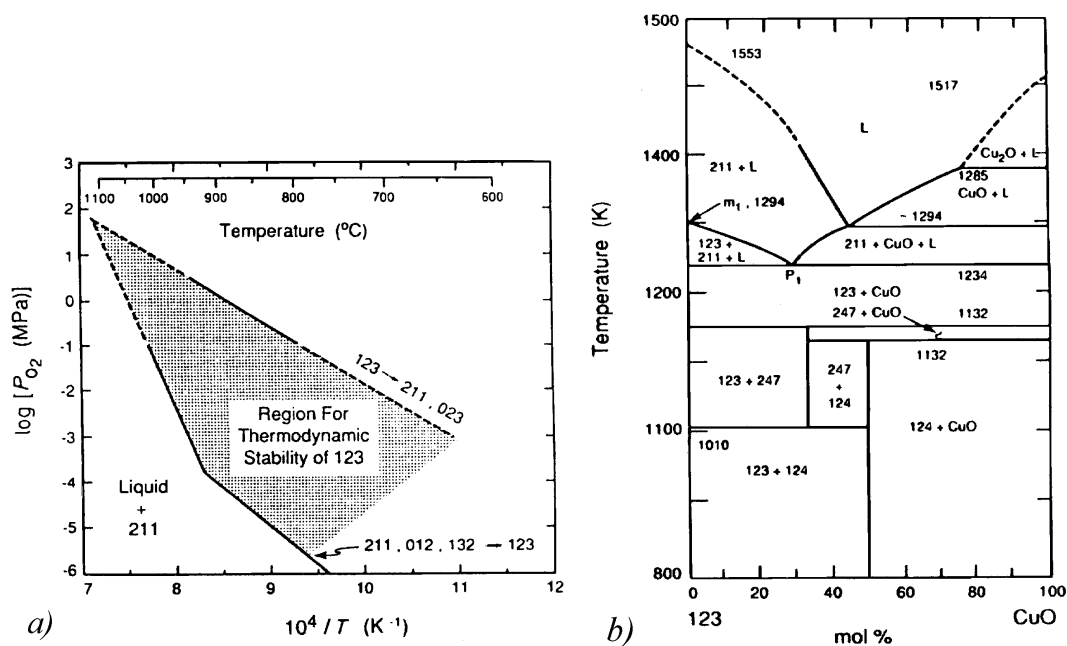


Fig 4.9 a) Temperature oxygen partial pressure stability regime for YBCO, b) YBCO-CuO section of CuO-BaO- Y_2O_3 diagram at 10^5 Pa (after Lindemer *et al.* (1991))

There are certain processing methods that require the formation of a liquid phase to favour the formation of textured grains (melt texturing or flux growth methods) (Salama *et al.* (1994)). However, for this study it was necessary to produce a series of polycrystalline specimens with different densities so that it is possible to evaluate the effect of porosity and of the presence of grain boundaries in the diffusion process, therefore the formation of liquid phase during the sintering process was avoided.

The heat treatments consisted in a series of ramps at 240 °C/min to 950, 940 and 930°C, holding the samples at that temperature for 10-12 hours in a 100 % oxygen atmosphere and leaving the sample to cool in the furnace to room temperature. The densities of the samples were measured with a pycnometer and they were found to

range between 81 % and 94 % of the theoretical density. Samples with densities below 91 % of the theoretical density exhibit open porosity whereas above this value the pores between the grains are closed.

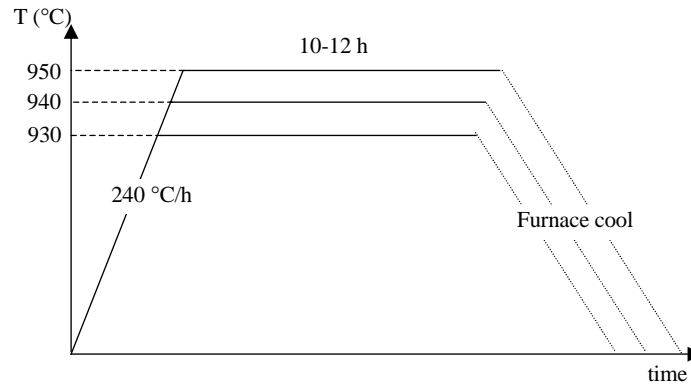


Fig. 4.10 Schematic of sintering process in 1 atm O_2

4.4.3 Single crystals

The single crystals were kindly supplied by Dr. Chen of the Clarendon Physics Laboratory in Oxford. These crystals were grown by the flux growth method in a $BaZrO_3$ crucible with the following heat treatment: heated to 920 °C and cooled (in air) to 600 °C at 100 °C/h, then from 600 to 400 °C cooled at 10 °C/h and to room temperature again at 100 °C/h, and ranged in size between 250 μm to a few millimetres.

Fig. 4.11 Single crystal 0.3 mm

4.5 Characterisation techniques

The characterisation techniques reviewed in this section were used regularly during the course of the measurements to corroborate the results obtained using thermogravimetry.

4.5.1 Microscopy

Optical microscopy was used to examine the microstructure of the polycrystalline samples and single crystals. The best viewing conditions for the microstructure of YBCO exist in reflected polarised light. In these conditions the high-oxygen orthorhombic phase shows a characteristic twinned structure. This structure is a consequence of the accommodation of the stress generated in the crystal structure when the lattice parameters of the unit cell change during the oxygenation process (see chapter 1).

The extent of the twinning gives an idea of the degree of oxygenation of the grains/single crystals. The tetragonal regions have lower oxygen content and appear untwinned.

Camscan S2 electron microscopes were used in examination of the shapes of powder particles as well as fracture surfaces of polycrystalline pellets. All images were formed at a beam intensity of 40 kV.

4.5.2 X-ray diffraction

The diffraction patterns of specimens were taken using a Philips PW1370 vertical diffractometer. Powder samples were mounted on a silicon substrate to eliminate background signals and polycrystalline samples were directly mounted on the sample holder aligned to the correct position in the diffraction cell.

Continuous θ - 2θ scanning was carried out over the 2θ range $10^\circ < 2\theta < 100^\circ$, and plots of X-ray intensity against 2θ were obtained. Step scans were also carried out. Scan rates of $0.02^\circ/\text{min}$ and preset times of 2-4 seconds were employed and the data was also plotted in intensity vs. 2θ angle graphs. The 2θ range used was the same as in

the continuous scans ($10^\circ < 2\theta < 100^\circ$). The long counting times over narrow angular ranges allowed to measure the peak positions precisely. Peak data were used to estimate the oxygen stoichiometry in YBCO, calculating the lattice parameters from the characteristic peak positions.

4.5.3 T_c measurements

An AC magnetic induction method can be used to monitor the diamagnetic response of a sample placed between two induction coils. This response is directly related to the oxygen content of the sample. The equipment used for making these measurements was a ‘Lakeshore Cryotronic’ AC Susceptometer. The sample under study was initially cooled in zero field. Then an a.c. signal of 333.3 Hz frequency and 79.6 A/m was applied to the coils, and both the in-phase and out-of-phase components of the magnetic susceptibility were recorded on heating the samples from approximately 4 K to 100 K at 3 K/min.

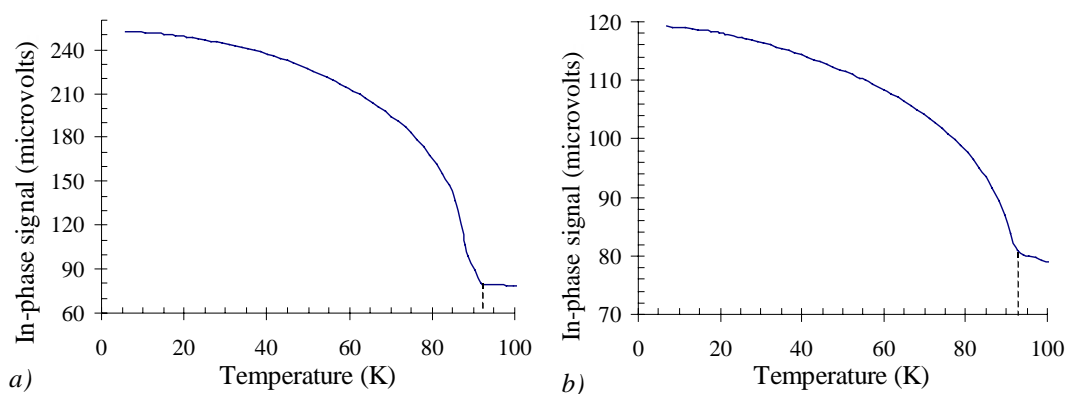


Fig. 4.13 AC susceptometer traces of powder oxygenated at: a) 400 °C in pure oxygen and b) in a 20%O₂-80%Ar mixture at 450 °C. Note how in spite of the different oxygen contents of the samples (6.97 and 6.9 respectively) the T_c appears to have the same value for both, when, according to Poulsen *et al.* (1991) a decrease in the T_c should have been observed in the sample oxygenated at the lower partial oxygen pressure and higher oxygenating temperature (b)).

Measurements were carried out on a number of samples with a range of oxygen contents, from fully oxygenated at 400 °C to fully deoxygenated in Ar at 900 °C. Fig. 4.12 shows the results obtained from a sample oxygenated in pure oxygen at 400 °C and another powder sample oxygenated in 20 % O₂ at 450 °C. Both samples appear to have the same critical temperature. It has already been pointed out in chapter 1 (see section 1.3, Table 1.1) that there is a certain degree of uncertainty in the literature

concerning the relationship between oxygen content and critical temperature of YBCO samples; therefore, it was decided not to use this technique to determine accurately the oxygen contents of the specimens.

4.6 Experimental procedures

4.6.1 Deoxygenation of samples

In order to be able to study the oxygenation behaviour of YBCO it was necessary to produce oxygen-poor samples before carrying out the oxygenating experiments. Deoxygenation of powders, polycrystals and single crystals was done heating the specimen in Ar at 50 °C/min to either 750 or 800 °C, and holding the specimen at that temperature until no further weight change was observed. The samples were cooled to room temperature at 50 °C/min.

4.6.2 Isothermal experiments

The aim of these experiments was to be able to calculate a value for the diffusion coefficient that could be used later on to analyse the rest of the data collected:

4.6.2.1 Powder samples

Due to the small particle size of the powders it was not possible to heat powder samples to a very high temperature, as the sample reached the equilibrium oxygen content before it was heated to the final temperature set. Therefore, the range of temperatures had a maximum limit of 450 °C. This is a consequence of the increase in diffusion coefficient with temperature (these aspects are covered in more detail in chapter 5).

The powder was heated at a ramp rate of approximately 90 °C/min to 300, 350, 400 and 450 °C and it was held at those temperatures until no further weight change was observed. The sample was subsequently cooled at a rate of 90 °C/min.

Additional experiments at different partial oxygen pressures were also carried out. The pressures chosen were 20%, 50%, and 80% O₂ in Ar.

4.6.2.2 Single crystal samples

The size of the single crystals used ranged between 212 μm to ≈ 7 mm. Their larger size (diffusion distance) compared to the powder specimens increased the time it took to equilibrate the samples in the low temperature range. Therefore, these single crystals were used to study the oxygenation behaviour at the temperatures that were too high for powder samples. The heating and cooling procedure is the same as for the powders, with higher equilibration temperatures: from 400 to 550 °C. Data from these experiments are combined with those from powder samples to be able to study the diffusion process over a wide temperature range. All of these isothermal runs were carried out in a pure oxygen atmosphere.

4.6.2.3 Polycrystalline samples

The oxygenation experiments using polycrystalline samples were carried in the same temperature range as the powder specimens (300 to 450 °C) in spite of their larger particle size. The ramp rates during oxygenation (heating and cooling) were 90°C/min.

4.6.3 *Non-Isothermal experiments*

Non-isothermal experiments were carried out on powders, polycrystals and single crystal samples. After having deoxygenated the specimens, they were heated up to 700°C at the following ramp rates: 1, 10, 30, 50 and 90 °C/min. The samples were held at 700 °C until no weight change was observed and they were cooled at the same rate as they were heated up. These experiments were also carried out in a pure oxygen atmosphere.

4.7 Conclusions

This chapter has presented a description of the diffusion model developed to become a theoretical basis of the study of oxygen diffusion in YBCO. The model will be used to predict the oxygen contents of the samples after oxygenation and the distribution of these contents within the samples used. It will also provide with a means to optimise oxygenation times during processing (see chapter 5).

Thermogravimetry, the experimental technique used in this thesis for the study of oxygen diffusion has been presented. This is followed by a description of the YBCO powder and single crystals specimens as well as the preparation method of the bulk samples used in these experiments. The chapter concludes with a description of the experimental methods followed in the course of the experiments, covering the deoxygenation pre-treatment and the isothermal and non-isothermal oxygenations carried out.

Chapter 5

Results and discussion

5.1 Introduction

This chapter presents the experiments performed in this diffusion study and discusses the results obtained. Their analysis is used to clarify the current situation on the value of the oxygen diffusion coefficient in $\text{YBa}_2\text{Cu}_3\text{O}_{7-\delta}$. It has already been shown (chapter 3) that the scatter in values of \tilde{D} published is quite large. The aim of this thesis is to study the reasons behind this scatter as well as to give a value for the chemical diffusion coefficient that is not affected by compositional or microstructural features.

The results presented were obtained from diffusion studies carried out with powder, single crystal and polycrystalline samples. These are discussed for experiments done under isothermal and non-isothermal conditions. The section that describes the diffusion analysis done on powder samples includes a comparison of the experimental results with those from the theoretical calculations obtained with the model of the oxygenation process developed (see chapter 4).

The final section of this chapter is dedicated to further applications of the model for hypothetical oxygenation experiments. These have been performed to optimise the oxygenation step during the processing of YBCO.

5.2 Isothermal experiments

The purpose of this first set of experiments was to calculate a value for the diffusion coefficient of YBCO. The expression for D obtained will be used later on to analyse the rest of the data collected and it will become a reference value for future applications.

The technique used in these experiments was thermogravimetry (see chapter 4 for experimental procedure followed). Monitoring the rate of change of the sample weight it is possible to calculate the value of the chemical diffusion coefficient of oxygen in YBCO (see chapter 2).

The state of aggregation of the sample can alter the final result of the measurements, so it is necessary to make the following considerations:

The use of polycrystalline samples introduces a large number of factors whose effects on diffusion are unknown or difficult to measure, such as the effect of porosity (open and closed), the presence of grain boundaries, the temperature region in which grain boundary diffusion is dominant (short-circuit diffusion), the presence of a range of grain sizes within the sample, etc.

These microstructural parameters could be eliminated if a more simple form of the material was chosen: for example, a single crystal. Unfortunately, the large sizes of these crystals increase diffusion times so much that the experimentation times are prolonged beyond practicality. The duration of the experiments can be decreased increasing the diffusion temperature, but it would be more interesting if, instead of extrapolating high-temperature results to the low temperature regions, the experiments could be carried out at these lower temperatures, closer to those at which the samples would achieve a high level of oxygenation. It has already been mentioned in chapter 1 that highly oxygenated samples have good superconducting properties. The distribution of this oxygen within the sample to optimise the superconducting properties is very important, the aim being an evenly distribution of oxygen within the material.

Using YBCO in powder form solves most of these problems as each powder particle is a very small single crystal. This allows one to study of the diffusion process at low temperatures with more reasonable oxygenation times.

These points explain the strategy followed in this diffusion study. The first part is dedicated to the oxygenation of powder; this is followed by a study of the oxygenation of small single crystals and polycrystalline samples of different densities.

The following sections are going to deal with the experiments performed and the analysis of the results obtained in this study of oxygen diffusion in YBCO.

5.2.1 Powders

Section 4.3.1 describes the fabrication process of the YBCO powder used. Its final particle size ranges between 2 and 10 μm in diameter (see Fig. 4.7).

In order to standardise the initial condition of the specimens used, all of them were deoxygenated beforehand. The samples were heated in the thermogravimetric analyser (TGA) in Ar up to temperatures between 700 and 800 $^{\circ}\text{C}$, and maintained at that temperature until no further weight change was observed. At the end of the deoxygenation stage they were cooled at 90 $^{\circ}\text{C}/\text{min}$ to room temperature.

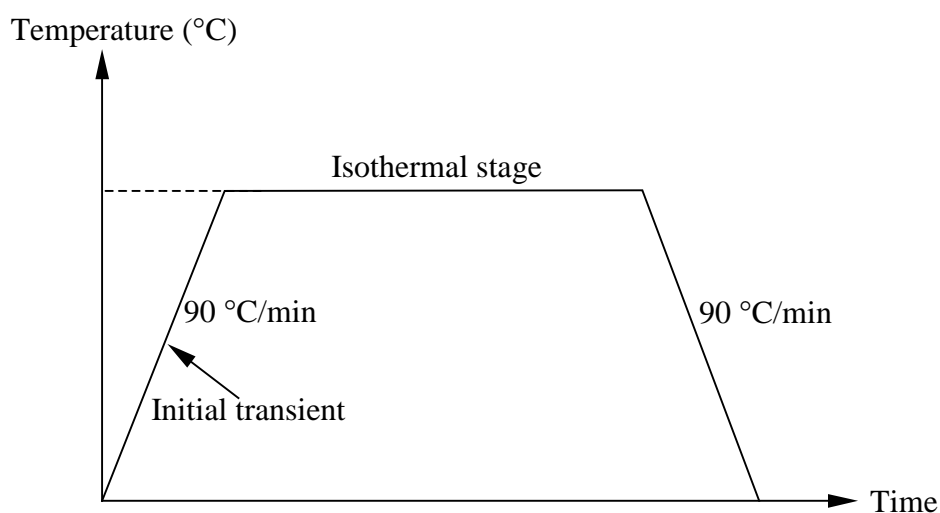


Fig. 5.1 Schematic of isothermal heat treatment

During the isothermal heat treatments the weight changes experienced by the powder samples were recorded with respect to time and temperature. The samples were heated in pure oxygen at 90 $^{\circ}\text{C}/\text{min}$ to the temperature chosen for the oxygenation study (Fig. 5.1), held at this temperature until the weight stabilised and cooled to room temperature at the same rate of 90 $^{\circ}\text{C}/\text{min}$.

The particle size of the powder used limits the temperature range of the experiments ($D \approx x^2/t$); for a same value of the diffusion coefficient, if the particle size is small, the diffusion distance is short and oxygenation times are shorter. Since the value of the diffusion coefficient increases with increasing temperature, if the oxygenating

temperature chosen is high, diffusion of oxygen will occur more readily. This process could speed up so much that the amount of oxygen absorbed during the initial ramp to the isothermal stage (heating transient) is so high that no information about \tilde{D} can be drawn from the isothermal stage. Section 5.3 explains how this absorption of oxygen during the heating stage can also yield information about \tilde{D} and be applied to optimise the oxygenation stage during the processing of YBCO.

This section, however, deals with the analysis of the diffusion process under isothermal conditions, so the aim is to be able to reduce the amount of oxygen absorbed during the initial heating transient. It was observed that if the isothermal temperature was higher than 450 °C, the amount of oxygen absorbed at constant temperature was too small (and if the temperature was increased high enough, even non-existent) to be able to carry out any diffusion analysis of the data collected. 450°C was therefore taken to be the upper limit of the range of temperatures chosen.

The lower limit is again determined by the length of the oxygenation steps (given the particle size of the sample), and it was taken to be 300 °C. The isothermal experiments were done at 300, 350, 400 and 450 °C; weight gain of the powder samples was recorded with time and when their weight stabilised, the samples were cooled at 90 °C/min to room temperature. A typical weight gain trace is shown in Fig. 5.2.

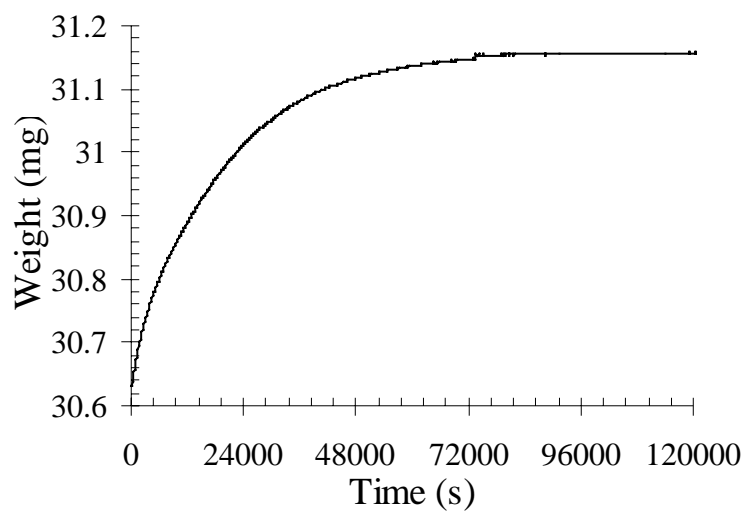


Fig. 5.2 Oxygenation of powder at 300 °C (isothermal temperature reached after ≈ 180 s)

Once the weight variation with time was obtained, the next step was to calculate the diffusion coefficient characteristic for each temperature. A number of methods have been used and their results are going to be reviewed in the following section.

5.2.1.1 Diffusion in a slab and in a cylinder

It has already been described in chapter 2 how setting the appropriate boundary conditions to Fick's second law it is possible to obtain an expression that describes the diffusion process in the system considered.

The first condition taken for this work is that the diffusion coefficient is independent of concentration. Some groups have observed that the diffusion coefficient depends on the oxygen content of the sample but there is no agreement between the authors in the type of variation, as some say it increases with decreasing oxygen content while others do not observe this behaviour (see chapter 3 for a review of the results published in the literature). It has been considered that the variation of \tilde{D} with concentration will never be as large as the existing scatter of seven orders of magnitude present in the values of \tilde{D} itself, so for this study it has been assumed that \tilde{D} is independent of concentration.

Diffusion in YBCO takes place preferentially in the *ab* plane, diffusion in the *c* direction being approximately 10^6 times slower. Therefore, it was decided that the initial theoretical study of the value of \tilde{D} could be characterised as a diffusion in a plane sheet.

To calculate the solution to Fick's second law in this case, the concentrations at the surfaces of the sheet are considered to be constant and equal throughout the experiment. The initial concentration of diffusing substance is constant within the sheet, and it is assumed for simplicity that the size of the sheet does not change during the absorption process (see chapter 2).

The solution of the diffusion equation with these boundary conditions is:

$$\frac{M_t}{M_\infty} = 1 - \sum_{n=1}^{\infty} \frac{8}{(2n+1)^2 \pi^2} \exp\left(-\tilde{D} \frac{(2n+1)^2 \pi^2 t}{4l^2}\right), \quad (5.1)/(2.32)$$

where M_t is the total amount of material absorbed at time t , M_∞ is the material absorbed after infinite time, and l is one half of the sheet thickness.

Substituting in (5.1) the known values of powder particle size, l , and time it takes to equilibrate the oxygen content of the sample for each temperature it is possible to generate a series of oxygenation profiles (fractional weight change, M_t/M_∞ , vs. t) that vary with the value chosen for the diffusion coefficient, as it can be seen in Fig. 5.3

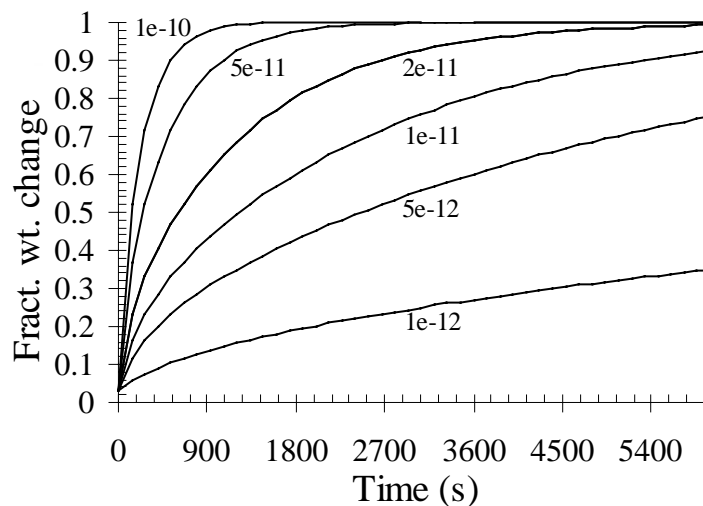


Fig. 5.3 Variation in weight gain during oxygenation with different diffusion coefficients for a particle with a $5 \mu\text{m}$ radius. Numbers next to curves are the values of D for each case (cm^2/s)

If instead of a flat sheet a cylindrical geometry was considered, this diffusion analysis would be carried out following the same steps using the solution for diffusion in a cylinder (Eq. (5.2)). This is going to be covered in more detail later in this section.

Comparing the theoretical and experimental curves and changing the value of the diffusion coefficient of the theoretical curve, it is possible to find a value of \tilde{D} for which the difference between both curves is minimum. Repeating this process for each one of the experiments carried out at 300, 350, 400 and 450 °C we obtain a series of values for the diffusion coefficient at each temperature.

Fig. 5.4 shows one of the comparisons made between the experimental data and the result of the solution to the diffusion equation for a particle $5.2 \mu\text{m}$ wide. It can be seen how the fit is very good. The graph includes two extra theoretical absorption curves that show how the choice of the diffusion coefficient with this method does not

introduce a large error in the calculations. A small variation in the value of \tilde{D} has a pronounced effect on the shape of the fractional weight change curve.

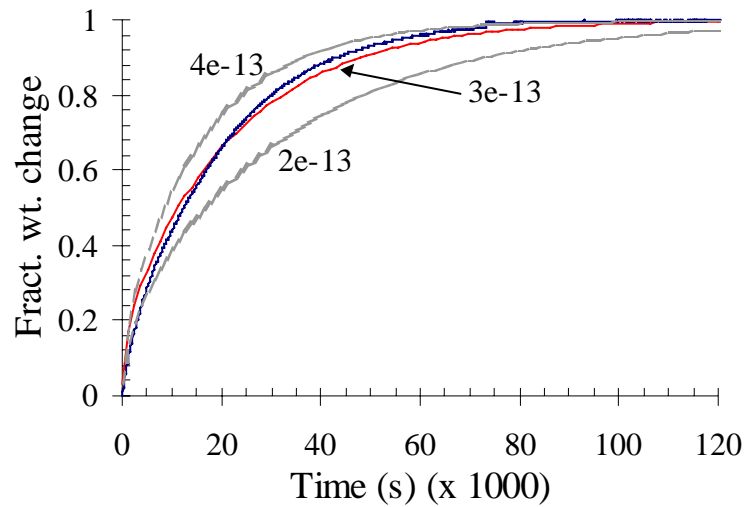


Fig. 5.4 Comparison between weight gain traces of an experimental oxygenation of powder at 300 °C (in blue) and the theoretical calculation of the same oxygenation using the solution to the case of diffusion in a flat sheet (in red). Diffusion distance: 2.6 μm ; $\tilde{D} = 3.0 \times 10^{-13} \text{ cm}^2/\text{s}$. Two extra theoretical lines with their respective values of the diffusion coefficients (in cm^2/s) are included for comparison (for the same diffusion distance)

It has already been described in chapter 4 that the diffusion model developed divides the powder particles into disks to carry out the diffusion calculations. It was thought necessary to assess the difference in the values of the diffusion coefficient when using a cylindrical geometry instead of a flat sheet.

Fig. 5.5 shows the two different situations considered: in the case of the sheet, diffusion occurs only in one direction, whereas in the case of a cylinder, the concentration gradient moves towards the centre of the cylinder in all directions.

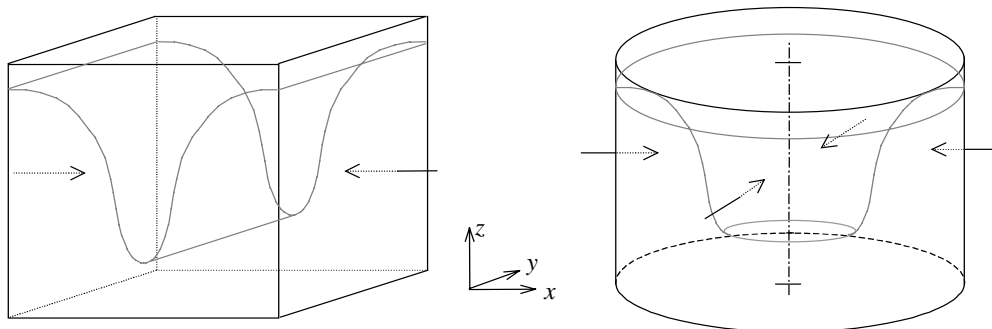


Fig 5.5 Diffusion in flat sheet and cylindrical geometries

The solution of the diffusion equation for this cylindrical geometry with the same boundary conditions mentioned above, takes the form:

$$\frac{M_t}{M_\infty} = 1 - \sum_{n=1}^{\infty} \frac{4}{a^2 \alpha_n^2} (-\tilde{D} \alpha_n^2 t), \quad (5.2)$$

where M_t and M_∞ are defined as in the previous case, a is the radius of the cylinder and α_n are the roots of $J_0(a\alpha_n) = 0$, where $J_0(x)$ is the Bessel function of the first kind of order zero. The values for these roots are tabulated in B.A.A.S., Mathematical tables, Vol. X (1952).

Following the same procedure as with the solution for sorption in a flat sheet, a series of curves is obtained, and these match the plots of experimental weight gain with respect to time (Fig. 5.6). The overlap of both curves is again very good. The diffusion coefficient obtained with the flat sheet solution is slightly faster than that obtained with the cylindrical geometry difference. It can be seen in Fig. 5.5 that a flat sheet with the same width as the radius of a cylinder can absorb more oxygen. This gives rise to a faster diffusion coefficient so that equilibrium is achieved in the same length of time. It is going to be seen in section 5.2.1.2 that the difference between both values is within the limits of the error introduced due to the change in particle size.

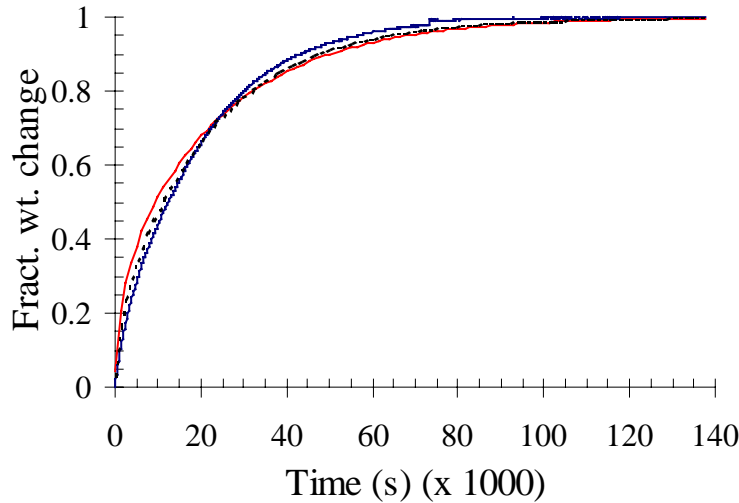


Fig. 5.6 Comparison between experimental (blue) and theoretical cylindrical geometry (red) weight gain when oxygenating at 300 °C (radius = 2.6 μm); $\tilde{D} = 1.5 \times 10^{-13} \text{ cm}^2/\text{s}$. Dashed line shows the solution for diffusion in a flat sheet (diffusion distance = 2.6 μm); $\tilde{D} = 3 \times 10^{-13} \text{ cm}^2/\text{s}$

From the above comparisons between experimental and theoretical diffusion model data it can be seen that the diffusion process is not surface reaction dependent. Neither of the theoretical solutions chosen describe a surface reaction limited process and the agreement with the experimental data is very good. Chemical diffusion occurs as a result of the presence of a concentration gradient in the sample, therefore it does not seem reasonable that the outer part of the sample oxygenates fully leaving the inside deoxygenated and that after this has occurred, diffusion proceeds slowly as a highly oxygenated front moving towards the centre of the specimen, as some authors suggest (Furukawa *et al.* (1992), Ikuma and Akiyoshi (1988), for example).

The diffusion process occurs in the presence of a decreasing gradient of oxygen content towards the centre of the sample. The value of the gradient will become smaller as diffusion continues until the sample is fully oxygenated and the oxygen content is uniform throughout. This will be seen more clearly in section 5.2.1.5 (see Fig. 5.18 for an example of evolution of concentration profiles within samples).

It should be considered that to do these calculations it has been necessary to input not only the value of \tilde{D} , but also the particle size (the diffusion distance). Since the powder used contains a range of particle sizes, the value of \tilde{D} was calculated for a number of them in order to find an average for the value of \tilde{D} that could describe the diffusion process with the minimum error possible. Table 5.1 shows the results of the calculations for these particle sizes. It can be seen how the difference between the values of \tilde{D} is always less than an order of magnitude. The choice of the maximum and minimum particle size is done according to the particle size distribution of the powder (see Fig. 4.7). 50 % of the powder particles have radii between 4.5 μm and 1.5 μm ; therefore these have been chosen to be the upper and lower error limit for the diffusion coefficient.

From the calculations of the average \tilde{D} calculated it is possible to obtain an expression of the diffusion coefficient from the slope (the activation energy) and intercept (pre-exponential factor) of a plot of the logarithm of these \tilde{D} values against $1/T$. The Arrhenius expression for the calculated \tilde{D} is:

$$\tilde{D} = 0.033 \exp(-1.24(\text{eV})/kT) \quad (5.3)$$

Temperature (°C)	$\tilde{D}_{1.5\ \mu\text{m}}$ (cm^2/s)	$\tilde{D}_{2.6\ \mu\text{m}}$ (cm^2/s)	$\tilde{D}_{4.5\ \mu\text{m}}$ (cm^2/s)	Average (cm^2/s)
300	1.0×10^{-13}	3.0×10^{-13}	9.4×10^{-13}	4.5×10^{-13}
350	9.3×10^{-13}	1.9×10^{-12}	5.6×10^{-12}	2.8×10^{-12}
400	4.9×10^{-12}	9.5×10^{-12}	2.8×10^{-11}	1.4×10^{-11}
450	2.5×10^{-11}	6.0×10^{-11}	1.8×10^{-10}	8.8×10^{-11}

Table 5.1 Diffusion coefficients at different temperatures and particle sizes (diffusion distance) obtained from the solution to the equation describing diffusion in a flat sheet

5.2.1.2 Estimation of errors in the calculations

The errors associated to all these calculations and measurements are going to be reviewed in this section.

The first error is that of the experimental measurements. According to the manufacturer, the thermogravimetric analyser TGA 7 carries an error in its measurements of $\pm 1\ \mu\text{g}$. Taking a more conservative approach and considering the error to be one order of magnitude bigger, i.e. $\pm 10\ \mu\text{g}$, the measurements of the weight change during oxygenation of a 35 mg sample with an initial oxygen content of 6.2 would carry an error of $\approx 1\%$, which is reasonable in view of the errors that are introduced during the theoretical calculations, as it will be seen in this section.

The next factor to consider is the effect of the initial heating rate in the oxygenation of the sample. It is not possible to heat up the material instantaneously to the temperature at which the isothermal experiment is going to take place (see Fig. 5.7). Therefore, during the initial heating stage some oxygen diffuses in the sample, increasing its weight before the isothermal stage begins.

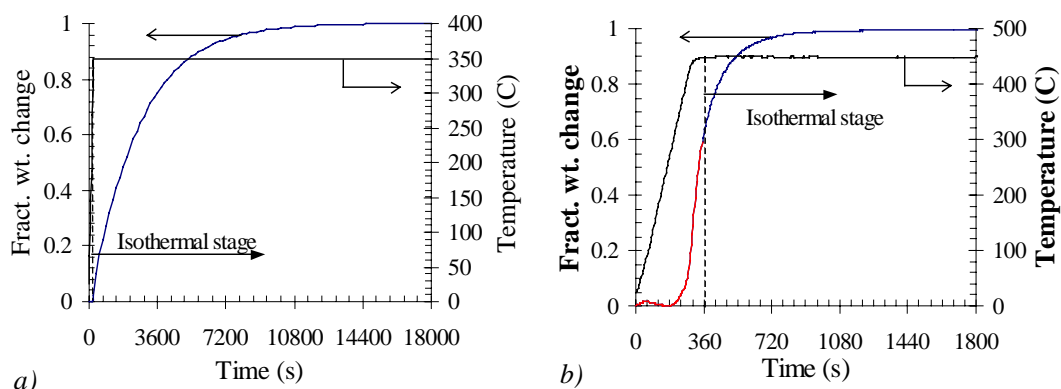


Fig. 5.7 Comparison between oxygenation of powder at 10 °C/min to: a) 350 °C and b) 450 °C with the initial transient (temperature ramp to the required temperature)

The amount of oxygen that diffuses in during this transient depends on the heating rate and the temperature of the isothermal step. More oxygen will diffuse in the sample when slow heating rates are used, although the effect is smaller if the isothermal stage temperature is low. The use of fast heating rates reduces the amount of oxygen absorbed during this initial transient (see Fig. 5.8). The initial absorption of oxygen would be eliminated if an infinitely fast heating rate could be used.

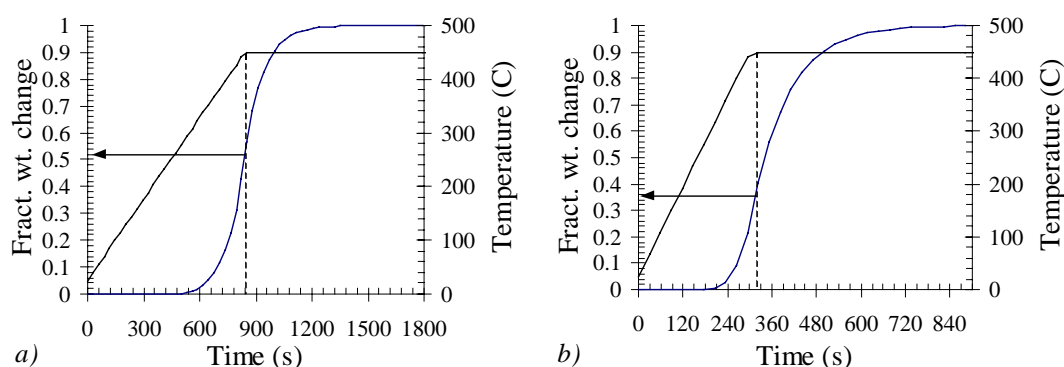


Fig. 5.8 Variation in initial oxygen content when heating a sample with a 2.1 μm radius to 450 °C at: a) 30 °C/min., and b) 90 °C/min (theoretical calculation)

It must be pointed out that one of the assumptions of this work is the independence of the oxygen content of the diffusion coefficient. This initial transient does not, in principle, present any problems for the calculation of the value of \tilde{D} . However, the ideal situation would be that where all the weight gain occurred during the isothermal stage.

The heating rate used for all the isothermal experiments was 90 °C/min, the fastest possible while still keeping the temperature lag in the TGA 7 to less than 20 °C. The

time spent heating the sample was so short that the maximum amount of oxygen absorbed during the non-isothermal stage was never higher than 35% of the total amount at 450 °C and much less at lower temperatures

When carrying out the theoretical calculations to overlap the theoretical weight gain curve with the experimental curve, two aspects should be considered: the diffusion distance taken and the choice of \tilde{D} . With respect to the diffusion distance, it has already been mentioned that the powder samples have a range of particle sizes. The value of \tilde{D} was calculated for a number of these sizes in order to know the amount of error introduced in the calculations. This error is the largest of all calculated here. The value of the diffusion coefficient given in this work is an average of the values of \tilde{D} calculated for a number of particle sizes (see Table 5.1). Fig. 5.9 shows its variation with temperature compared to the range of values obtained from literature with the error bars that result from the variation in particle size in the calculations. The line in bold is the variation of the \tilde{D} calculated using a cylindrical diffusion model. It can be seen how the values obtained are within the error region of the diffusion coefficient calculated using a sheet geometry.

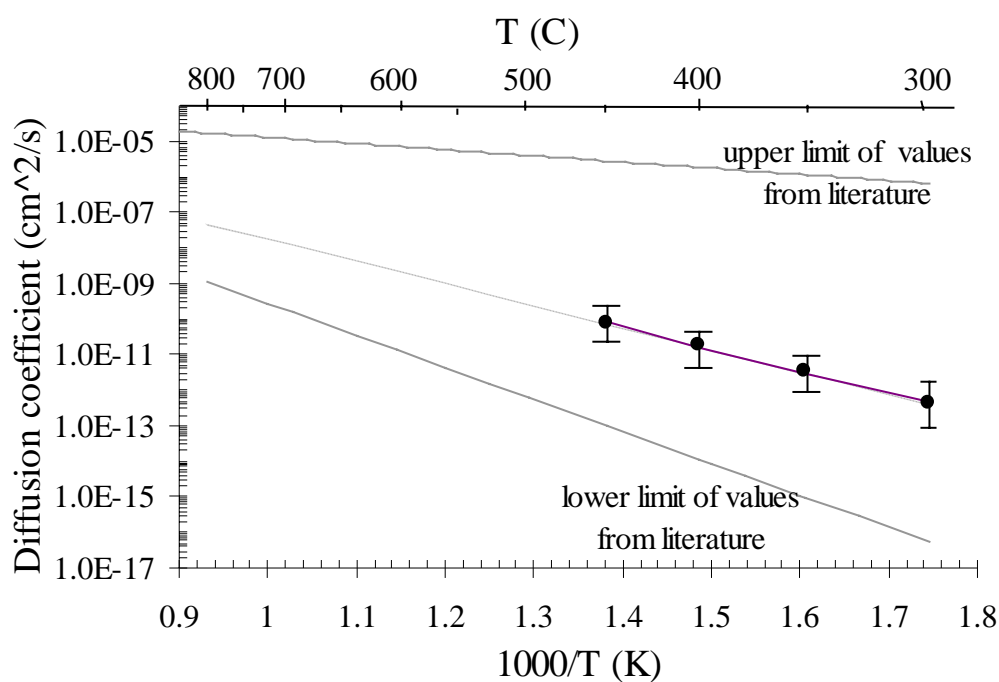


Fig. 5.9 Calculated \tilde{D} values (with error bars) obtained with the solution of diffusion in a slab. Line in bold shows \tilde{D} values obtained for the solution of diffusion in a cylinder. These values are shown within the upper and lower limits of diffusion data collected from the literature

The second aspect to consider is the choice of \tilde{D} once the diffusion distance is set. It has been shown in the previous section (Fig. 5.4) that small changes in the value of \tilde{D} alter considerably the shape of the weight gain trace with time. The error introduced by the choice of \tilde{D} is much smaller than that introduced by the variation in particle size.

5.2.1.3 Other methods used to calculate \tilde{D}

Two other theoretical methods can be used to estimate the value of the diffusion coefficient at each temperature; these concentrate respectively on the weight changes observed at the beginning and at the end of the oxygenation process. These calculations are included here as a confirmation of the previous results obtained.

- Initial rates of absorption

It has been shown in section 5.2.1.2 that the influence of the initial transient on the overall shape of the experimental weight gain curve compared to the theoretical case with no initial transient is minimum. Therefore, it is possible to carry out an analysis of the initial rates of absorption of oxygen to calculate the diffusion coefficient at each temperature.

As it was explained in chapter 2, for small times and in the case of constant \tilde{D} , it is possible to simplify the expression of the relative weight gain with time (5.1) to:

$$\frac{M_T}{M_\infty} = \frac{4}{\pi^{1/2}} \left(\frac{\tilde{D}t}{l^2} \right)^{1/2} \quad (5.4)$$

The value of \tilde{D} can be calculated from the slope of the straight line obtained when plotting the relative weight change of the sample vs. the square root of time.

Fig. 5.10 shows the line and slope of the line obtained during an oxygenation carried out at 350 °C after ramping to that temperature at 90 °C/min. According to the manufacturer the average particle size of the powder is 5.2 μm in diameter, so the value of the diffusion coefficient calculated with this diffusion distance from the slope of the line is: 3.1×10^{-12} cm²/s; this agrees very well with the diffusion coefficient value obtained using the flat sheet solution.

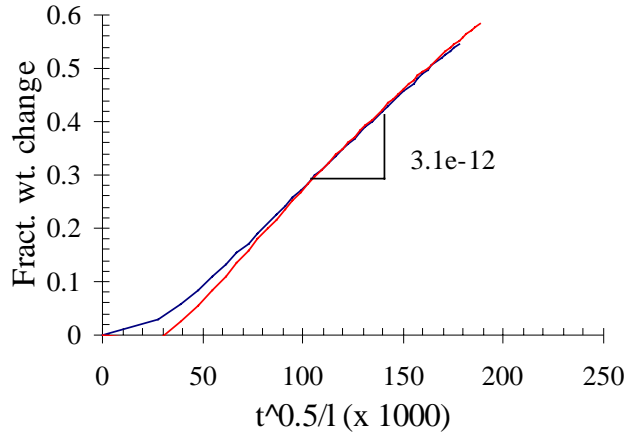


Fig. 5.10 Fractional weight change (M_t/M_∞) vs. $t^{1/2}/l$ for oxygenation of powder at 350 °C (in blue. Particle size: 2.6 μm radius). Line in red represents theoretical fractional weight change for oxygenation at 350 °C using the solution to the case of diffusion in a flat sheet.

The experimental line has a slightly different slope than the solution to the diffusion equation. This can be attributed to the experimental error of the measurements. However, the variation in values of \tilde{D} for the three different cases is within the error calculated above that results from the variation in grain size (diffusion distance). The simplification of the equation that includes a summation to a one-term expression also reduces the accuracy of the result.

- Final rates of absorption

In the same way as the analysis of the initial rates of absorption, if the diffusion is independent of composition it is possible to calculate the value of the diffusion coefficient from the final stages of the absorption of oxygen. The solution to the diffusion equation (5.1) for a plane sheet becomes in this simplified case:

$$\frac{d}{dt}(\ln(M_\infty - M_t)) = -\frac{\tilde{D}\pi^2}{l^2} \quad (5.5)$$

A plot of $\ln(M_\infty - M_t)$ against t will be a straight line of slope equal to $\tilde{D}\pi^2/l^2$, where l is the diffusion distance.

Fig 5.11 shows such a plot for data from an oxygenation of powder at 400 °C. The value of the diffusion coefficient obtained for this case from the slope of the line is 6.4×10^{-12} cm²/s. This value is within the experimental error margin calculated in 5.2.1.2

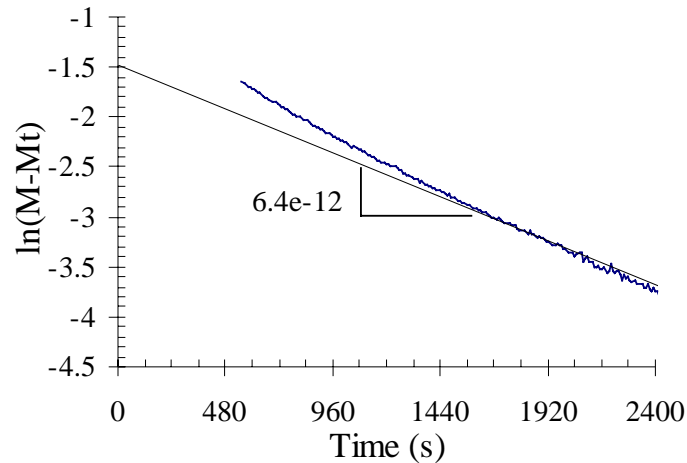


Fig. 5.11 Plot of $\ln(M_\infty - M_t)$ vs. t characteristic of an oxygenation of YBCO powder at 400 °C (particle size: 2.6 μm radius). Value next to slope in graph is the calculated diffusion coefficient following the analysis explained above.

5.2.1.4 Comparison with literature

Fig. 5.9 showed the position of the data calculated with the results from these experiments with respect to all the range of data published in this subject. This section is going to review the differences found with results published in the literature (see chapter 3):

- Tracer diffusion (Fig. 5.12)

Comparing the results presented above with data collected in tracer diffusion experiments, it is interesting to see that even though most of these were carried out using polycrystalline samples there are a number of them that agree with the results of the chemical diffusion in powder samples obtained in this work.

The results from Rothman *et al.* (1989), (1991), for example, lie quite close to our results even though the samples were polycrystalline with a density close to 99% of the theoretical density. Similar results obtained for single crystals by Tsukui *et al.* (1991-b) in the *ab* plane are one order of magnitude higher than those of Rothman and

co-workers, but this variation could be a result of the difficulty in carrying out SIMS measurements along the *ab* plane, as it is necessary to have a thick crystal which is not always available. It is not known whether the samples achieved equilibrium during the pre-oxygenation stage; this technique could be more sensitive to these initial conditions than thermogravimetry (see section 5.1) and a lower saturation of oxygen could favour a faster substitution with the isotope.

However, their *c* axis results agree quite well with those obtained by Bredikhin *et al.* (1991), whose *ab* data also agrees within one order of magnitude with that of Rothman *et al.* and with that obtained from this chemical diffusion study. Tracer data calculated by Turrillas *et al.* (1989) also agrees within the order of magnitude error mentioned above.

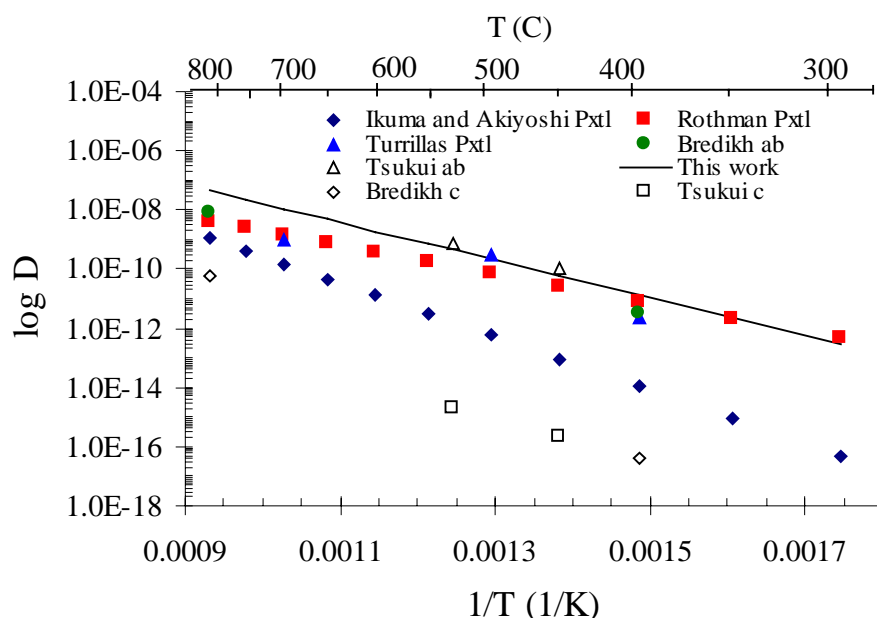


Fig. 5.12 Tracer diffusion data from literature compared to the chemical diffusion in powder result

The tracer diffusion result by Ikuma and Akiyoshi (1988) differs markedly from the rest of the tracer data in the literature. They used thermogravimetry to study the diffusion of ^{18}O in polycrystalline samples previously oxygenated in ^{16}O . Their initial oxygenation conditions were altered by a slow heating rate and it is possible that the presence of impurities could have modified the final results of the measurements. The activation energy calculated in their experiments is unreasonably high: 1.8 eV (the activation energy for vacancy diffusion is usually around 1 eV; see chapter 2). They suggest a surface reaction mechanism controlling the diffusion process, but the

formation of a surface layer that may hinder diffusion has not yet been observed in any of the traces obtained with SIMS, which probably rules out this explanation. It has been suggested by Rothman's group that the measurements could be of something else other than oxygen diffusion.

- Resistance measurements (Fig. 5.13)

There is a lot of work published with results obtained from resistance measurements, but most of these only calculate values of the activation energy of the diffusion process, which limits the comparison to the value of A_e .

In order to do a complete study of the diffusion process it is not only necessary to know the value of the activation energy, but also that of the pre-exponential factor. In this way the straight line with a slope of A_e is anchored at the intercept for $1/T = 0$, which allows one to know the values of \tilde{D} for the whole temperature range. It has been observed that rearrangement of the oxygen atoms within the lattice can be measured at low temperatures. This could mean that this technique can be used to measure not only diffusion of oxygen into and out from the sample, but also its distribution once it is inside the structure. This should be taken into account when analysing the results from these resistance measurements.

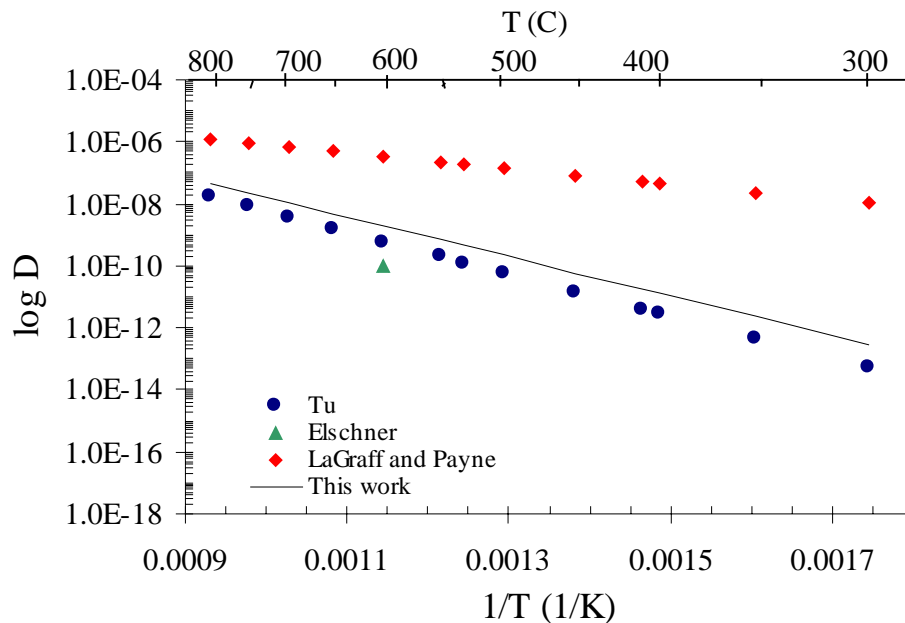


Fig. 5.13 Diffusion data from resistance measurements in literature compared to the result of chemical diffusion in powder

Only Tu *et al.* (1988-a), (1988-b) and LaGraff and co-workers (1993-a) give a full Arrhenius expression for the diffusion of oxygen in YBCO. The values obtained by Tu and co-workers were calculated from a dynamic (changing temperature) measurement of the resistance during oxygenation and deoxygenation of polycrystalline samples similar to the non-isothermal studies that are going to be presented in section 5.3. It is interesting to see that their values lie quite close to those obtained in this study of chemical diffusion in powder samples. The effects of porosity and grain boundary diffusion would be expected to alter the final results giving a faster diffusion coefficient than that obtained with thermogravimetry, but it can be seen that for most of the temperature range the values obtained by Tu *et al.* are less than one order of magnitude lower than those of chemical diffusion. This set of values lies within the experimental error region calculated in section 5.2.1.2.

LaGraff *et al.* (1993-a), (1993-b) studied out- and in-diffusion in polycrystalline and single crystal samples under isothermal conditions and they have carried out a calculation of the activation energy of oxygen diffusion in YBCO: the first value, equal to 0.96 eV, is calculated from measurements of resistivity in single crystals, and the second, 0.5 eV, from polycrystalline samples. The latter is suggested to be characteristic of grain boundary and pore diffusion and the former, with a higher value, is thought to be typical of bulk diffusion. The value of 0.96 eV is in good agreement with the diffusion of oxygen via vacancies mentioned earlier on (~ 1 eV).

The work by Elschner *et al.* (1992) concentrates on the studying the effect of microstructure in the diffusion process. They differentiate between diffusion along cracks, which has a null activation energy, and bulk diffusion, with an activation energy of approximately 1 eV. They have calculated a value for intragrain diffusion of 10^{-10} cm²/s at 600 °C, although they do not give a mathematical expression for the variation of \tilde{D} with temperature. This diffusion value appears to be slightly low compared to the other results, but it may be a consequence of the effects of the microstructure, most probably due to the presence of closed porosity that may slow the diffusion process to the centre of the sample.

- Chemical diffusion (Fig. 5.14)

The widest scatter in data appears to be in the results obtained with studies of chemical diffusion using thermogravimetric analysis. This technique is very sensitive to the alteration in microstructural features of the specimens, so it is thought that the change in density and grain size of the samples could be the reason for the wide range of values published. All the samples used were polycrystalline, with varying density and particle size.

As it is going to be seen in section 5.2.3, the study of diffusion in polycrystalline samples is very complex. It requires taking into account the effect of grain boundaries, and the presence of open or closed or open porosity. Grain boundaries provide a fast path for the transport of oxygen content at low temperatures (short-circuit diffusion). The amount of grain boundaries is determined by the degree of porosity and the grain size of the sample.

If the presence and effects of grain boundaries are ignored the analysis would be limited to setting the diffusion distance. It has already been discussed in chapter 3 that in the case of porous samples, the diffusion distance chosen should be the average between open pores, whereas if the sample is fully dense it should be the size of the specimen. The wrong choice of the sample size as diffusion distance can affect considerably the result of the calculation of \tilde{D} .

The data presented by Kishio *et al.* (1989-b) differs considerably in the value of the activation energy with respect to any of the other results presented in the literature and those calculated in this work (see Table 3.1 and Fig. 5.14). Their study of the variation of oxygen content with partial oxygen pressure is very complete, and although it agrees with other studies of the same type (Ikuma and Akiyoshi (1988)), their calculation of the diffusion coefficient seems to disagree with most of the data. Their polycrystalline samples had a density of 98 % of the theoretical density and a grain size of 50 μm , the largest obtained compared to most of the other groups. It is possible that the time spent at each pressure and temperature was not enough to equilibrate the sample; this, together with the high density of the sample could have given rise to calculations of oxygen diffusion in a material that had not achieved equilibrium at the

end of the oxygenation process, introducing a larger degree of error in the calculations of the diffusion coefficient.

Differential scanning calorimetry studies of oxygen diffusion in YBCO powder by Glowacki *et al.* (1988) have also yielded a high value of the activation energy for this process, between 1.5-1.6 eV, close to the results by Kishio *et al.* (1989-b). However, the calculation of the pre-exponential factor, D_0 , located the series of diffusion values quite close to the results obtained in this thesis using thermogravimetry, as well as those published by Haller *et al.* (1989) and Mozahev and co-workers (1992), (1994) (see Fig. 5.14). The slight difference in the results is probably a result of experimental errors, such as the temperature lag of the differential scanning calorimeter with heating rate. A re-evaluation of the activation energy once the temperature lag has been estimated would yield a more reliable value for the activation energy of oxygen absorption in YBCO. The use of differential scanning calorimetry to study oxygen diffusion presents the advantage of providing information about the evolution of this process from very low temperatures (if the heating rate is not faster than 50 °C/min). Low temperature diffusion data is difficult to obtain sometimes using other techniques. More work should be carried out in this field to investigate the possibilities of applying DSC to the study of oxygen diffusion.

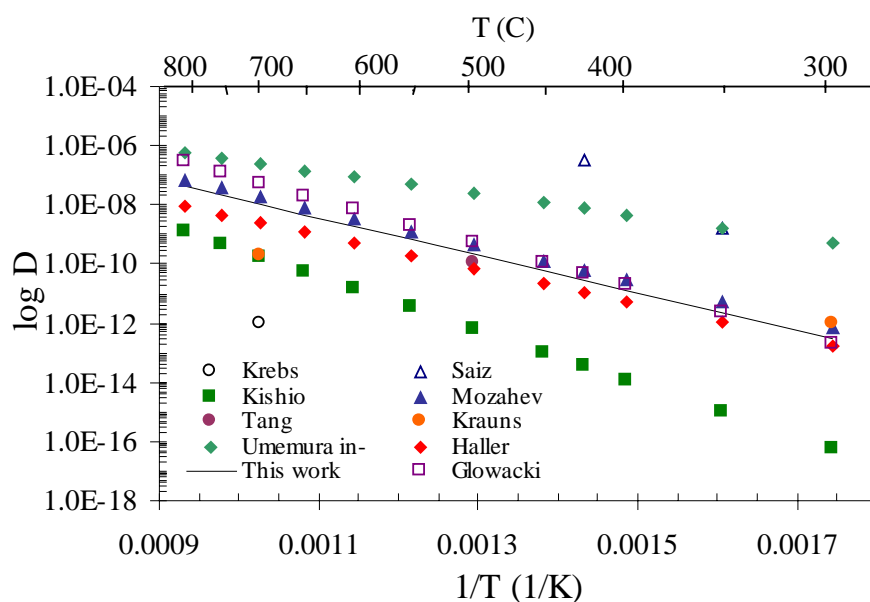


Fig. 5.14 Chemical diffusion data from the literature compared to the results of chemical diffusion in powder

The work carried out by Mozahev and co-workers (1992), (1994) combined studies of oxygenation of very fine powders with polycrystalline samples of varying density. They studied diffusion in the powder and low density polycrystals using the solution to Fick's second law characteristic of diffusion in a sphere. The study of the higher density samples was done using the solution to diffusion in a plane sheet, taking the diffusing distance to be the size of the polycrystalline sample, instead of the grain size. This could be the reason for the slightly higher values (a longer diffusion distance than the real distance results in a faster diffusion coefficient), but they lie within the region of experimental error of the diffusion values calculated in this thesis.

The high values of the diffusion coefficient obtained by Umemura *et al.* (1989) could again be explained due to a miscalculation of the diffusion distances in the polycrystalline sample. Their choice of solution of the diffusion equation to be applied was probably not very accurate, as it required to take into account the height and diameter of the sample (which they assume to be a cylinder) suggesting that they consider diffusion along the three crystallographic axes, when diffusion occurs primarily in the *ab* plane. The values of the activation energy calculated are quite low (0.7 and 0.5 eV), which could be characteristic of grain boundary diffusion, as suggested by LaGraff *et al.* (1993-a). (1993-b) in their electrical resistance studies.

Krauns and Krebs (1993) carried out two measurements of \tilde{D} for a polycrystalline sample with open porosity. They found that the diffusion coefficient was strongly dependent on composition, with the activation energy changing as much as 0.8 eV between specimens. The activation energy that can be calculated from the two diffusion values given is quite low (see table 3.1); this corroborates the analysis presented at the beginning of this section concerning the form of the material for the experiments. Polycrystals are very complex and the use of powder samples was thought to introduce less variables in the study of the diffusion process.

Tang and Lo (1991) also studied the oxygenation of oxygen in YBCO in a very porous polycrystalline sample, and the only diffusion value mentioned agrees with the diffusion coefficient calculated in this work. The data by Haller *et al.* (1988) also agrees quite well with the results presented in section 5.2.1.1 obtained using powder samples, although Haller and co-workers used polycrystalline specimens for their

studies. The porosity of their samples and perhaps the choice of a slightly large diffusion distance yield lower values for the diffusion coefficient than those obtained in the work presented in this thesis. However, the agreement is within the order of magnitude error mentioned in 5.2.1.2.

5.2.1.5 Modelling of the diffusion process under isothermal conditions

Once the expression for \tilde{D} was calculated it was possible to reproduce the experimental results with the computational model developed described in chapter 4.

The calculated values of the pre-exponential factor and activation energy for diffusion are entered in the programme and the variation in weight of a powder particle with a set grain size (average grain size of the powder sample) can be calculated for the oxygenation treatment chosen.

This first step taken was to test the validity of the model, setting a theoretical calculation of the weight gain recorded in the isothermal runs shown in the previous section. Fig. 5.15 shows the results obtained for two of these runs. The first one is an oxygenation with a fast ramp rate to a low temperature (90 °C/min to 350 °C) and the second is an oxygenation to a higher temperature with a slower ramp rate (10 °C/min to 450 °C). This experimental result was not used in the calculation of \tilde{D} , but is included to show that the model can reproduce any kind of experimental situation.

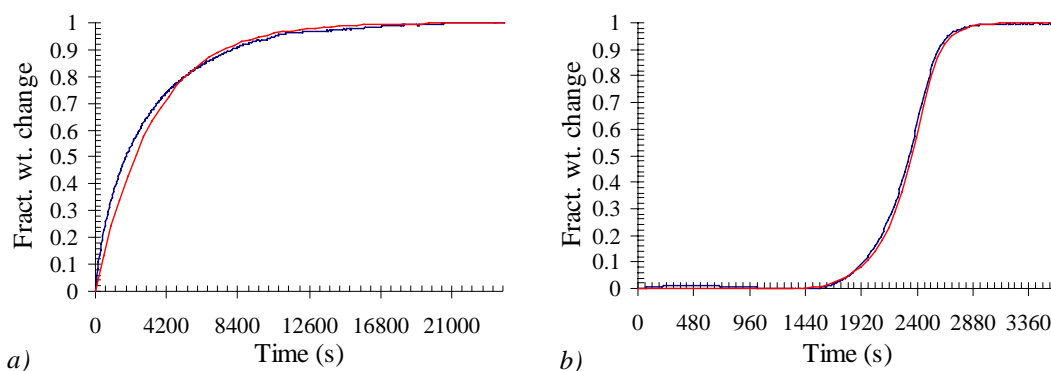


Fig. 5.15 a) 90 °C/min to 350 °C, and b) 10 °C/min to 450 °C. Experimental data shown in blue and model data in red. Particle radius: 2.1 μm

The reproduction of the weight change with temperature (or time) is very useful, as it can help in the design of experiments where it is necessary to know the diffusion time

for any type of oxygenation treatment as well as what weight change is expected. To complement further the analysis of oxygenation, this model also calculates the change in the oxygen distribution gradient within the sample as the oxygenation occurs. This feature is very useful when it is necessary to know the distribution of oxygen of a sample after a certain heat treatment.

The choice of particle radius equal to 2.1 μm was made so that both isothermal and non-isothermal theoretical studies agreed with the experimental results. This difference in the diffusion distance could be a consequence of the slight disagreement in shape between the real powder particles and the spherical powder particles assumed in the computer model.

Fig. 5.16 shows how the model can successfully reproduce oxygenation experiments at low and at higher temperatures (90 $^{\circ}\text{C}/\text{min}$ to 350 $^{\circ}\text{C}$, Fig. 5.16 a), and 90 $^{\circ}\text{C}/\text{min}$ to 450 $^{\circ}\text{C}$, Fig. 5.16 b), respectively).

It can be seen how during the treatment at low temperature the amount of oxygen absorbed during the heating transient is minimum, while when the temperature is raised the distribution of oxygen in the specimen at the beginning of the isothermal step is much higher (marked by red lines in the oxygen distribution).

Fig. 5.16 c) shows an extreme case of very slow heating rate: 10 $^{\circ}\text{C}/\text{min}$ to 450 $^{\circ}\text{C}$. From its characteristic weight gain plot and oxygen distribution graph it can be seen that the oxygen starts being absorbed at 260 $^{\circ}\text{C}$ and most of the oxygenation occurs during the initial transient mentioned in the previous sections. By the time the isothermal stage is reached (at 450 $^{\circ}\text{C}$) almost 90 % of the total amount of oxygen has been absorbed. The distribution is not yet uniform, as the equilibrium oxygen content for that temperature in a pure oxygen atmosphere is 6.97, so the concentration gradient through the sample continues decreasing with time until equilibrium is reached. The same occurs when heating at a faster rate, although in this case most of the oxygenation occurs during the isothermal stage (see Fig. 5.7 a)).

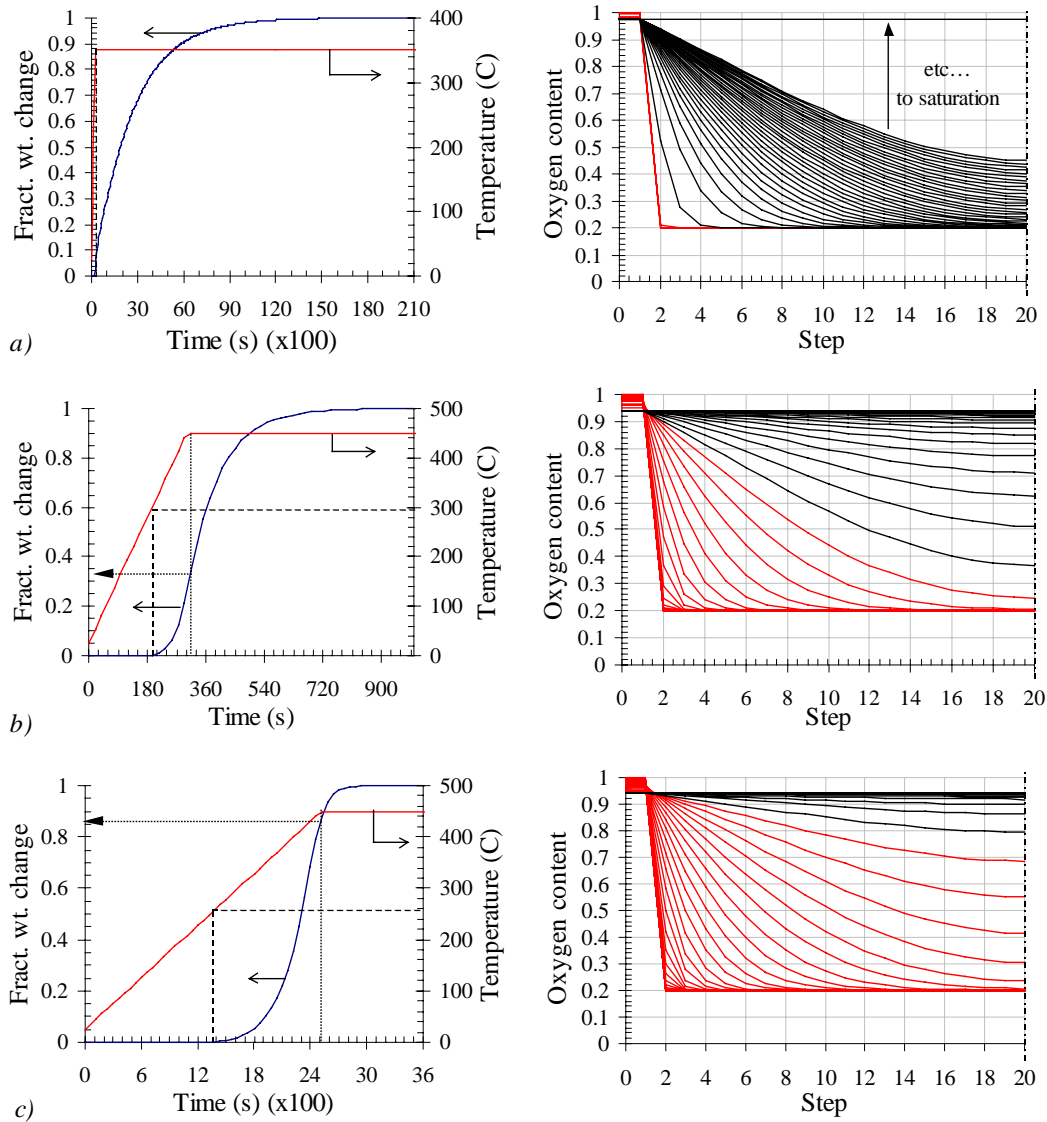


Fig. 5.16 Concentration profile within a sample during oxygenations at: a) 90 °C/min to 350 °C, b) 90 °C/min to 450 °C (time between concentration lines: 30 s), and c) 10 °C/min to 450 °C (time between concentration lines: 60 s). Red lines show oxygenation during transient stage. Black lines show oxygenation during isothermal stage. Sample size: 2.1 μm radius

It has already been mentioned that high, uniform oxygen contents are the aim of the manufacturing and processing of YBCO samples. Using the model developed to reproduce the heat treatment will allow manufacturers and researchers to find out the true oxygenation of the sample, i.e. its amount and distribution, which will be of great help when it comes to analysing the results of experiments whose value depends on oxygen content.

- Use of initial and final rates of absorption

The results obtained from theoretical oxygenations with the model developed can also be analysed in the same way as the experimental data. This section shows that an analysis of the initial and final rates of absorption of these theoretical oxygenations yields very similar results to those presented in section 5.2.1.3 (Other methods used to calculate \tilde{D}).

Fig 5.17 shows the straight line obtained in the study of the initial rate of absorption of a theoretical computation of an oxygenation at 90 °C/min to 350 °C using the oxygenation model developed. The particle radius used was 2.1 μm . The value of the diffusion coefficient obtained from the slope of the line is $1.3 \times 10^{-12} \text{ cm}^2/\text{s}$. The red line in the graph shows the fractional weight change obtained using the solution to the case of diffusion in a flat sheet (no initial transient).

It can be seen from Fig. 5.17 that the diffusion coefficient obtained from this analysis of the theoretical data gives a value for this coefficient quite similar to that obtained from the experimental oxygenation. The difference in the values could be due to small inaccuracies due to shape variation between the real sample and the theoretical model and perhaps due to the combination of the oxygenations of powder particles of different sizes.

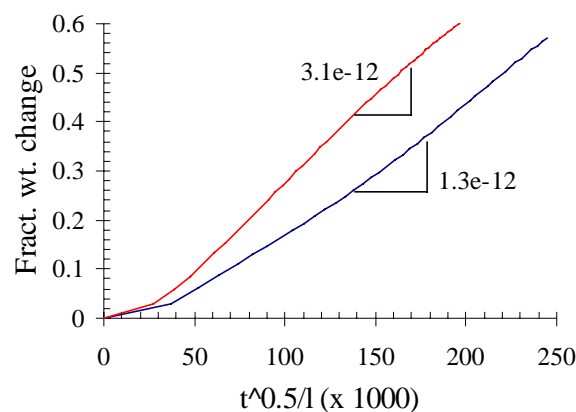


Fig. 5.17 Fractional weight change (M_t / M_∞) vs. $t^{1/2}/l$ for a theoretical oxygenation at 350 °C calculated with the diffusion model developed (particle size: 2.1 μm radius) (in blue). Line in red represents theoretical fractional weight change for oxygenation at 350 °C using the solution to the case of diffusion in a flat sheet (see Fig. 5.10)

Concerning the analysis of the final rates of absorption, Fig. 5.18 shows a plot of the data from an oxygenation at 400 °C oxygenation reproduced with the diffusion model

developed. The diffusion coefficients obtained for this case obtained from the slope of the line is equal to $8.0 \times 10^{-12} \text{ cm}^2/\text{s}$. This value is within the error margin calculated for the diffusion measurements presented in section 5.2.1.3.

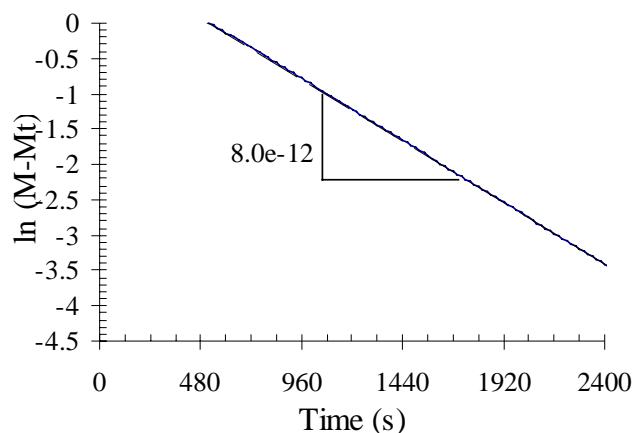


Fig. 5.18 $\ln(M_\infty - M_t)$ vs. t for a theoretical oxygenation of powder at 400 °C (ramp at 90 °C/min) calculated with the diffusion model developed (particle size 2.1 μm radius). $\tilde{D} = 8.0 \times 10^{-12} \text{ cm}^2/\text{s}$

5.2.2 Oxygenation of polycrystalline and single crystal samples

In order to follow the natural extension of this oxygenation work, a preliminary study of the behaviour of polycrystalline and single crystal specimens was carried out.

It has already been pointed out that the oxygenation process in polycrystals is very complex. The presence of grain boundaries, open and closed porosity and an unknown range of particle sizes increases the difficulty in the analysis of the results obtained. The oxygenation of polycrystalline samples is beyond the scope of this thesis and these results are only included as preliminary steps towards the complete analysis of the diffusion process in YBCO.

Two polycrystalline samples were made with SSC powder following the process described in section 4.4.2 of chapter 4. The densities of these specimens were determined by pycnometry and were 85 and 94 % of the theoretical density respectively. The average grain size of both samples was measured using optical microscopy; it was found to be 12.5 μm for the 85 % dense polycrystal and 150 μm for the 94 % dense sample.

Following the same oxygenation study carried out with powder samples, the polycrystalline specimens were deoxygenated in Ar at 750 °C and subsequently oxygenated at different temperatures in the range 300 - 450 °C.

Fig. 5.19 a) and b) show that the oxygenation traces obtained in the case of polycrystalline specimens had a different shape in the initial stages of the process: instead of an exponential behaviour (see oxygenation of powder samples in 5.2.1; Figs. 5.2 and 5.6, for example), the increase in weight appears to be linear with time until most of the oxygenation has occurred. This behaviour was observed at low temperatures for both polycrystalline specimens.

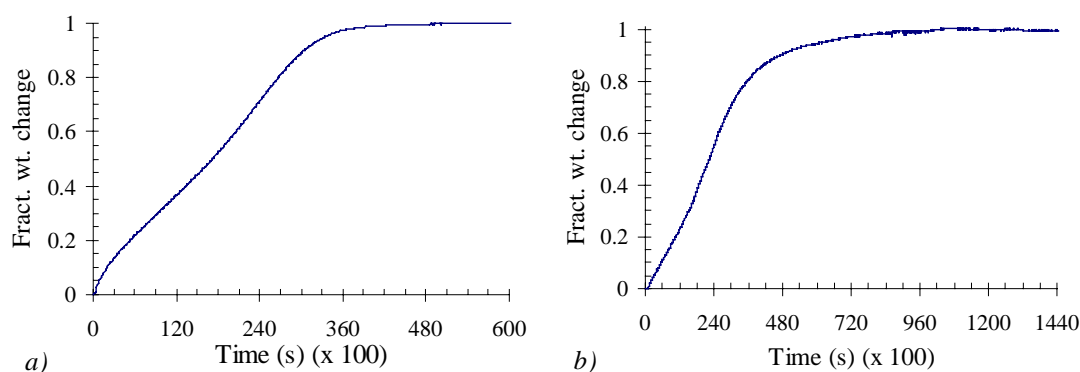


Fig. 5.19 a) Oxygenation at 300 °C of 85 % dense polycrystal, and b) oxygenation at 300 °C of 94% polycrystal

As the temperature of the isothermal oxygenations increased, this linear increase in weight with time became less pronounced, disappearing altogether at high temperatures, as it can be seen in Fig. 5.20 a) and b).

It is not known why this initial linear weight gain occurs. The fact that it disappears as the oxygenation temperature increases suggests that it might be linked to grain boundary diffusion. It is known that this type of diffusion has a low activation energy (lower than bulk diffusion) at low temperatures. However, the effect of grain boundaries is thought to enhance the diffusion process, and the linear increase in weight with time appears to be slowing down the absorption of oxygen in the sample. This effect should be studied in more detail.

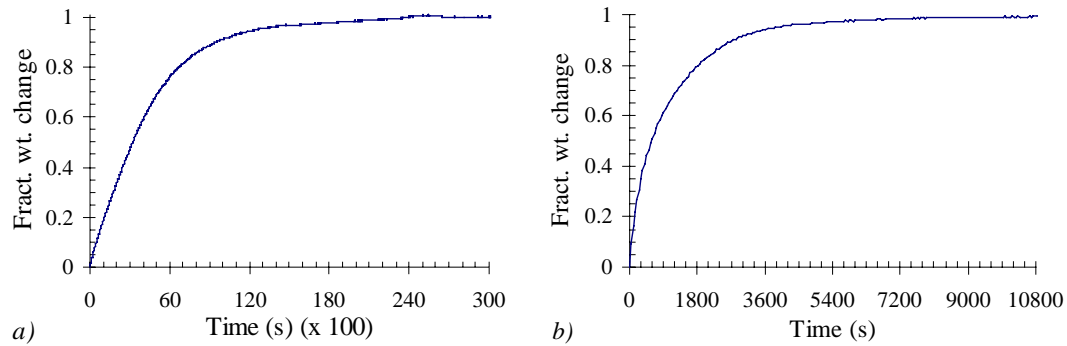


Fig. 5.20 Oxygenation of 94% polycrystal at: a) 350 °C, and b) 400 °C

The calculation of the diffusion coefficient for polycrystalline samples was carried out in the same way as it was done with powder data: the solution to the diffusion equation for the case of diffusion in a slab was fitted to the experimental fractional weight change. Using the values of the grain sizes measured with optical microscopy, the curves were matched to the final variation in weight change, irrespectively of the shape of the initial part of the curve (Fig. 5.21). Due to the small grain size of the 85% dense polycrystal the temperature range over which the isothermal experiments were carried out was very limited (300 – 350 °C) and it was not possible to carry out a calculation of the value of the diffusion coefficient without incurring in a large error. The value of the diffusion coefficient in a polycrystalline sample was calculated using data from the oxygenation of the 94 % dense polycrystal.

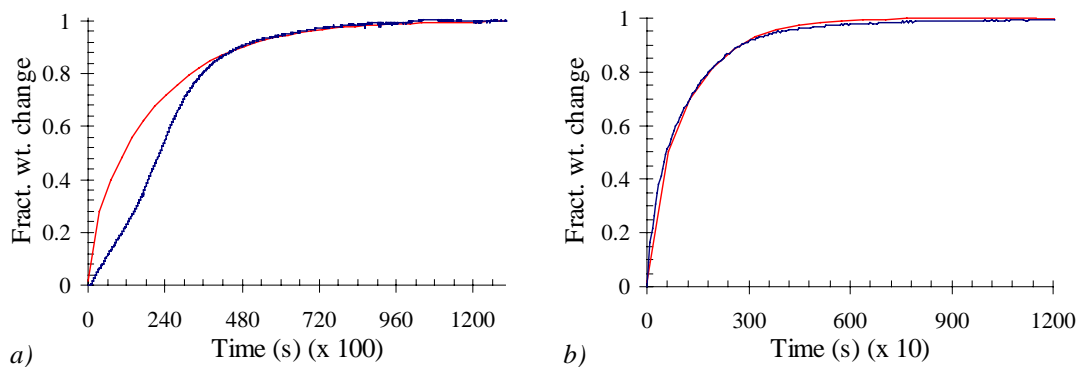


Fig. 5.21 Oxygenation of 94 % polycrystal at: a) 300 °C ($D = 1.2 \times 10^{-8} \text{ cm}^2/\text{s}$), and b) 400 °C ($D=1.7 \times 10^{-7} \text{ cm}^2/\text{s}$). Blue line: experimental data; red line: solution to the diffusion equation. (Diffusion distance: $x = 0.05 \text{ cm}$)

The diffusion coefficients for the 94 % dense sample were calculated ignoring the effect of grain boundary diffusion in this specimen with closed porosity. The diffusion distance used was therefore one half of the dimensions of the specimen. This was

calculated to be approximately 0.5 mm. The values obtained for the diffusion coefficients obtained were:

Temperature ($^{\circ}\text{C}$)	D 94 % dense polycrystal (cm^2/s)
300	1.2×10^{-8}
350	5.1×10^{-8}
400	1.7×10^{-7}
450	4.8×10^{-7}

Table 5.2 Values of the diffusion coefficient calculated for a 94 % dense polycrystal with an average diffusion distance of 0.05 cm

Oxygenation experiments carried out with single crystal samples at higher temperatures than those used with powder samples also yielded very high values of the oxygen diffusion coefficient (see Fig. 5.22). It is not known why diffusion occurs faster in these single crystals (average size: $1 \times 1 \times \sim 0.05$ mm) than in powder samples.

It has been observed that ageing a powder sample for 2½ weeks in a high CO_2 environment increased the diffusion coefficient above the error margin calculated in section 5.2.1.2 (see Fig. 5.22). The presence of impurities in the single crystals introduced during processing could be one of the reasons for the faster diffusion behaviour observed.

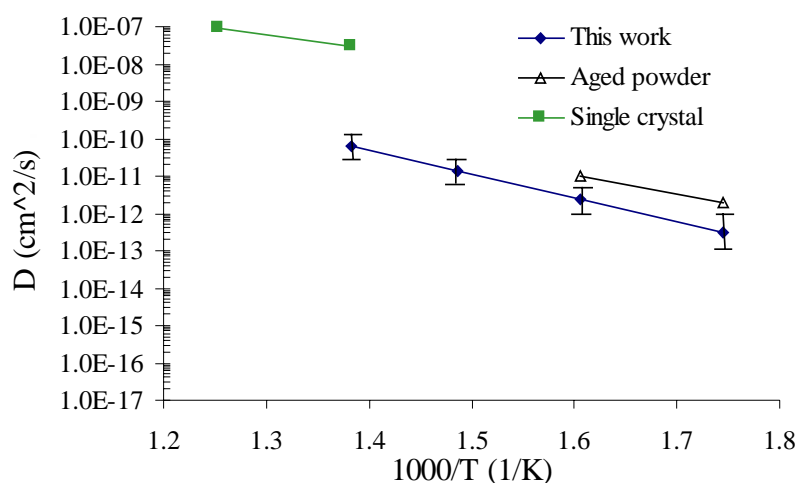


Fig 5.22 D vs. $1/T$ results for single crystal specimens (diffusion distance: $50 \mu\text{m}$) and aged SSC powder (radius: $2.6 \mu\text{m}$) compared to the chemical diffusion results presented in section 5.2.1.2 (Fig. 5.9)

5.2.3 Summary

This section has presented a study of oxygen diffusion in YBCO using thermogravimetry under isothermal conditions.

Thermogravimetry is a very useful technique for the measurement of chemical diffusion, as it records weight changes as a function of time and temperature in a controlled atmosphere. The atmosphere is chosen so that a chemical gradient is established across the sample and oxygen (in this case) is driven in or out of the specimens.

Using the solution to Fick's second law for diffusion in a slab it has been possible to calculate a value for the chemical diffusion of oxygen in YBCO comparing the theoretical results obtained using this solution (see Eq. (5.1)) from this solution with the experimental data.

The value of \tilde{D} obtained has been compared to the results published in the literature, suggesting possible reasons for the differences observed between these and the results obtained in this thesis. The effect of sample microstructure (use of polycrystals, single crystals or powder specimens) appears to be quite important. This justifies the choice of YBCO powder for the thermogravimetric study presented here. The choice of this form of material eliminates the effects of microstructural characteristics such as grain boundaries, presence of secondary phases, etc. In addition, the size of the powder particles is so small that it has allowed one to carry out the experiments at temperatures close to those ideally used for the oxygenation of samples during processing.

The computer programme developed to study the diffusion process theoretically has already been described in chapter 4. The diffusion parameters used are calculated from the thermogravimetry experiments. The validity of the programme has been checked, and section 5.2.1.5 shows that it has been possible to reproduce theoretically the experimental results from isothermal oxygenations at a series of heating rates.

Since it has been proven that it is possible to reproduce experimental data using the diffusion programme developed, the effect of the initial heating rate on the oxygenation results has been studied using only theoretical results. This has allowed

one to carry out a study of the diffusion process that would have otherwise taken a long time and a large number of samples if it had been carried out in practice.

A preliminary analysis of diffusion data for polycrystalline and single crystal samples has been carried out, but the number of factors affecting the process, such as grain boundary diffusion, porosity (for single crystals) and the presence of impurities in the sample (single crystals) have been observed to alter the oxygenation behaviour. A full study of these factors and their effect on the diffusion process should be carried out to complete the study of oxygen diffusion in YBCO.

5.3 Non-Isothermal experiments

One of the limitations of the use of powders is that, as it has been mentioned before (section 5.2.1), the maximum temperature at which the experiments can be carried out is limited by their particle size. If the particle size is very small, the temperature range will be reduced because the maximum temperature at which isothermal experiments can be carried out is low. Should this temperature value be exceeded, the sample will oxygenate to its equilibrium value during the initial heating transient. The same effect would be observed if the heating rate was reduced to very slow values. Under these circumstances full oxygenation of the sample occurs during the heating stage, and it is not possible to extract any information about the diffusion process (the value of \tilde{D}) with the methods described in the previous sections.

However, it was thought that the analysis of non-isothermal experiments could yield interesting information about the diffusion process, as well as providing one with a novel approach to the oxygenation step of the samples during processing (this will be discussed in more detail at the end of this chapter). This section presents the analysis of the experimental results obtained from oxygenations of powder, polycrystalline and single crystal samples under non-isothermal conditions.

5.3.1 Powders. *Effect of ramp rates*

Powder samples were deoxygenated following the heat treatment in Ar mentioned in 4.6.1. These samples were then heated in an oxygen atmosphere (1 atm) at different

rates: 1, 10, 30, 50 and 90 °C/min to 700 °C. They were held at 700 °C for a few minutes and then cooled to room temperature at the same rate as they were heated up.

The shape of the weight gain curve in these non-isothermal experiments is very characteristic (Fig. 5.23):

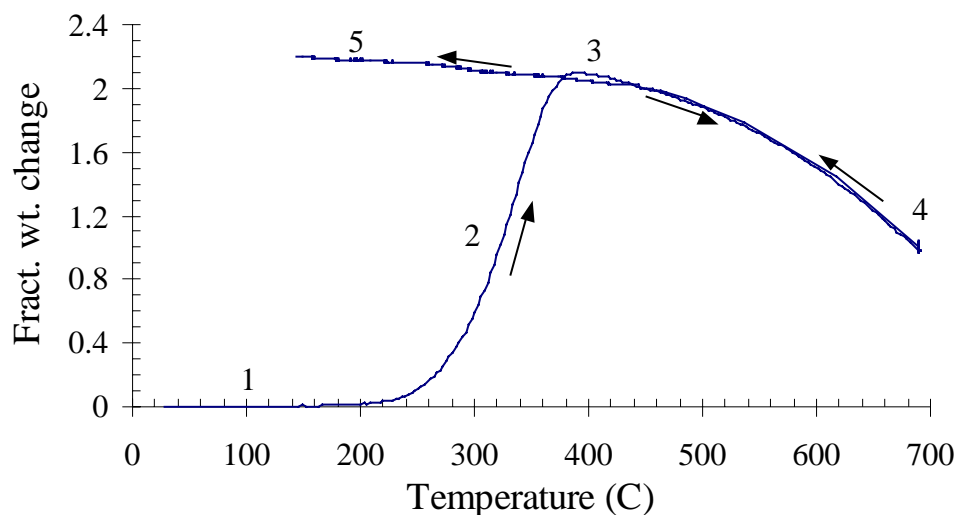


Fig. 5.23 Characteristic weight gain during a non-isothermal oxygenation of YBCO powder at 1 °C/min to 700 °C in a pure oxygen atmosphere and cooling to room temperature at the same rate

During the first part of the experiment, the weight of the sample remains constant (1). When the temperature increases above a certain value, T_{onset} , the weight of the sample starts increasing (2). This weight gain is steady until a certain point (3), where a maximum occurs. The temperature at which this maximum weight gain is observed is going to be referred to as maximum temperature, T_{max} . After this point, the weight of the sample starts decreasing continuously with increasing temperature (4). When the maximum temperature of the heat treatment is reached and the sample is cooled down, the change in weight of the specimen follows the last part of the heating curve (4), weight increasing with decreasing temperature. When the point of maximum weight is reached (3) and the temperature is decreased further, the sample continues to gain weight (5) slowly until it stabilises in the very low temperature range.

These changes in weight can be directly related to the change in oxygen content of the originally deoxygenated YBCO sample. The explanation is as follows:

At low temperatures (1) the weight of the sample remained constant because the value of the diffusion coefficient is too small for diffusion to take place. As temperature

increases, \tilde{D} increases too, and at a certain point, (2), the value of this coefficient has increased so much that the oxygen present in the furnace chamber has enough time to diffuse in the sample, faster as temperature increases. This diffusion of oxygen is observed in an increase in weight of the sample.

The weight gain continues until a certain temperature, T_{max} , when a maximum is reached (3). At this point the sample is saturated with oxygen. The equilibrium oxygen content at any temperature above this point is lower than that at the maximum of the weight curve. Therefore, as the temperature increases the sample starts losing oxygen (4). During this part of the non-isothermal heating curve the sample is always at its equilibrium oxygen content.

During cooling of the sample in the same atmosphere, it will absorb oxygen at the same rate as it lost it during the last part of the heating curve (4). As the temperature decreases below the point at which the maximum in weight occurred during heating, the weight gain becomes more sluggish until it stops altogether at low temperatures (5).

The temperatures at which the oxygenation process starts, T_{onset} , (point at which the weight gain begins) and at which the maximum in weight is reached, are determined by the diffusion coefficient and heating rate.

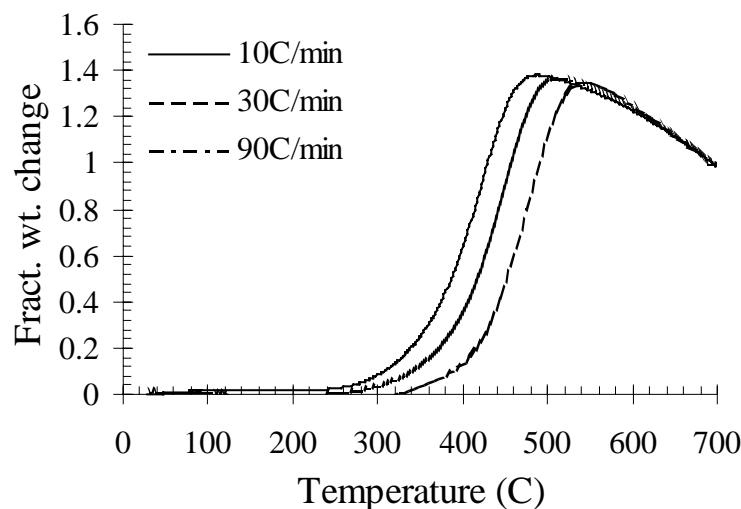


Fig. 5.24 Non-isothermal experiments: powder samples heated in 100 % O_2 to 700 °C at 10, 30 and 90°C/min

Fig. 5.24 shows that the values of the minima and maxima shift to higher temperatures with increasing heating rates. This occurs because as the ramp rate increases the time spent at each temperature is shorter, and the oxygen absorption during each time step is smaller. The onset of absorption will then be observed at higher temperatures.

It is possible to calculate the activation energy of the absorption process from the dependence on the heating rate of the temperature at which diffusion starts and T_{\max} :

The process taking place is that of oxygen diffusion inside the sample along the ab planes. Therefore, there is a flux of oxygen that alters the concentration according to the flux equation (in 1-D):

$$J = -\tilde{D} \frac{\partial C}{\partial x} \quad (5.6)/(2.1)$$

\tilde{D} is the chemical diffusion coefficient of oxygen in the sample, and it can be expressed with an Arrhenius equation:

$$\tilde{D} = D_o \exp(-A_e / kT). \quad (5.7)$$

According to Fick's second law, the variation in concentration with time can be expressed as:

$$\frac{\partial C}{\partial t} = \nabla J = \tilde{D} \frac{\partial^2 C}{\partial x^2}, \quad (5.8)$$

provided the diffusion coefficient is independent of concentration. It is possible to integrate this expression with respect to time in order to calculate the total change in concentration:

$$C = \int_0^t \nabla J dt = \int_0^t \tilde{D} \frac{\partial^2 C}{\partial x^2} dt. \quad (5.9)$$

Being a non-isothermal experiment, the temperature changes with time, and it is possible to change the integral variable:

$$C = \int_{RT}^{T_{\max}} \tilde{D} \frac{\partial^2 C}{\partial x^2} \frac{dt}{dT}, \quad (5.10)$$

where T_{\max} is the temperature at which the maximum in concentration occurs. Substituting the expression for the diffusion coefficient and rearranging terms the integration becomes:

$$C \left(\frac{dT}{dt} \right) = \left(D_o \frac{\partial^2 C}{\partial x^2} \right) \left(\frac{kT_{\max}^2}{A_e} \right) \exp \left(\frac{-A_e}{kT_{\max}} \right) \quad (5.11)$$

Taking logarithms of both sides, it is possible to see that the activation energy for oxygenation can be calculated from the slope of a plot of $\ln(dT/dt)$ vs. $1/kT_{\max}$. It would also be possible to plot $\ln((dT/dt)/T_{\max}^2)$ vs. $1/kT_{\max}$. Fig. 5.25 shows a plot of the results from both expressions, whose slopes give activation energies equal to 1.4 eV and 1.2 eV respectively given a total concentration change, C , of 0.4. These results agree with the activation energy calculated using the diffusion analysis of isothermal diffusion presented in the previous section (5.2.1.2)

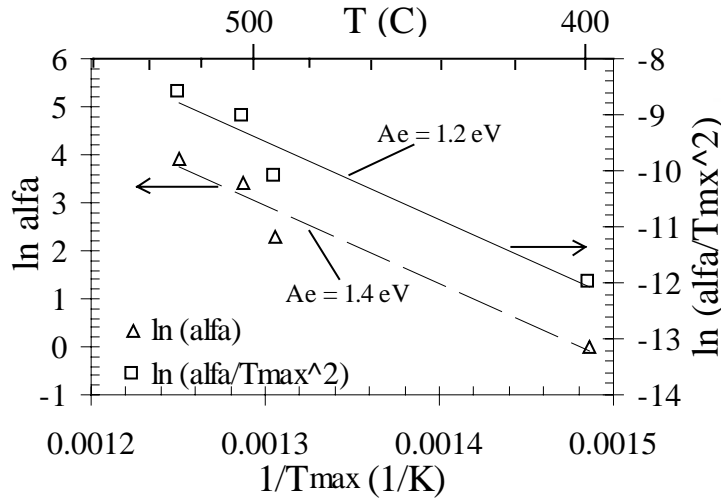


Fig. 5.25 Plots of $\ln(\alpha/T_{\max}^2)$ and $\ln(\alpha)$ vs. $1/T_{\max}$ for non-isothermal oxygen absorption at several heating rates

The values obtained in this calculation have an inherent error associated to the temperature lag of the furnace, which has been calculated to be around 20 °C at high temperatures. The average activation energy obtained is: 1.3 ± 0.1 eV. Having into account that this is a rough initial calculation using data collected under dynamic (non-equilibrium) conditions, this value agrees (within the experimental error limits) with that obtained using the methods described in sections 5.2.1.1 and 5.2.1.3.

5.3.2 Comparison with results from model

The computer model developed can reproduce quite accurately the experimental results under non-isothermal conditions, as it can be seen in Fig. 5.26 a). The curves obtained with this model reproduce slow and fast heating rate experiments.

The difference in maximum height between the curve modelled with the program and the experimental trace is attributed to the choice of a single particle size to calculate the theoretical curve, whereas the powder consists of a range of particle sizes. Their overall effect is a reduction in the height of the maximum weight. This can be clearly seen in Fig. 5.26 b). This figure shows a series of curves obtained for different particle sizes and their average for the same heat treatment. The maximum in the fractional weight change decreases and shifts to higher temperatures because the slower relative weight gain of bigger particles counteracts the effect of smaller particles and decreases the maximum in the average fractional weight change profile.

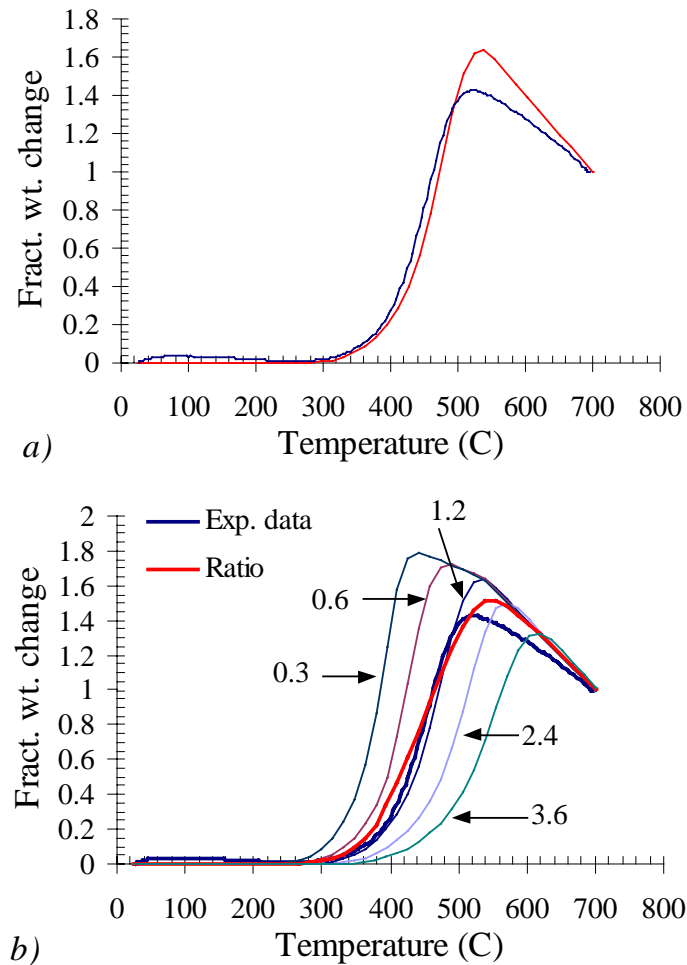


Fig. 5.26 Comparison of non-isothermal experimental and model curves. a) 50 °C/min to 700 °C (in red) for a particle with a radius of 2.1 μm (experimental result for the same heat treatment in blue), and b) model curves at different particle sizes (in microns) and their average (in red) compared to the experimental data (in blue). Heat treatment: 50 °C/min to 700 °C

The advantage of the use of this model is that it allows one to follow the evolution of the oxygenation process in the specimen while the temperature increases, as it calculates the concentration profile inside the sample. The variation in the oxygen distribution is shown in Fig. 5.27.

At the beginning (1) there is no weight change; only an outer cylinder of the disc is oxygenated at the equilibrium oxygen content for RT, representing the surface of the sample. In (2) the diffusion coefficient increases and the sample starts absorbing oxygen, decreasing the concentration gradient from the surface to the centre.

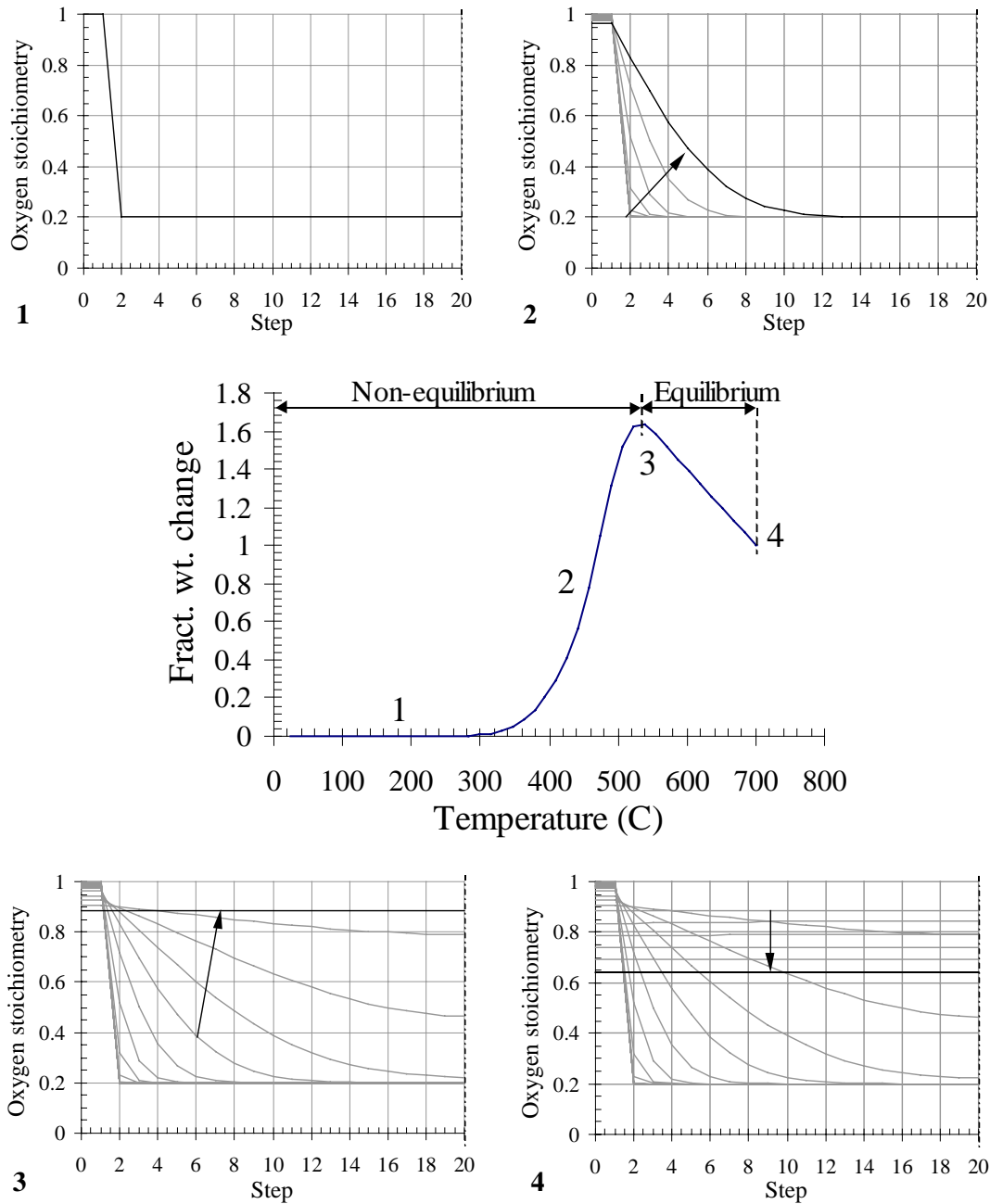


Fig. 5.27 Concentration profiles at different points during the heating in oxygen of a sample under non-isothermal conditions ($50\text{ }^{\circ}\text{C}/\text{min}$ to $700\text{ }^{\circ}\text{C}$). Time between lines 40 s . Particle radius: $2.1\text{ }\mu\text{m}$

During (1) and (2) the sample is not at its equilibrium oxygen content because the ramp rate and the slow diffusion coefficient at these low temperatures the sample cannot oxygenate completely. But when the temperature is sufficiently high (the diffusion coefficient has become faster), the sample has absorbed enough oxygen to have a uniform distribution within the sample, and it has the value of the equilibrium oxygen content at that temperature (3). From this point onwards the distribution of

oxygen in the sample is at equilibrium and decreases uniformly until the maximum temperature of the non-isothermal run is reached (4).

With respect to the cooling part of this non-isothermal experiment, it is very interesting to see that as the temperature decreases, the sample is at the equilibrium oxygen content (with a uniform distribution) until the temperature is decreased to T_{max} . Below this point, the diffusion coefficient becomes slower and the time spent at each temperature (determined by the cooling rate) is not long enough for full oxygenation of the sample to occur. This means that at the end of the cooling cycle, the sample has highly oxygenated edges and a centre with a lower oxygen content (see Fig. 5.28).

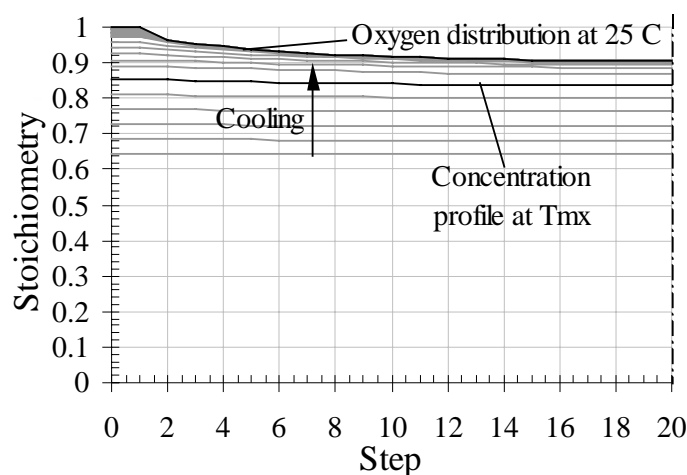


Fig. 5.28 Theoretical calculation of the concentration profiles at different points during the cooling in oxygen at 50 °C/min from 700 °C of a 2.1 μm radius sample under non-isothermal conditions. Time between lines: 20 s

5.3.3 Summary

This section has analysed the characteristic shape of non-isothermal oxygenation of YBCO powders. It has been shown how an analysis of this dynamic measurement can also yield information about the diffusion process.

The diffusion programme developed has successfully reproduced the experimental data taking into account the range of particle sizes present in the powder. The possibility of following the evolution of the oxygen concentration profile during the heat treatment corroborates the transition from a non-equilibrium situation where the

diffusion coefficient is too slow to oxygenate the sample fully, to a high temperature regime where the sample is always at its equilibrium oxygen content. This regime has a very interesting application that is going to be described in the following section.

5.4 Further applications of the model

5.4.1 *Quasi-equilibrium cooling*

It has been shown throughout this chapter that the model of the diffusion process developed can be applied to the study of oxygenation under isothermal and non-isothermal conditions. This model not only reproduces with accuracy the fractional weight changes of specimens under these conditions but also provides extra information, calculating the variation in the distribution of the oxygen content within the sample during the oxygenation process. Knowledge of this oxygen distribution is very important, as it can help predicting (or explaining) their superconducting behaviour.

This section is going to describe the development of a novel cooling procedure that could be introduced in the processing of YBCO specimens to give optimum superconducting properties by maximising their oxygen content in shorter oxygenation times.

It is known that in order to have a sample with good superconducting behaviour, its oxygen content must be above 6.9, and if possible it should be uniformly distributed. It has been shown in section 5.3.1 that during the cooling part of the non-isothermal experiments, the region above T_{max} corresponds to a uniform increase in oxygen content, where the sample is always at the equilibrium content for each temperature. The point at which this maximum occurs depends on the cooling rate, and it decreases with slower cooling rates (Fig. 5.29).

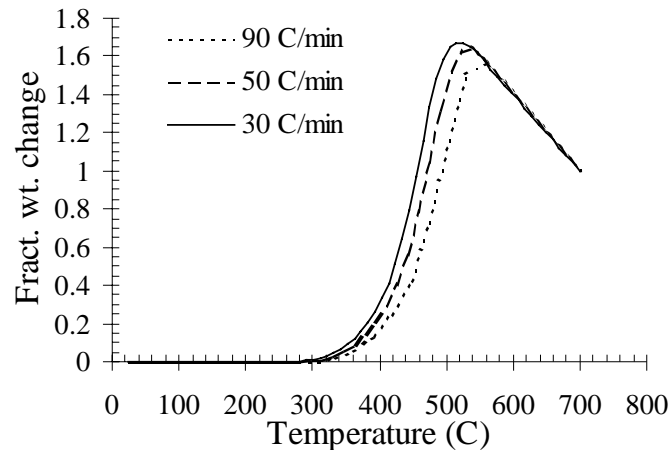


Fig. 5.29 Theoretical non-isothermal runs at 30, 50 and 90 °C/min showing the decrease in peak temperature with slower heating rates for a particle size 2.1 μm in radius

The cooling procedure developed here combines these two factors: on one hand, the possibility to cool a sample to a certain temperature, T_{max} , while its oxygen content is uniformly distributed and at equilibrium, and on the other hand being able to decrease this temperature, T_{max} , (below which the sample is no longer at “equilibrium”) slowing the cooling rate. The cooling process developed keeps the sample at its equilibrium oxygen content while the sample is being cooled decreasing the cooling rate. The change in oxygen content is only possible if the equilibrium condition is altered for a short period of time, establishing a concentration gradient across the sample. Therefore, this improved oxygenation process is going to be referred to as *quasi-equilibrium cooling*.

Two assumptions have been made in the development of this cooling procedure:

- The cooling rate of the sample is never faster than 90 °C/min,
- The material used for these preliminary theoretical experiments is powder with an average particle size of 2.1 μm in radius.

The first step is to obtain an expression relating the maximum temperatures to the cooling rates. There is an exponential relationship between them that can be calculated empirically from the slope and intercept of the straight line obtained when plotting $\log(\text{cooling rates})$ vs. T_{max} (Fig. 5.30). The expression obtained is:

$$\text{Cooling rate} = 8 \times 10^{-7} \exp(0.0338 \times T_{max}) \quad (5.12)$$

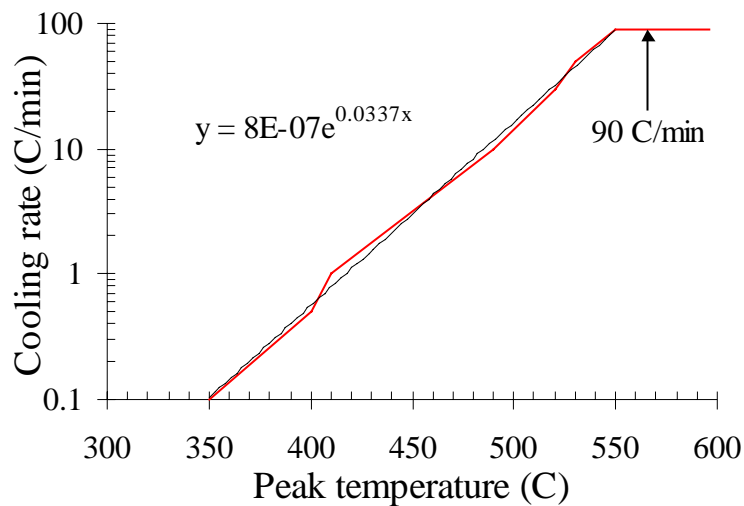


Fig. 5.30 Plot of cooling rates, α (log scale), against maximum temperature, T_{max} characteristic of a particle with a radius equal to $2.1 \mu\text{m}$

Fig. 5.28 shows that the distribution of the oxygen absorbed during cooling is uniform as long as the temperature is higher than T_{max} (schematic (3) in Fig. 5.27). Below this temperature, the absorption ceases to be uniform because the diffusion coefficient becomes too slow; at these lower temperatures oxygen concentrates on the outer regions of the particle. This sets a limit in the uniform distribution of oxygen within the specimen as well as on the value of its oxygen content. The final distribution is not going to be constant, as shown in Fig. 5.28. But it is guaranteed to be *at least* as high as the equilibrium oxygen content for T_{max} of the heating rate used. Oxygen will be uniformly distributed in the sample up to this content. The values of the equilibrium oxygen content of each T_{max} considered are therefore going to be taken as the oxygen contents obtained when applying the *quasi-equilibrium procedure*. This gives a certain margin of error, as the oxygen content is always going to be somewhat higher than the values given in the following tables and graphs.

Table 5.2 shows a series of cooling rates, their characteristic peak temperatures obtained from the non-isothermal experiments carried out with powder samples and the equilibrium oxygen contents for those temperatures (from Gallagher (1987)). These data have been represented in Fig. 5.31 below.

α ($^{\circ}\text{C}/\text{min}$)	T_{\max} ($^{\circ}\text{C}$)	Oxygen content
0.1	350	6.95
0.5	400	6.95
1	410	6.95
10	490	6.91
30	515	6.89
50	530	6.87
90	550	6.85

Table 5.2 Cooling rates, associated maximum temperatures and their equilibrium oxygen content for powder samples (experimental data)

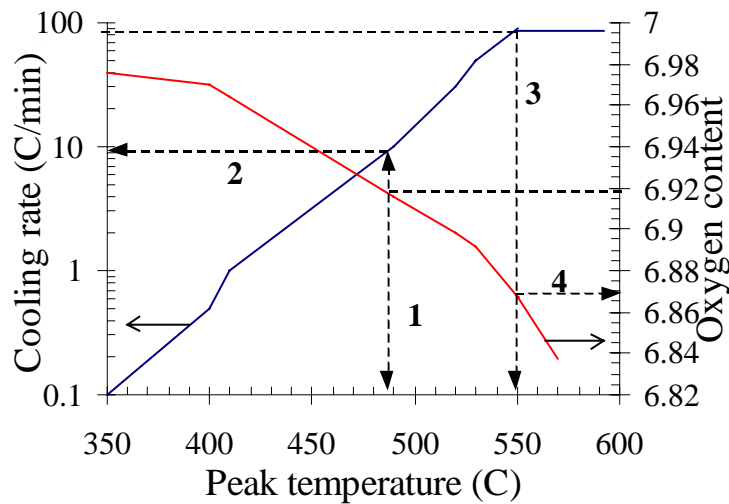


Fig. 5.31 Plot of cooling rates vs. T_{\max} and equilibrium oxygen content vs. T_{\max}

Fig. 5.31 can be used to make the predictions mentioned above:

If the minimum oxygen content required for a sample is 6.92, taking this point in the oxygen content vs. T_{\max} line, it is possible to see that the temperature at which 6.92 is the equilibrium content is approximately 485 $^{\circ}\text{C}$ (line 1). This temperature is the T_{\max} of a cooling rate that can be read from the α vs. T_{\max} line (line 2). The cooling rate for which 480 $^{\circ}\text{C}$ is T_{\max} is ~ 9 $^{\circ}\text{C}/\text{min}$, therefore, if this sample is cooled at 9 $^{\circ}\text{C}/\text{min}$ from 700 $^{\circ}\text{C}$ to room temperature, its oxygen content will be *at least* 6.92.

If, on the other hand, the powder has been cooled at 90 $^{\circ}\text{C}/\text{min}$, the peak temperature characteristic of this rate is 550 $^{\circ}\text{C}$ (line 3), which means that the oxygen content of

the powder will be *at least* 6.87 (line 4). This amount will be uniformly distributed in the powder particles.

Knowing the cooling rate it is possible to calculate the time it will take to decrease the temperature from 700 °C to T_{max} :

T_{max} (°C)	α (°C/min)	Cooling time from 700 °C	Oxygen content
350	0.1	58 h 20 min	6.98
400	0.4	12 h 30 min	6.97
415	1	4 h 75 min	6.96
480	9	24 min 26 s	6.92
518	25	7 min 17 s	6.90
530	45	3 min 45 s	6.89
550	90	1 min 40 s	6.87

Table 5.3 Cooling times from 700 °C to the T_{max} characteristic of each cooling rate, α , for a 2.1 μm radius particle

If the oxygen content required is high, the maximum temperature will be low; this means that the powder should be cooled at a very slow rate. However, it can be seen from Table 5.3 that there is no need to keep the cooling rate constant in order to cool the specimen in the quasi-equilibrium conditions described. Fast rates can be used at high temperatures and slower rates at low temperatures to obtain the same final oxygen concentration. Provided the temperature is never below the characteristic T_{max} for each rate chosen the material will be at equilibrium, and it will be possible to combine the cooling rates so that if the final oxygen content is 6.97. Taking these temperature steps to be the as big (and different in size) as those in the table above, the cooling procedure would be:

From 700	to 550 °C at	90 °C/min	1 min 40 s
From 550	to 530 °C at	45 °C/min	24 s
From 530	to 518 °C at	25 °C/min	29 s
From 518	to 480 °C at	9 °C/min	4 min 13 s
From 480	to 410 °C at	1 °C/min	1 h 10 min
From 410	to 400 °C at	0.4 °C/min	<u>25 min</u>
Total			~ 1 h 51 min

The difference in total cooling time between the single-rate cooling to 400 °C (at 0.4°C/min) to the step-cooling shown above is quite large: approximately 10 h.

This *quasi-equilibrium cooling* procedure can be improved setting the temperature intervals to be of a certain size. This would allow the construction of a table with the time it takes to cool down from one temperature to another. The reduction in temperature could be set to occur in 20 °C intervals, for example, and the cooling rates for each of them would be the characteristic rates of the lower temperatures in the step. Table 5.4 shows an example of these *quasi-equilibrium cooling* times.

To obtain a powder sample with an oxygen content of 6.97, for example, the table shows how long it would take to cool from 700 °C and the cooling rates required for each one of the temperature intervals. As it has been shown above, the final temperature of the cooling procedure should be 400 °C, and the cooling time would be 1 h. The column on the right hand side shows the time it would have taken to cool to that temperature using only the characteristic cooling rate for 400 °C (0.42°C/min): approximately 12 hours.

The data from this table can also be presented in the form of a graph showing the equilibrium oxygen content and reduced cooling times (see Fig. 5.32). Extended times (single cooling rate) are included for comparison. The overlap of these two curves at high temperatures is due to the limitation in cooling rate mentioned at the beginning of this section: rates cannot be faster than 90 °C/min, which means that cooling to 560°C will always be carried out at the same rate, and reduced and extended times will coincide. Below this temperature, the curves separate showing the difference in cooling times between both procedures (single cooling rate and quasi-equilibrium cooling).

Oxygen content	Peak T (°C)	Cooling rate (°C/min)	Reduced time from 700 °C	Extended time from 700 °C
6.98	300	0.01	28 h 42 min	19 days 16 h 42 min
6.98	320	0.03	14 h 36 min	13 days 17 h
6.98	340	0.06	7 h 27 min	4 days 14 h 22 min
6.97	360	0.11	3 h 48 min	53 h
6.97	380	0.22	1 h 57 min	25 h 28 min
<u>6.97</u>	<u>400</u>	<u>0.42</u>	<u>60 min</u>	<u>12 h 10 min</u>
6.96	420	0.83	31 min	5 h 47 min
6.95	440	1.64	17 min	2 h 45 min
6.93	460	3.23	9 min	1 h 17 min
6.92	480	6.34	6 min	36 min
6.91	500	12.47	3 min	17 min
6.89	520	24.52	2 min	8 min
6.88	540	48.20	2 min	4 min
6.85	560	90	1 min	2 min
6.82	580	90	1 min	1 min
6.80	600	90	1 min	1 min
6.76	620	90	< 1 min	1 min
6.73	640	90	< 1 min	< 1 min
6.70	660	90	< 1 min	< 1 min
6.67	680	90	< 1 min	< 1 min
<u>6.64</u>	<u>700</u>			

Table 5.4 Comparison between reduced and extended times for quasi-equilibrium cooling from 700 °C of powder with 1.2 μm radius particles

Fig. 5.32 shows the same example used to demonstrate the application of the *quasi-equilibrium cooling* table: 6.97 is the equilibrium oxygen content at 400 °C, which means that cooling from 700 °C to this temperature following the quasi-equilibrium procedure it would take 1 h, while it would take approximately 12 h to achieve the same oxygen concentration using a single cooling rate. The time needed to cool to room temperature would be added to this value to give the total time of the cooling step.

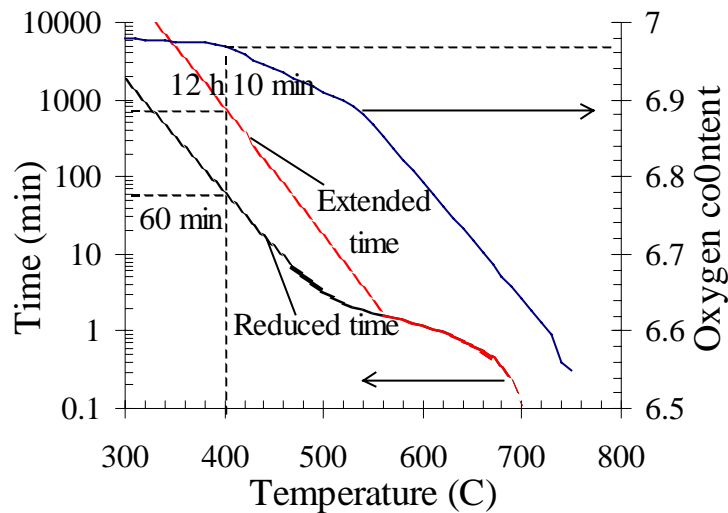


Fig. 5.32 Combination plot showing equilibrium oxygen content, reduced and extended cooling times vs. T_{max} (diffusion distance: $2.1 \mu m$)

The starting temperature can be altered to suit the processing route, and the temperature intervals can be modified to accommodate to the programming options of the furnace used. If the temperature steps were very small, the total cooling stage would be reduced to shorter times, but this would not be very practical experimentally, because furnaces have a limited number of heat treatment steps. However, no matter what the size of the temperature steps is, the *quasi-equilibrium cooling* procedure always provides an alternative oxygenation with shorter processing times.

5.4.2 Extrapolation to different particle sizes

The alternative cooling route presented in the previous section is valid for small powder particles ($2.1 \mu m$ in radius). However, the size of the specimens used for practical applications often bigger than just a few microns (sometimes of the order of tens of mm), so it would be ideal if these curves were available for a range of particle sizes.

One way of calculating these quasi-equilibrium cooling procedures for a number of particle sizes would be to carry out experimentally a series of non-isothermal oxygenations and calculating the relationship between cooling rate and maximum temperature from the peaks obtained. This presents a problem that has already been referred to at the beginning of the chapter: as the size of the specimen increases (the

diffusion distance increases) diffusion times increase too, slowing the data gathering process considerably.

The diffusion model developed can be used to calculate theoretically the non-isothermal experiments required to establish the relationship between cooling rates and maximum temperatures. This can be done either fixing the grain size and recalculating the expression of cooling rate (α) vs. T_{max} , as it has been shown in the previous section, or extrapolating these values from a known group of particle sizes to the required particle size.

In the first case, Fig. 5.33 shows that an increase in the particle size requires a decrease in the cooling rates used. If the rates are too fast, the sample will only be partially oxygenated at the end of the process. The relationship between cooling rates and T_{max} obtained for a 10 μm radius particle is:

$$\text{Cooling rate} = 2 \times 10^{-5} \exp(0.0219 \times T_{max}) \quad (5.13)$$

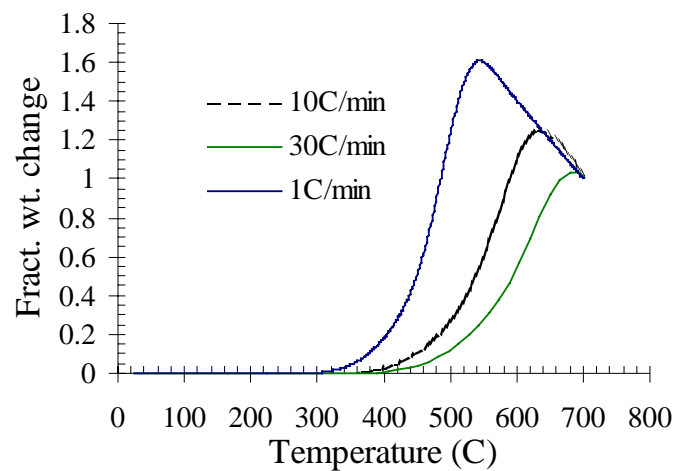


Fig. 5.33 Theoretical non-isothermal oxygenations of a 10 μm radius particle. Note the slower cooling rates compared with those used to oxygenate a 2.1 μm radius particle (Fig. 5.29)

This reduction in ramp rates means that the oxygenation times are going to increase considerably, but as it is shown in Table 5.5 and Fig. 5.34, the *quasi-equilibrium cooling* procedure developed still offers a faster alternative way of oxygenating the specimens.

Oxygen content	Peak T ($^{\circ}\text{C}$)	Cooling rate ($^{\circ}\text{C}/\text{min}$)	Reduced time from 700°C	Extended time from 700°C
6.98	300	0.03	1 day 8 h 48 min	9 days 16 h 40 min
6.98	320	0.04	21 h 9 min	5 days 22 h 38 min
6.98	340	0.07	13 h 40 min	3 days 15 h 12 min
6.97	360	0.11	8 h 49 min	2 days 5 h 9 min
6.97	380	0.17	5 h 41 min	1 days 8 h 17 min
<u>6.97</u>	<u>400</u>	<u>0.26</u>	<u>3 h 40 min</u>	<u>19 h 32 min</u>
6.96	420	0.40	2 h 22 min	11 h 46 min
6.95	440	0.61	1 h 32 min	7 h 3 min
6.93	460	0.95	59 min	4 h 12 min
6.92	480	1.48	38 min	2 h 29 min
6.91	500	2.29	25 min	1 h 27 min
6.89	520	3.54	16 min	51 min
6.88	540	5.49	10 min	29 min
6.85	560	8.51	7 min	16 min
6.82	580	13.19	4 min	10 min
6.80	600	49.08	3 min	5 min
6.76	620	76.06	2 min	3 min
6.73	640	90	1 min	1 min
6.70	660	90	1 min	1 min
6.67	680	90	< 1 min	< 1 min
<u>6.64</u>	<u>700</u>			

Table 5.5 Comparison between reduced and extended times for quasi-equilibrium cooling from 700°C of powder with $10\ \mu\text{m}$ radius particles. Note the increase in cooling time and decrease in ramp rates for the same oxygen contents (and peak temperatures)

Going back to the case of oxygenation to 6.97 again, the time it would take to increase the oxygen content to that value using the quasi-equilibrium cooling method would be approximately 3 h 40 min, which is a much better alternative than the $\sim 19\frac{1}{2}$ hours it would take using a single cooling rate (Table 5.5 and Fig. 5.34).

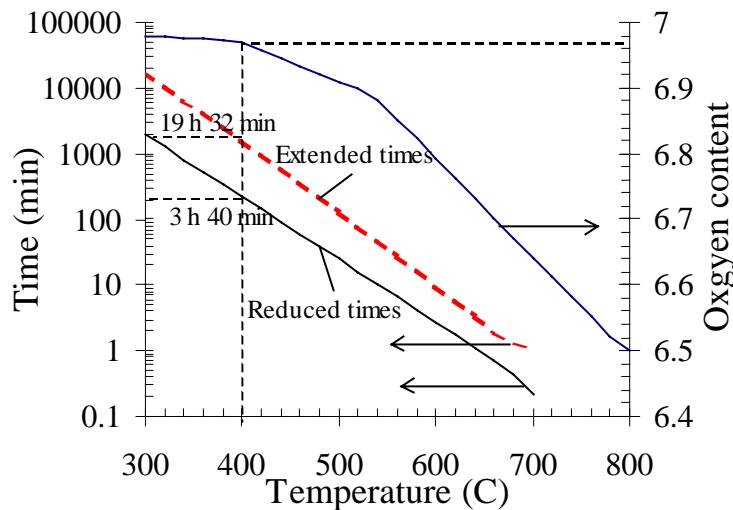


Fig. 5.34 Combination plot showing equilibrium oxygen content, reduced and extended cooling times vs. T_{max} for a particle with a $10\ \mu\text{m}$ radius (note that the cooling rates are much slower in the case of a $2.1\ \mu\text{m}$ particle (Fig. 5.32))

If instead of fixing the particle size the study was carried out setting the cooling rates constant, the procedure would be the following:

In the first place, it is necessary to obtain the empirical relationship between particle size and T_{max} for a chosen cooling rate. This relationship has been found to be logarithmic; taking the maximum temperatures and cooling rates characteristic for a $2.1\ \mu\text{m}$ radius particle (Eq. (5.12)), those for a $10\ \mu\text{m}$ particle (Eq. (5.13)) and similar data for other different particle sizes, it has been found that grouping the theoretical results by cooling rates and plotting T_{max} vs. $\log(\text{particle size})$ gives a series of parallel lines with the same slope. Fig. 3.35, for example, shows the change in T_{max} that corresponds to a cooling rate of $0.1\ ^\circ\text{C}/\text{min}$.

An increase in the grain size results in an increase of the temperature below which the sample is not at its equilibrium oxygen content. This means that the temperature at which the cooling procedure starts may have to be increased to 800 or $900\ ^\circ\text{C}$.

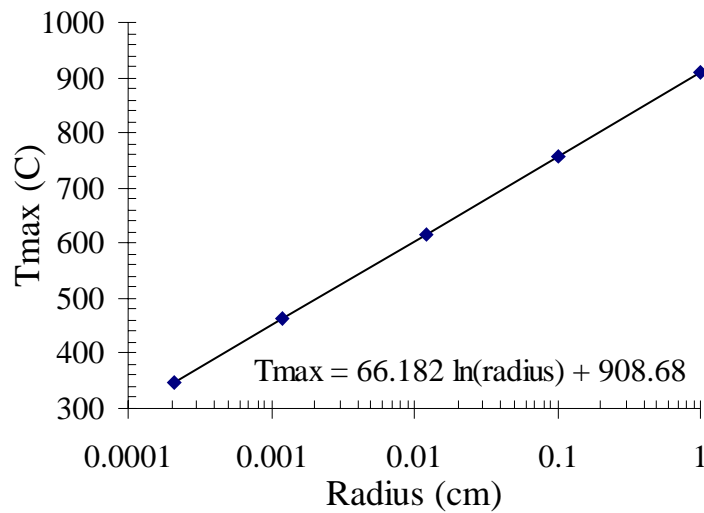


Fig. 5.35 Empirical relationship between grain sizes (radii) and maximum temperatures for a cooling rate of 0.1 °C/min

It has already been mentioned that the slope of the line relating T_{max} and particle radius is the same for any cooling rate (α) chosen, so in order to complete Fig. 3.35 for a wider range of cooling rates, it is only necessary to shift the T_{max} characteristic of the 0.1 °C/min rate so that it intersects at the different T_{max} - α points already calculated for one of the particle sizes (see Fig. 5.36).

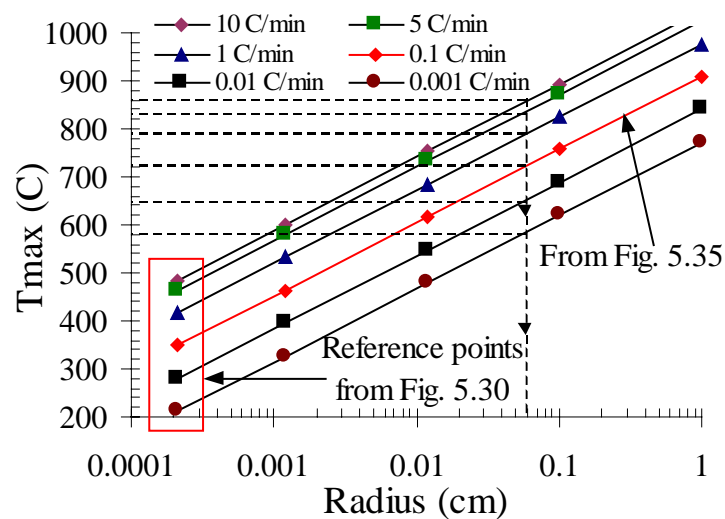


Fig. 5.36 Empirical relationships between grain sizes (radii) and maximum temperatures for a series of cooling rates

The graph that results from this series of relationships can be used as a guide of the temperature range and cooling rates that need to be used for a *quasi-equilibrium*

oxygenation of specimens of any size; this would allow the calculation of the oxygenation times that would result from using the cooling rates shown.

If the specimen to oxygenate had the dimensions $1 \times 1 \times 1 \text{ mm}^3$, the diffusion distance would be equal to 0.5 mm. For a particle with a radius equal to 0.5 mm, the following cooling procedure (from $\sim 900 \text{ }^\circ\text{C}$ in pure oxygen) can be drawn up from the data plotted in Fig. 5.36 (approximate oxygen contents characteristic of each temperature are shown in brackets):

Cool:	at $10 \text{ }^\circ\text{C}/\text{min}$ to	880 $^\circ\text{C}$	(6.41)	
	at $5 \text{ }^\circ\text{C}/\text{min}$ to	830 $^\circ\text{C}$	(6.46)	10 min
	at $1 \text{ }^\circ\text{C}/\text{min}$ to	790 $^\circ\text{C}$	(6.50)	50 min
	at $0.1 \text{ }^\circ\text{C}/\text{min}$ to	720 $^\circ\text{C}$	(6.59)	11 h 40 min
	at $0.6 \text{ }^\circ\text{C}/\text{h}$ to	650 $^\circ\text{C}$	(6.70)	4 days 20 h 40 min
	at $1.4 \text{ }^\circ\text{C}/\text{day}$ to	580 $^\circ\text{C}$	(6.82)	<u>1 month 18 days 14 h</u>
				~1 month 23 days

This cooling procedure will yield a sample with an oxygen content equal to ~ 6.82 . However, this content is very low for the material to have good superconducting properties, so it would be necessary to decrease the temperature further. Due to the increased particle size and slower diffusion rates at low temperatures, continuing the oxygenation to increase the oxygen content using the quasi-equilibrium cooling procedure would require the use of slower cooling rates (of the order of degrees per month), which would result in unreasonably long cooling times.

The application of this oxygenation procedure for larger particles at lower temperatures appears to be very complex due to the slow cooling rates needed. However, it should be pointed out that these large specimens are usually polycrystals, and diffusion in these materials occurs not only through the bulk, but combines with grain boundary diffusion in the lower temperature range. The effects of other microstructural features, such as porosity or presence of impurities should also be taken into account. This could result in a faster overall diffusion process that would involve faster cooling rates and yield shorter oxygenation times.

5.4.3 Summary

This section describes the development of a dynamic cooling procedure that can be introduced in the processing of YBCO to yield highly oxygenated samples with a uniform distribution of oxygen. This procedure has been termed *quasi-equilibrium cooling* and has been developed based on data collected experimentally during non-isothermal oxygenations of powder samples at different rates.

Using the diffusion model developed it has been possible to obtain theoretical results of non-isothermal oxygenations of larger particles that would have otherwise taken a very long time to carry out and it has been possible to present an initial extrapolation of this cooling procedure to bigger samples. The application of this *quasi-equilibrium cooling* procedure to oxygenate large specimens is still in an initial stage. All the work carried out in this thesis has been done using a bulk diffusion coefficient, but polycrystalline samples have a different effective diffusion coefficient, incorporating grain boundary diffusion at lower temperatures. More work should be carried out to evaluate the use of this cooling procedure in the oxygenation of polycrystalline samples.

5.5 Conclusions

This chapter has presented an analysis of the results obtained using thermogravimetry to measure the oxygenation of YBCO powder samples. Fitting a solution to Fick's first law with the appropriate boundary conditions it has been possible to calculate the pre-exponential coefficient, D_0 , and the value of the activation energy of this diffusion process that can be described with an Arrhenius equation. The values obtained for the variation of the oxygen diffusion coefficient with temperature have been compared to the results published in the literature.

The diffusion model developed described in chapter 4 uses the values of D_0 and the activation energy calculated from the experimental data. It has been shown that this model can be successfully applied to the analysis and prediction of isothermal oxygenations. The evolution of the oxygen concentration profile within the sample can also be followed using the programme developed; this is of great interest as this

information could be applied to the analysis of the superconducting properties of oxygenated specimens.

This isothermal study of powder samples is followed by a brief account of the work done on polycrystalline specimens of different density. The results obtained show that the diffusion process in polycrystals is very complex, as it has already been pointed out in chapters 2 and 3. The analysis of the data collected with the solution to Fick's first law used for the study of oxygenation of powder specimens has only attempted to calculate a rough estimate of the oxygen diffusion coefficient for polycrystalline samples.

The final section of this chapter concentrates on the study of non-isothermal oxygenations. It analyses the characteristic shape of non-isothermal oxygenation traces; these curves can be divided into a non-equilibrium region during which the sample absorbs oxygen at a rate too slow to achieve full oxygenation, and an equilibrium region in which the specimen is at the equilibrium oxygen content for each temperature. A preliminary analysis of the non-isothermal results has allowed one to calculate a value for the activation energy of the oxygenation process that agrees well with that calculated from isothermal oxygenations.

The characteristic behaviour of the non-isothermal oxygenation trace at high temperatures has been used to develop a novel cooling procedure that consists in decreasing the temperature of the specimen from the last high-temperature stage during manufacturing at a series of cooling rates that ensure that the sample is at the equilibrium oxygen content of each temperature. This procedure has been termed *quasi-equilibrium cooling*.

It has been calculated that the *quasi-equilibrium cooling* procedure reduces the duration of the oxygenation step; this difference increases with the size of the samples. Therefore, the procedure could be implemented at the end of the processing of YBCO superconducting samples instead of the isothermal oxygenation stage usually employed. This would eliminate (or reduce the effects of) one of the problems linked to the use of high temperature superconductors in industrial applications: the need of long oxygenation stages that become increasingly long with sample size; this makes

the manufacturing process of YBCO for high temperature superconducting applications not viable commercially.

The diffusion programme has been used to calculate the final distribution of oxygen in the sample at the end of the *quasi-equilibrium cooling*. It has been possible to extrapolate diffusion results to larger samples reducing the overall experimentation time in this thesis and completing the design of novel cooling procedures for samples of different sizes. These extrapolated values can be used as a guideline to design the cooling/oxygenating procedure appropriate for the size of the sample used in each case. This study should be developed further using a diffusion expression typical of polycrystalline YBCO that took the effects of grain boundaries and porosity in the diffusion process. This would allow the development of cooling procedures for samples used in large-scale applications.

The study of isothermal and non-isothermal oxygenations of YBCO carried out using thermogravimetry and the development of a diffusion model to reproduce these results theoretically have allowed one to gain more information about the oxygen diffusion process. Using the programme to reproduce oxygenation experiments theoretically it has been possible to develop an oxygenating procedure that could reduce the length of the processing of YBCO specimens for large scale applications.

Chapter 6

Direct Current Zoning effect

6.1 Introduction

The previous chapters have presented a study of the diffusion of oxygen in $\text{YBa}_2\text{Cu}_3\text{O}_{7-\delta}$ (YBCO). It has already been pointed out that the properties of superconducting oxides are strongly dependent on the oxygen non-stoichiometry and its distribution over the whole sample. Because of this non-stoichiometry YBCO behaves as a solid mixed conductor at high temperatures, showing predominantly electronic conductivity but also a significant ionic mobility; its overall resistivity increases steeply for $T > 400$ °C due to the loss of oxygen and the increase in the scattering of carriers. Above this temperature the oxygen ion conductivity (similar to that of fast ionic conductors at high temperatures, see Fig. 6.26) becomes significant in the conduction process. The subject of this chapter is directly related to the mixed conductor behaviour of YBCO and to the diffusion of oxygen ions in this material.

This chapter presents a brief review of the high temperature electrical properties of YBCO together with a review of the work carried out to study the Direct Current Zoning effect. This is followed by a presentation and analysis of the work done and concludes with the description of the computer model developed to reproduce the effect of Direct Current Zoning in an ideal sample.

6.2 Direct Current Zoning effect (DCZ)

It has been observed that when a DC current is applied to a polycrystalline bar of YBCO (and other superconducting materials) a hot zone forms at a certain point along the bar. The zone has been observed to drift towards the cathode. This phenomenon is known as Direct Current Zoning (DCZ), and it is going to be reviewed in the following sections.

The formation of a hot zone when a DC current is applied across the sample is related to the increase in mobility of the oxygen ions in the sample with temperature and the resulting change in ionic conductivity as well as to the steep increase in the resistivity of the sample with temperature (see Fig. 6.3). Inhomogeneities in composition, density or cross sectional area of the sample are thought to be the nucleation points of the zone, although the precise combination of factors that determine the onset of zone formation is not at present understood. The hot zone moves towards the negative electrode. This drift is related to the migration of oxygen ions towards the anode due to the potential difference, and within and out of the sample due to the changes in temperature. The fast ionic motion of the ions in the structure could introduce the use of YBCO as an oxygen sensor and it can also help in the understanding of the complex kinetics and thermodynamics during the processing of high temperature superconductors. The following sections present the work carried out by other groups.

6.2.1 DCZ in YBCO

Apart from the work reported here, three other groups world-wide have studied this phenomenon and the results published disagree in certain aspects. The materials studied by the different groups were: YBCO (Osip'yan *et al.* (1988), Bobrov *et al.* (1990) and Nefedov *et al.* (1992)), Bi-Pb-Sr-Ca-Cu-O (Yanmaz *et al.* (1992), (1993)) and GdBCO (Okamoto *et al.* (1994-a) (1994-b)). All of the work reported has been carried out on untextured polycrystalline ceramic samples.

Osip'yan *et al.* (1988) applied a DC current to YBCO bars and observed the formation of a hot zone drifting towards the negative electrode. This behaviour was associated with a non-linear dependence of the resistivity of the material with temperature and the evolution of oxygen during Joule heating. They pointed out that such a loss would be accompanied by the formation of a high concentration of positively charged oxygen vacancies whose mobility in an electric field would determine the drift of the zone. In another report by the same group, Bobrov *et al.* (1990) propose a model for the presence of the hot zone in YBCO. In this model the effects of heat release and heat transfer are linked to the increase in resistance and the oxygen vacancy concentration and diffusion through the material.

However, the I-V characteristic of the formation of the zone and the relationship between domain drift velocity and current do not agree with reports published later and with the work presented in this report.

Bobrov *et al.* (1990) claim that an increase in current increases the speed at which the zone moves. But it has been observed in this work that the zone becomes immobile when the voltage is increased above a certain value. This results in an increase in the resistance of the sample, which in turn raises the temperature of the zone up to the point where catastrophic failure could occur, melting the sample.

Nefedov *et al.* (1992) reported the DC treatment on the YBCO superconducting ceramics at 77K and observed that light impurities (Na, K, Cl) and oxygen migrate towards the appropriate electrode, resulting in a change of the properties of the material.

Fig. 6.1 Sequence photograph after applying a DC voltage of 7V to $GdBa_2Cu_3O_{7.8}$. The pictures are taken at 2 min intervals. The movement reverses each time the polarity is reversed (after Okamoto *et al.* (1994-b))

Okamoto *et al.* (1994-a), (1994-b) report the same DCZ effect for samples of GdBCO when a DC voltage of 7 V is applied at room temperature. They studied the effects of partial oxygen pressure in the generation and movement of the zone. They reported that the current necessary to create and maintain the hot zone appeared to be very sensitive to the oxygen pressure in the atmosphere, and once the zone was present it was observed to increase size with increasing voltage (Fig. 6.2). This group observed

that the total current after the appearance of the hot zone was independent of the applied voltage, which contradicts the measurements presented in this chapter. They report that the value of the current needed to create a zone increased with increasing oxygen pressure and so did the drift velocity of the zone, agreeing with Bobrov *et al.* (1990). They conclude that these variations in oxygen pressure affect the oxygen migration in the hot zone.

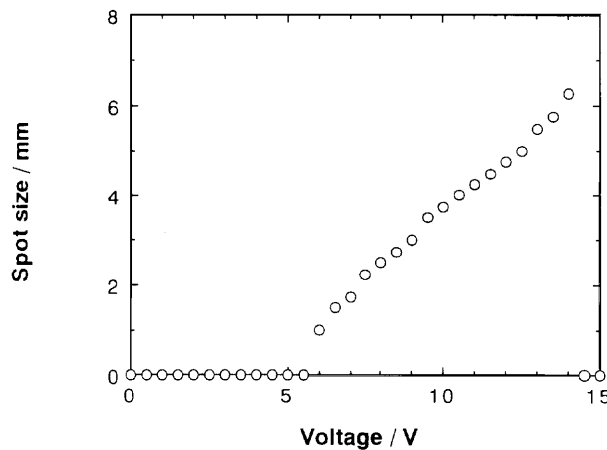


Fig. 6.2 Voltage dependence of the spot size (after Okamoto *et al.* (1994-b))

Migration of the hot spot is explained by Okamoto and co-workers in the following way:

“[...] The oxygen ions in the hot zone move easily due to the high temperature and high concentration of oxygen vacancies. When oxygen ions move to the positive potential side of the hot spot, the resistivity increases on the negative side and decreases on the positive side. [...] Because the system tries to stay in equilibrium, oxygen will diffuse into the sample at the positive side which will further decrease the resistivity and the temperature. At the side of the negative electrode oxygen will be released from the sample, hence the resistivity and the temperature will increase. Consequently, the spot will move to the negative electrode”.

This is a very good description of the phenomenon that is going to be explained in more detail in section 6.4.

6.2.2 DCZ in other materials: Bi-Pb-Sr-Ca-Cu-O

Yanmaz *et al.* (1992), (1993) report another application of this heating effect by applying an electric field across the sample. They observed that an increase in 0.2 A produced another zone in the sample once the first one appeared. The passing of the zone was observed to alter the final microstructure of the specimen. The formation of two zones in the bar has also been observed in the experiments carried out for this dissertation (see section 6.4). This result does not agree with the I-V characteristic of the DCZ effect shown by Okamoto *et al.* (1994-a), where the current was constant once a zone formed, independently of the voltage applied.

Yanmaz and co-workers observed the modification of the microstructure of the zoned samples, and so have the other authors like Bobrov *et al.* (1990), for example, who reported a change in the structure of the sample from orthorhombic to tetragonal where the zone was present and a change to orthorhombic again once the zone had moved towards the negative electrode. They agreed with Bobrov *et al.* (1990) in that the speed of the zone increased with increasing current.

The suggested explanation for the DCZ effect by Yanmaz *et al.* (1992), (1993) is not very clear. They propose that the creation and movement of the zone could be due to solid electrolysis, with O^- ions migrating under an electric field gradient from the negative to the positive electrode, thus increasing:

“[...] the O^- ion concentration at the positive electrode with a consequent increase in electrical resistance. This results in a “hot spot” and the creation of a zone due to resistance heating. Because the material becomes hot, oxygen is lost, the resistance falls and the zone then moves to another high resistance region”.

This decrease in resistance with decreasing oxygen ion concentration contradicts the reported change in the electrical properties of YBCO with increasing temperature: as temperature increases, the oxygen content decreases and the resistivity of the material increases, as it is going to be seen in section 6.3 (e.g. Gurvitch and Fiori (1987)).

6.2.3 Effect of different atmospheres

Osip'yan *et al.* (1994-b) and Bobrov and co-workers studied the effects of different atmospheres on the DCZ effect and found that the zone drift velocity increased when the samples were studied in oxygen atmosphere, and the size of the zone and the drift velocity decreased when using helium. In vacuum a hot zone appeared but no drift was observed. This resulted in a continuous heating of the sample and led to catastrophic failure by melting at the zone. This difference in behaviour when changing the oxygen content of the atmosphere means that the movement of oxygen ions is very important in this process but a full explanation to this phenomenon has not been presented yet.

6.3. High temperature transport properties

6.3.1 Review

After the discovery of YBCO much of the experimental and theoretical work on the electronic behaviour of this material concentrated on the range of temperatures around and below T_c in order to explain the mechanism of superconductivity in this regime. But interest has also developed in the study of normal state electronic properties of high temperature superconductors with the hope that such properties might help in understanding the mechanism of high T_c superconductivity.

Conductivity measurements provide information about the product of the mobility of the charge carriers and their concentration in the sample. However, in the work published on the YBCO system there has been an accumulation of conflicting reports concerning its structural and electrical properties. Most of the work concentrates in the determination of data within very limited regimes which does not allow one to draw general conclusions concerning the defect structure of the oxide phase or its electrical properties. In spite of this there is a general agreement on the decrease of conductivity with decreasing oxygen content.

In order to be able to study the Direct Current Zoning process it is necessary to know how the conductivity of YBCO changes at high temperatures. This section presents a review of the work carried out in this field.

Grader *et al.* (1987) observed a variation in the slope in the plot of resistivity vs. temperature in a region near the orthorhombic-tetragonal transition and associated this change in resistivity to the phase change in the crystal structure. This has also been suggested by Fiori *et al.* (1987) (Fig. 6.3), Fisher *et al.* (1987) and Davidson *et al.* (1988).

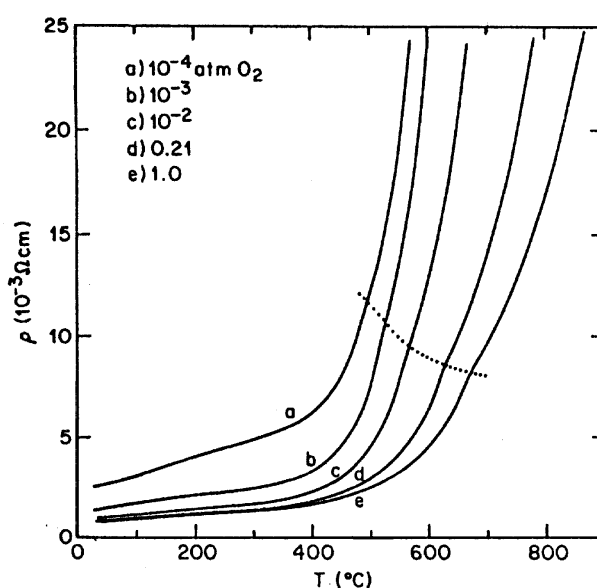


Fig. 6.3 Temperature dependence of the resistivity of YBCO at various partial oxygen pressures (after Fiori *et al.* (1987))

However, Park and Kim (1988) and Yamaguchi *et al.* (1988) did not link this change in slope with the order-disorder transition. It has been corroborated by other authors that it occurs due to a change in the charge transport behaviour from metallic to semiconducting. The temperatures at which this change is observed vary from 427 °C in air (Munakata *et al.* (1987)), higher than 400 °C (Park and Kim (1988)), approximately 500 °C in air (Brabers *et al.* (1988)) to 620 °C in air and 680 °C in O₂ (Park *et al.* (1988)). The last two values seem too high compared with the rest.

This variation in conducting behaviour is directly related to the oxygen non-stoichiometry of the sample; since its distribution and the measurement of oxygen motion in the sample appears to be very dependent on microstructure (see chapter 3),

some scatter in the values is expected. The conductivity of the specimen is determined by its thermal history, its microstructure and the measuring technique used.

The change in slope in the conductivity has also been measured in terms of oxygen content. The values at which this change in slope has been observed to occur range from 6.3 (Leonidov *et al.* (1989)) and 6.5 (Yamaguchi *et al.* (1988)), to 6.8 (Yoo and Lee (1994)). The result from Leonidov *et al.* (1989) seems to be too low for the temperatures considered (around 400-500 °C). In this temperature range the equilibrium oxygen content is much higher, closer to the 6.8 given by Yoo and Lee (1994).

The strong dependence on the non-stoichiometry could be another explanation for the hysteresis observed in the conductivity (resistivity) values during heating and cooling cycles of the sample observed by Yamaguchi *et al.* (1988) and Freitas and Plaskett (1987).

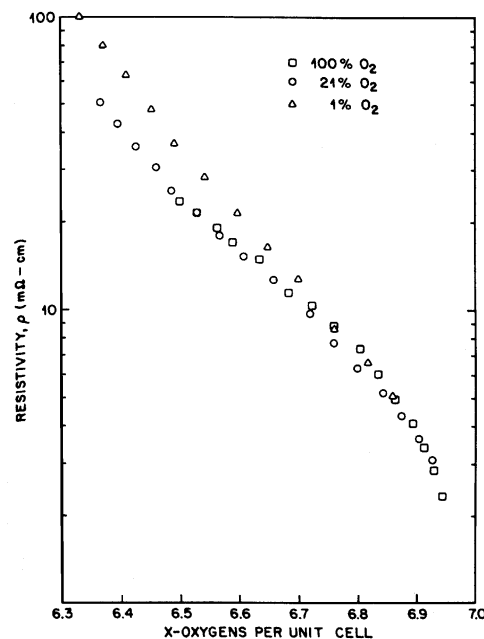


Fig. 6.4 Resistivity of YBCO as a function of oxygen content (after Grader *et al.* (1987))

All the authors agree on a dependence of the resistivity on temperature and partial oxygen pressure; this is a direct consequence of the relationship between the stoichiometry and the transport properties. However, there are slight discrepancies as to what this dependence is. Leonidov *et al.* (1989) suggest a dependence of $\sigma \propto pO_2^{1/6}$ or $pO_2^{1/4}$, Yoo (1989) observed a $\sigma \propto pO_2^{1/2}$ between 400 and 700 °C, Davidson *et al.*

(1988) also suggest a square root dependence on partial oxygen pressure and Ronay (1987) and Chang *et al.* (1988) observed a square root dependence in the tetragonal phase, and $\sigma \propto pO_2^{1/4}$ in the orthorhombic phase. This dependence is directly related to the type of current carrier, agreed by all authors to be holes.

During the study of the electrical resistivity of YBCO a change in the transport process from p to n is observed to occur when the partial oxygen pressure is reduced to very low values (10^{-3} - 10^{-4} atm at 700 °C to 800 °C (Chang *et al.* (1988)) or if the temperature is increased (877 °C, according to Yoo and Lee (1994)).

The transport model has been suggested to be small polaron hopping by most authors: Yoo (1989), Su *et al.* (1988), Nowotny and Rekas (1990), Davidson *et al.* (1988). Fisher *et al.* (1987) proposed a narrow band model, applicable for the tetragonal region, and Ronay suggested a different method based on the law of mass action.

Fig. 6.5 summarises some of the results published for the conductivity of YBCO at different temperatures. The measurements carried out by the different groups measure the total conductivity of the material; this will be mainly due to electron motion at low temperatures with an increasing contribution of the ionic conductivity as temperature increases. Fig. 6.24 in section 6.4.3 shows the increasing value of the ionic conductivity of YBCO calculated using the relationship between ionic conductivity and the diffusion coefficient of the ions in the material.

With respect to the direct measurement of the ionic conductivity of YBCO, the amount of work carried out is not very great and the reports give quite scattered values: Carrillo-Cabrera *et al.* (1989) have measured a conductivity of $1 \Omega^{-1}\text{cm}^{-1}$ at 500 °C (in air), while Park *et al.* (1988) give a value of $1.6 \times 10^{-6} \Omega^{-1}\text{cm}^{-1}$ for the same temperature (in oxygen). There is a serious discrepancy between these two results. It has already been mentioned that the ionic conductivity is proportional to the concentration and mobility of the diffusing species. The stoichiometry of this material in air and oxygen changes only by approximately 0.3 atoms per formula unit (Gallagher (1987)), which leads one to think that the measurements must have been affected by an extra factor that has given rise to such a difference in the values.

The activation energies calculated for ionic conductivity also present a large variation: from 1.23 eV and 1.5 eV (Vischjager *et al.* (1990)) to around 2.5 eV (Carrillo-Cabrera *et al.* (1989)), and 2.46 in the tetragonal phase or 1.6 eV in the orthorhombic phase (Yoo (1989)). These variations could be a consequence of the different methods used to measure this conductivity (DC two-probe conductivity, AC impedance, four point probe, etc.) and it is very likely that the microstructure of the polycrystalline sample affects the final result in the same way as it affects the diffusion measurements carried out. This could be due to an irregular distribution of the oxygen in the grains or the presence of grain boundaries, pores or impurities that can interfere with the measurement.

It will be seen in the next section (6.3.2) that the value of the ionic conductivity can be linked to the diffusion coefficient (Eq. (6.16)) using the Nernst-Einstein equation (Eq. (6.7)). It seems surprising that of all the authors that have studied the ionic conductivity of YBCO, only Park *et al.* (1988) have completed their work by relating their values of the ionic conductivity to the oxygen diffusion in the material. They obtained a value for the diffusion coefficient equal to $9.5 \times 10^{-8} \text{ cm}^2/\text{s}$ at 500 °C. This value is two orders of magnitude slower than that calculated for oxygen diffusion in a polycrystalline material presented in chapter 5 (section 5.2.2).

This brief review shows that in spite of all the work carried out for the study of the high temperature transport properties of YBCO the situation still presents conflicting points over the transport mechanism as well as the value of the electronic and ionic conductivity of the material. The dependence of this behaviour on the non-stoichiometry introduces variables in the study similar to those considered in the study of oxygen diffusion. This suggests that more work should be conducted in this topic so that conclusive values for the electronic and ionic conductivity are produced.

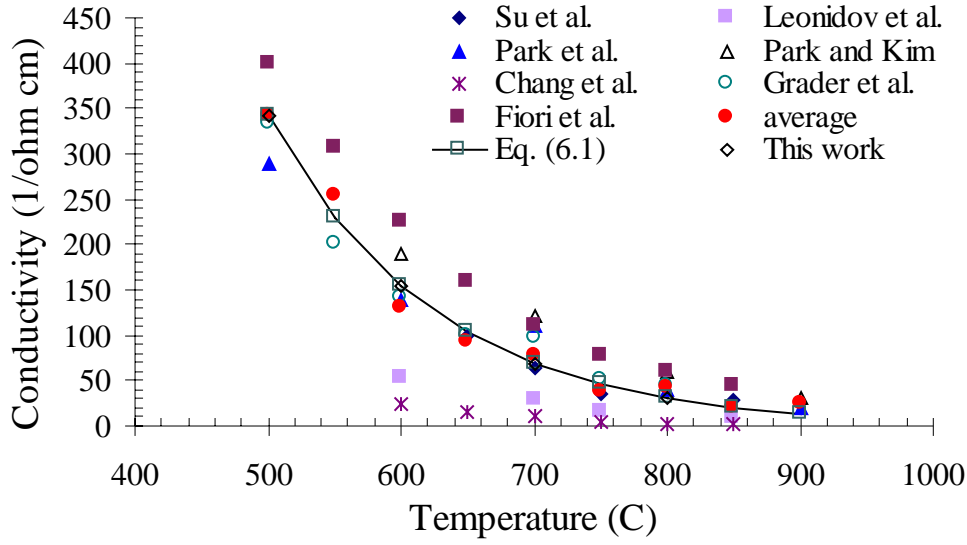


Fig. 6.5 Literature data for the electronic conductivity of YBCO ($pO_2 = 1 \text{ atm}$)

In order to be able to carry out the analysis of the Direct Current Zoning effect, it was necessary to obtain an expression for the average of the electronic conductivity in YBCO. The value of the conductivity that is going to be used in the calculations presented in section 6.4.3 of this chapter was calculated from the average of the literature values (see Fig. 6.5). It was assumed to vary exponentially with temperature (in °C) and has the form:

$$\sigma = 1.8 \times 10^4 \exp(-8.0 \times 10^{-3} T) \quad (6.1)$$

6.3.2 Nernst-Einstein equation. Correlation between diffusion and conductivity

In order to be able to study the causes of the Direct Current Zoning effect, it is necessary to look at the motion of both ions and electrons in a concentration or activity gradient and their simultaneous transport in an electric field (drift). Chemical diffusion occurs in a concentration gradient and drift is due to electric field effects, so while diffusion occurs for all species, drift (or electromigration) affects only charged species.

The study of diffusion in a concentration gradient has already been discussed in chapter 2. The net flux of particles in a concentration (or chemical potential) gradient is expressed by Fick's first law:

$$j = -D (\partial C / \partial x), \quad (6.2)/(2.1)$$

when diffusion occurs only in the x direction. D is the diffusion coefficient and C is the concentration at each point.

The relationship between the diffusion coefficient and the mobility can be derived as follows:

The chemical potential of the diffusing particles takes the form:

$$\mu = \mu^\circ + RT \ln C, \quad (6.3)$$

where μ° is the chemical potential in the standard state, C is the concentration of the particles, R is the gas constant and T the absolute temperature. The relation is valid for mobile ions as well as for defects (e.g. vacancies).

In the absence of an electric field the diffusive force experienced by each particle is:

$$\mathbf{F} = - (1/N_A) (\partial \mu / \partial x) = - (RT/N_A C) (\partial C / \partial x)_{P,T}. \quad (6.4)$$

where N_A is Avogadro's number. The ion mechanical mobility, B , can be defined as the average drift velocity per unit force. Therefore the particle velocity, v , is equal to:

$$v = B \mathbf{F}. \quad (6.5)$$

Since the flux of diffusing particles is equal to the net amount of particles moving per unit time, the flux of particles in a concentration gradient can also be expressed by:

$$j = C v = - (BRT/N_A) (\partial C / \partial x)_{P,T}. \quad (6.6)$$

Comparison with Fick's first law of diffusion (Eq. (6.2)) gives:

$$D = BRT/N_A = BkT. \quad (6.7)$$

This expression shows the direct proportionality between diffusion coefficient and mobility. It is known as the Nernst-Einstein relation (k is the Boltzmann constant).

If the particle was driven by the potential difference of an electric field of strength $E = -\partial \phi / \partial x$, the force on each particle due only to the applied electric field would be:

$$\mathbf{F} = -ze (\partial\phi/\partial x) = zeE, \quad (6.8)$$

where z is the charge of the migrating species (2 in the case of oxygen ions). The average velocity at which the ions move is:

$$v = \mathbf{BF} = \mathbf{BzeE}. \quad (6.9)$$

Using the expression for the velocity of the ions and Eq. (6.6), the flux of ions would be equal to:

$$j = C v = \mathbf{CBzeE}. \quad (6.10)$$

Substituting the Nernst-Einstein equation (Eq. (6.7)), the mobility may then be replaced by the diffusion coefficient of the ions:

$$j = \mathbf{CDzeE/kT}. \quad (6.11)$$

Therefore, the flux of particles (the number of particles per unit area and time, Eq. (6.10)) can be expressed by:

$$j = -D [(\partial C/\partial x) - zC (F/kT) (\partial\phi/\partial x)], \quad (6.12)$$

where the second term on the right hand side represents electromigration. This term shows the importance of charge of the species, z , and of the value of the electric field gradient, $\partial\phi/\partial x$. F is Faraday's number, the charge of a mole of electrons.

The conductivity of a material is a result of the movement of all ions and all other charge carriers (electrons or holes) in the material under the influence of an electric field. As long as the electric field is not too strong we can assume that there is a linear relationship between the total flux of the charged particles (the electrical current density), J , and the electric field, E . Ohm's law is then valid:

$$J = \sigma E; \quad (6.13)$$

σ is the electrical conductivity (assumed in this derivation to be independent of the direction in the crystal). The total conductivity, σ , is the sum of the partial conductivities σ_i of the various types of particles, i , if the different charge carriers are transported independently of one another.

$$J = \sum J_i = \sum \sigma_i E, \quad \text{so:} \quad \sigma = \sum \sigma_i. \quad (6.14)$$

Mobility and conductivity are related in the following way:

Assuming that only one type of ion is mobile, the flux of charge carried by the flowing ions, j , is defined as:

$$j = J/(z F) = \sigma E / (z F). \quad (6.15)$$

Substituting equation (6.11) above, the relation between partial electrical conductivity, the mechanical mobility and the diffusion coefficient of the moving ions is:

$$\sigma = DC(zF)^2/RT, \quad (6.16)$$

and in terms of mobility: $\sigma = CBz^2eF.$ (6.17)

To calculate roughly the value of the ionic conductivity in YBCO at a temperature of 500°C, it is sufficient to know the value of the diffusion coefficient at that temperature. For this preliminary calculation, D is going to be taken as $1.2 \times 10^{-6} \text{ cm}^2/\text{s}$ (see chapter 5 for diffusion coefficient of polycrystals). The charge of the mobile species, z , is -2 and the concentration of ions is: $8.7 \times 10^{-3} \text{ moles/cm}^3$ in air (the equilibrium oxygen content at this temperature is ~ 6.88). Substituting these values in equation (6.16) the oxygen ionic conductivity has a value of roughly $6 \times 10^{-2} \Omega^{-1} \text{ cm}^{-1}$. This differs with the value calculated by Park *et al.* (1988) in four orders of magnitude and with that calculated by Carrillo-Cabrera *et al.* (1989) in two orders of magnitude. The dependence of these values on the non-stoichiometry of the sample and its microstructure could be the reason for the difference observed.

Charge transport is also sometimes expressed in terms of the electronic mobility, b , defined as the drift velocity of charge carriers per unit electric field:

$$b = v/E, \quad (6.18)$$

so that from (6.9):

$$b = B z e, \quad (6.19)$$

and: $J = C z F v = n z e b E,$ (6.20)

where n is the ion density (ions per unit volume) and:

$$\sigma = n z e b, \quad (6.21)$$

following the convention for charge transport in semiconductors and metals.

6.4 Results and discussion

The previous sections have discussed the phenomenon of Direct Current Zoning and the work that has been carried out in this topic. This has been followed by a study of the research done on the electrical properties of YBCO at high temperatures (section 6.3.1). YBCO has a high oxygen ion mobility at high temperature. This is associated to the increase in the ionic conductivity at these temperatures (above 600 °C this conductivity becomes significant, as it is going to be seen in section 6.4.3), and makes YBCO a candidate for fast ionic conductor applications, although this field has not been developed yet.

This review of the electronic and ionic conductivity values published in the literature has been followed by a derivation of the relationship between conductivity and diffusion. This is going to be used in the study of the motion of the zone combining the effects of ionic conductivity and chemical diffusion on the distribution of oxygen ions within the specimen (see section 6.3.2).

This section is going to present and discuss the work carried out in the analysis of the Direct Current Zoning effect.

The first section describes the experimental procedure. This is followed by a discussion of the results obtained, pointing out the unique characteristics of the DCZ effect. The drop in the power needed to maintain the zone present in the bar and the stopping of the zone are discussed. The third section presents an analysis of the processes that take place simultaneously during the DCZ effect: the change in the temperature profile when the zone appears, the variation in electronic and ionic conductivity with temperature, and the magnitude and direction of the ionic fluxes due to the potential difference established as well as to the concentration gradient present. This analysis has corroborated the description of the process presented by Okamoto and co-workers (1994-b) (see section 6.2). Reasons for the stopping of the zone have been suggested.

This is followed by a description of the computer model developed to reproduce the formation of the zone. This programme has carried out for the first time theoretical calculations of the processes that take place in the Direct Current Zoning effect: from the moment when a current is applied to the YBCO bar to the formation of the zone and its motion. The results from this model have been compared to experimental data, finding a very good agreement between them. The suggestions made in the previous sections concerning the motion of the zone, the change in the temperature profile with time and the variation in the oxygen concentration within the sample have been corroborated by the model, which, in spite of being at an early stage of development, has produced very good results that have contributed to the understanding of the processes taking place in the Direct Current Zoning effect. This section is followed by a summary of the work presented.

6.4.1 Sample preparation and experimental procedure

For the DCZ experiments the YBCO samples were prepared via a polymer processing technique. Polymer processed sheets were produced by a technique known as calendering. It consists of mixing YBCO powder with a binder (PVB), a plasticiser and a solvent (cyclohexanone) in the correct amounts in a rolling mill (see Appendix 2A). Extensive mixing of the components during successive rolling steps results in a rubbery paste that can be rolled into a tape of controlled thickness with a homogeneous distribution of the material. The tape forms what is known as “green body” and it is an unreacted mixture of the components. It can be pressed in a further step so that proper compaction is ensured and it is then cut to shape. The resulting tape produced was about 15 cm wide and approximately 1.5 mm thick. After pressing it was cut in thin strips 1-2 mm wide.

These strips required further processing. The binder is eliminated from the mixture in a burn-off step at around 500 °C. This is followed by a sintering step at high temperatures (see Fig. 6.6). It is essential that the binder is burned off carefully to avoid the presence of large pores in the microstructure. A typical binder burn-off period for samples 1-2 mm thick consists of a slow heating (1 to 2 °C/min) to 500 °C. After this first step, conventional processing of the material is carried out, sintering at

temperatures around 900 °C for 10 hours. The atmosphere used during the burn-off and sintering steps is air. In order to make highly oxygenated specimens, the strips were cooled to 500 °C and held in pure oxygen (with a flow of 30 mm³/min) for approximately 10 hours. This produces compact oxygenated polycrystalline samples.

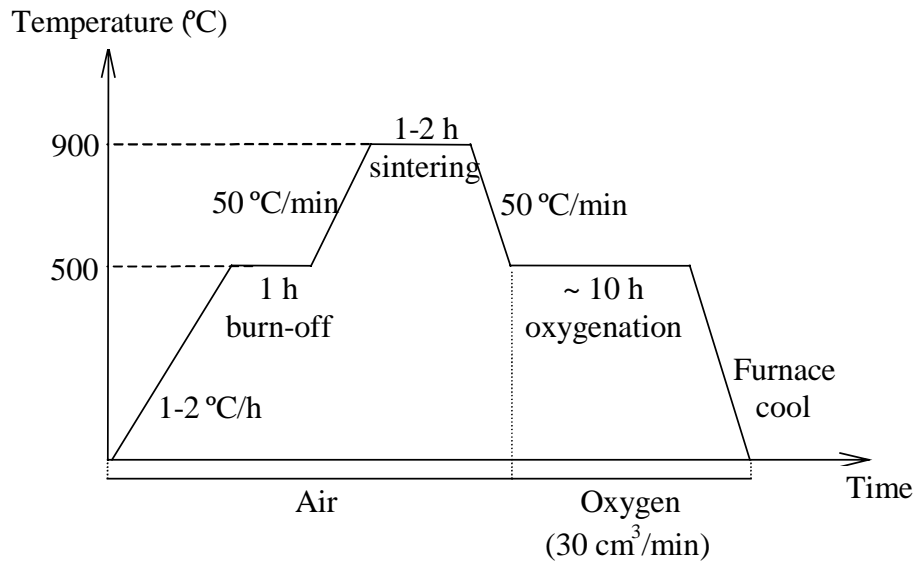


Fig. 6.6 Schematic of heat treatment

The ends of the samples were impregnated with silver paste and contact silver wire was mounted to the sample with the same paint to reduce contact resistance. An increasing voltage was applied using a Coutant LQT 200 power supply. The experimental setup is shown in Fig. 6.7.

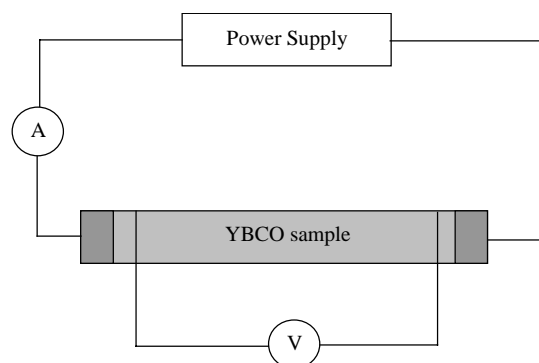


Fig. 6.7 Schematic of setup

The change in current with increasing voltage is monitored with a 4-point measurement as pictured above. Temperature measurements were carried out using a K-type thermocouple.

6.4.2 Results and discussion

An increase in the voltage by 0.1 V every minute resulted in a linear increase of the current passing through the sample. When the voltage and current reached a certain value, a decrease in the current was observed (see Fig. 6.8); this is characteristic of the onset in the formation of a hot zone. This hot region becomes visible when its temperature is above 550-600 °C, and the drop in current was not always associated to the presence of a visible zone. If this was the case, it was necessary to increase the voltage further to raise the temperature of the sample and make the zone visible.

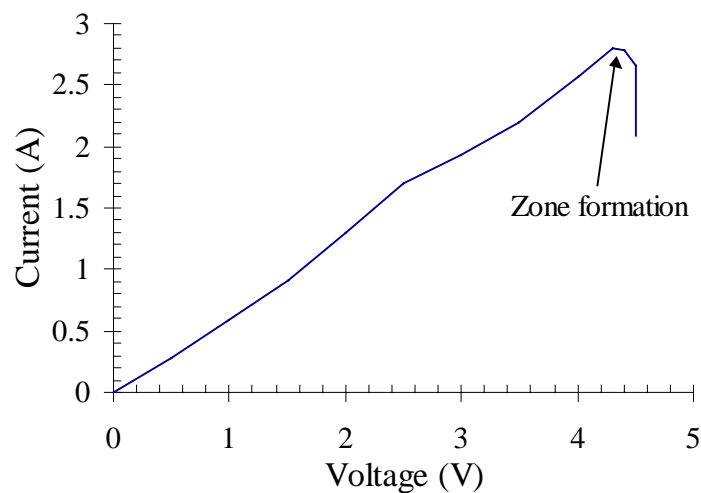


Fig. 6.8 I-V characteristic of one of the samples

It should be noted that once the zone appeared in the sample, the amount of power required to keep the zone present in the bar was reduced considerably compared to the power applied just before it occurred. This decrease in power could be as high as 25%. This characteristic of the formation of the zone is going to be studied in more detail later on in this section.

It was observed that holding the current and voltage constant after the zone occurred it was possible to see that it moved towards the negative electrode at speeds that ranged between 2 to 0.3 mm/min. Specimens with lower porosity exhibited zones that moved more slowly; this suggests that the speed at which the zone moves along the sample is strongly correlated to the degree of intergranular contact in polycrystalline samples and to the variation in the diffusion process due to the microstructure of the sample.

Figure 6.9 shows the initial stages of the formation of the zone and its motion along the sample.

+ + + + + + + +

- - - - - - - -

Fig. 6.9 Sequence of photographs while applying a DC voltage of 5.3 V to an YBCO bar. The pictures are taken at 10min intervals. Note the change of colour of the zone at the formation indicating a change in temperature. Distance between lines on the marker beside the sample: 5 mm

A change in the polarity was observed to reverse the direction of travel:

+ + + + - - - -

- - - - + + + +

Fig. 6.10 Sequence of photographs showing the change in direction of the mobile zone when the polarity is reversed. $V = 5.2$ V and $I = 3.6$ A. Time interval between pictures: 10 min. Distance between lines on the marker beside the sample: 5 mm

An increase in the voltage was observed to increase the current, contrary to what was reported by Okamoto *et al.* (1994-a), (1994-b), and Yanmaz *et al.* (1992), (1993). The current was observed to decrease every time the increase in voltage stopped. Increasing the voltage once the zone is present in the sample increases the overall temperature of both, which, instead of increasing its travelling speed (Bobrov *et al.* (1990)), slowed down to a halt. The continuous increase of the potential difference across the sample and its associated increase in temperature always resulted in an

increase in the width of the zone followed by catastrophic failure due to melting of the sample at the zone (see Fig. 6.2).

The zone disappeared when the voltage was decreased. If the sample was allowed to cool down and then V was increased again, the zone always appeared at the point where it had first occurred unless some damage had been done to the sample while the previous zone was present, such as partial melting. If this was the case, the zone was always observed to appear at the damaged region.

When observed under the optical microscope, the areas along which the zone had moved presented a tetragonal structure, while the “unzoned” areas showed golden-coloured orthorhombic grains with a large number of twins in them, typical of the orthorhombic structure (see Fig. 6.12). The “zoned” regions showed in some cases a small degree of twinning in the grains, but the twins were less noticeable. This means that the transformation from orthorhombic to tetragonal had not been completed in the time the zone moved along the bar. This result agrees with the changes in the microstructure of the samples due to the effects of the zone reported by Osip'yan *et al.* (1988) and Bobrov and co-workers: an increase in the amount of tetragonal phase present after the passage of a hot zone. To confirm this change, the samples were analysed with XRD, and it can be seen in the graphs enclosed (Fig. 6.11) that the orthorhombic sample shows very clearly the two peaks at 32 degrees, first a smaller one and then a larger one, whereas the zoned area gives a diffraction pattern where the small peak is just showing to the right of the larger peak, which is characteristic of the tetragonal phase. But the difference between them is not very pronounced probably due to the uncompleted phase change mentioned before.

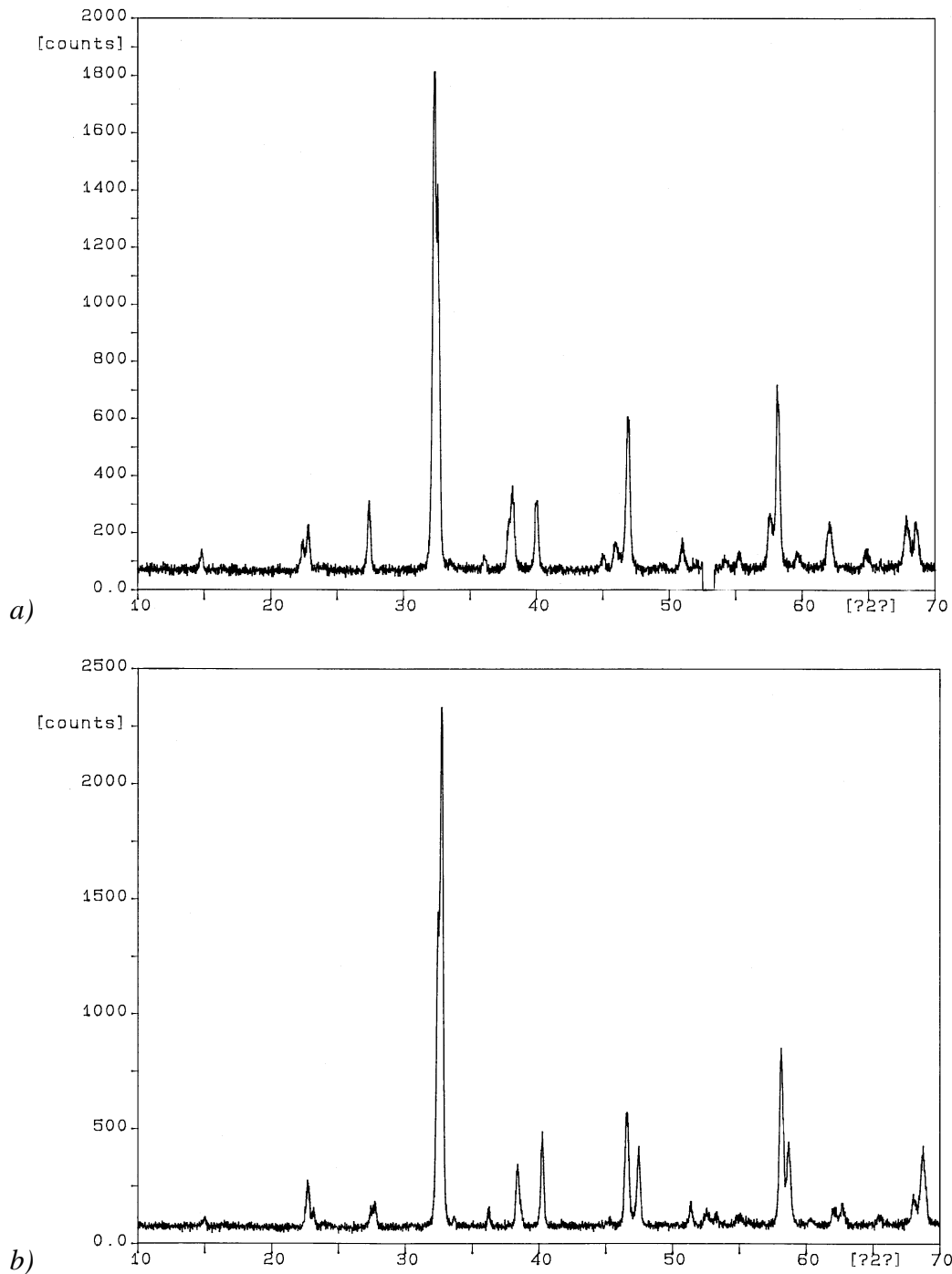


Fig. 6.11 XRD patterns of a) tetragonal region in DCZ sample, and b) orthorhombic area in DCZ sample

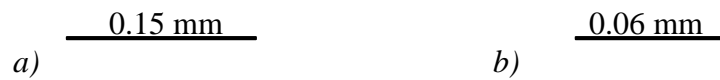


Fig. 6.12 Microstructures of: a) zoned area (tetragonal) and b) unzoned area (orthorhombic, showing characteristic twins in the grains)

The absence of microstructural changes in terms of grain size change is attributed to the high porosity of the samples, since the starting size of the grains was small and they were not very strongly interconnected. There is one case, however, where the microstructure showed some grain growth (Fig. 6.13): in this sample the zone remained immobile for a long period of time after which it melted the bar. The area next to where the zone melted the specimen shows considerable grain growth compared to the grain size of the regions in the surroundings. The increase in temperature of the zone and the time it remained immobile at this high temperature allowed grain growth to occur.

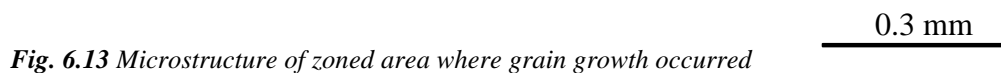


Fig. 6.13 Microstructure of zoned area where grain growth occurred

Temperature measurements were carried out to follow the evolution of the temperature profile along the bar (Fig. 6.14):

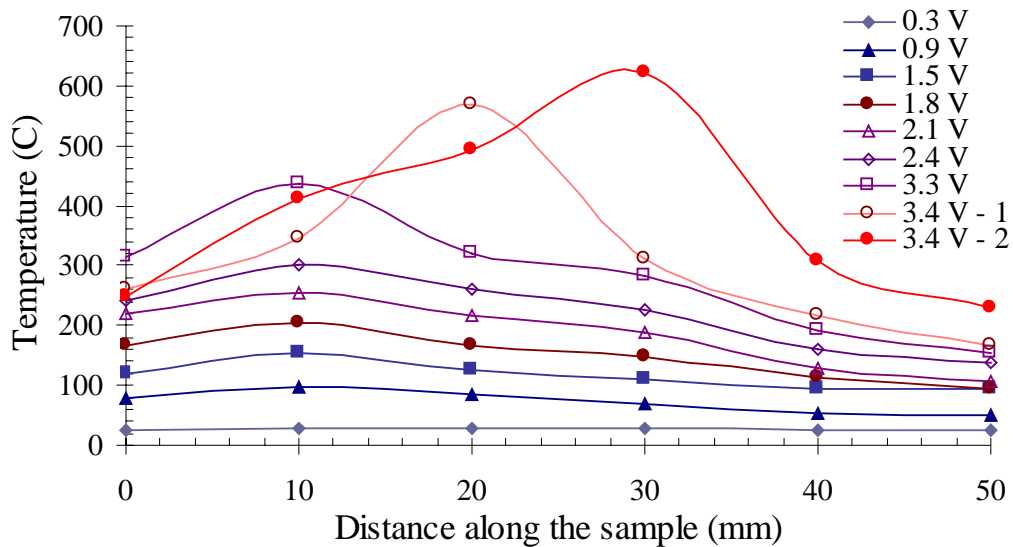


Fig. 6.14 Temperature profile of the sample with increasing voltage. Zone became visible at 3.4 V

It is interesting to note that before the zone becomes visible the temperature profile appears to indicate the nucleation point of the zone. A slight increase in temperature is observed 10 mm away from the left hand end of the sample (the anode). This region with higher temperature moves towards the cathode (the right hand side) while the voltage is increased. Raising the current that passes down the specimen increases the temperature and the irregularity becomes more pronounced until it becomes visible at ~ 3.4 V.

There is still no consensus on the mechanism leading to zone formation. It is normally attributed to a fluctuation in the resistivity of the material that increases the temperature so much that the heat cannot be dissipated fast enough and the perturbation remains in the form of a zone. The change in the temperature can be explained as follows:

The temperature of the sample increases uniformly with voltage due to the Joule effect. The resistivity of the sample changes accordingly with the increase in temperature (Fig. 6.5) and this change occurs uniformly along the sample. If a small fluctuation (increase) of the resistivity occurs, the temperature increases at that point. This fluctuation is thought to occur at a microstructural irregularity such as a crack or

a region of high porosity in the sample. The reduction in cross sectional area increases the heating due to the Joule effect at that point, giving rise to the formation of the zone.

When the heat generated by this increase in resistivity is small, it is transferred to the surroundings by convection, conduction and radiation and the sample returns to its previous stable state. However, if the fluctuation is so large that the heat generated is transferred to the surroundings with a net increase in the temperature, the resistivity gradient formed becomes stable in the sample. The width of the zone generated due to this resistivity gradient is controlled by the amount of heat dissipated away from the sample by radiation and along the sample by conduction. The zone moves along the sample due to the motion of oxygen ions driven across the zone towards the anode by the potential difference established. These changes in the temperature profile are shown schematically in Fig. 6.15.

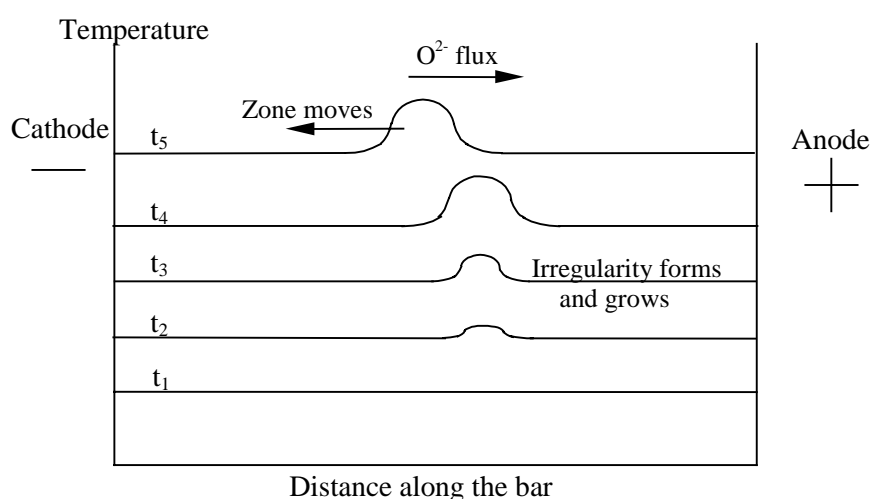


Fig. 6.15 Zone generation process

Other possible reason for the formation of a zone is the presence of impurities or variations in concentration in the material that increase the local current density and local heating so that the temperature raises to such levels that a zone is generated. This has been observed in some of the specimens that had impurities adhered to the surface, probably from a slight contamination of the furnace. These impurities could have the effect of hindering the dissipation of heat from the sample, hence creating a hot region that would give rise to a high resistivity nucleus, triggering the formation of the zone.

Sometimes the zone was observed to pin at one point in the sample, probably where there was high porosity, a crack or a high concentration of defects. These irregularities could anchor the hot spot in the sample. Making a notch of considerable depth in the bar, the zone was observed to occur at the centre of this notch and remain immobile at that point. At this moment a second zone formed in the sample. This zone moved along the sample whereas that at the notch remained stationary. Once the mobile zone disappeared it was necessary to increase the voltage (and current) again to form another mobile zone.

Figure 6.16 shows the second occasion when two zones were observed in a sample. In this case the zone that had initially formed, remained immobile and faded with time. When the voltage was increased to make it reappear, two zones were observed to form: one hotter than the other. The voltage had to be decreased so that the hotter zone did not melt the specimen and at this moment the zone that was at a lower temperature disappeared. The zone that formed in the second place began to move along the sample as it has already been observed in Figs. 6.9 and 6.10.

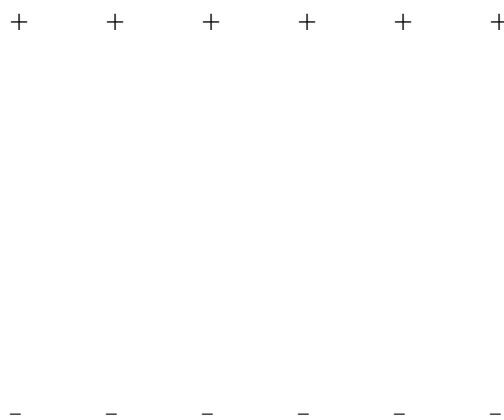


Fig. 6.16 Sequence of photographs showing the formation of two zones in a sample (see text above). Initial voltage applied: 4.6 V (3.8 A). Voltage was increased to 5.1 V (4.2 A) between the second and third photograph. Time between photographs: ~ 10 min. Distance between lines on the marker beside the sample: 5 mm

A possible explanation of the movement of the zone towards the negative electrode in the DCZ effect is the following:

An increase in temperature increases the oxygen diffusion coefficient, favouring the flow of oxygen within and out of the sample. This reduction in oxygen content

increases the resistivity of the material, raising the temperature of the sample until at a certain point a hot zone appears (see Fig. 6.17).

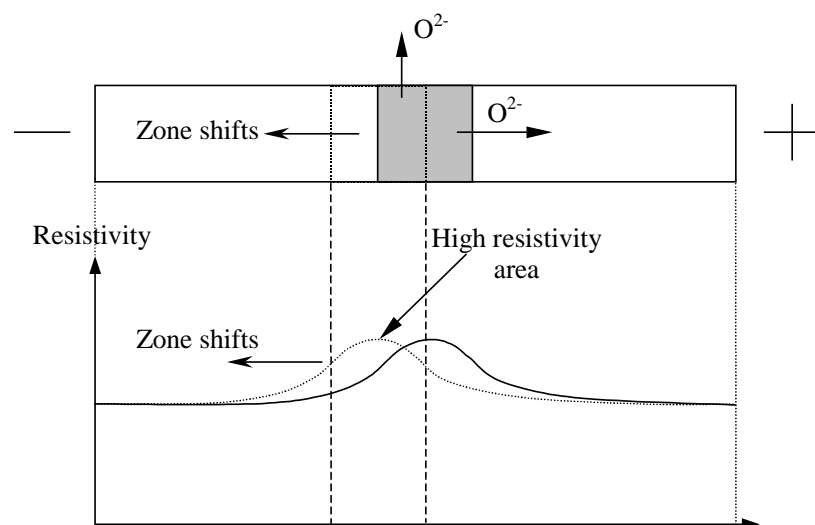


Fig. 6.17 Schematic of movement of zone towards the negative electrode and variation in resistivity within the sample associated to the presence of a zone

The movement of this hot region towards the cathode occurs because the oxygen ions are diffusing both out of the sample and within it as a result of the temperature gradient established and the electric field applied. This movement of ions creates an oxygen-rich area on the positive side of the zone and an oxygen-depleted area on the negative side of the zone. The resistivity of YBCO is related to its stoichiometry (see Fig. 6.4), oxygen-rich samples being less resistive than oxygen-poor samples. Therefore, the oxygen-rich end has a lower resistivity (and lower temperature) than the oxygen-depleted end, that will be at a higher temperature as a result of this increase in resistivity.

The changes in resistivity along the sample in the DCZ effect give rise to the temperature profile presented in Fig. 6.14. A more detailed study of the heat transfer processes that are taking place during this effect can be used to explain the drop in current when the zone appears. These calculations have been introduced in the program developed to model the DCZ effect (see section 6.4.4) and are presented in Appendix 2B.

It is thought that the drop in current once the zone has formed (see Fig. 6.8), this is, the drop in power when the zone forms could be linked to the following variation in the temperature profile:

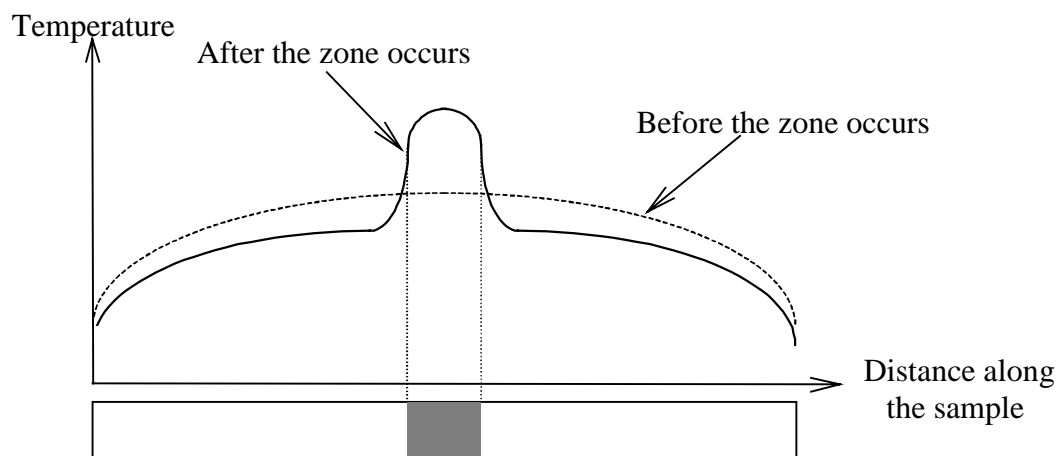


Fig. 6.18 Possible variation in the temperature profile before and after the zone forms

In order to compensate for the local sharp increase in temperature at the zone, the rest of the sample temperature decreases. This occurs to maintain the amount of power supplied constant. However, the decrease in resistivity that compensates the local increase at the zone results in an overall decrease in temperature and a decrease in the power needed to keep the zone present in the sample. Unfortunately, this could not be seen clearly from the measurements taken (Fig. 6.14) due to the low accuracy of the temperature measurement. However, the results from the computer simulation developed that are going to be discussed in section 6.4.4 confirm this suggestion (see Fig. 6.31).

6.4.3 DCZ: Analysis

In order to characterise fully the phenomenon of Direct Current Zoning there are two areas where further study is required:

1) Analysis of the current flow in a mixed ionic conductor, the mechanism by which a zone originates and the reasons for this instability to occur.

2) Modelling of the steady state motion of a stable zone after it has formed.

The mechanism of nucleation of a zone in the bar is very complex, as it involves an irreversible transition from an essentially uniform high dissipation state to a heterogeneous state with lower overall dissipation. The experimental work carried out in this section of the thesis has concentrated on the analysis of the movement of the

zone. Once the study of this aspect of the Direct Current Zoning effect is completed, it will be possible to incorporate to it the effects of the microstructure, being able to carry out a full characterisation of the DCZ effect.

This section is going to study the ionic fluxes established due to the potential difference applied across the bar as well as due to the concentration gradient present in the sample (Joule effect). Their change in magnitude depending on the value of the electric field, E , and the change in concentration are used to explain the observed stopping of the zone. This is followed by an analysis of the changes in ionic and electronic conductivity, the number of mobile ions due to each type of flux and their direct link to the speed at which the zone moves. It will be seen at the end of this section that the calculations carried out are in very good agreement with the experimental results.

Therefore, let us consider the zone already present in an YBCO bar. Fig. 6.19 shows the characteristic temperature profile and the variation in oxygen distribution in the bar. This oxygen distribution is due to the increase in the value of the diffusion coefficient, D , and the decrease in the value of the equilibrium oxygen content with temperature (see Figs. 5.9 and 1.5, respectively). Oxygen ions will tend to diffuse into or out of the sample until the equilibrium content for each temperature is reached.

The initial temperature and concentration profiles considered for these calculations are those shown in Fig. 6.19. Looking at the oxygen motion due to chemical diffusion, the ions move within the sample due to the gradient established and out of the sample due to the high temperatures reached at the zone. The following paragraphs present a preliminary calculation of the out-diffusion process to assess its contribution to the DCZ effect.

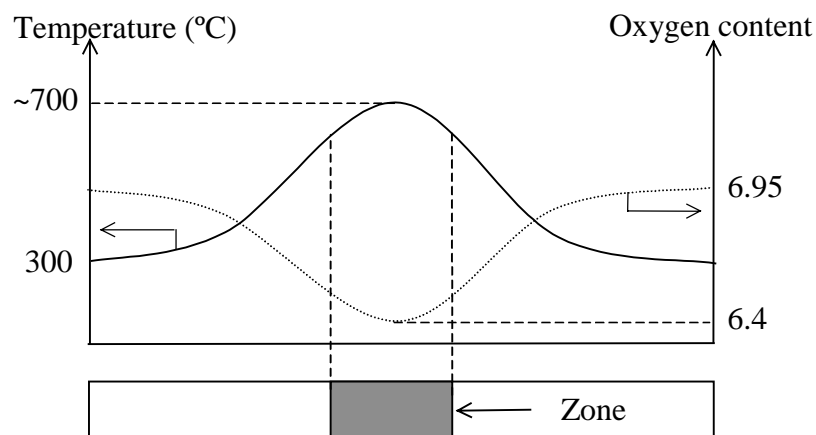


Fig. 6.19 Schematic of temperature profile and distribution of oxygen content in an YBCO bar with a zone

Table 6.1 shows the values of oxygen diffusion in polycrystalline samples calculated from a diffusion expression fitted to the results obtained in chapter 5 (section 5.2.2). See values of the diffusion coefficients used in Table 6.3). If the bar is 2 mm thick and oxygen ions diffuse from the centre of the sample, the time it will take one oxygen ion to get from the centre to the surface can be calculated ($D \approx x^2/t$):

<i>Temperature (°C)</i>	<i>Time</i>
400	16.3 h
500	2.3 h
600	~ 30 min
700	9.4 min
800	3.5 min

Table 6.1 Time it would take an oxygen ion to diffuse from the centre of an YBCO bar with a zone to the surface of the bar (diffusion distance, $x = 0.1$ cm)

It has already been mentioned in this section that the zone was observed to move at speeds up to 2 mm/min in the samples used. It can be seen in Table 6.1 that oxygen out-diffusion from the centre of the specimen takes longer to occur than what it takes the zone to move down the bar. Therefore, diffusion within the sample dominates the process and only the oxygen atoms that are very close to the surface diffuse out of the specimen in the timescale of the experiment.

Taking again the 2 mm/min at which the zone moves along the sample, and assuming that the experiment has been carried out for one minute, the zone will have shifted

2mm. Looking at an oxygen ion in the region where the material is at 800 °C, during this period of time it will have moved 6.9×10^{-2} mm. This distance is one order of magnitude larger than the size of the YBCO unit cell (along the a or b axes), but not very long on a macroscopic scale. Therefore, during this minute, only the oxygen ions that are within $\sim 7 \times 10^{-2}$ mm from the surface of the bar diffuse to the surrounding atmosphere. Since the zone is moving continuously and the temperature distribution is also changing, the ions will be diffusing at the fastest speeds (at the highest temperatures) for shorter periods of time than that considered above, so it can be assumed that the effect of out-diffusion is negligible compared to that due to the electric field. Therefore, the diffusion of oxygen out of the sample is not going to be considered in the following calculations.

Fig. 6.20 shows an element of the bar considered. The processes taking place can be expressed mathematically with Eq. (6.12). This equation describes the flux of matter in a specimen under the effect of a concentration gradient ($-D\partial C/\partial x$) and an electric field ($DzCF/kT (-\partial\phi/\partial x)$):

$$j = -D [(\partial C/\partial x) - zC (F/kT) (\partial\phi/\partial x)]. \quad (6.12)$$

The electric field drives the oxygen ions towards the anode ($j_{\text{Electrical}}$) and, at the same time, the change in the temperature distribution (see Fig. 6.19) gives rise to a redistribution of the oxygen ions in the structure (j_{Fick}). These ions move out of the sample and within it so that the equilibrium oxygen content is achieved. It has already been shown that the phenomenon of out-diffusion can be ignored for these initial calculations due to the small effect it would have on the final result. The magnitude of the two fluxes ($j_{\text{Electrical}}$, j_{Fick}) on the motion of oxygen ions within the sample is discussed below:

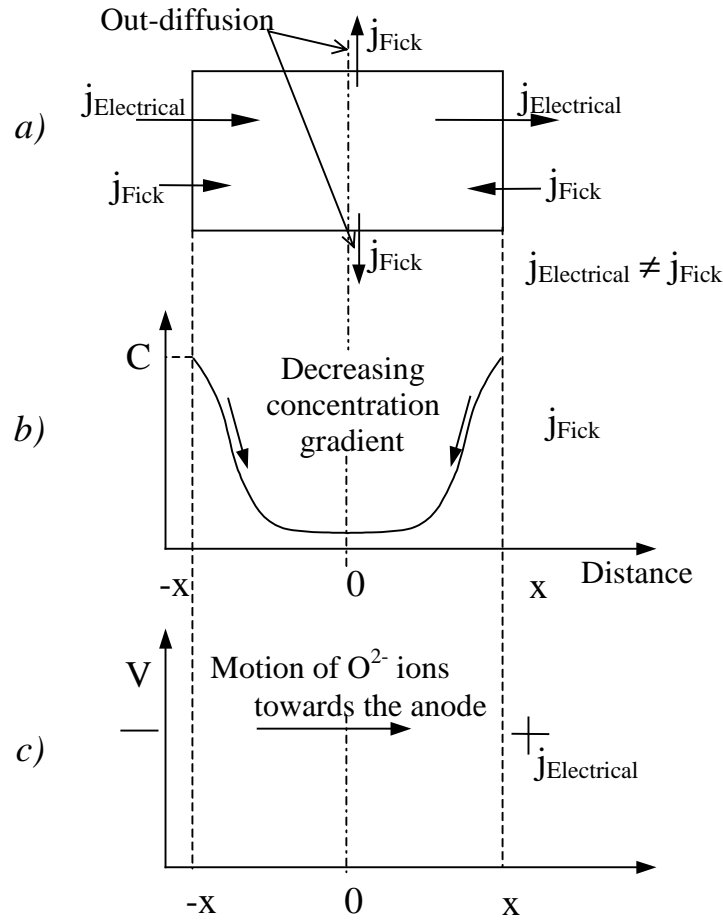


Fig. 6.20 a) Schematic of the two types of ion flux taking place in the zone, b) shape of the concentration gradient established across it, and c) potential difference at the zone

Fig. 6.20 shows the two processes that contribute to the motion of oxygen ions in the sample: the driving force of the potential gradient present across the bar and the concentration gradient that results from the non-uniform heating of the sample (see also Eq. (6.12)). In order to evaluate the importance of each process, the current generated by the ions moving due to the chemical concentration gradient has been calculated, and it has been compared with that due to the presence of an electric field.

It has already been shown that the temperature profile varies continuously along the sample, with a pronounced increase closer to the zone region (Figs. 6.14 and 6.19). In order to perform the calculations that follow it is necessary to divide this continuous distribution in steps of a certain length. For this initial calculation, the steps are taken every $100\text{ }^{\circ}\text{C}$. Each of these temperature steps has a characteristic oxygen content from which the value of $\partial C/\partial x$ can be calculated. For a 5 cm bar, the approximation of

the temperature distribution used in the following calculations is shown in Fig. 6.21 a).

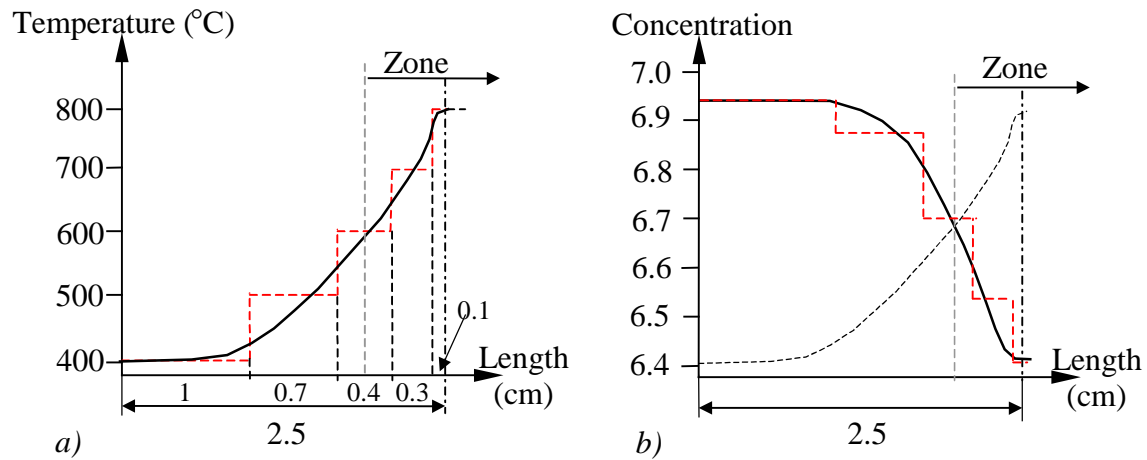


Fig. 6.21 Schematics showing: a) variation in temperature and step temperature subdivision (in red) of half a bar of YBCO where there is a zone present (at the centre of the bar), and b) variation in concentration in the same half bar of YBCO. The line in red shows the concentration steps between each temperature from which $\partial C/\partial x$ is calculated

If the sample has an initial oxygen content of 6.95 and the concentration profile corresponds to the equilibrium oxygen content of YBCO for each temperature (see Fig. 6.21 b)), then the change with temperature of the two fluxes expressed in terms of current is shown in the table below (6.2):

T ($^{\circ}\text{C}$)	Concentration	dx (cm)	I_{Fick} (A)	I_E (A)
400	0.95	1	0	4.8×10^{-5}
500	0.88	0.7	6.6×10^{-6}	6.0×10^{-4}
600	0.70	0.4	1.3×10^{-4}	4.2×10^{-3}
700	0.53	0.3	5.4×10^{-4}	2.1×10^{-2}
800	0.40	0.1	3.4×10^{-3}	8.5×10^{-2}

Table 6.2 Variation of current due to chemical diffusion of ions in the concentration gradient established as shown in Fig. 6.20 due to the formation of a zone in an YBCO bar compared with the current due to the potential difference across the bar (see Table 6.4)

It can be seen that for the concentration gradients assumed the motion of oxygen ions is dominated by the electric field applied, with values around one to two orders of magnitude higher than that due to chemical diffusion (see Fig. 6.22).

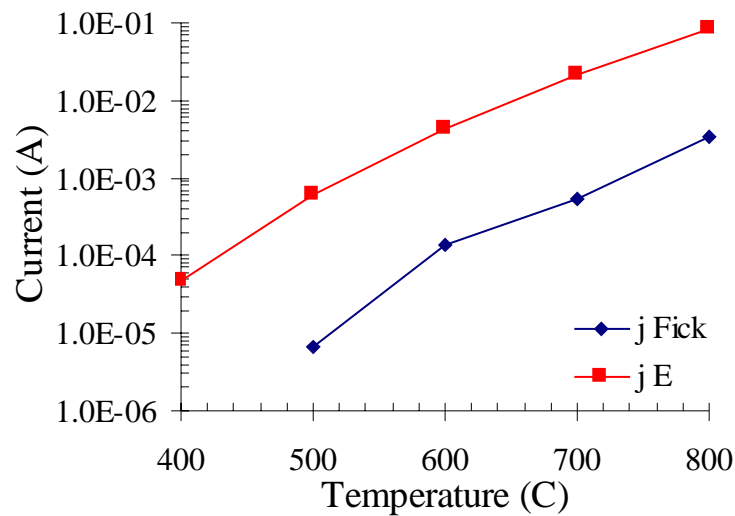


Fig. 6.22 Variation of currents flowing in the sample due to the voltage applied and chemical diffusion when a zone is present in an YBCO bar. The flow of ions due to the electric field dominates oxygen motion in the sample

This flux analysis can be used to explain why a moving zone stops at a certain point along the bar (see section 6.4.2). There are two situations where the zone has been observed to stop moving:

In the first case, the zone stops at a point where there is a defect in the sample, such as a notch or perhaps a change in the microstructure (a region with higher porosity, for example). This defect increases locally the resistivity of the bar and the zone stops at that point. Some of these defects have also been observed to be the nucleation points of immobile zones in a sample (section 6.4.2).

In the second case, the zone moves down the sample and it stops due to an increase in the current that passes through the bar. This results in an increase of the overall temperature of the bar and the zone. Considering this case in terms of ion fluxes, when the current is increased the electrical and chemical diffusion fluxes could become equal in magnitude and balance each other at the anode end of the zone (see schematic of zone element in Fig. 6.23). This would result in a decrease in the number of oxygen ions flowing, and the zone would stop. If, at any moment the accumulation of oxygen due to the flux from the cathode end into the zone increased the content above the equilibrium value, this oxygen would leave the sample through the out-diffusion, although it has already been discussed that for this preliminary study out-diffusion would be neglected in these calculations.

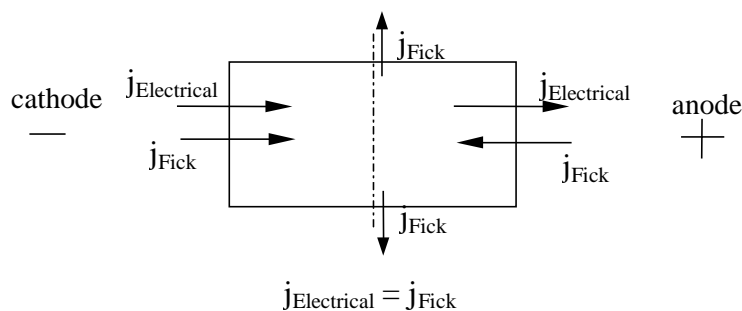


Fig.6.23 Schematic of fluxes in an element of zone when the zone is stationary

The results obtained using the DCZ model developed that are going to be discussed in section 6.4.4 show the change in concentration gradient within the sample due to these two fluxes. The combined effect of the electrical and chemical diffusion (Fick) fluxes at the cathode end gives rise to a smooth concentration gradient that decreases towards the high temperature region in the zone. At the anode end, the drift of ions due to the potential difference across the sample shifts them towards lower temperature regions. Fick diffusion becomes more sluggish and this results in an accumulation of ions (see Fig. 6.32). The zone stops when the concentration gradient created due to this higher concentration of ions at the anode end is such that the driving force on the oxygen ions due to the potential difference is not strong enough to overcome the concentration difference.

The main effect in DCZ is the motion of oxygen ions in the sample through the grain boundaries (faster) and the grains (more slowly) under the effects of the electric field (electromigration) and the temperature (diffusion), as it is going to be discussed in the next section.

As it has been mentioned in this section, The sample is assumed to be always at the equilibrium oxygen content for each temperature. The conductivity of oxygen ions in YBCO can be calculated using Eq. (6.16) provided the chemical diffusion coefficient of the oxygen ions in the sample is known. This series of values is taken from the measurements of diffusion in polycrystalline YBCO samples presented in chapter 5:

Temperature (°C)	Diffusion coefficient (cm ² /s)	Ionic conductivity (Ω ⁻¹ cm ⁻¹) ⁽¹⁾	Electronic conductivity (Ω ⁻¹ cm ⁻¹) ⁽²⁾
400	1.7×10 ⁻⁷	1.1×10 ⁻²	757.9
500	1.2×10 ⁻⁶	6.0×10 ⁻²	341
600 ⁽³⁾	5.4×10⁻⁶	1.9×10⁻¹	153.6
700	1.8×10⁻⁵	4.3×10⁻¹	69.2
800	4.7×10⁻⁵	7.7×10⁻¹	31.2

Table 6.3 Variation of the diffusion coefficient, ionic and electronic conductivity with temperature

Assuming that the whole cross sectional area contributes to the conduction process, the current density is equal to:

$$J = I / \text{cross sectional area of sample} = 3 \text{ A} / 3 \times 10^{-2} \text{ cm}^2 = 1.0 \times 10^2 \text{ A/cm}^2.$$

Continuing the calculations, the values for the change of electric field with position in the zone can be obtained using Ohm's law. From the value obtained, the ion current density and the current carried by the oxygen ions as they move along the sample can be calculated:

Temperature (°C)	Electric field (V/cm)	Ionic current density (A/cm ²)	Ionic current (A)
400	0.2	1.6×10 ⁻³	4.9×10 ⁻⁵
500	0.3	2.1×10 ⁻²	6.2×10 ⁻⁴
600	0.8	0.1	4.3×10⁻³
700	1.7	0.7	2.2×10⁻²
800	3.7	2.9	8.7×10⁻²

Table 6.4 Variation of the electric field, ionic current density and ionic current with temperature

The decrease in electronic conductivity with increasing ionic conductivity can be seen very clearly in the graph below:

⁽¹⁾ Ionic conductivity (Eq. (6.16)) = $DC(zF)^2 / RT$ (Ω⁻¹cm⁻¹).

⁽²⁾ The electronic conductivity has been calculated from Eq. (6.1)

⁽³⁾ Temperatures from 400 °C to 800 °C are shown in the calculations, although the temperatures reached in the zone are 600 °C to 800 °C (in bold). The other temperatures are presented as a reference only in order to fully appreciate the variation with temperature of the diffusion coefficient, conductivity, ionic current and number of mobile ions.

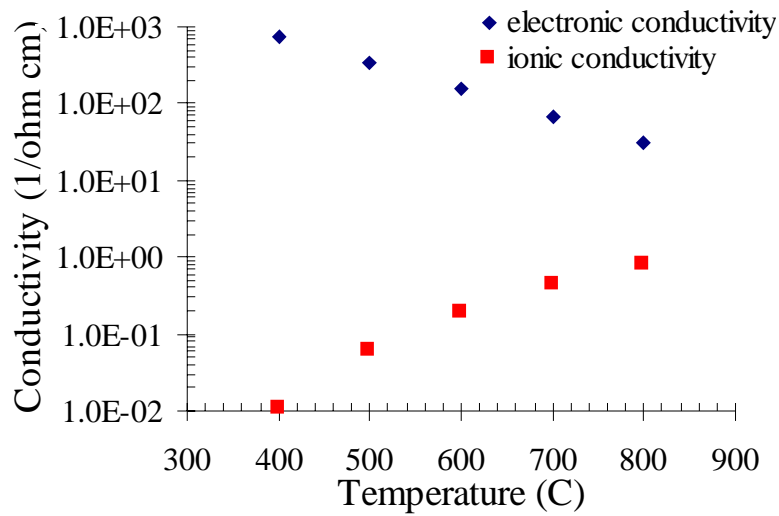


Fig. 6.24 Variation of total conductivity and ionic (O^{2-}) conductivity of $YBa_2Cu_3O_{7-\delta}$

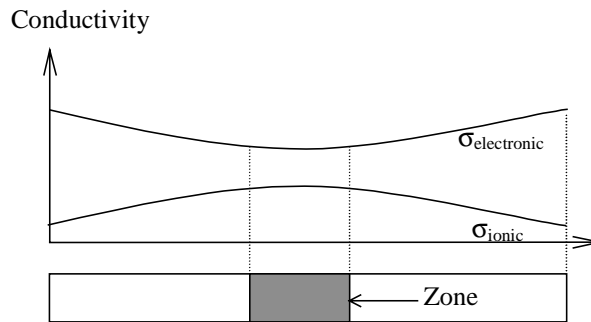


Fig. 6.25 Schematic of variation in electrical and ionic conductivities

The values of the oxygen ion conductivity of YBCO in this temperature range are comparable to those of other fast ionic conductors, as it can be seen in Fig. 6.26.

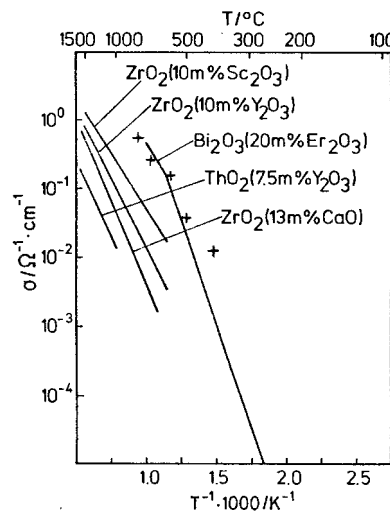


Fig. 6.26 Comparison between ionic conductivities of oxygen ion conductors (from Rickert (1982)). Crosses show the values of the oxygen ion conductivity in YBCO calculated in this chapter (see Table 6.3)

If the zone (at 800 °C) is taken to move at 1 mm/min (approximately 17 $\mu\text{m/s}$), calculating the number of mobile ions in the whole volume of a slab 17 μm (1.7×10^{-3} cm) wide, the number of ions, N_i , that will have moved to the next 17 μm towards the anode per unit time is:

$$\text{Volume of a } 17 \mu\text{m slab} = 1.7 \times 10^{-3} \times 3 \times 10^{-2} = 5.1 \times 10^{-5} \text{ cm}^3$$

$$\text{Number of mobile ions per unit volume, } n_i = 2.4 \times 10^{21} \text{ ions/cm}^3 \text{ (for 6.4)}$$

$$\text{Mobile ions in } 17 \mu\text{m slab, } N_i = 2.4 \times 10^{21} \times 5.1 \times 10^{-5} = 1.2 \times 10^{17} \text{ ions}$$

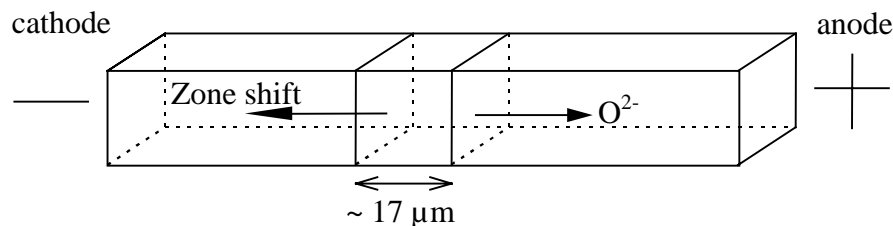


Fig. 6.27 Schematic of the slab at the zone moving along sample towards the cathode

Calculating the number of oxygen ions flowing due to the potential difference applied across the YBCO bar:

Since $1\text{A} = 1/2e$ ions/s:

$$N = I/2e \quad \text{where:} \quad \begin{array}{l} e = \text{electronic charge (C)} \\ I = \text{ionic current (A)} \\ N = \text{number of mobile ions per second} \end{array}$$

Temperature (°C)	Mobile ions/s
400	9.7×10^{13}
500	1.3×10^{14}
600	1.2×10^{15}
700	7.6×10^{16}
800	4.0×10^{17}

Table 6.5 Variation in the number of mobile ions with temperature

It can be seen that calculations of mobile ions per unit time at different temperatures and the value calculated above for the 17 μm slab agree very well.

It has been shown that the combination of chemical diffusion and drift of the oxygen ions due to the presence of an electric field gives rise to the formation of a zone where

the increase in temperature gives rise to an ionic contribution to the conduction process that would not take place otherwise. The motion of oxygen ions due to the potential difference and the concentration gradients present has been related to the speed at which the zone moves. It has been proposed that the effects of ionic drift and chemical diffusion on the distribution of oxygen in the sample can, under certain circumstances, decrease the travelling speed of the zone, sometimes making it stop at one point. This effect is going to be observed in the theoretical analysis of DCZ presented in the next section. This analysis shows the direct link between the fast ionic conductor behaviour of YBCO and the DCZ effect.

Changes in the electric field along the sample due to alterations in the microstructure should be monitored to assess the extent of the effect of these variations. Further insight into the subject of conductivity and oxygen ion diffusion is required to carry out a more accurate study of the DCZ phenomenon.

6.4.4 Computer model of the Direct Current Zoning effect

To complete this initial study of the DCZ effect, a computer program was developed to reproduce the experimental results theoretically. This model was written in collaboration with Dr. Ilan Blech during his stay in the laboratory as a visiting researcher, and it applies finite element analysis to calculate the I-V characteristic of an YBCO bar across which a certain potential difference, V , is established. The value of V can be kept constant or changed to suit the reproduction of the experimental results in the same way as they were obtained.

The program calculates the variation in temperature with time resulting from drawing a current through the sample. As it has been mentioned in the previous sections this heating has a direct effect on the mobility of oxygen ions in the YBCO bar. The increase in the value of the oxygen diffusion coefficient with temperature and the presence of an electric field (electromigration) increase the mobility of mobile species and their concentration. These two factors determine the electrical properties of the material.

The variation in the distribution of oxygen in the YBCO bar results in a change in the value of the electronic and ionic conductivity (Fig. 6.21); this, in turn, alters the temperature of the sample. At this point, the series of calculations starts again.

The computer model developed calculates the temperature variation with time of the whole bar as well as the distribution of oxygen across it. This distribution determines the total resistive behaviour of the sample, allowing one to follow the variation in the amount of current passing through the sample at each moment in time for the voltage applied.

Therefore, it is possible to reproduce theoretically the I-V characteristics obtained in the experiments while being able to observe the changes in temperature and in oxygen content experienced by the sample (discussed in the previous sections) that give rise to the formation of a hot zone. Although the model is a highly simplified representation of the real situation it will be seen that the main characteristic of zone formation, drift and the tendency for zones to halt at high currents are successfully reproduced by it.

The computer algorithm was written in QBASIC. It calculates the variations in the value of the temperature, oxygen ion concentration and resistivity of an YBCO long cylindrical bar divided into a certain number of parallel segments of length *seglen*, as shown in the figure:

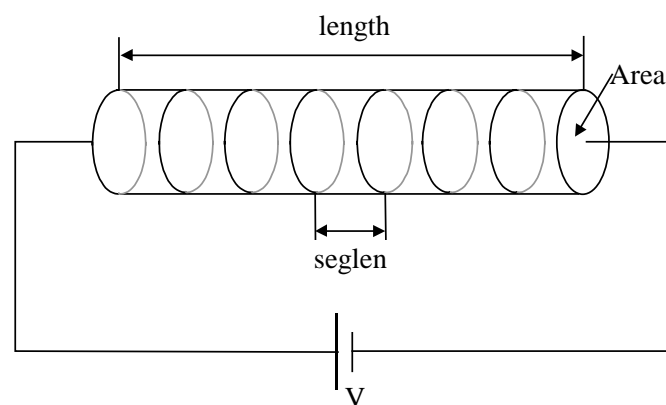


Fig. 6.28 Schematic of YBCO bar with segments

The geometrical factors characteristic of the bar: diameter, length, surface area, cross sectional area, etc., the diffusion and the conductivity parameters are stored as constants in the programme. D_o and A_e are taken from the expression for diffusion in a dense polycrystal presented in chapter 5 (section 5.2.5), and the conductivity

parameters are taken from the average of the change in conductivity with temperature calculated in section 6.2.1 (Eq. (6.1)).

The user then inputs the value of the initial oxygen concentration of the bar and the initial value of the potential difference established across it. The value of V can be altered once the program has started to simulate the experimental conditions of increasing the voltage at a constant rate or reducing it to study the effects of the variation in voltage on the concentration profile as well as the changes in temperature associated to it.

The program starts calculating the resistance of the bar for the initial conditions of temperature and oxygen concentration. It continues evaluating the heat generated in each of the segments due to the Joule effect and calculating the total heating along the bar by subtracting the total power from the heat dissipated by radiation, convection and conduction. This heating results in an increase in temperature of the bar and the temperature values are updated.

Heating the sample increases the value of the oxygen diffusion coefficient; this means that some of the oxygen is going to diffuse out of the sample. The new equilibrium concentration of oxygen in the bar due to the increase in temperature is then calculated.

Oxygen ions also move in the bar due to the potential difference established across it (electromigration), so the next step calculates the drift of oxygen ions towards the positive electrode. A gradient in concentration is generated, and the resulting shift of ions in this gradient is used to update once more the value of the concentration profile. The change in the distribution of oxygen ions at the end of each time step alters the conductivity of the segments, which in turn modifies the generation of heat with time and current passing through each of them.

Each one of these blocks of calculations (power generated, temperature distribution, variation in concentration, etc.) is carried out for each segment in the bar so that it is possible to follow the evolution of the change in temperature and concentration along the whole sample.

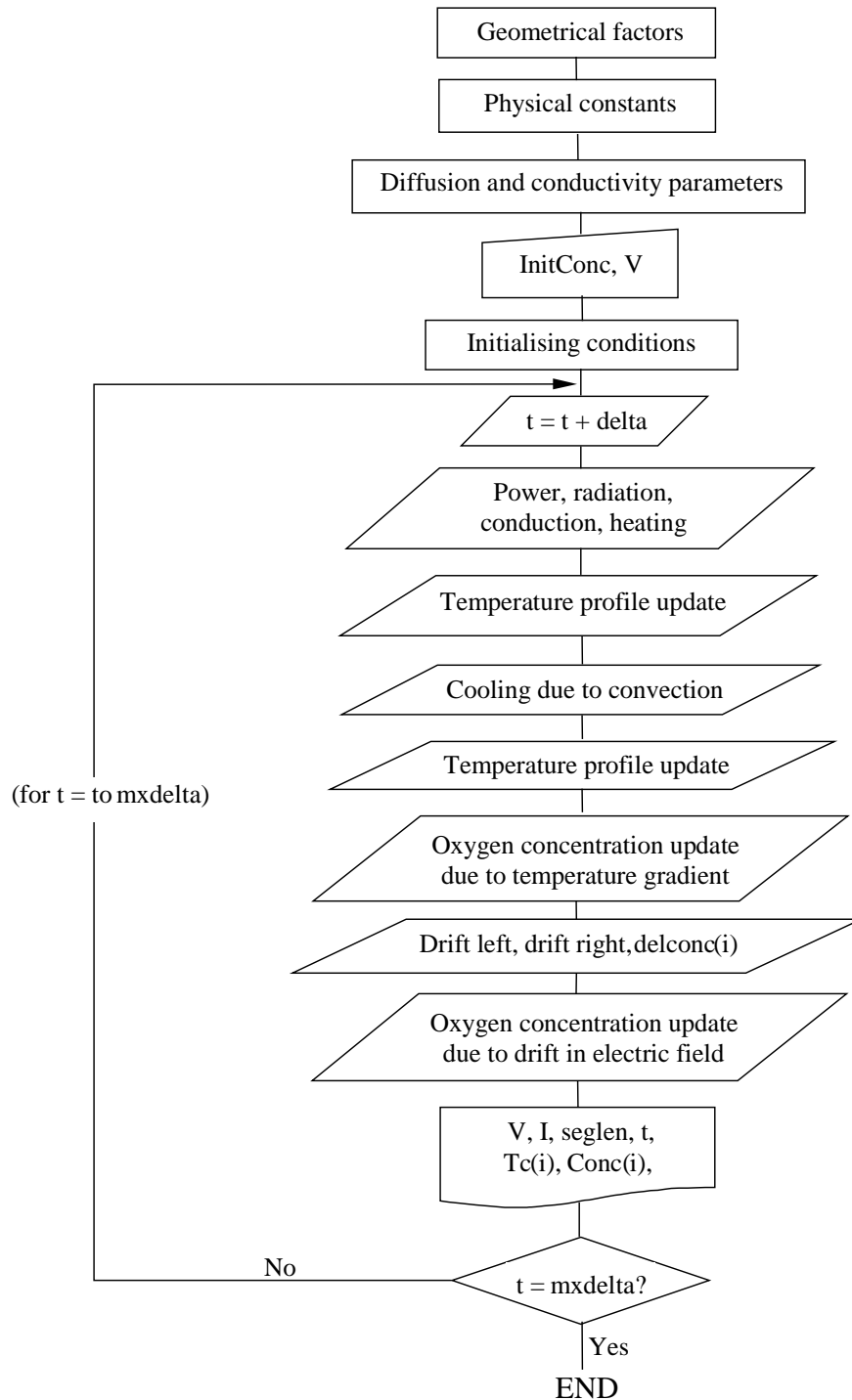


Fig. 6.29 Flowchart of the algorithm developed to model the DCZ effect

The values of current and voltage, the variation in the concentration profile along the bar and the temperature distribution are exported to a file that can be read in spreadsheet form so that the theoretical results can be compared with the experimental data. The listing of this program is included in Appendix 2C.

The results obtained from the theoretical calculations using the model developed are a good first approximation for the calculation of the I-V characteristic of the sample during the DCZ effect. This model reproduces quite well the variations in temperature occurring due to the movement of oxygen ions within the sample as a result of the Joule effect. The changes in the oxygen content calculated confirm the presence of oxygen-rich and oxygen-depleted areas at the zone that give rise to its movement along the sample.

6.4.4.1 Comparison with experimental results

It has been observed that the initial slope of the I-V characteristic of the experimental runs varies from one sample to another. This is thought to be due to microstructural aspects such as the density of the polycrystalline bar, grain size, presence of impurities, etc.

The resistance of the bars used depends on their density. In order to be able to reproduce the experimental results it is therefore necessary to adjust the value of the initial resistance to match the theoretical and experimental situations.

Fig. 6.30 shows one of the results obtained from modelling the increase in voltage to 4.5 V. It can be seen that the agreement between the curves is very good. The drop in current is larger in the theoretical calculation. This could be due to the need for a more accurate calculation of the resistivity values and the heat dissipation from the sample.

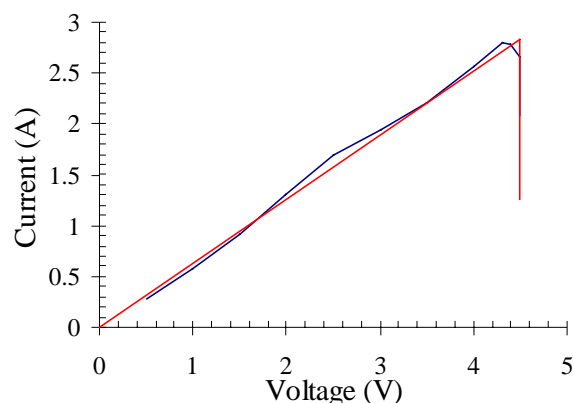


Fig. 6.30 I-V characteristics of experimental run shown in Fig. 6.8 (in blue) and theoretical model of the same experiment (in red)

The variation in temperature with time during this theoretical experiment had the form:

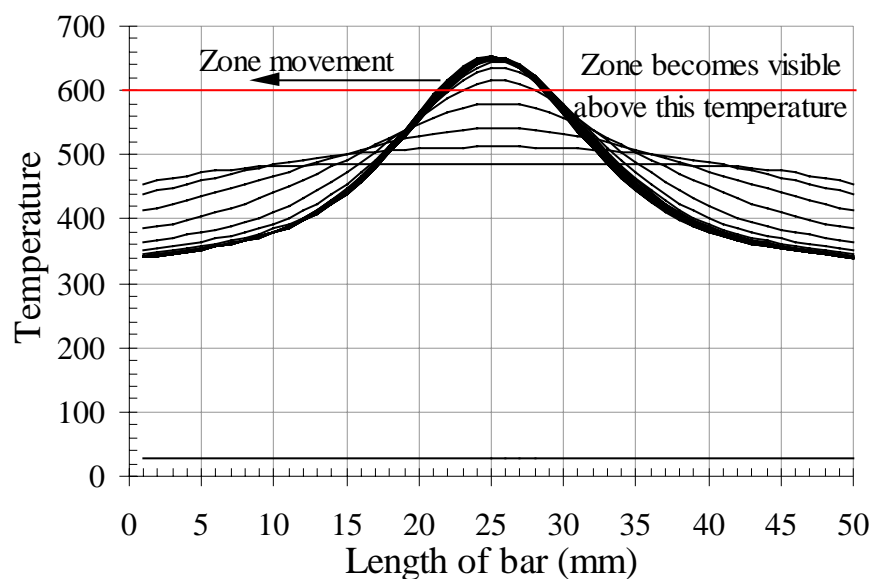


Fig. 6.31 Variation in temperature profile with time when a potential difference of 4.5 V is applied to a polycrystalline YBCO bar. Time between temperature profiles: 30 s

It can be seen how the variation in temperature calculated (Fig. 6.31) is quite similar to that measured experimentally (see Fig. 6.14). The decrease in the temperature at the ends of the bar when the zone forms corroborates the calculations and suggestions presented in section 6.4.2 concerning the variation in electric power supplied: the formation of the zone is associated to a drop in the power dissipated by the sample. This is accommodated by a reduction in the temperature of the regions away from the zone.

The increase in temperature is associated with faster chemical diffusion of the oxygen ions and their electromigration due to the electric field. This modifies the initial oxygen distribution in the sample as shown in Fig. 6.32. There is an accumulation of oxygen ions in the region immediately to the right of the zone due to the combined effects of the electromigration and Fick diffusion of ions. This region is at a lower temperature, and chemical diffusion occurs more slowly. This creates an oxygen-rich area with a low resistivity, whereas to the left of the zone the opposite effects of the drift due to the potential difference and chemical diffusion to reduce the concentration

gradient and away from the zone (see section 6.4.3 and Fig. 6.22), create an oxygen depleted region where there is a less abrupt concentration gradient.

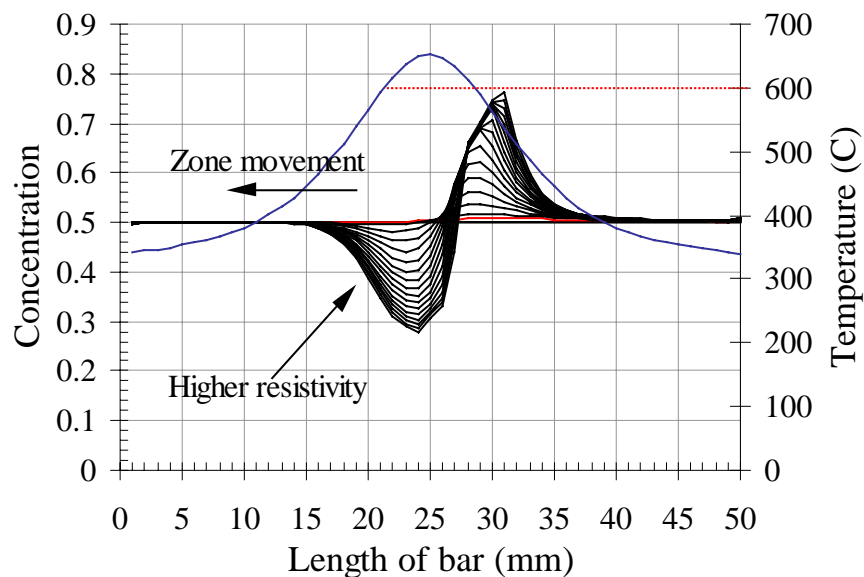


Fig. 6.32 Variation in the distribution of oxygen in the sample when a potential difference of 4.5 V is applied to a polycrystalline YBCO bar. Time between lines: 30 s

This oxygen depleted region has a high resistivity and the slope of the concentration gradient within it determines whether the zone remains mobile or immobile in the sample. If the gradient is small, the electric field established across the sample is going to be strong enough to drive oxygen ions across the gradient towards the anode. In this case the zone moves. However, if the gradient is large (due to an increase in the power supplied to the sample), the flux due to the electric field may not be strong enough to overcome the difference in concentration and the ions will not move towards the anode

It has been observed during the theoretical experiments that in certain cases the zone did not move. This is probably due to the effect mentioned in section 6.4.3 where the effects of chemical diffusion and ionic drift due to the potential difference give rise to the formation of a sharp concentration gradient that the ionic drift cannot overcome. The accumulation of ions at the cathode end of the zone in the example presented in Fig. 6.32 is quite large; this gives rise to a steep concentration gradient. The zone was observed to move very slowly in this case.

The development of this model has for the first time given the opportunity to carry out a calculation of the effects of the different processes that combine to produce the Direct Current Zoning effect. There is still need for more improvement of the modelling, evaluating the dependence of the conductivity on the density of the bar, as well as the effects of other microstructural features on this value. For the purposes of a simplified calculation it was assumed that the oxygen content of the sample segments was always the equilibrium content for the temperature of the segment. It has been mentioned in section 6.4.2 that the speed at which the ions move due to the change in temperature is much slower than the speed at which the zone moves. This would result in smaller changes in concentration than those calculated with this model. Further development of the program to incorporate a more accurate calculation of the chemical diffusion in the sample was beyond the scope of this thesis. For the following studies of the DCZ effect it will be very interesting to introduce such modification in the program in order to be able to calculate more accurately the contribution of chemical diffusion in the process.

The study of diffusion in polycrystalline samples presented in chapter 5 has shown that the microstructure has a very important effect on the chemical diffusion process. In order to be able to model the DCZ effect more accurately it would be necessary to know the dependence of the value of the oxygen diffusion coefficient on the density of the samples used.

6.4.5 Summary

This section has presented a more complete analysis of the Direct Current Zoning effect than those carried out so far. It has corroborated the suggestions made by other groups concerning the motion of oxygen ions within the sample that result in the formation of a zone when a potential difference is applied across a polycrystalline bar of YBCO.

The formation of a zone in a sample is associated to a reduction in the power supplied to it. This has been explained in terms of the variation in temperature of the sample before and after the zone appeared.

It has been shown that the chemical diffusion and drift of oxygen ions are directly related to the speed at which the zone moves along the sample, and it has been possible to suggest a reason for its remaining stationary considering the magnitude and direction of these ionic fluxes.

The development of a computer model to reproduce this phenomenon has corroborated the suggestions made concerning the changes in temperature within the sample before and after the zone appears and it has also calculated the change in the oxygen distribution within the sample once the zone is present and moving. This evolution of the concentration gradients with time has corroborated the suggestion made relating chemical diffusion and drift of the oxygen ions in the presence of an electric field that cause the zone to stop at a certain point.

6.5 Conclusions

The oxygen non-stoichiometry of YBCO and its behaviour as a solid mixed conductor at high temperatures are thought to be the reason behind what is known as the Direct Current Zoning effect. This effect consists on the formation of a hot region in a bar of polycrystalline YBCO when a DC voltage is applied across it.

This chapter has presented an initial study of the processes occurring during the formation of this hot zone, combining the increase in temperature due to the Joule effect with the variation in the conductivity of the sample and chemical diffusion of oxygen within it because of the increase in temperature. This chapter has developed a more thorough study than any of those carried out to date, and it presents an analysis of the motion of oxygen ions due to electromigration and chemical diffusion that supports the proposed mechanism for the motion of the zone.

A more exhaustive analysis of the conditions in which the zone forms will help to characterise it fully (zone nucleation, speed, size and temperature), such as more accurate measurements of the temperature of the bar (with an infrared pyrometer, for example) and the effects of sample microstructure on ion conduction and chemical diffusion.

It is still unknown why the zone forms although it is thought that it occurs at some point along the sample where there is a higher degree of porosity or to the presence of impurities that increase the temperature of the sample locally, triggering the formation of the zone but allowing it to move away from this point towards the negative electrode.

To complete this preliminary study of the DCZ effect a computer model has been developed taking into account the three processes that take part in the formation and motion of the hot zone along the bar: temperature change (Joule effect), increase in the oxygen conductivity and variation in the value of oxygen chemical diffusion in the sample. The theoretical I-V characteristics obtained match quite well the experimental results. The model calculates the variation in temperature with time during the theoretical reproduction of the experiments as well as the variation in the distribution of oxygen due to the increase in the value of the chemical diffusion and the electromigration of the oxygen ions due to the potential difference established across the sample. This model has given the opportunity to study for the first time all the processes that take part simultaneously in the Direct Current Zoning effect. The results from the computer programme have corroborated the suggestions made during the experimental stage of the study concerning the variation in temperature and oxygen content in the sample. The program has also given an insight as to why the zone sometimes stops at some point in the sample.

Chapter 7

Conclusions and further work

7.1 Conclusions

This thesis has presented a study of the phenomenon of oxygen diffusion in $\text{YBa}_2\text{Cu}_3\text{O}_{7-\delta}$ (YBCO). Analysis of the thermogravimetric results from experimental isothermal oxygenations of YBCO powder has yielded an Arrhenius expression for the variation of the oxygen diffusion coefficient with temperature in this material. This study of the diffusion process includes the development of a computer model for oxygen diffusion in YBCO particles.

YBCO was one of the first high temperature superconductors discovered, and its superconducting properties are strongly dependent on its oxygen stoichiometry. A large amount of work has been done on the variation of this stoichiometry and its effect on the superconducting properties of the material. Since the critical temperature (T_c) of YBCO increases with oxygen content (Fig. 1.4), processing of this material for optimum superconducting properties concentrates on achieving the highest oxygen content possible.

However, the manufacturing of YBCO samples for superconducting applications requires very high temperatures, and in this region the equilibrium oxygen content is low (Fig. 1.5). In order to increase the oxygen content of the material it is necessary to include an oxygenation step at lower temperatures.

For a given sample size, the duration of this step is determined by the value of the oxygen diffusion coefficient. This is crucial to optimise the superconducting properties and it is one of the reasons why such a large amount of work has been dedicated to the calculation of the value of the diffusion coefficient of oxygen in YBCO.

However, in spite of all the work done, the results published in the literature are quite scattered (see Fig. 7.1). The present study has tried to reconcile the data available, taking into account the factors that may have affected these calculations of the oxygen diffusion coefficient (chapter 3).

The first aspect to consider is the fact that depending on the technique used, the diffusion coefficient measured is different. Chemical diffusion, self diffusion and tracer diffusion are the three types of coefficients measured. The driving force for diffusion is different in each case, and in order to compare them it is necessary to take into account the factors that relate each of them with the rest. These factors have been reviewed in chapter 2.

The second aspect concerning the analysis of diffusion results is the effect of the sample microstructure on the results obtained with each measuring technique. Tracer diffusion and internal friction methods are not affected by the type of sample used, although there are some difficulties associated to tracer diffusion measurements in the *c* direction due to the reduced size of the single crystals along this axis. However, resistance measurements and thermogravimetry, for example, are highly sensitive to the sample microstructure. The effect of microstructural features becomes more important when using polycrystalline specimens. The microstructural features of these samples introduce a series of factors that in most cases have unknown effects on the diffusion process. The presence of grain boundaries introduces the possibility of grain boundary diffusion occurring if the experiment is carried out at low temperature, although the range of temperatures within which it is predominant over bulk diffusion is not yet known.

Other microstructural features of polycrystalline samples, such as the presence of open or closed porosity may also alter the diffusion results obtained. If the sample has a high degree of porosity, oxygen will be able to reach the most inner regions of the sample without any opposition (open porosity). This should be taken into account when the diffusion distance is established in the analysis of diffusion data. In this case the diffusion length will be one half of the distance between interconnected pores (if the effect of grain boundaries is not taken into account). In the case of samples with closed porosity, the diffusion length should be one half of the dimensions of the

sample (assuming again that grain boundary diffusion is not active in the temperature range considered). The estimation of the diffusion distance is one of the main sources of error in diffusion studies.

The effect of secondary phases and impurities introduced during the processing of polycrystalline and single crystal specimens should also be taken into account when analysing diffusion results.

After the analysis of the literature data it seemed clear that the use of a polycrystalline sample to study the oxygen diffusion coefficient in YBCO would not help in the clarification of the scattered results. The use of powder samples, however, would eliminate the effects mentioned above from the analysis of the diffusion process, so it was decided to carry out a series of oxygenations of powder samples to determine a value of the diffusion coefficient that was not affected by microstructural defects.

The study presented in this thesis has been divided into two sections:

The first section consists in the analysis of *isothermal oxygenations* of powder specimens using thermogravimetry. This technique allows the calculation of the value of the chemical diffusion coefficient, \tilde{D} , because the weight changes of the powder samples are directly related to the change in oxygen stoichiometry of the material. The analysis of the data was made fitting the results of two different solutions of Fick's second law assuming that \tilde{D} was independent of the concentration of oxygen in the sample. An Arrhenius expression relating the change in the value of the diffusion coefficient with temperature was obtained with the calculated values of the chemical diffusion coefficient at different temperatures.

It is possible to calculate the length of the oxygenation step needed to obtain an YBCO sample with high oxygen content (above 6.9 for optimum superconducting properties) knowing the value of the diffusion coefficient at each temperature. The optimisation of the time it takes to oxygenate YBCO specimens has been a matter of concern for large scale applications. The shorter diffusion distances of thin films mean that full oxygenation can be completed during manufacturing without increasing processing time considerably. However, due to the larger diffusion distances of bulk samples, oxygenation times can increase to weeks, months or even years. The increase

in processing time due to the long oxygenation steps needed reduces the practical applications of this type of samples.

The problem of increased oxygenation times has been solved in the second section of this diffusion study:

In the course of the oxygenation experiments, it was observed that the weight gain traces obtained during *non-isothermal oxygenations* (heating slowly to high temperatures) had a very characteristic shape (Fig. 5.26) that could be divided in two regions: an initial part where oxygen was absorbed by the specimen at low temperatures (non-equilibrium regime) up to a certain temperature, T_{\max} , and a second part at higher temperatures where the weight of the sample decreased following the equilibrium oxygen content for each temperature (quasi-equilibrium regime). If the sample was cooled at the same rate as it had been heated up, the weight change of the sample followed this *quasi-equilibrium* trace until the temperature decreased to T_{\max} . At this temperature \tilde{D} becomes too slow to oxygenate the whole sample in the time set by the cooling rate. Provided the temperature of the specimen is always kept above the T_{\max} of the rate at which it is cooled, its oxygen content will be distributed uniformly in the sample and will always be at the equilibrium value for each temperature.

Non-isothermal oxygenations of powder samples at different rates showed that T_{\max} decreased with decreasing heating rate. The possibility of cooling the samples following the equilibrium oxygen content trace slowing the cooling rate with decreasing temperature (thus decreasing the value of T_{\max} and broadening the range of temperatures at which the sample is at equilibrium) offered an alternative way of oxygenating YBCO samples. Cooling from a high temperature at a series of cooling rates (faster at high temperatures and more slowly at low temperatures), as shown in chapter 5, allows a reduction of oxygenation times of up to 12 hours for powder particles $\approx 5 \mu\text{m}$ in diameter.

It has already been pointed out that the oxygenation of small powder particles or thin films is not a problem because of their small dimensions. The situation becomes more problematic when larger samples need to be oxygenated. To be able to apply the *quasi-equilibrium* procedure developed to the oxygenation of bulk samples for large

scale superconducting applications, it was necessary to draw up the relationship between cooling rates and T_{\max} for larger particle sizes (as the diffusion length increases cooling rates become slower and longer times are required for full oxygenation to be achieved). Carrying out experimentally the non-isothermal oxygenations needed to obtain this data would have taken a very long time, so the diffusion programme developed was used instead to calculate theoretically the results from non-isothermal oxygenations of larger samples allowing one to obtain the relationships between cooling rates and maximum temperatures for a series of sample sizes. It has been shown in chapter 5 that these *quasi-equilibrium cooling* procedures offer a fast alternative to isothermal oxygenation of bulk samples.

The diffusion programme developed has proved to be highly versatile. It reproduces fractional weight changes under isothermal and non-isothermal conditions, and it gives further insight to the oxygen diffusion process, calculating the evolution of the concentration profile during these oxygenations. This is particularly interesting as it could be of help when studying the superconducting behaviour of the samples. The programme can also be used to predict oxygenation times of larger samples without having to carry out trial-and-error experiments, reducing considerably research times.

This diffusion programme has also been applied to the study of the evolution of oxygenations under non-isothermal conditions. It has been particularly useful in calculating oxygenations of large samples to develop the *quasi-equilibrium cooling* procedure proposed in this thesis. This novel oxygenation step can be introduced at the end of the processing of YBCO bulk samples for large scale applications reducing oxygenation times and producing samples with the required oxygen contents.

The following chapter (chapter 6) presents a preliminary analysis of the Direct Current Zoning (DCZ) effect. The generation of a hot zone in a bar of polycrystalline superconductor when a certain potential difference is applied across it is directly linked to the motion of oxygen ions in the material due to the effects of electromigration and diffusion in a temperature and concentration gradient. A small number of groups have studied this effect. The work presented in this thesis includes a more detailed analysis of the DCZ effect, studying the variation in electronic and ionic conductivity and how these changes give rise to the presence of a hot mobile zone in

the bar. The work done has concentrated on the stability and motion of the zone along the polycrystalline sample. It has been observed that in some samples the zone remained immobile, and reasons for this behaviour have been suggested.

The study of this phenomenon includes the development of a computer model that reproduces the DCZ effect. This is the first model that has been written to study the effect theoretically, and it takes into account the combination between electromigration and diffusion processes. The results obtained using this computer programme have corroborated the proposed variation in temperature and oxygen distribution along the polycrystalline sample. The model has also supported the suggestions made concerning the stopping of the zone as it is moving along the bar.

7.2 Further work

With respect to the chemical diffusion study, the analysis of the data in the literature has brought up a large number of questions that have not been looked into in detail and that are very important if the diffusion of oxygen in YBCO is to be characterised fully.

Most of these are related to the microstructure of the samples used. Oxygen diffusion in polycrystalline materials has been studied undifferentiated from diffusion in powders or single crystals, and this seems to be associating an highly complex diffusion behaviour to the same group as single diffusion events.

The effects that grain boundary diffusion have on the diffusion process and the temperature range over which this short-circuit diffusion occurs have not been studied, and it would be very interesting to be able to study the possibility of combining the effects of fast grain boundary and bulk diffusion cycling the temperature to design an alternative oxygenation procedure.

The presence of open and closed porosity has also been mentioned. It would be very interesting to carry out a thorough study of the effects of density on the value of the diffusion coefficient. But great care will have to be taken in the correct characterisation of the sample, taking into account the grain size and the degree of open and closed porosity.

The possibility of blocking the diffusion process in certain regions of the sample due to misaligned grains (*c*-axis oriented) combined with grain boundary diffusion seems to be a matter that will only be possible to analyse theoretically. This brings up the need to develop a computer model that considers the effects of grain boundary diffusion and bulk diffusion in their respective temperature ranges as well as introducing changes in grain size. This is a challenging project that could only be carried out after experimental studies have been performed clarifying the points mentioned above.

With respect to the Direct Current Zoning effect, once the matters of diffusion in a polycrystalline material have been dealt with, it will be possible to carry out a complete study of the phenomenon. It would also be necessary to clarify the electrical behaviour of YBCO at high temperatures (> 300 K) in polycrystalline samples of different densities. The continuation of the DCZ project would study the reasons behind the generation of the zone, its motion down the polycrystalline bar and why, on occasions, the zone remains immobile at one point in the sample.

Meanwhile, however, it would be very interesting to use the relationship between the oxygen diffusion and oxygen ion conductivity (Nernst-Einstein equation) to control the oxygen content of YBCO samples applying a potential difference across them monitoring the temperature of the sample. This could be the topic of an interesting study that would assess the potential use of electrochemistry as a faster means of controlling the oxygen stoichiometry of superconducting samples.

APPENDIX 1

1A Listing of the computer model developed to study oxygen diffusion in a spherical powder particle

The following programme calculates the variation in weight change and the change in the oxygen content distribution in a spherical particle. The results obtained with this programme have been discussed in chapter 5 (see flowchart of the algorithm used in section 4.2.4).

```

CLS          '' Initializing the screen and clearing

      DEFDBL A-H      '' Double precision numbers
      DEFDBL O-V      '' Double precision numbers
      DEFINT I-N      '' Integers
      DEFSNG W-Z      '' Single precision numbers

''Variables:
      DIM C1(40, 40), V(40, 40), C2(40, 40), Se(40, 40), re(40, 40)
      DIM radio(40), alfa(40), Vr(40), suma(40), grade(40, 40),
gradi(40, 40)
      DIM WeightT(5000), Tst(10), Ten(10), tstart(10), tend(10)

'' Diffusion parameters:
      B = 1.38066E-23          ''Boltzmann constant
      si = 8.617E-05 / 1.38066E-23 ''Ratio eV/J
      d0 = .033              ''Diffusion pre-exponent cm2/s
      q = 1.24                ''Activation energy for diffusion
in eV
      q = q / si              ''Activation energy in J

'' Geometrical factors:
      Pi = 4 * ATN(1): rd = Pi / 180
      r = .00021              '' Radius of particle in cm
      nr = 20: na = 20        '' Number of divisions of sphere:
'' nr = number of slices in semisphere
'' na = number of rings in each slice.
      dh = r / nr             '' Division of radius to
calculate the                '' sections of
the semisphere

'' Calculation of the angles that limit each section of the sphere
considered: FOR kr = 1 TO nr
      cose = (kr - 1) * dh / r: '' Sine of the angle
      GOSUB 1000:              '' To cos-1 subroutine:
      alfa(kr) = Pi / 2 - angu:

NEXT kr
alfa(nr + 1) = Pi / 2
Vu = 2 / 3 * Pi * r ^ 3: Su = 2 * Pi * r * dh
FOR kr = 1 TO nr
      F = SIN(alfa(kr + 1)) - SIN(alfa(kr))
      F = F - (SIN(alfa(kr + 1))) ^ 3 / 3 + (SIN(alfa(kr))) ^ 3 / 3
      Vr(kr) = Pi * r ^ 3 * F
      radio(kr) = (Vr(kr) / Pi / dh) ^ .5
NEXT kr

```

```

'' Data input:
PRINT
PRINT "Enter initial concentration, x, (YBCO(6+x)); : INPUT
conc0
PRINT
PRINT "You have the choice of doing:"
PRINT "a) a study of the change in concentration with
increasing T"
PRINT "b) a study of the change in concentration at constant
T"
PRINT "c) a combination of the above (ramp + isothermal)"
PRINT
PRINT "Data saved in file (enter filename - default:
matrix.dat)"; : INPUT file$
PRINT "Concentration data saved in file (enter filename -
default: h:\conc.dat)"; : INPUT concfile$
IF file$ = "" THEN file$ = "matrix.dat"
IF concfile$ = "" THEN concfile$ = "h:\conc.dat"
PRINT
PRINT "Enter number of heat treatment cycles"; : INPUT Ncyc
PRINT "Enter initial T"; : INPUT T0
initialt = 0
Ten(0) = T0

OPEN concfile$ FOR OUTPUT AS #3
PRINT #3, "Initial Concentration=" + STR$(conc0)
FOR m = 1 TO Ncyc
PRINT "Step no. "; m
PRINT "Enter delta time"; : INPUT dtime
PRINT "Enter final T"; : INPUT T1
PRINT #3, "Step no.=" + STR$(m) + CHR$(9) + "Delta
time=" + STR$(dtime) + CHR$(9) + "Final T=" + STR$(T1)
Tst(m) = Ten(m - 1)
Ten(m) = T1
tstart(m) = initialt
initialt = initialt + dtime
tend(m) = initialt
NEXT m
PRINT #3, "ka"
PRINT #3,
FOR ka = 1 TO na
PRINT #3, STR$(ka)
NEXT ka
CLOSE #3

'' Calculation of the total heat treatment time:
numheaders = Ncyc + 1
tiTot = tend(Ncyc) * 60

'' "Slice" section. Calculation of the change in concentration in
each slice
'' considered:
FOR kr = 1 TO nr

'' Geometric factors:
dr = radio(kr) / na

'' Calculation of the external radius of each ring (re), volume of
each
'' ring (V), external surface of each ring (SE) and initial
concentration
'' (C1):
FOR ka = 1 TO na
V(kr, ka) = Vr(kr) * (2 * (na - ka) + 1) / (na ^ 2)

```

```

re(kr, ka) = radio(kr) - (ka - 1) * dr
Se(kr, ka) = 2 * Pi * re(kr, ka) * dh
C1(kr, ka) = conc0
NEXT ka
NEXT kr

ti = 0          '' Initial time in seconds

'' Calculation of the total time of the heat treatment:
dti = .1       '' Time interval chosen (in s)
kесcribe = 1   '' Each kесcribe iterations C1 is displayed
on screen

'' Main calculation:
FOR kr = 1 TO nr
  kr = 1
  dr = radio(kr) / na
  SCREEN 12          '' Graphic screen 640x480
  CLS
  GOSUB 2000: GOSUB 3000  '' Draw grids

'' Time count starts here:
  FOR ti = 0 TO tiTot STEP dti
    Minconc = 0
    Maxconc = .987#
    FOR m = 1 TO Ncyc
      IF ti < tend(m) * 60 AND ti >= tstart(m) * 60 THEN
        stepno = m
      NEXT m
      deltat = ti - tstart(stepno) * 60
      tinterval = tend(stepno) * 60 - tstart(stepno) * 60
      tempint = Ten(stepno) - Tst(stepno)

      T = Tst(stepno) + tempint / tinterval * deltat

'' Calculation of diffusion coefficient:
      D = d0 * EXP(-q / B / (T + 273))
      SELECT CASE T
        CASE IS < 396
          Equconc = -.0000705 * T + 1
        CASE 396 TO 535
          Equconc = -.0006 * T + 1.21
        CASE 535 TO 783
          Equconc = -.0015 * T + 1.692
        CASE IS > 783
          Equconc = -.001 * T + 1.3
      END SELECT

'' Concentration of outer ring(ka=1):
      C2(kr, 1) = Equconc
      IF C2(kr, 1) > Maxconc THEN C2(kr, 1) = Maxconc
      IF C2(kr, 1) < Minconc THEN C2(kr, 1) = Minconc

'' Concentration of the rest of the rings:
      FOR ka = 2 TO na - 1
        grade(kr, ka) = (C1(kr, ka - 1) - C1(kr, ka)) / dr
        gradi(kr, ka) = (C1(kr, ka) - C1(kr, ka + 1)) / dr
        C2(kr, ka) = C1(kr, ka) + Se(kr, ka) * D * dti *
        grade(kr, ka) / V(kr, ka)
        C2(kr, ka) = C2(kr, ka) - Se(kr, ka + 1) * D * dti
        * gradi(kr, ka) / V(kr, ka)
        IF C2(kr, ka) > Maxconc THEN C2(kr, ka) = Maxconc
        IF C2(kr, ka) < Minconc THEN C2(kr, ka) = Minconc
      NEXT ka

```

```

'' Concentration of innermost ring (ka=na):
  FOR ka = na TO na
    grade(kr, ka) = (C1(kr, ka - 1) - C1(kr, ka)) / dr
    gradi(kr, ka) = 0
    C2(kr, ka) = C1(kr, ka) + Se(kr, ka) * D * dti *
    grade(kr, ka) / V(kr, ka)
    C2(kr, ka) = C2(kr, ka) - Se(kr, ka + 1) * D * dti
    * gradi(kr, ka) / V(kr, ka)
    IF C2(kr, ka) > Maxconc THEN C2(kr, ka) = Maxconc
    IF C2(kr, ka) < Minconc THEN C2(kr, ka) = Minconc
  NEXT ka

'' Change C1 to C2 so that this value can be carried into
the next '' iteration:
  FOR ka = 1 TO na
    C1(kr, ka) = C2(kr, ka)
  NEXT ka

k$ = INKEY$          ''waiting for trapping
keystrokes
  IF LEN(k$) = 1 THEN
    IF LEN(k$) = 1 AND ASC(k$) = 27 THEN
      END              '' Exit
    END IF
    IF LEN(k$) = 1 AND k$ = "c" OR k$ = "C" THEN
      GOSUB 4000: GOSUB 3000    '' Clear
    END IF
    IF LEN(k$) = 1 AND ASC(k$) = 13 THEN
      INPUT c          '' Stop until key is
      pressed
    END IF
  END IF

'' Print label:
  LOCATE 1, 12

  PRINT USING "Temperature= ####.#"; T;
  PRINT USING "oC   time=##"; FIX(ti / 3600);
  PRINT " hours ";
  PRINT USING "##.#"; (ti / 60) - 60 * FIX(ti / 3600);
  PRINT " min";
  LOCATE 2, 15: PRINT "Exit press ESC";
  LOCATE 2, 34: PRINT "Clear the top screen press C";

'' (Draw line every kescribe iteration)
  IF INT(ti/dti)/INT(kescribe/(dti)) =
  INT(INT(ti/dti)/INT(kescribe/(dti))) THEN

    GOSUB 5000          '' Open a data file
    COLOR 2
    LOCATE 23, 1
    IF T > 1000 THEN
      COLOR 31
      PRINT "The temperature is too close to the
      melting point"
    END
  END IF

'' Plot concentration profile:
  FOR ka = 1 TO na - 1
    LINE (offsetx + ka * sx, offsety+900 * C1(kr,
    ka) * sy)-(offsetx + (ka + 1) * sx, offsety+900 *
    C1(kr, ka + 1) * sy)

```

```

        NEXT ka
        COLOR 15
        '' Calculation of the weight change of the sphere with
oxygenation:
        n = INT(ti / kescribe)
        eightA = dr * C1(kr, 1)
        FOR ka = 2 TO na
            WeightA = WeightA + dr * (C1(kr, ka - 1) +
C1(kr, ka))/2
        NEXT ka
        WeightT(n) = WeightA
        WeightT(0) = 0
        '' Plot Mass-t curve
        COLOR 2
        IF n = 0 THEN
            LINE (x01 + 0 * dx1, y02 - WeightT(0) / dy1)-
(x01 + 0 * dx1, y02 - WeightT(0) / dy1)
        END IF
        IF n = 1 OR n > 1 THEN
            LINE (x01 + (n - 1) * dx1, y02 - WeightT(n -
1) / dy1)-(x01 + (n) * dx1, y02 - WeightT(n) / dy1)
        END IF
        GOSUB 6000          '' Save data in file
        GOSUB 7000          '' Close the data file
        COLOR 15
        '' Export data:
        OPEN concfile$ FOR INPUT AS #2
        OPEN "C:\temp\conctmp.dat" FOR OUTPUT AS #3
            '' Read headers and write
            out again:
        FOR ix = 1 TO numheaders
            LINE INPUT #2, inline$
            PRINT #3, inline$
        NEXT ix
        LINE INPUT #2, inline$
        PRINT #3, inline$ + CHR$(9) + STR$(ti)
        LINE INPUT #2, inline$
        PRINT #3, inline$ + CHR$(9) + STR$(T)
        FOR ka = 1 TO na
            LINE INPUT #2, inline$
            PRINT #3, inline$ + CHR$(9) + STR$(C1(kr,
ka))
        NEXT
        CLOSE #2
        CLOSE #3
        KILL concfile$
        SHELL "copy c:\temp\conctmp.dat " + concfile$
        END IF
    NEXT ti
NEXT kr
END

1000      '' cos-1 subroutine
IF ABS(cose) > 10 ^ (-9) THEN 1010
angu = Pi / 2: RETURN
1010 IF 1 - ABS(cose) > 10 ^ (-6) THEN 1030
angu = Pi / 2 * (1 - SGN(cose)): RETURN
1030 angu = ATN((1 - cose * cose) ^ .5 / cose)
IF angu < 0 THEN angu = Pi + angu: RETURN

2000      '' Sub to draw axes for Mass-t, labels etc.
CLS
sy = -.27          '' Scale factor y direction
sx = 500 / na      '' Scale factor x direction

```

```

offsety = 280
offsetx = 35
COLOR 15

dy1 = 6.5 * 10 ^ -7#
dx1 = 3

x01 = 150: x02 = 450    '' Scale factor x direction
y01 = 300: y02 = 475    '' Scale factor y direction

LINE (x01, y01)-(x01, y02)
LINE (x01, y02)-(x02, y02)

RETURN

3000          '' Draw grid
COLOR 15
FOR tt = 0 TO 900 STEP 90
    LINE (offsetx + sx, offsety + tt * sy)-(offsetx + (na + 1) *
sx, offsety + tt * sy)
NEXT tt
FOR j = offsetx + sx TO offsetx + (na + 1) * sx + 1 STEP na / 10 * sx
    LINE (j, offsety)-(j, offsety + 900 * sy)
NEXT j

SCREEN 12

COLOR 15
LOCATE 10, 1: PRINT "  x  "
LOCATE 3, 3: PRINT " 7.0 "
LOCATE 6, 3: PRINT " 6.8 "
LOCATE 9, 3: PRINT " 6.6 "
LOCATE 12, 3: PRINT " 6.4 "
LOCATE 15, 3: PRINT " 6.2 "
LOCATE 18, 3: PRINT " 6.0 "
LOCATE 20, 37: PRINT "radius (cm)";
LOCATE 19, 7: PRINT USING "#.####"; (re(kr, 1));
LOCATE 19, 38: PRINT USING "#.####"; (re(kr, 1) / 2);
LOCATE 19, 70: PRINT (0);

RETURN

4000          '' Clear the top of the screen
FOR u = 1 TO 30
    LOCATE u, 1: PRINT TAB(78);
NEXT u
RETURN

5000
OPEN "h:\" + file$ FOR APPEND AS #1
RETURN

6000
WRITE #1, ti, WeightT(n) * 10 ^ 4, T
RETURN

7000
CLOSE #1
RETURN

```

APPENDIX 2

2A Preparation of mixture for polymer processing of YBCO tapes

The mixture of YBCO powder, plasticiser and binder used had the following proportions;

110 g of $\text{YBa}_2\text{Cu}_3\text{O}_{7-\delta}$

5.6 g of PBV

6.7 g of cyclohexanone

2 b of dibutylphthalate

The components were mixed together and worked through a rolling mill until the tapes had a uniform appearance and strong consistency.

2B Calculation of heat dissipation in the YBCO bar used in the computer model developed

During the process of formation and movement of the zone along the bar, three types of heat transfer take place that determine the final temperature of the sample for a given power VI supplied to the sample: radiation, convection and conduction. The program developed to model the motion of the zone in the sample (see section 2C below) takes them into account in order to calculate the variation in temperature along the specimen. They are described by the following equations:

$$\text{Radiation: } Q^R = A\varepsilon\sigma(T^4 - T_{\text{ambient}}^4)$$

where: ε = emissivity of the material (0.915)

σ = Stefan-Boltzmann constant = $5.67 \times 10^{-8} \text{ W/m}^2\text{K}^4$

A = area through which the heat is dissipated

T = temperature of the surface (in K)

T_{ambient} = ambient (room) temperature (in K)

$$\text{Conduction: } Q^C = A_c k (T - T_{\text{initial}}) / x$$

where: k = thermal conductivity of the material (W/m^2)

A_c = cross sectional area through which the heat is dissipated

x = distance over which the temperature difference is

measured.

Convection: $Q = A_s h (T_{\text{sample}} - T_{\text{atmosphere}})$

where: h = convective heat transfer coefficient ($\text{W}/\text{m}^2 \text{ } ^\circ\text{C}$)

A_s = surface area through which the heat is dissipated

T_{ambient} = ambient (room) temperature (in K)

The latter form of heat dissipation in this case is natural convection of air. In this situation the transfer of heat occurs at a low rate since the natural convection currents move rather slowly. The flow of air around the YBCO bar is assumed to be non-turbulent near the surface. The thermal conductivity of a horizontal pipe for streamline flow of air takes the form (Coulson and Richardson (1977)):

$$h = 1.18 (\Delta T/d)^{1/4}.$$

It has been assumed in the calculations below that the thermal conductivity varies in 0.0001 every time the temperature of the sample increases $1 \text{ } ^\circ\text{C}$.

The calculation of the increase in temperature in the program is carried out subtracting the heat lost by radiation, convection and conduction from the power supplied, VI . This allows to estimate the difference in temperature after each time step. This new temperature profile is used in the next set of calculations: oxygen diffusion coefficient, resistivity and once more the new temperature profile of the sample.

2C Listing of the computer model developed to study the Direct Current Zoning effect

The following programme calculates the variation in temperature and the change in the oxygen content distribution in a polycrystalline rod during the Direct Current Zoning effect. The results obtained with this programme have been discussed in chapter 6 (see flowchart of the algorithm used in section 6.4.4).

```
SCREEN 0: CLS ''Initializing the screen and clearing

'' Geometrical factors:
diameter = .0023 '' Diameter in m
area = 3.14159 * diameter ^ 2 / 4 '' Cross sectional area
length = .05 '' Total length in m
surface = 3.14159 * diameter * length '' Wire surface area in m^2

'' Physical constants:
emissivity = .915
Density = 5.8 '' Density in gr/cm^3
Density = Density * .001 * 10 ^ 6 '' Density in Kg/m^3
ThermalCond = 2.67 '' Thermal conductivity in
W/(m K)
SpecificHeat = .431 '' Specific heat in J/(g K)
```

```

SpecificHeat = SpecificHeat * 1000          '' Specific heat J/(kg K)
ThermalTempCof = .0001                    '' 1/°C assumed temp coefficient
RT = 25                                    '' of the thermal conductivity
                                           '' Room temperature in °C

concoefficient = 1.18                      '' Convection coefficient in
W/m²K
    '' Convection is assumed to follow:
    '' Convection loss=coefficient*(temp-
ambient)^0.25/diameter^0.25

convection = concoefficient / diameter ^ .25
    '' Convection is now used in the following equation -
    '' Convection loss = convection*(temp-ambient)^0.25

endeffect = 1    '' This allows a larger loss at the ends to be
effectuated
                '' endeffect=1 means no increased loss at the end
                '' endeffect>1 means increased loss at the end

'' Physical constants:
stefan = 5.67E-08                            '' Stefan-Boltzmann
constant W/(m²K⁴)
si = 8.617E-05 / 1.38066E-23                '' Ratio eV/J
k = 1.38066E-23                             '' Boltzmann constant J/K

'' The ion concentration in x-6 units the oxygen ion concentration is
'' assumed to obey the relation:
'' IF T<400 THEN
''     ionconc = InitConc
''     ELSEIF ionconc < -0.015*Tc(i) +1.55057 THEN
''         ionconc = InitConc
''     ELSE ionconc = -0.015*Tc + 1.55057

ze = 2 * 1.6E-19                            '' Charge transported by the oxygen ions
conc = 3.408 * 10 ^ 27                      '' Mobile ions/m³ (for x=6.6, or x-6=0.6)
Maxconc = .987#                             '' Maximum oxygen concentration
firstread = 0                               '' A flag
                                           '' The first reading occurs when the temperature
tempdiff = 5                                '' of the zone is within tempdiff of the last
reading
                                           '' after which the 'firstread' flag is set to 1.

'' Diffusion parameters:
d0 = .23                                    '' Diffusion pre-exponent cm²/s (from chapter
5)
d0 = d0 / 10000                            '' m²/s
q = .8                                     '' Activation energy for diffusion in eV (from chapter
5)
q = q / si                                  '' Activation energy in J

'' Total = total conductivity data
Total4 = 34100!                            '' Conductivity at 400°C (from chapter
6)
Total8 = 2093!                             '' Conductivity at 850°C (from chapter
6)

'' Since the experimental conductivity is 8 times lower we
'' divide the conductivity by 8

Total4 = Total4 / 8                        '' Conductivity at 400°C
Total8 = Total8 / 8                        '' Conductivity at 850°C

```

```

b = LOG(Total4 / Total8) / 450 '' Find exponential to fit the
following
c = Total4 / EXP(-b * 450) '' equation: conductivity=c*exp(-b*t)
'' Find the pre-exponent

'' Linear simulation of a wire divided by n segments:
N = 50 '' Number of segments, maximum 100
'' Tc = Temperature in °C
'' Tk = Temperature in K
'' heating = heat production
'' cooling = heat loss
'' conc = oxygen concentration in x-6
'' delconc = change in concentration

DIM Tc(101), heating(101), cooling(101), conc(101), delconc(101)

PRINT "Enter initial oxygen concentration (in x-6 units):";
INPUT InitConc
'' Uniform distribution of Tc, the temperature at room temp
'' and concentration at InitConc

FOR i = 1 TO N
    Tc(i) = RT
    conc(i) = InitConc
NEXT i

PRINT "Do you want to enter a depleted oxygen region? (y/n)";
INPUT YesNo$

IF YesNo$ = "y" THEN GOSUB 5000 '' Create an area with a different
concentration

'' Initialising:
oldcurrent = 0
oldvoltage = 0

'' Calculate temperature rise with time time sequence starts at t=0
and
'' continues with m steps of delta until time totaltime (in sec) is
reached

totaltime = 5000 '' Total length of calculation in
seconds
delta = .1 '' Interval in seconds
m = totaltime / delta '' m*delta = total time

seglen = length / N '' Segment length

PRINT "Enter voltage in V:"; : INPUT v0

mm = -1 '' mm is a counter
SCREEN 12 '' Graphic screen 640x480
GOSUB 1000: GOSUB 2000 '' Draw grids

ss = 1 / SpecificHeat / Density / area / seglen * delta '' Temp,
increase °C/W

OPEN "h:\qbprogs\Tprodcz.dat" FOR OUTPUT AS #2
PRINT #2, "initial concentration= " + STR$(InitConc)
PRINT #2, "i"
FOR i = 1 TO N
    PRINT #2, STR$(i)
NEXT i
CLOSE #2

```

```

OPEN "h:\qbprogs\VIDcz.dat" FOR OUTPUT AS #3
PRINT #3, "initial voltage =" + STR$(v0)
PRINT #3,
PRINT #3, "T, V, current"
CLOSE #3

OPEN "h:\qbprogs\condcz.dat" FOR OUTPUT AS #8
PRINT #8, "initial concentration=" + STR$(InitConc)
PRINT #8, "i"
  FOR i = 1 TO N
    PRINT #8, STR$(i)
  NEXT i
CLOSE #8

FOR T = 0 TO m * delta STEP delta      '' Start main loop
  Resistance0 = 0
  '' Find the resistance: Total=total conductivity
  FOR i = 1 TO N
    Tk = 273 + Tc(i)                    '' Temperature in K
    D = d0 * EXP(-q / k / Tk)          '' Diffusion coefficient
    '' ionconc is the ion concentration (max=maxconc-6)
    SELECT CASE Tk
      CASE IS <= 435 + 273
        ionconc = -.00009 * Tc(i) + 1
      CASE (435 + 273) TO (705 + 273)
        ionconc = -.001653 * Tc(i) + 1.68
      CASE IS >= (705 + 273)
        ionconc = -.001163 * Tc(i) + 1.334
    END SELECT
    IF ionconc > 1 THEN ionconc = Maxconc
    IF Tk < 673 THEN
      electr = Total4
    ELSE electr = c * EXP(-b * Tc(i))
    END IF
    '' Ionic is now the conductivity due to the conc(i)
    ionic = (D / k / Tk) * ze ^ 2 * conc(i) * conc / .6
    '' Total is now the real total conductivity
    Total = electr + ionic

    resistivity = 1 / Total              '' Resistivity in 1/Ωm
    Resistance0 = Resistance0 + resistivity * seglen / area
    '' Sum all the individual segments to give the value of
the
    '' total resistance resistance0 of the wire.
  NEXT i

  current = v0 / Resistance0
  V = 0

  FOR i = 1 TO N
    '' Heat generation in the segments and radiation + convection loss:
    Tk = 273 + Tc(i)
    D = d0 * EXP(-q / k / Tk)
    SELECT CASE Tk
      CASE IS <= 435 + 273
        ionconc = -.00009 * Tc(i) + 1
      CASE (435 + 273) TO (705 + 273)
        ionconc = -.001653 * Tc(i) + 1.68
      CASE IS >= (705 + 273)
        ionconc = -.001163 * Tc(i) + 1.334
    END SELECT

    IF Tk < 673 THEN

```

```

        electr = Total4
ELSE electr = c * EXP(-b * Tc(i))
END IF

ionic = (D / k / Tk) * ze ^ 2 * conc(i) * conc / .6
Total = electr + ionic

resistivity = 1 / Total
resistance = resistivity * seglen / area
power = current ^ 2 * resistance      '' Joule heating
V = V + current * resistance         '' Voltage drop
radiation = emissivity * stefan * surface / N * ((Tc(i) +
273) ^ 4 - (RT + 273) ^ 4)

'' Radiation loss
'' Add convection term:
'' if Tc(i)-RT<0 then Tc(i)=RT
    radiation = radiation + convection * surface / N * (Tc(i)
    - RT)^.25
'' add convection term
'' special treatment for ends

        IF i = 1 OR i = N THEN
            radiation = radiation + emissivity * stefan * area
            * ((Tc(i) + 273) ^ 4 - (RT + 273) ^ 4)
''add convection term
            radiation = endeffect * radiation + convection *
            area * (Tc(i) - RT) ^ .25
        END IF

'' ss = tempearture increase in oC/W after delta seconds
    heating(i) = (power - radiation) * ss''oC

    Tc(i) = Tc(i) + heating(i)      '' Update temperature profile
    '' if Tc(i)<RT then Tc(i)=RT

NEXT i

'' Cooling due to thermal conduction along the rod
FOR i = 2 TO N - 1
    cof = 1 - ThermalTempCof * Tc(i)
    '' Thermal conductivity at Tc(i) in W/(Km)
    cooling = -ThermalCond * cof * area / seglen * (2 * Tc(i)
    - Tc(i - 1) - Tc(i + 1))      '' W
    cooling(i) = cooling * ss      '' cooling in oC
NEXT i

'' Special treatment for the first and last segments:
'' Conduction into the rod only:
    cof = 1 - ThermalTempCof * Tc(i)
    '' Thermal conductivity at Tc(1) W/(mK)
    cooling = -ThermalCond * cof * area / seglen * (Tc(1) - Tc(2))
    '' W
    cooling(1) = cooling * ss      '' oC
    cof = 1 - ThermalTempCof * Tc(i)
    '' Thermal conductivity at Tc(n) W/(mK)
    cooling = -ThermalCond * cof * area / seglen * (Tc(N) - Tc(N -
    1))      '' W
    cooling(N) = cooling * ss      '' oC

'' Update the temperature profile:
FOR i = 1 TO N
    Tc(i) = Tc(i) + cooling(i)    '' if Tc(i)<RT then Tc(i)=RT
NEXT i

```

```

'' Calculate concentration changes:
  FOR i = 1 TO N
    Tk = Tc(i) + 273
    D = d0 * EXP(-q / k / Tk)
    SELECT CASE Tk
    CASE IS <= 435 + 273
      ionconc = -.00009 * Tc(i) + 1
    CASE (435 + 273) TO (705 + 273)
      ionconc = -.001653 * Tc(i) + 1.68
    CASE IS >= (705 + 273)
      ionconc = -.001163 * Tc(i) + 1.334
    END SELECT

'' ionconc is the equilibrium oxygen concentration in x-6 units:
    tau = (diameter / 2) ^ 2 / D ''Diffusivity time constant
    conc(i) = conc(i) + (ionconc - conc(i)) * (delta / tau)
    IF conc(i) > ionconc THEN conc(i) = ionconc
  NEXT i

'' Ion drift calculation:
  FOR i = 1 TO N
    Tk = Tc(i) + 273
    D = d0 * EXP(-q / k / Tk)
    Tkleft = Tc(i - 1) + 273

    IF i = 1 THEN
      Dleft = 0
    ELSE Dleft = d0 * EXP(-q / k / Tkleft)
    END IF
    SELECT CASE Tkleft
    CASE IS <= 435 + 273
      ionconc = -.00009 * Tc(i - 1) + 1
    CASE (435 + 273) TO (705 + 273)
      ionconc = -.001653 * Tc(i - 1) + 1.68
    CASE IS >= (705 + 273)
      ionconc = -.001163 * Tc(i - 1) + 1.334
    END SELECT

    IF Tkleft < 673 THEN
      electr = Total4
    ELSE electr = c * EXP(-b * Tc(i))
    END IF
    ionic = (Dleft / k / Tkleft) * ze ^ 2 * conc(i - 1) *
conc / .6
    Total = electr + ionic
    resistivityl = 1 / Total
    Vleft = current / area * resistivityl

    driftleft = (Vleft) * Dleft / k / Tkleft * ze
    Tkrightright = Tc(i + 1) + 273

    IF i = N THEN
      Dright = 0
    ELSE Dright = d0 * EXP(-q / k / Tkrightright)
    END IF
    SELECT CASE Tkrightright
    CASE IS <= 435 + 273
      ionconc = -.00009 * Tc(i + 1) + 1
    CASE (435 + 273) TO (705 + 273)
      ionconc = -.001653 * Tc(i + 1) + 1.68
    CASE IS >= (705 + 273)
      ionconc = -.001163 * Tc(i + 1) + 1.334
    END SELECT

```

```

        IF Tkrightr < 673 THEN
            electr = Total4
        ELSE electr = c * EXP(-b * Tc(i))
        END IF
        ionic = (Drightr / k / Tkrightr) * ze ^ 2 * conc(i + 1) *
conc / .6
        Total = electr + ionic

        resistivityr = 1 / Total
        Vright = current / area * resistivityr
        driftright = (Vright) * Drightr / k / Tkrightr * ze
        delconc(i) = (conc(i - 1) * driftleft - conc(i + 1) *
driftright) * delta / seglen

'' Chemical gradients:
        fick = (-(conc(i) - conc(i - 1)) * Dleft + (conc(i + 1) -
conc(i)) * Drightr) / seglen
        delconc(i) = delconc(i) + fick * delta / seglen
    NEXT i

'' Update concentration due to drift:
    FOR i = 1 TO N
        conc(i) = conc(i) + delconc(i)
        IF conc(i) > Maxconc THEN
            conc(i) = Maxconc
        END IF
        IF conc(i) < .2 THEN
            conc(i) = .2
        END IF
    NEXT i

    k$ = INKEY$
    IF LEN(k$) = 1 THEN
        IF LEN(k$) = 1 AND ASC(k$) = 27 THEN
            END          ''exit
        END IF
        IF LEN(k$) = 1 AND ASC(k$) = 13 THEN
            INPUT c      '' Hold calculation until next
keystroke

        END IF
        IF LEN(k$) = 1 AND k$ = "c" OR k$ = "C" THEN
            GOSUB 3000: GOSUB 2000          '' Clear
        END IF
        IF LEN(k$) = 1 AND k$ = "a" OR k$ = "A" THEN
            GOSUB 1000: GOSUB 2000        '' clear
all

        END IF
        IF LEN(k$) = 1 AND k$ = "h" OR k$ = "H" THEN '' Hot spot
            GOSUB 5000
        END IF
    END IF

    IF LEN(k$) = 1 AND k$ = "p" OR k$ = "P" THEN
        GOSUB 4000          '' Draw concentration profile
    END IF

    IF LEN(k$) = 2 THEN
        IF ASC(MID$(k$, 2, 1)) = 80 THEN
            v0 = v0 - .1          '' Down arrow, decrease voltage
        END IF
        IF ASC(MID$(k$, 2, 1)) = 72 THEN
            v0 = v0 + .1          '' Up arrow, increase voltage
        END IF
    END IF
END IF

```

```

mm = mm + 1                                '' mm = number of iterations
IF mm / 300 - INT(mm / 300) = 0 THEN
    '' Draw line every 50th
    calculation
    mmprint = 6                            '' Calculate every mmprint cycles
'' Print label
LOCATE 1, 1: PRINT TAB(78);
LOCATE 1, 1
PRINT "V=";
PRINT USING "####.##"; V;
PRINT "V    I=";
PRINT USING "####.##"; current;
PRINT "A    R=";
PRINT USING "####.##"; Resistance0;
PRINT "^    ";
PRINT "T=";
PRINT USING "####.##"; Tc(N / 2);
PRINT "oC   time=";
PRINT USING "####.##"; T;

GOSUB 6000
IF mm / mmprint - INT(mm / mmprint) = 0 THEN
    '' Find location of max
    temp
    oldmaxtemp = maxtemp                    '' Old value of
temperature
    maxtemp = -1E+37
    FOR i = 1 TO N
        IF Tc(i) > maxtemp THEN
            maxtemp = Tc(i): maxtemploc = i
        END IF
    NEXT i

    IF mm > mmprint THEN
        '' First time to start calculations:
        '' First time (zero point) to start measuring average drift
        '' when the zone temp is stable within tempdiff remember firsttime
        '' and firsloc=segment when max temp occurred at time=firsttime
        '' then set firstread=1

        IF ABS(oldmaxtemp - maxtemp) < tempdiff AND
        firstread = 0 THEN
            firstread = 1: firsttime = T: firstloc
            = maxtemploc
        END IF
    END IF
    IF mm > mmprint THEN
        speed = (maxtemploc - oldmaxtemploc) * seglen
        / (delta * mmprint) * 1000 * 60      '' In
        mm/min
    END IF
    LOCATE 18, 40: PRINT "Hot zone velocity=";
    PRINT USING "####.##"; speed;
    PRINT " mm/min ";
    IF firstread > 0 AND T > firsttime THEN
        LOCATE 19, 40: PRINT "Av. zone velocity=";
        avspeed = (maxtemploc - firstloc) * seglen /
        (T - firsttime) * 1000 * 60        '' In mm/min
        PRINT USING "####.##"; avspeed;
        PRINT " mm/min ";
    END IF

```

```

LOCATE 20, 40: PRINT "At";
PRINT USING "####"; INT(Tc(maxtemploc));
PRINT "oC, Ionic drift=";
Tk = Tc(maxtemploc) + 273
D = d0 * EXP(-q / k / Tk)

SELECT CASE Tk
CASE IS <= 435 + 273
    ionconc = -.00009 * Tc(i) + 1
CASE (435 + 273) TO (705 + 273)
    ionconc = -.001653 * Tc(i) + 1.68
CASE IS >= (705 + 273)
    ionconc = -.001163 * Tc(i) + 1.334
END SELECT

IF Tk < 673 THEN
electr = Total4
ELSE electr = c * EXP(-b * Tc(i))
END IF
ionic = (D / k / Tk) * ze ^ 2 * conc(maxtemploc) *
conc / .6
Total = electr + ionic
resistivity = 1 / Total
Vseg = current / area * resistivity
PRINT USING "####.##"; -(Vseg) * D / k / Tk * ze *
1000 * 60;
PRINT " mm/min";

IF mm > 0 THEN
    oldmaxtemploc = maxtemploc
    'old value of segment# where max temp
    occurred
END IF

END IF
'' Plot temperature profile:
COLOR 14
FOR i = 1 TO N - 1
    LINE (offsetx + i * sx, offsety + Tc(i) * sy)-
    (offsetx + (i + 1) * sx, offsety + Tc(i + 1) * sy)
NEXT i
OPEN "h:\qbprogs\Tprodcz.dat" FOR INPUT AS #1
OPEN "c:\temp\dcz1.dat" FOR OUTPUT AS #2
'' Read headers and write out again
LINE INPUT #1, inline$
PRINT #2, inline$
LINE INPUT #1, inline$
PRINT #2, inline$ + CHR$(9) + STR$(T)
FOR i = 1 TO N
    LINE INPUT #1, inline$
    PRINT #2, inline$ + CHR$(9) + STR$(Tc(i))
NEXT i
CLOSE #1
CLOSE #2
KILL "h:\qbprogs\Tprodcz.dat"
SHELL "copy c:\temp\dcz1.dat " + "h:\qbprogs\Tprodcz.dat > nul"

OPEN "h:\qbprogs\condcz.dat" FOR INPUT AS #8
OPEN "c:\temp\dczcon.dat" FOR OUTPUT AS #7
'read headers and write out again
LINE INPUT #8, inline$
PRINT #7, inline$
LINE INPUT #8, inline$
PRINT #7, inline$ + CHR$(9) + STR$(T)

```

```

FOR i = 1 TO N
  LINE INPUT #8, inline$
  PRINT #7, inline$ + CHR$(9) + STR$(conc(i))
NEXT i
CLOSE #8
CLOSE #7
KILL "h:\qbprogs\condcz.dat"
SHELL "copy c:\temp\dczcon.dat " + "h:\qbprogs\condcz.dat >
nul"

'' Plot V-I curve:
COLOR 10
IF oldcurrent < 8 AND current < 8 THEN
  LINE (x01 + oldvoltage * dx1, y02 - oldcurrent *
dy1)-(x01 + V * dx1, y02 - current * dy1)
END IF
oldvoltage = V: oldcurrent = current
GOSUB 7000      '' To save V-I values
GOSUB 8000      '' Close V-I file values

'' Draw strip every 50 calculations
FOR i = 1 TO N
  COLOR 0
  IF Tc(i) > 600 THEN
    COLOR 4      ''brownish
  END IF
  IF Tc(i) > 700 THEN
    COLOR 12     ''reddish
  END IF
  IF Tc(i) > 800 THEN
    COLOR 14     ''yellow
  END IF
  IF Tc(i) > 950 THEN
    COLOR 15     ''white
  END IF
  LINE (offsetx + i * 2, offsety + 20)-(offsetx + i *
2, offsety + 30)
  LINE (offsetx + i * 2 + 1, offsety+20)-(offsetx + i
* 2 + 1, offsety + 30)
NEXT i
END IF
COLOR 15
NEXT T
END

1000      '' sub to draw axes for V-I, labels, etc.
CLS
sy = -.215      '' Scale factor y direction
sx = 500 / N    '' Scale factor x direction
offsety = 215
offsetx = 10
COLOR 15
LINE (offsetx, offsety)-(offsetx + N * sx, offsety)

'' Outline of the rod:
leftx = 1
LINE (offsetx + leftx, offsety + 19)-(offsetx + leftx, offsety + 31)
LINE (offsetx + leftx + 1 + 2 * N, offsety + 19)-(offsetx + leftx + 1
+ 2 * N, offsety + 31)
LINE (offsetx + leftx, offsety + 19)-(offsetx + leftx + 1 + 2 * N,
offsety + 19)

```

```

LINE (offsetx + leftx, offsety + 31)-(offsetx + leftx + 1 + 2 * N,
offsety + 31)

'' V-I axes drawing:
maxa = 4: maxv = 5          '' max I, max V
dyl = 40: y01 = 280: y02 = y01 + maxa * dyl
dx1 = 50: x01 = 10: x02 = x01 + maxv * dx1

FOR i = 0 TO maxv
    LINE (x01 + i * dx1, y01)-(x01 + i * dx1, y02) '' 1 V steps
NEXT i
FOR j = 0 TO maxa STEP 1
    LINE (x01, y02 - j * dyl)-(x02, y02 - j * dyl) '' 1 A steps
NEXT j

COLOR 15
LOCATE 17, 1: PRINT "Current (A)"
LOCATE 18, 1: PRINT "4"
LOCATE 23, 1: PRINT "2"
LOCATE 29, 30: PRINT "Voltage (V)";
LOCATE 29, 1: PRINT "0";
LOCATE 29, 8: PRINT "1";
LOCATE 29, 15: PRINT "2";
LOCATE 29, 21: PRINT "3";
LOCATE 29, 27: PRINT "4";

'' Instructions:
xr = 41          '' Left column
yr = 22         '' Top row
LOCATE yr, xr: PRINT "Exit press ESC";
LOCATE yr + 1, xr: PRINT "Increase voltage press "; CHR$(24);
LOCATE yr + 2, xr: PRINT "Decrease voltage press "; CHR$(25);
LOCATE yr + 3, xr: PRINT "Clear the top screen press C";
LOCATE yr + 4, xr: PRINT "Create a hot spot press H";
LOCATE yr + 5, xr: PRINT "Concentration profile press P";

x1 = 640 * xr / 80 - 20          '' 640x480 pixels are 80x30
col*rows
y1 = 480 * yr / 30 - 20
x2 = 640 * (xr + 29) / 80
y2 = 480 * (yr + 5) / 30 + 5
LINE (x1, y1)-(x2, y1)
LINE (x2, y1)-(x2, y2)
LINE (x2, y2)-(x1, y2)
LINE (x1, y2)-(x1, y1)

'' Drift information border
yr = 18
xr = 41
x1 = 640 * xr / 80 - 20          '' 640x480 pixels are 80x30
col*rows
y1 = 480 * yr / 30 - 20
x2 = 640 * (xr + 35) / 80
y2 = 480 * (yr + 2) / 30 + 5
LINE (x1, y1)-(x2, y1)
LINE (x2, y1)-(x2, y2)
LINE (x2, y2)-(x1, y2)
LINE (x1, y2)-(x1, y1)
RETURN

2000          '' Draw grid
COLOR 15
FOR tt = 0 TO 900 STEP 100

```

```

        LINE (offsetx, offsety + tt * sy)-(offsetx + N * sx, offsety +
tt * sy)
NEXT tt

FOR j = offsetx TO offsetx + N * sx + 1 STEP N / 10 * sx
    LINE (j, offsety)-(j, offsety + 900 * sy)
NEXT j

COLOR 15
LOCATE 2, 65: PRINT "900oC"
LOCATE 6, 65: PRINT "600oC"
LOCATE 10, 65: PRINT "300oC"
LOCATE 14, 65: PRINT "0oC"
LOCATE 15, 47: PRINT "Distance mm";
LOCATE 15, 31: PRINT INT(length * 500 + .5);
T$ = "TEMPERATURE"
FOR j = 1 TO LEN(T$)
    LOCATE j + 2, 72
    PRINT MID$(T$, j, 1)
NEXT j
RETURN

3000
FOR u = 1 TO 14          '' Clear the top of the screen
    LOCATE u, 1: PRINT TAB(78);
NEXT u
RETURN

4000
GOSUB 3000: GOSUB 2000
LOCATE 2, 65: PRINT "6.9  "
LOCATE 6, 65: PRINT "6.6  "
LOCATE 10, 65: PRINT "6.3  "
LOCATE 14, 65: PRINT "6.0  "
T$ = "      x      "
FOR j = 1 TO LEN(T$)
    LOCATE j + 2, 72
    PRINT MID$(T$, j, 1)
NEXT j
COLOR 14
FOR i = 1 TO N - 1
    LINE (offsetx + i * sx, offsety + 1000 * conc(i) * sy)-(offsetx
+ (i + 1) * sx, offsety + 1000 * conc(i + 1) * sy)
NEXT i
111 k$ = INKEY$: IF k$ = "" THEN 111
    GOSUB 3000
    GOSUB 2000
RETURN

5000          '' Create an area with a different concentration
LOCATE 1, 1: PRINT TAB(78);
LOCATE 1, 1: PRINT "Enter start,end of spot in % of length:"; : INPUT
stpct, endpct
LOCATE 1, 1: PRINT TAB(78);
LOCATE 1, 1: PRINT "Enter oxygen concentration (in x-6):"; : INPUT
spot
FOR sp = INT(stpct / 100 * N) TO INT(endpct / 100 * N)
    conc(sp) = spot
NEXT sp
RETURN

6000
OPEN "h:\qbprogs\VIDcz.dat" FOR APPEND AS #3
RETURN

```

```
7000  
WRITE #3, T, V, current  
RETURN
```

```
8000  
CLOSE #3  
RETURN
```

REFERENCES

- A.A. Abrikosov, *Sov. Phys. JETP*, Vol. **5** (1957) pp. 1174-1182.
- M.A. Alario-Franco and C. Chaillout, *Solid State Ionics*, Vol. **32/33** (1989) pp. 1056-1063.
- M. Asta, D. de Fontaine, G. Ceder, E. Salomons and M. Kraitichman, *J. Less-Common Metals*, Vol. **168** (1991) pp. 39-51.
- M. Ausloos and A. Pękaliski, *Phys. Rev. B*, Vol. **52** (1995) pp. 4577-4582.
- H. Bakker, J.P.A. Westerveld and D.O. Welch, *Physica C*, Vol. **153-155** (1988) pp. 848-849.
- H. Bakker, J.P.A. Westerveld, D.M.R. Lo Caschio and D.O. Welch, *Physica C*, Vol. **157** (1989) pp. 25-36.
- J.G. Bednorz and K.A. Müller, *Z. Phys. B*, **64** (1986), pp. 189-193.
- A. Belzner, T.M. Gür and R.A. Huggins, *Solid State Ionics* Vol. **40-41** (1990) pp. 535-538.
- V.S. Bobrov, E.A. Brener, S.E. Esipov, A.N. Izotov, Yu A Koval', V.V. Korshunov, R.K. Nikolaev, L.A. Novomlinskii, Yu A Ossipyan, N.S. Sidorov and V Sh Shekhtman. B.C.H. Steele. R (1990)/01 (private communication).
- A. Bourdillon and N.X. Tan Broudillon, “*High temperature superconductors: processing and science*”, Academic Press (1994).
- V.A.M. Brabers, W.J.M. de Jonge, L.A. Bosch, C. van der Steen, A.M.W. de Groot, A.A. Verheyen and C.W.H.M. Vennix, *Mat. Res. Bull.*, Vol. **23** (1988) pp. 197-207.
- S.I. Bredikhin, G.A. Emel'chenko, V.Sh. Shechtman, A.A. Zhokhov, S. Carter, R.J. Chater, J.A. Kilner and B.C.H. Steele, *Physica C*, Vol. **179** (1991) pp. 286-290.
- J.J. Capponi, C. Chaillout, A.W. Hewat, P. Lejay, M. Marezio, N. Nguyen, B. Raveau, J.L. Soubeyroux, J.L. Tholence and R. Tournier, *Europhys. Lett.*, Vol. **3** (1987) pp. 1301-1307.
- W. Carrillo-Cabrera, H-D. Wiemhöfer and W. Göpel, *Solid State Ionics*, Vol. **32-33** (1989) pp. 1172-1178.
- H.S. Carslaw and J.C. Jaeger, “*Conduction of heat in solids*”, Oxford Science Publications, 2nd Ed. (1959).

- R.J. Cava, B. Batlogg, C.H.Chen, E.A. Tietman, S.M. Zahurak and D. Wereder, *Nature*, Vol. **329** (1987) pp. 423-425.
- R.J. Cava, A.W. Hewat, E.A. Hewat, B. Batlogg, M. Marezio, K.M. Rabe, J.J. Krajewski, W.F. Peck Jr. and L.W. Rupp Jr., *Physica C*, Vol. **165** (1990) pp. 419-433.
- G. Ceder, M. Asta, W.C. Carter, M. Kraitichman, D. de Fontaine, M.E. Mann and M. Sluiter, *Phys. Rev. B*, Vol. **41** (1990) pp. 8698-8701.
- E.K. Chang, D.J.L. Hong, A. Mehta and D.M.Smyth, *Mat. Lett.*, Vol. **6** (1988), pp. 251-253.
- J-S. Choi, M. Sarikaya, I.A. Aksay and R. Kikuchi, *Phys. Rev. B*, Vol. **42** (1990) pp. 4244-4254.
- K. Conder, E. Kaldis, M. Maciejewski, K.A. Müller and E.F. Steigmeier, *Physica C*, Vol. **210** (1993) pp. 282-288.
- K. Conder, Ch. Krüger, E. Kaldis, D. Zech and H. Keller, *Physica C*, Vol. **225** (1994) pp. 13-20.
- J.R. Cost and J.R. Stanley, *J. Mater. Res.*, Vol **6** (1991) pp. 232-243.
- J.M. Coulson and J.F. Richardson, “*Chemical engineering. Volume 1. Fluid flow, heat transfer and mass transfer*”, 3rd Ed., Pergamon Press, (1977).
- J. Crank, “*The mathematics of diffusion*”, 2nd Ed., Oxford Science Publications, (1975).
- M. Cyrot and D. Pavuna, “*Introduction to superconductivity and high T_c materials*”, World Scientific, (1992).
- T. Datta, “*Concise encyclopedia of magnetic and superconducting materials*”, Ed. J.E. Evetts, Pergamon Press, (1992).
- A. Davidson, P. Santhanam, A. Palevski and M.J. Brady, *Phys. Rev. B*, Vol. **38** (1988) pp. 2828-2831.
- S. Elschner, W. Becker, H. Bestgen and M. Brand, *Physica C*, Vol. **202** (1992) pp. 401-407.
- A. Erb, B. Greb and G. Müller-Vogt, *Physica C*, Vol. **259** (1996) pp. 83-91.
- F. Faupel and T. Hehenkamp, *Z. Metallkd.*, Vol. **84** (1993) pp. 529-533.
- A.T. Fiory, M. Gurvitch, R.J. Cava and G.P. Espinosa, *Phys. Rev. B*, Vol. **36** (1987) pp. 7262-7265.
- J.C. Fisher, *J. Appl. Phys.*, Vol. **22** (1951) pp. 74-77.

- B. Fisher, E. Polturak, G. Koren, A. Kessel, R. Fischer and L. Harel, *Solid State Commun.*, Vol **64** (1987) pp. 87-88.
- D. de Fontaine, M.E. Mann and G. Ceder, *Phys. Rev. Lett.*, Vol. **63** (1989) pp. 1300-1303.
- D. de Fontaine, G. Ceder and M. Asta, *Nature*, Vol. **343** (1990-a) pp. 544-546.
- D. de Fontaine, G. Ceder and M. Asta, *J. Less-Common Metals* Vol. **164-165** (1990-b) pp. 108-122.
- P.P. Freitas and T.S. Plaskett, *Phys. Rev. B*, Vol. **36** (1987) pp. 5723-5726.
- P.P. Freitas and T.S. Plaskett, *Phys. Rev. B*, Vol. **37** (1988) pp. 3657-3659.
- T. Furukawa, T. Shigematsu and N. Nakanishi, *Physica C*, Vol **204** (1992) pp. 103-108.
- P.K. Gallagher, *Adv. Cer. Mat.*, Vol. **2** (1987) pp. 632-639.
- B.A. Głowacki, R.J. Highmore, K.F. Peters, A.L Greer and J.E. Evetts. *Supercond. Sci. Technol.*, Vol **1** (1988) pp. 7-11.
- G.S. Grader, P.K. Gallagher and E.M. Gyorgy, *Appl. Phys. Lett.*, Vol. **51** (1987) pp. 1115-1117.
- M. Gurvitch and A.T. Fiory, *Phys. Rev. Lett.*, Vol. **59** (1987) pp. 1337-1340.
- I. Haller, M.W. Shafer, R. Figat and D.B. Goland, “*Chemistry of oxide superconductors*”, Ed. C.N.R. Rao, Blackwell Scientific Publications IUPAC (1988) pp. 93-100.
- M.S. Islam, *Supercond. Sci. Technol.*, Vol. **3** (1990) pp. 531-536.
- Y. Ikuma and S. Akiyoshi, *J. Appl. Phys.*, Vol. **64** (1988) pp. 3915-3917.
- J.A. Jacobson, J.M. Newsam, D.C. Johnston, J.P. Stokes, S. Bhattacharya, J.T. Lewandowski, D.P. Goshorn, J.M. Higgins and M.S. Alvarez, “*Chemistry of oxide superconductors*”, Ed. C.N.R. Rao, Blackwell Scientific Publications IUPAC (1988) pp. 43-61.
- J.D. Jorgensen, M.A. Beno, D.G. Hinks, L.Solderholm, K.J.Volin, R.L. Hitterman, J.D. Grace, I. K.Schuller, C.U. Segre, K. Zhang and M.S. Kleefisch, *Phys. Rev. B*, Vol. **36** (1987-a) pp. 3608-3616.
- J.D. Jorgensen, B.W. Veal, W.K.Kwok, G.W. Crabtree, A. Umezawa, L.J. Nowicki and A.P.Paulikas, *Phys. Rev. B*, Vol. **36** (1987-b) pp. 5731-5734.
- J.D. Jorgensen, B.W. Veal, A.P. Paulikas, L.J. Nowicki, G.W. Crabtree, H. Claus and W.K. Kwok, *Phys. Rev. B*, Vol. **41** (1990) pp. 1863-1877.

- K. Kishio, J. Shimoyama, T. Hasegawa, K. Kitazawa and K. Fueki, *Jpn. J. App. Phys.*, Vol. **26**, (1987), pp. L1228-L1230.
- K. Kishio, K. Kitazawa, K. Suzuki, T. Hasegawa and K. Fueki, *Physica C*, Vol. **162-164** (1989-a) pp. 55-56.
- K. Kishio, K. Suzuki, T. Hasegawa, T. Yamamoto and K. Kitazawa, *J. Solid State Chemistry*, Vol. **82** (1989-b) pp. 192-202.
- C. Krauns and H-U. Krebs, *Z. Phys. B*, Vol. **92** (1993) pp. 43-46.
- Ch. Krüger, K. Conder and E. Kaldis, *Physica C*, Vol. **213** (1993) pp. 219-223.
- T. Kwok, P. S. Ho and S. Yip, *Phys. Rev. B*, Vol. **29** (1984-a) pp. 5354-5362.
- T. Kwok, P. S. Ho and S. Yip, *Phys. Rev. B*, Vol. **29** (1984-b) pp. 5363-5371.
- J.R. LaGraff, P.D. Han and D.A. Payne, *Physica C*, Vol. **169** (1990) pp. 355-360.
- J.R. LaGraff, P.D. Han and D.A. Payne, *Phys. Rev. B*, Vol. **43** (1991) pp. 441-447.
- J.R. LaGraff and D.A. Payne, "*Physics and Materials Science of High Temperature Superconductors, II*", R. Kossowski *et al.* (eds.), Kluwer Academic Publishers (1992), pp. 225-246.
- J.R. LaGraff and D.A. Payne, *Phys. Rev. B*, Vol. **47** (1993-a) pp. 3380-3390.
- J.R. LaGraff and D.A. Payne, *Physica C*, Vol. **212** (1993-b) pp. 470-477.
- J.R. LaGraff and D.A. Payne, *Physica C*, Vol. **212** (1993-c) pp. 478-486.
- S-F. Lau, A.B. Rosenthal, N.P. Pyrras, J.A. Graham and H.N. Cheng, *J. Mater. Res.*, Vol. **6** (1991) pp. 227-231.
- A.D. Le Claire, "*Treatise in Solid State Chemistry*, Vol. 4, Reactivity of Solids" N.B. Hannay (Ed.), Plenum (1975), p.1.
- I.A. Leonidov, Ya.N. Blinovskov, E.E. Flyatau, P.Ya. Novak and V.L. Kozhevnikov, *Physica C*, Vol. **158** (1989) pp. 287-292.
- T.B. Lindemer, F.A. Washburn, C.S. MacDougall, R. Feenstra and O.B. Cavin, *Physica C*, Vol. **178** (1991) pp. 93-104
- F. London and H. London, *Proc. Roy. Soc. (London)*, Vol. **A155** (1935) pp. 71.
- J.R. Manning, "*Diffusion kinetics for atoms in crystals*", Van Nostrand (1968) p. 95.
- J.L. McManus, D.J. Fray and J. Evetts, *Supercond. Sci. Technol.* Vol. **1** (1989) pp. 291-295.

- J.L. McManus, D.J. Fray and J. Evetts, *Physica C*, Vol. **169** (1990) pp. 193-200.
- J.L. McManus, D.J. Fray and J. Evetts, *Physica C*, Vol. **190** (1992) pp. 511-521.
- W. Meissner and R. Ochsenfeld, *Naturwissenschaften*, Vol. **21** (1933) pp. 787.
- R. Mogilevsky, R. Levi-Stetti, B. Pashmakov, L. Liu, K. Zhang, H.M. Jaeger, D.B. Buchholz, R.P.H. Chang and B.W. Veal, *Phys. Rev. B*, Vol. **49** (1994) pp. 6420-6423.
- A.P. Mozahev and S.V. Chernyaev, *J. Mater. Chem.*, Vol **4** (1994) pp. 1107-1110.
- A. P. Mozhaev, S.V. Chernyaev, T.I. Udalt'sova and N.M. Kotov, *Russ. J. Inorg. Chem.*, Vol. **37** (1992) pp. 1111-1113.
- F. Munakata, K. Shinohara, H. Kanetsuka, N. Hirosaki, A. Okada and M. Yamanaka, *J. Jnl. Appl. Phys.*, Vol. **26** (1987) pp. L1292-L1293.
- V.I. Nefedov, A.N. Solokov, A.R. Vinogradov, T.A. Fomina, N.G. Shuranova, K.G. Oksenoid, G.I. Ramendik and E.A. Volkov, *Medeleev Commun.*, (1992) pp. 21-22.
- J. Nowotny and M. Rekas, *J. Am. Ceram. Soc.*, Vol. **73** (1990) pp. 1054-1061.
- H.M. O'Bryan and P.K. Gallagher, *Adv. Cer. Mat.*, Vol. **2** (1987) pp. 640-648.
- H.M. O'Bryan and P.K. Gallagher, *Solid State Ionics*, Vol. **32-33** (1989) pp. 1143-1148.
- T. Okamoto, B. Huybrechts and M. Takata, *Jpn. J. Appl. Phys.*, Vol. **33** (1994-a) pp. L1212-L1214.
- T. Okamoto, B. Huybrechts and M. Takata, *MRS Fall Meeting '94* (1994-b).
- H.K. Onnes, *Leiden Comm.*, Vol. **120b**, **122b**, **124c** (1911).
- Yu.A. Osip'yan, R.K. Nikolaev, N.S. Sidorov, V.S. Bobrov and V.S. Tsoi, *JETP Lett.*, Vol. **47** (1988) pp. 310-314.
- E.J.M. O'Sullivan and B.P. Chang, *Appl. Phys. Lett.*, Vol. **52** (1988) pp. 1441-1443.
- G. Ottaviani, C. Nobili, F. Nava, M. Affronte, T. Manfredini, F.C. Maticotta and E. Galli, *Phys. Rev. B*, Vol. **39** (1989) pp. 9069-9073.
- T. Ozawa, *J. Thermal Analysis*, Vol. **2** (1970) p. 301.
- M.V. Patrakeev, I.A. Leonidov, V.L. Kozhevnikov, V.I. Tsidilkovskii and A.K. Demin, *Physica C*, Vol. **210** (1993), pp. 213-220.
- J. S. Park and H.G. Kim, *Jpn. J. Appl. Phys.*, Vol. **27** (1988) pp. L191-L194.
- J-H. Park, P. Kostic and J.P. Singh, *Mat. Lett.*, Vol. **6** (1988) pp. 393-397.

- N.L. Peterson, "Diffusion in solids, Recent developments", A.S. Nowick and J.J. Burton (Eds.), Academic Press (1975), pp. 115-170.
- H.F. Poulsen, N.H. Andersen, J.V. Andersen, H. Bohr and O.G. Mouritsen, *Nature*, Vol. **349** (1991) pp. 594-596.
- H. Rickert, "Electrochemistry of solids. An introduction", Springer Verlag (1982).
- G.P. Rodríguez-Donoso, J. Ruiz, B.J. Fernández and A.J. Vázquez-Vaamonde, *Mat. and Design*, Vol. **16** (1995) pp. 163-166.
- M. Ronay, *Phys. Rev. B*, Vol. **36** (1987) pp. 8860-8862.
- M. Ronay and P. Nordlander, *Physica C*, Vol. **153-155** (1988) pp. 834-835.
- A.C. Rose-Innes, E.H. Rhoderick, "Introduction to Superconductivity", Pergamon, (1988).
- S.J. Rothman, J.L. Roubort and J.E. Baker, *Phys. Rev. B*, Vol. **40** (1989) pp. 8852-8860.
- S.J. Rothman, J.L. Roubort, U. Welp and J.E. Baker, *Phys. Rev. B*, Vol. **44** (1991) pp. 2326-2333.
- J.L. Roubort, N. Chen, K.C. Goretta and S.J. Rothman, *ICMC '90 Conference "High-Temperature Superconductors, Materials Aspects"*, (1990).
- J.L. Roubort and S.J. Rothman, *J. Appl. Phys.*, Vol. **76** (1994) pp. 5615-5628.
- J. Ruiz, J.B. Fernández and J.M. Belló, *2nd Seminar of Surface Engineering with High Energy Beams Sci. and Techn.* (1989) pp. 161-172.
- E. Saiz and J.S. Moya, *Mater. Lett.*, Vol. **6** (1988) pp. 369-373.
- J. Sabras, G. Peraudeau, R. Berjoan and C. Monty, *J. Less Common Metals*, Vol. **164-165** (1990) pp. 239-246.
- K. Salama and D.F. Lee, *Supercond. Sci. Technol.*, Vol. **7** (1994) pp. 177-193.
- E. Salomons and D. de Fontaine, *Phys. Rev. B*, Vol. **41** (1990) pp. 11159-11167.
- I.K. Schuller, D.G. Hinks, M.A. Beno, D.W. Capone II, L. Soderholm, J.-P. Locquet, Y. Bruynseraede, C.U. Segre and K. Zhang, *Solid State Comm.*, Vol. **63** (1987) pp. 385-388.
- Y. Scolnik, E. Sabatani and D. Cahen, *Physica C*, Vol. **174** (1991) pp. 273-279.
- S. Semenovskaya and A.G. Khachatryan, *Phys. Rev. B*, Vol. **46** (1992) pp. 6511-6534.

- H. Shaked, J.D. Jorgensen, J. Faber Jr., D.G. Hinks and B. Dabrowski, *Phys. Rev. B*, Vol. **39** (1989) pp. 7363-7366.
- D. Shi, *Phys. Rev. B*, Vol. **39** (1989) pp. 4299-4305.
- D. Shi "High temperature superconducting materials science and engineering: new concepts and technology", Pergamon, (1995).
- E.D. Specht, C.J. Sparks, A.G. Dhere, J. Brynstead, O.B. Cavin, D.M. Kroeger and H.A. Oye, *Phys. Rev. B*, Vol **37** (1988) pp. 7426-7434.
- H. Strauven, J.P. Locquet, O.B. Verbeke and Y. Bruynseraede, *Solid State Comm.*, Vol. **65** (1988) pp. 293-296.
- P. Strobel, J.J. Capponi, M. Marezio and P. Monod. *Solid State Comm.*, Vol. **64** (1987) pp. 513-515.
- M.-Y. Su, S.E.Dorris and T.O.Mason, *J. of Solid State Chem.*, Vol. **75** (1988) pp. 381-389.
- T. Suzuoka, *J. Phys. Soc. Jap.*, Vol. **19** (1964) pp. 839-851.
- J.L. Tallon and M.P. Staines, *J. Appl. Phys.*, Vol. **68** (1990) pp. 3998-4001.
- T.B. Tang and W. Lo, *Physica C*, Vol. **174** (1991) pp. 463-466.
- S. Tsukui, T. Yamamoto, M. Adachi, K. Kawabata, N. Fukuoka, A. Yanase and Y. Yoshioka, *Physica C*, Vol. **185-189** (1991-a) pp.929-930.
- S. Tsukui, T. Yamamoto, M. Adachi, Y. Shono, K. Kawabata, N. Fukuoka. S. Nakanishi, A. Yanase and Y. Yoshioka, *Jpn. J. App. Phys.*, Vol. **30** (1991-b) pp. L973-L976.
- K.N. Tu, C.C. Tsuei, S.I. Park and A. Levi, *Phys. Rev. B*, Vol. **38** (1988-a) pp. 772-775.
- K.N. Tu, N.C. Yeh, S.I. Park and C.C. Tsuei, *Phys. Rev. B*, Vol. **38** (1988-b) pp. 5118-5121.
- K.N. Tu, N.C. Yeh, S.I. Park and C.C. Tsuei, *Phys. Rev. B*, Vol. **39** (1989) pp. 304-314.
- X. Turrillas, J.A. Kilner, I. Kontoulis and B.C.H. Steele, *J. Less Common Metals*, Vol. **151** (1989) pp. 229-236.
- T. Umemura, K. Egawa, M. Wakata and K Yoshizaki, *Jpn. J. of App. Phys.*, Vol. **28** (1989) pp. L1945-L1947.
- B.W. Veal, H. You, A.P. Paulikas, H. Shi, Y. Fang and J.W. Downey, *Phys. Rev. B*, Vol. **42** (1990-a) pp. 4770-4773.

- B.W. Veal, H. You, A.P. Paulikas, H. Shi, Y. Fang and J.W. Downey, *Phys. Rev. B*, Vol. **42** (1990-b) pp. 6305-6316.
- D.J. Vischjager, A.A. van Zomeren, J. Schoonman, I. Kontoulis and B.C.H. Steele, *Solid State Ionics*, Vol. **40-41** (1990) pp. 810-814.
- R.T.P. Whipple, *Phil. Magazine*, Vol. **45** (1954) pp. 1225-1236.
- W.K. Wu, J.R. Ashburn, C.J. Torng, P.H. Hor, R.L. Meng, L. Gao, Z.J. Huang, Y.Q. Wang and C.W. Chu, *Phys. Rev. Lett.*, Vol. **58** (1987), pp. 908.
- X.M. Xie, T.G. Chen and Z.L. Wu, *Phys. Rev. B*, Vol. **40** (1989) pp. 4549-4556.
- S. Yamaguchi, K. Terabe, A. Imai and Y. Iguchi, *Jpn. J. of App. Phys.*, Vol. **27** (1988) pp. L220-L222.
- E. Yanmaz, I.R. Harris and J.S. Abell, *J. of Alloys and Compounds*, Vol. **185** (1992) pp. 311-320.
- E. Yanmaz, K. Donnelly, I.R. Harris and J.S. Abell, *J. of Alloys and Compounds*, Vol. **195** (1993) pp. 39-42.
- H-I. Yoo, *J. Mater. Res.*, Vol **4** (1989) pp. 23-27.
- H-I. Yoo and S-M. Lee, *J. Am. Ceram. Soc.*, Vol. **77** (1994) pp. 3131-3136.
- J. Zaanen, A.T. Paxton, O. Jepsen and O.K. Andersen, *Phys. Rev. Lett.* Vol. **60** (1988) pp. 2685-2688.
- J.X. Zhang, G.M. Lin, W.G. Zeng, K.F. Liang, Z.C. Lin, G.G. Siu, M.J. Stokes and P.C.W. Fung, *Supercond. Sci. Technol.*, Vol. **3** (1990-a) pp. 113-117.
- J.X. Zhang, G.M. Lin, W.G. Zeng, K.F. Liang, Z.C. Lin, G.G. Siu, M.J. Stokes and P.C.W. Fung, *Supercond. Sci. Technol.*, Vol. **3** (1990-b) pp. 163-172.
- Z. Zhao, L. Chen, Q. Yang, Y. Huang, G. Chen, R. Tang, G. Liu, C. Cui, L. Chen, L. Wang, S. Guo, S. Li and J. Bi, *Kexue Tongbao*, Vol. **32** (1987) pp. 1098.